UNIVERSITY OF SALERNO

DOCTORAL THESIS

# Particle physics and quantum field theory approaches to dark matter

*Author:*
Aniello QUARANTA

*Supervisor:*
Prof. Antonio CAPOLUPO

*A thesis submitted in fulfillment of the requirements for the degree of Doctor of Philosophy*

*in the*

Department of Physics “E. R. Caianiello”

Academic Year 2020–2021

“*And for some time light must be called darkness*”

F. W. Nietzsche, *Thus Spoke Zarathustra*

UNIVERSITY OF SALERNO

# *Abstract*

Department of Physics “E. R. Caianiello”

Doctor of Philosophy

**Particle physics and quantum field theory approaches to dark matter**

by Aniello QUARANTA

This thesis collects the results obtained during my doctorate course. The main topic is the nature of dark matter, investigated from the point of view of particle physics and quantum field theory. The research involves various aspects of the physics beyond the standard model, including the quantum field theory of particle mixing, neutrino physics, gravitational interactions and axionlike particles. The thesis is organized in three parts. In the first part we develop the quantum field theory of neutrino mixing in curved space, deriving new general oscillation formulae and analyzing the rich condensate structure of the flavor vacuum. We show that in a cosmological metric with De Sitter expansion of the scale factor, the flavor vacuum behaves as a pressure-less perfect fluid akin to dark matter. The second part is devoted to axions and axionlike particles, which to date represent the most promising dark matter candidates. We devise two novel detection strategies, making use of quantum entanglement and neutron interferometry. The third part deals with the phenomenology of flavor mixing and neutrino interactions. We show how the dark-matter-like properties of the flavor vacuum may in principle be revealed in ensembles of cold Rydberg atoms. We discuss the possibility to simulate the gravitational interactions of neutrinos with trapped ions. Finally we introduce a new quantum mechanical approach to study the dissipative effects of neutrino propagation in matter.

# *Acknowledgements*

I wish to thank all those who helped me during my doctorate.

I am immensely grateful to my supervisor Prof. Antonio Capolupo, who guided me in my research. His broad vision and his tireless work have inspired me to continuosly improve and give my best in the research.

I am thankful to Prof. Gaetano Lambiase, Prof. Salvatore Marco Giampaolo and Dr. Sante Carloni for the illuminating discussions and the work done together.

Finally I thank my family for their constant and unconditional support.

# Contents

# List of Figures

# Notation

Throughout the thesis we adopt the mostly minus signature of the Minkowski metric tensor $\eta_{\mu\nu} = \mathrm{diag}\,(1, -1, -1, -1)$. Unless otherwise specified, the Einstein summation convention over repeated indices is used, e.g. $A^\mu B_\mu \equiv \sum_\mu A^\mu B_\mu$.

Lowercase greek indices $\alpha, \beta, \gamma \ldots$ are used to denote the components of $4-$vectors and $4-$tensors and range between 0 and 3. Lowercase latin indices $a, b, c \ldots$ are used to denote the spatial components of 4-vectors and 4-tensors and range between 1 and 3. Uppercase latin indices $A, B, C \ldots$ are used to denote spinor components, with values $1, 2, 3, 4$. The imaginary unit is written $i$.

Boldface letters $\boldsymbol{a}, \boldsymbol{b}, \boldsymbol{c} \ldots$ denote spatial 3-vectors. The symbol $\cdot$ is used for the euclidean scalar product, and more generally for the sum $\boldsymbol{a} \cdot \boldsymbol{b} = \sum_{i=1,2,3} a_i b_i$. The boldface sigma indicates the vector of Pauli matrices $\boldsymbol{\sigma} \equiv (\sigma_x, \sigma_y, \sigma_z)$, where

$$\sigma_x = \begin{pmatrix} 0 & 1 \\ 1 & 0 \end{pmatrix} \; ; \; \sigma_y = \begin{pmatrix} 0 & -i \\ i & 0 \end{pmatrix} \; ; \; \sigma_z = \begin{pmatrix} 1 & 0 \\ 0 & -1 \end{pmatrix} \, .$$

If $z$ is a complex quantity, $\Re z$, $\Im z$, $z^*$ and $|z|$ denote respectively the real part, the imaginary part, the complex conjugate and the modulus of $z$. The adjoints of matrices $M$ and operators $O$ are denoted $M^\dagger$ and $O^\dagger$.

When dictated by convenience the Dirac bra–ket notation is employed. Inner products and expectation values are written $\langle A | \, B \rangle$ and $\langle A | \, O \, | A \rangle$, for given states $|A\rangle \, , |B\rangle$ and operator $O$.

Only a rare and circumstancial use of acronyms is made, interchangeably with the extended form. These are: **QFT** (**Q**uantum **F**ield **T**heory); **SM** (**S**tandard **M**odel); **F(L)RW** (**F**riedman–(**L**emaître)–**R**obertson–**W**alker); **VEV** (**V**acuum **E**xpectation **V**alue); **ALP** (**A**xion **L**ike **P**article); **MSW** (**M**ikheev–**S**mirnov–**W**olfenstein).

Natural units with $c = 1 = \hbar$ are used throughout the thesis. The mass/energy units are specified whenever needed.

# Introduction

Two of the greatest achievements of the 20th century are undoubtedly the formulation of General Relativity and the Standard Model of particle physics. These theories represent the basis for our current understanding of the universe. Many of the recent groundbreaking experimental discoveries, from the Higgs boson [1] to the detection of gravitational waves [2], are to be traced back to either of the two theories. Together they are able to explain most of the observed phenomena, yet they give us an incomplete and fragmented picture, gravitation being described by a classical theory and particle physics by a fully quantum mechanical model. Over the years a significant amount of evidence, hinting at theories beyond the standard model and general relativity, has been accumulated. The discovery of neutrino oscillations [3–5] has revealed that neutrinos are massive particles and that they can change flavor during their propagation. The origin of their mass, as well as the fundamental mechanism behind flavor oscillations, cannot be explained within the standard model and remain debated. Even more compelling are the long-standing puzzles of modern cosmology. The early phases of the universe pose a huge challenge to theoretical physics in several respects. Going backwards in time, to epochs that are closer and closer to the Big Bang, two fundamental steps are expected to take place: the unification of all the gauge interactions or "Grand Unification" [6–9] and the attainment of the Quantum Gravity [10–13] regime. Likewise, the original baryon asymmetry [9, 14–16] that has given rise to the excess of matter over antimatter must be traced back to the first phases of the universe. All these phenomena require theories beyond the standard model. The content of the universe at the present age is no less mysterious. Only about 5% of its total energy density is in the form of ordinary matter (baryons), while the great majority is made up by "dark" components [17]. The accelerated expansion of the universe is fueled by *dark energy* [18–20], that represents about 70% of the total energy density. The nature of dark energy is essentially unknown, with possible explanations in terms of new particles [21] and in terms of extended theories of gravity [22, 23]. The remaining $\sim 25\%$ of the total energy density is in the form of *dark matter*. As the name suggests, this substance does not emit electromagnetic radiation, contrary to the visible (baryonic) matter. We can infer its existence only due to its gravitational effects. The first evidence of dark matter comes indeed from the gravitational stability of the large scale structures in the universe. The rotation curves of spiral galaxies require additional, invisible, matter to be explained [24–27]. At larger scales, dark matter is responsible for holding galaxy clusters together, and accounts for the discrepancy between their visible mass and the related gravitational lensing [28]. At cosmological level the dark portion is needed to explain the observed amount of matter in the universe [17, 29]. Given the evidence at different scales, it is today accepted that dark matter constitutes the majority $\sim 85\%$ of the matter content of the universe, representing a basic ingredient in the standard cosmological model ($\Lambda$CDM) [30]. Nevertheless, there is no consensus on the fundamental nature of dark matter. Several hypotheses have been put forward, ranging from primordial black holes [31, 32] to supersymmetric weakly interacting particles [33], but none of them has proven to be conclusive.

The central topic of this thesis is the nature of dark matter, explored from a particle physics perspective. The discussion is necessarily tied to the physics beyond the standard model, and deals with transversal issues, encompassing strictly theoretical subjects as well as phenomenological analyses. Among these stands the phenomenon of flavor mixing, and more generally the issues related to neutrino physics. Earlier works [34–38] have shown, building upon the quantum field theory of fermion mixing, that the vacuum of the theory may have dark-matter-like properties. This hints at the intriguing possibility that dark matter may be explained, at least partially, by means of a pure field theoretic effect, without the need to introduce new particles. The idea that the quantum field theoretic vacuum might be related to the dark components of the universe is not entirely new (see e.g. [39, 40]). Yet the naive computation of the energy density in quantum field theory leads to the notorious cosmological constant problem [41, 42], exceeding the actual value by several orders of magnitude. The quantum field theory of particle mixing eases the tension, bringing along a much milder ultraviolet behaviour (logarithmic as opposed to power-law) in the momentum integral for the energy density. In addition, the flavor vacua of bosons and fermions show, respectively, a dark-energy-like and a dark-matter-like behaviour, granting the possibility to explain both phenomena in the same framework. Interesting as they are, these results were obtained in the context of Minkowskian quantum field theory.

In the first part of the thesis we pursue a more realistic approach, involving quantum field theory in curved space. To this end we construct a proper generalization of the mixing quantum field theory to curved space. The peculiar structure of the flavor space is there interlaced with the intrinsic ambiguities of the field theory on curved backgrounds, resulting in a theory of remarkable complexity. We introduce new general oscillation formulae and discuss the issues related to their transformation properties. The formalism we develop to tackle the unique combination of mixing and spacetime curvature proves to be versatile enough to describe neutrino mixing in many spacetimes of interest, including the cosmological Friedmann-Robertson-Walker metrics and the Schwarzschild black hole metric. We derive oscillation formulae for neutrinos in these spacetimes, showing their deviation from their quantum mechanical and flat counterparts, both in the amplitude and in the phase of the oscillations. The so-developed quantum field theory of fermion mixing in curved space then provides the basis for a curved space analysis of the flavor vacuum. In this respect we obtain results that confirm and generalize those obtained in flat space. We show that the flavor vacuum may account for a dark matter component in a cosmological Friedmann-Robertson-Walker spacetime, in the case of a De Sitter expansion, deriving the associated equation of state. This constitutes the first attempt at a consistent study of its dark-matter-like properties. The relevance of our analysis of neutrino mixing in curved space is certainly not limited to the possibility of explaining dark matter. Neutrinos have indeed played a fundamental role during the first phases of the universe, and are decisive in the evolution of stars. In these environments neutrino physics cannot be fully understood without assessing the impact of gravitation on the particle mixing phenomenon.

In the second part of the thesis we deal with the particle explanations for dark matter. Indeed, besides the field theoretical explanation, dark matter may be understood in terms of new particles. Over the years a huge number of theories, extending the standard model by the addition of one or more fields, has been proposed. A whole *dark sector*, with its own "dark" gauge bosons [43] has been inspected. But axions and axionlike particle models are arguably the best motivated. A compelling theoretical motivation for their existence is that they emerge naturally from the Peccei–Quinn [44] mechanism, which represents an elegant solution to the strong CP problem. Furthermore axions and axionlike particles emerge from various string theoretic models [45–47]. Their relevance as a dark matter component is a consequence of their small interactions with the standard model fields. The chance to solve two puzzles at once has motivated a wide and long–lasting interest in axions and axionlike particles, both from the theoretical point of view, with the development of more and more refined models, and from the experimental point of view, with countless experiments aimed at their revelation. To date, however, there is no clear evidence for their existence. In the second part of the thesis we develop two new detection strategies for axions and axionlike particles. The core of these proposals is the new interaction between fermions due to axion exchange. By extension our methods apply to any new pseudoscalar particle which is capable of mediating interactions between fermions, and thus are akin to "fifth force" experiments. Our proposals adjoin seemingly distant branches of physics, borrowing tools and ideas from quantum information theory and interferometry in order to probe the existence of new particles and forces. We first investigate the quantum entanglement induced by the axion–mediated interaction on fermions. We show that the entanglement properties of the fermion states depend on the coupling to axions and that the axion–induced interaction shows up in entanglement measures. We then discuss how to isolate the axion contribution from other unwanted sources of entanglement, and provide a specific physical observable, an entanglement witness, to measure the effects due to the axion–induced interaction. The second detection method is based on neutron interferometry. We demonstrate that the axion–mediated neutron–neutron interaction affects the phase of neutrons. We then devise an interferometric setup to reveal the axion–induced phase, that can eventually be used to probe the existence of new pseudoscalar particles. The limits and the advantages of our proposals are thence discussed.

In the third part of the thesis we study the phenomenology of flavor mixing and neutrino interactions. The difficulty in experimentally probing dark matter components is not limited to axions and axionlike particles. Also the dark-matter-like behaviour of the flavor vacuum is hard to be revealed, since it is mainly relevant on the cosmological scales and only a poor experimental control over neutrinos is possible. We partially remedy the situation, by introducing appropriate simulations that, preserving the essential physics, can replicate the phenomena in a controlled environment. Atomic physics offers, in this respect, the ideal ground to test theories and models that would be otherwise hardly accessible. These include the dark-matter-like properties of the flavor vacuum and the tiny gravitational interactions among neutrinos. We show that the phenomenology of flavor mixing can be reproduced with Rydberg atoms. The latter represent a versatile analogue of oscillating neutrinos, allowing for the fine tuning of the inter-atomic interactions and a precise control over the thermodynamic parameters. We explicitly demonstrate the formal analogy between Rydberg atoms and oscillating neutrinos, arguing that the physical vacuum for the Rydberg atoms has the same dark-matter-like properties as the flavor vacuum of neutrinos. We show that, in particular, this affects the energy and the thermodynamic quantities of the atomic ensemble, rendering the effect potentially observable. Similarly, we prove that ions placed in trapping potentials, originated through electric or magnetic fields, can simulate the neutrino-neutrino gravitational interactions. The phenomenology predicted for gravitationally interacting neutrinos is thus replicated with trapped ions. We then further investigate neutrino interactions in dense media, in an effort to go beyond the matter potential approximation. We introduce a simple quantum mechanical approach to take into account the matter-induced dissipation. We describe the decoherence due to the interactions with matter and discuss the effective violation of the discrete symmetries due to the medium. The study has possible implications in astrophysical environments.

The purposes of the research work collected in this thesis are manifold. On the one hand is the development of theories capable to explain, at least partially, dark matter. On the other hand is the understanding of exquisitely particle physics issues, including the description of flavor mixing in curved space. Today the largest available source of observational data is the cosmos, from the local to the cosmological scale. Therefore it is no surprise that cosmology and astrophysics are the main driving forces behind the development of particle physics. The particle physics beyond the standard model is necessarily entwined with the fundamental questions of modern cosmology. This is ostensibly reflected in our research work. The nature of dark matter makes no exception, by challenging our standard-model-based perspective and stimulating the progress of particle physics. Not only neutrinos, but also axions and axionlike particles have such a transversal relevance. No less important is the possibility to test the theories, by carefully analyzing the resulting phenomenology. In this respect we devise both “direct” detection strategies and quantum simulations.

The thesis is structured as follows.

Chapter I gives a brief introduction to flavor mixing in the quantum mechanical and in the quantum field theoretical approaches, with a particular emphasis on the condensate structure of the flavor vacuum.

Chapter II is devoted to the quantum field theory of flavor mixing in curved space. First we develop the formalism needed to compute the oscillation formulae, and apply it to various cases of interest. The same formalism is then employed to study the condensate structure of the flavor vacuum and its possible contribution to dark matter.

Chapter III is dedicated to axions and axionlike particles. After a review of their properties and their interactions, two novel detection strategies are presented and their feasability is discussed.

Chapter IV deals with the phenomenology of flavor mixing and neutrino interactions. Two atomic systems, Rydberg atoms and trapped ions, are used to simulate respectively the dark-matter-like behaviour of the flavor vacuum and the gravitational interactions among neutrinos. A quantum mechanical approach for the propagation of neutrinos in matter, including dissipative effects, is then presented. Finally we draw our conclusions. Chapters II to IV are entirely based on the research articles published by the author.

# Chapter 1

# Flavor Mixing

This introductory chapter is devoted to flavor mixing. The topic is extremely rich and is not completely understood in all of its aspects. Here we present the main features of the phenomenon, first in quantum mechanics [48, 49], and then in the framework of quantum field theory [50–53].

## 1.1 Flavor Oscillations in Quantum Mechanics

Consider a quantum system described by a time-independent Hamiltonian $H$, and denote its eigenstates as $|\psi_i\rangle$, for $i = 1, 2, ...d$, so that $H|\psi_i\rangle = E_i|\psi_i\rangle$. The dimensionality $d$ of the Hilbert space $\mathcal{H}$ of the system corresponds to the number of distinct flavors, and the most common occurrences are $d = 2$ and $d = 3$. Larger spaces can occur, for instance in neutrino mixing with one sterile neutrino $d = 4$. In what follows, the value of $d$, which we assume finite, and thus the number of distinct flavors, is irrelevant. Suppose that the physical states $|\psi_\sigma\rangle$ of the system, with $\sigma = A, B...$, are not eigenstates of the Hamiltonian. We call $|\psi_\sigma\rangle$ flavor states. The precise definition of flavor states depends on the underlying system: for neutrinos these are the states produced in the weak interaction processes [54]. The key point is that the flavor states are related to the energy eigenstates through a unitary operator $U$:

$$|\psi_\sigma\rangle = \sum_i U_{\sigma i}|\psi_i\rangle \ , \tag{1.1}$$

i. e. they are coherent superpositions of energy states. The matrix $U_{\sigma i}$ is known as the mixing matrix. Now let the initial state of the system be $|\psi(t=0)\rangle = |\psi_\sigma\rangle$. The state of the system at time $t$ shall be given by

$$|\psi_\sigma(t)\rangle = e^{-iHt}|\psi_\sigma\rangle = \sum_i U_{\sigma i} e^{-iE_i t}|\psi_i\rangle \ . \tag{1.2}$$

From the unitarity of $U$, i.e. $\sum_\sigma U^*_{\sigma j} U_{\sigma i} = \delta_{ji}$, we can invert the relation (1.1) to obtain

$$|\psi_i\rangle = \sum_\sigma U^*_{\sigma i}|\psi_\sigma\rangle \ . \tag{1.3}$$

Inserting the above equation in (1.2) we get

$$|\psi_\sigma(t)\rangle = \sum_{\sigma'}\left(\sum_i U_{\sigma i} U^*_{\sigma' i} e^{-iE_i t}\right)|\psi_{\sigma'}\rangle \equiv \sum_{\sigma'} A_{\sigma'\sigma}(t)|\psi_{\sigma'}\rangle \ , \tag{1.4}$$

where we have introduced the amplitude $A_{\sigma'\sigma}(t)$ for convenience. According to the principles of quantum mechanics $A_{\sigma'\sigma}(t) = \langle\psi_{\sigma'}|\,\psi_\sigma(t)\rangle$ represents the amplitude for the system to be found in the state $|\psi_{\sigma'}\rangle$ at time $t$, knowing that its initial state is $|\psi_\sigma\rangle$. By direct inspection we learn that

$$A_{\sigma'\sigma}(0) = \sum_i U_{\sigma' i} U^*_{\sigma i} = \delta_{\sigma'\sigma} \,, \tag{1.5}$$

so that the transition amplitude $A_{\sigma'\sigma}$ with $\sigma' \neq \sigma$ vanishes at $t = 0$, consistently with the assumption that the initial state is $|\psi_\sigma\rangle$. At $t > 0$ the transition amplitude is generally non zero, and flavor transitions occur with probability

$$P_{\sigma\to\sigma'}(t) = |A_{\sigma'\sigma}(t)|^2 = \sum_{i,j} U_{\sigma i} U^*_{\sigma' i} U^*_{\sigma j} U_{\sigma' j} e^{-i\left(E_i - E_j\right)t} \,. \tag{1.6}$$

It is immediate to verify that $\sum_{\sigma'} P_{\sigma\to\sigma'}(t) = 1$ for all $t$.

### 1.1.1 Two flavor oscillations

The simplest case is $d = 2$. Despite its simplicity, the formalism for two flavor oscillations describes a large number of physical systems, including neutral meson mixing, axion-photon mixing and neutrino oscillations in many experimentally relevant situations. Let us start with the Hamiltonian expressed on the flavor basis $|\psi_A\rangle, |\psi_B\rangle$:

$$H_f = \begin{pmatrix} H_{AA} & H_{AB} \\ H^*_{AB} & H_{BB} \end{pmatrix} \,. \tag{1.7}$$

Here the suffix $f$ stands for flavor, and it is understood that $H_{\sigma\sigma'} = \langle\psi_\sigma| H |\psi_{\sigma'}\rangle$ for $\sigma, \sigma' = A, B$. It is also assumed that the flavor basis is orthonormal. The Hamiltonian (1.7) can be easily diagonalized through a unitary operator $U$ of the form

$$U = \begin{pmatrix} \cos\theta & \sin\theta e^{i\phi} \\ -\sin\theta e^{-i\phi} & \cos\theta \end{pmatrix} \,, \tag{1.8}$$

provided that the mixing angle $\theta$ and the phase $\phi$ satisfy

$$\tan 2\theta = \frac{2|H_{AB}|}{H_{BB} - H_{AA}} \qquad e^{i\phi} = \frac{H_{AB}}{|H_{AB}|} \,. \tag{1.9}$$

The change of basis described by the matrix (1.8) indeed brings the Hamiltonian into its diagonal form

$$H_d = U^\dagger H_f U = \begin{pmatrix} H_1 & 0 \\ 0 & H_2 \end{pmatrix} \tag{1.10}$$

with

$$H_{1,2} = \frac{1}{2}\left(H_{AA} + H_{BB} \mp \sqrt{\left(H_{BB} - H_{AA}\right)^2 + 4|H_{AB}|^2}\right) \,. \tag{1.11}$$

The energy eigenstates $|\psi_1\rangle, |\psi_2\rangle$ are then related to the flavor states via the mixing matrix of eq. (1.8), explicitly

$$\begin{aligned} |\psi_A\rangle &= \cos\theta\, |\psi_1\rangle + \sin\theta e^{i\phi}\, |\psi_2\rangle \\ |\psi_B\rangle &= -\sin\theta e^{-i\phi}\, |\psi_1\rangle + \cos\theta\, |\psi_2\rangle \,. \end{aligned} \tag{1.12}$$

Now it is immediate to deduce the time evolution of the flavor states. By a straightforward application of the time evolution operator $e^{-iHt}$ to equations (1.12) we find

$$\begin{aligned} |\psi_A(t)\rangle &= \cos\theta e^{-iH_1t}|\psi_1\rangle + \sin\theta e^{i\phi}e^{-iH_2t}|\psi_2\rangle \\ |\psi_B(t)\rangle &= -\sin\theta e^{-i\phi}e^{-iH_1t}|\psi_1\rangle + \cos\theta e^{-iH_2t}|\psi_2\rangle \ . \end{aligned} \tag{1.13}$$

The transition amplitudes follow by evaluating the scalar products with the aid of eqs. (1.13). Taking into account the orthogonality of the energy eigenstates, one finds

$$\begin{aligned} P_{A\to B}(t) &= P_{B\to A}(t) = |\langle\psi_B(0)|\,\psi_A(t)\rangle|^2 = \sin^2 2\theta \sin^2\left(\frac{(H_2-H_1)\,t}{2}\right) \\ P_{A\to A}(t) &= P_{B\to B}(t) = |\langle\psi_A(0)|\,\psi_A(t)\rangle|^2 = 1-\sin^2 2\theta \sin^2\left(\frac{(H_2-H_1)\,t}{2}\right) \\ &. \end{aligned} \tag{1.14}$$

### 1.1.2 Neutrino oscillations

A unique case among the elementary particles, neutrinos undergo the phenomenon of flavor oscillations. They are produced abundantly in nuclear reactions and interact only through gravitation and the weak interaction. They take part in the weak interactions as flavor neutrinos, that is, as fields with a definite flavor. Three flavors are currently known, namely $\nu_e, \nu_\mu, \nu_\tau$, which carry the same lepton number as the corresponding charged leptons $L_e$ (electron), $L_\mu$ (muon), $L_\tau$ ($\tau$ particle). The flavor oscillations, i.e., transitions of the kind $\nu_e \leftrightarrow \nu_\mu$, occur because flavor neutrinos have no definite mass and they are not eigenstates of the free Hamiltonian, according to the mechanism described above. The first description of neutrino oscillations, due to Pontecorvo [48, 49], considers only the two flavors $\nu_e, \nu_\mu$. The neutrino mass term, written in the flavor basis $|\nu_e\rangle\,,|\nu_\mu\rangle$ has the form of eq. (1.7)

$$H = \begin{pmatrix} m_{ee} & m_{e\mu} \\ m_{e\mu} & m_{\mu\mu} \end{pmatrix} \tag{1.15}$$

with $m_{ee}, m_{e\mu}, m_{\mu\mu}$ positive real parameters with the dimensions of a mass. This corresponds to the field theoretic Hamiltonian density

$$\mathcal{H} = m_{ee}\bar{\nu}_e(x)\nu_e(x) + m_{\mu\mu}\bar{\nu}_\mu(x)\nu_\mu(x) + m_{e\mu}\left(\bar{\nu}_e(x)\nu_\mu(x) + \bar{\nu}_\mu(x)\nu_e(x)\right)\ , \tag{1.16}$$

where $\nu_e(x), \nu_\mu(x)$ are the neutrino flavor *fields* and the bar denotes the Dirac adjoint $\bar{\nu} = \nu^\dagger\gamma^0$. The Hamiltonian (1.15) is diagonalized as above, with mixing angle and eigenvalues

$$\begin{aligned} \tan 2\theta &= \frac{2m_{e\mu}}{m_{\mu\mu}-m_{ee}} \\ m_{1,2} &= \frac{1}{2}\left(m_{ee}+m_{\mu\mu} \mp \sqrt{(m_{\mu\mu}-m_{ee})^2+4m_{e\mu}^2}\right)\ . \end{aligned}$$

The corresponding eigenstates ($|\nu_1\rangle\,,|\nu_2\rangle$) are known as mass states and represent free particles propagating with a definite mass (and energy). The relativistic energy for a free particle of mass $m_j$, in a given frame, is $\omega_j = \sqrt{k^2+m_j^2}$, with $k^2 = |\boldsymbol{k}|^2$ and $\boldsymbol{k}$ the particle 3-momentum. Then the mass states at a given time are

$$|\nu_j(t)\rangle = e^{-i\omega_j t}|\nu_j\rangle \qquad j = 1, 2\,, \tag{1.17}$$

where we have denoted $|\nu_j\rangle = |\nu_j(t=0)\rangle$. Just as in equation (1.13), the flavor states at time $t$ are

$$\begin{aligned} |\nu_e(t)\rangle &= \cos\theta e^{-i\omega_1 t}|\nu_1\rangle + \sin\theta e^{-i\omega_2 t}|\nu_2\rangle \\ |\nu_\mu(t)\rangle &= -\sin\theta e^{-i\omega_1 t}|\nu_1\rangle + \cos\theta e^{-i\omega_2 t}|\nu_2\rangle \ . \end{aligned} \tag{1.18}$$

The oscillation probabilities are then

$$\begin{aligned} P_{e\to\mu}(t) &= P_{\mu\to e}(t) = \sin^2 2\theta \sin^2\left(\frac{\Delta\omega t}{2}\right) \\ P_{e\to e}(t) &= P_{\mu\to\mu}(t) = 1 - \sin^2 2\theta \sin^2\left(\frac{\Delta\omega t}{2}\right) \end{aligned} \tag{1.19}$$

with $\Delta\omega = \omega_2 - \omega_1$. Neutrinos are extremely light particles, so that their mass can be neglected with respect to their momentum $\boldsymbol{k}$. Expanding the energies around $m_j = 0$ as $\omega_j \approxeq k + \frac{m_j^2}{2k}$, we can write the energy difference as

$$\Delta\omega = \omega_2 - \omega_1 = \frac{m_2^2 - m_1^2}{2k} = \frac{\Delta m^2}{2k} \ . \tag{1.20}$$

Here we have introduced the squared mass difference $\Delta m^2 = m_2^2 - m_1^2$. On the other hand, neutrinos almost travel at the speed of light, so that the distance $z$ travelled from a source can be approximated (in natural units) with the time $t$ required to cover the distance $z \simeq t$. Identifying $z = t = 0$ with the time the neutrino leaves the source, and setting $L = \frac{4\pi k}{\Delta m^2}$, we can write the oscillation probabilities in terms of the distance travelled as

$$\begin{aligned} P_{e\to\mu}(z) &= P_{\mu\to e}(z) = \frac{1}{2}\sin^2 2\theta\left(1 - \cos\left(\frac{2\pi z}{L}\right)\right) \\ P_{e\to e}(z) &= P_{\mu\to\mu}(z) = 1 - \frac{1}{2}\sin^2 2\theta\left(1 - \cos\left(\frac{2\pi z}{L}\right)\right) \ . \end{aligned} \tag{1.21}$$

The form (1.21) is often preferred to the equivalent (1.19) in experimental analyses.

The neutrino Hamiltonian can also be written in another form. On the mass basis $|\nu_1\rangle, |\nu_2\rangle$ the Hamiltonian is diagonal and can be split as

$$H = \begin{pmatrix} \omega_1 & 0 \\ 0 & \omega_2 \end{pmatrix} = \frac{\omega_1 + \omega_2}{2}\begin{pmatrix} 1 & 0 \\ 0 & 1 \end{pmatrix} + \begin{pmatrix} -\frac{\Delta\omega}{2} & 0 \\ 0 & \frac{\Delta\omega}{2} \end{pmatrix} \ . \tag{1.22}$$

The first term, proportional to the identity matrix, produces a global phase factor which has no effect on the oscillation probabilities. Retaining only the second term, which encodes the oscillation dynamics, the Hamiltonian reads

$$H = \frac{\Delta m^2}{4k}\begin{pmatrix} -1 & 0 \\ 0 & 1 \end{pmatrix} \tag{1.23}$$

where we have used the equation (1.20). To obtain the Hamiltonian in the flavor basis we simply invert the equation (1.10):

$$H_f = \frac{1}{4k}\begin{pmatrix} -\Delta m^2\cos 2\theta & \Delta m^2 \sin 2\theta \\ \Delta m^2 \sin 2\theta & \Delta m^2 \cos 2\theta \end{pmatrix} \ . \tag{1.24}$$

Equations (1.15) and (1.24) represent, up to a term proportional to the identity, the neutrino propagation Hamiltonian in vacuum in the flavor basis. With very few modifications one can also describe the neutrino propagation in *matter*.

As mentioned above, neutrinos interact with matter only through gravitation and the weak interaction. Their gravitational interactions can be safely neglected in most of the environments and neutrinos effectively interact with mattter only through the weak processes. The scattering cross section is proportional to [54] $\sigma_0 = G_F^2 s = 2G_F^2 EM$, with $G_F \simeq 1.16 \times 10^{-5}\text{GeV}^2$ the Fermi constant and $s$ the squared center of mass energy, which in the laboratory frame equals $s = 2EM$ for a neutrino with energy $E$ and a target of mass $M$. To give an idea of how small the interaction rate is, consider that in a medium with a number density of nucleons of about $N = 10^{24}cm^{-3}$, each with mass $M \simeq 1\text{GeV}$, the neutrino mean free path $l = \frac{1}{N\sigma}$ is [54]

$$l = \frac{10^{12}\text{m}}{(E/\text{GeV})} . \tag{1.25}$$

Unless extremely energetic ($E \gg$ GeV) neutrinos or extremely dense media are taken into account, only the lowest order in weak interactions needs to be considered. At the lowest order only the elastic forward scattering, due to charged and neutral current processes, affects the neutrino propagation. The amplitudes for the elastic forward scattering add up coherently, resulting in neutrino refraction, which is described by an effective matter potential $V$, or equivalently by the momentum-dependent refraction index $n - 1 = \frac{V}{k}$. The matter potential $V$ is in general flavor-dependent. In an ordinary medium, made up of protons, neutrons and electrons, the electron neutrino experiences both charged current processes due to the electrons and neutral current processes due to neutrons, electrons and protons. On the other hand, the muon neutrino experiences only neutral current scattering. If the medium is electrically neutral, the neutral current contributions of electrons and protons to the matter potential cancel each other. Then the matter potential can be written as [54]

$$V_A = V_{CC}\delta_{Ae} + V_{NC} = \sqrt{2}G_F \left( N_e \delta_{Ae} - \frac{N_n}{2} \right) , \tag{1.26}$$

for $A = e, \mu$. Here $N_e$ and $N_n$ are the number densities of electrons and neutrons. In matrix form, on the flavor basis, this is

$$V = \sqrt{2}G_F \begin{pmatrix} N_e - \frac{N_n}{2} & 0 \\ 0 & -\frac{N_n}{2} \end{pmatrix} = \frac{-\sqrt{2}G_F N_n}{2} \begin{pmatrix} 1 & 0 \\ 0 & 1 \end{pmatrix} + \sqrt{2}G_F N_e \begin{pmatrix} 1 & 0 \\ 0 & 0 \end{pmatrix} . \tag{1.27}$$

Again the term proportional to the identity can be dropped, since it amounts to an irrelevant common phase factor. Adding up eqs. (1.24) and (1.27) we obtain the effective Hamiltonian for the neutrino propagation in matter

$$H_m = \frac{1}{4k} \begin{pmatrix} -\Delta m^2 \cos 2\theta + \mathcal{A} & \Delta m^2 \sin 2\theta \\ \Delta m^2 \sin 2\theta & \Delta m^2 \cos 2\theta \end{pmatrix} , \tag{1.28}$$

where we have denoted $\mathcal{A} = 4\sqrt{2}G_F k N_e$. Notice that this Hamiltonian depends explicitly on time $t$ and on the position $\boldsymbol{x}$ because of the space-time dependence of the electron number density $N_e(t, \boldsymbol{x})$. Nonetheless the Hamiltonian (1.28) has the same form as (1.7) and can be istantaneously diagonalized with a rotation as in eq. (1.10). The mixing angle can be read off eq. (1.9):

$$\tan 2\theta_m = \frac{\Delta m^2 \sin 2\theta}{\Delta m^2 \cos 2\theta - \frac{\mathcal{A}}{2}} \tag{1.29}$$

where $\theta_m$ denotes the instantaneous mixing angle in matter. The instantaneous eigenvalues are

$$\begin{aligned} H_{m(1,2)} &= \frac{1}{8k}\left(\mathcal{A} \mp \sqrt{\left(2\Delta m^2\cos 2\theta - \mathcal{A}\right)^2 + 4\left(\Delta m^2 \sin 2\theta\right)^2}\right) \\ \Delta E_m = H_{m2} - H_{m1} &= \frac{1}{4k}\sqrt{\left(2\Delta m^2\cos 2\theta - \mathcal{A}\right)^2 + 4\left(\Delta m^2 \sin 2\theta\right)^2} = \frac{\Delta m_m^2}{4k} \end{aligned} \tag{1.30}$$

where we have introduced the effective squared mass difference in matter $\Delta m_m^2$. Neutrino oscillations in matter are then formally described in the same way as in vacuum, except for the substitution $\theta \to \theta_m$ and $\Delta m^2 \to \Delta m_m^2$, with the (possibly space-time dependent) mixing angle in matter $\theta_m$ and squared mass difference in matter $\Delta m_m^2$. From the equation (1.29) we can see that the mixing angle in matter has a resonance at

$$\mathcal{A}_R = 2\Delta m^2 \cos 2\theta \tag{1.31}$$

where the matter mixing angle $\theta_m$ is maximal ($\theta_m = \frac{\pi}{4}$). The matter-induced enhancement of the oscillations close to the resonance condition is known as the Mikheyev-Smirnov-Wolfenstein (MSW) effect [55–57].

### Three flavor oscillations

The two flavor formalism employed above works in a variety of cases. Besides providing a good description of neutrino oscillations in many cases, when for some specific reason one of the original three flavors can be neglected, both in vacuum and in matter, the two flavor description suits well axion-photon mixing, photon-dark photon mixing and neutral meson mixing. Strictly speaking, however, the two flavor formalism is only an approximation in the context of neutrino oscillations, which generally involve all the three known flavors $|\nu_e\rangle, |\nu_\mu\rangle, |\nu_\tau\rangle$. The mass term of the Hamiltonian can be written, on the flavor basis, as

$$H = \begin{pmatrix} m_{ee} & m_{e\mu} & m_{e\tau} \\ m_{e\mu} & m_{\mu\mu} & m_{\mu\tau} \\ m_{e\tau} & m_{\mu\tau} & m_{\tau\tau} \end{pmatrix} \tag{1.32}$$

with $m_{AB}$ for $A, B = e, \mu, \tau$ real parameters with the dimensions of a mass. Right as in the two flavor case, the mass Hamiltonian is diagonalized by means of a rotation matrix $U$, although now $U \in SU(3)$ instead of $SU(2)$. In the usual parametrization [58] the three flavor mixing matrix takes the form

$$U = \begin{pmatrix} c_{12}c_{13} & s_{12}c_{13} & s_{13}e^{-i\delta_{CP}} \\ -s_{12}c_{23} - c_{12}s_{23}s_{13}e^{i\delta_{CP}} & c_{12}c_{23} - s_{12}s_{13}s_{23}e^{i\delta_{CP}} & c_{13}s_{23} \\ s_{12}s_{23} - c_{12}c_{23}s_{13}e^{i\delta_{CP}} & -c_{12}s_{23} - s_{12}c_{23}s_{13}e^{i\delta_{CP}} & c_{23}c_{13} \end{pmatrix}. \tag{1.33}$$

Here we have used the shorthand notation $c_{ij} = \cos\theta_{ij}, s_{ij} = \sin\theta_{ij}$. The matrix (1.33) is known as the Pontecorvo-Maki-Nakagawa-Sakata (PMNS) mixing matrix. Corresponding to three eigenstates $|\nu_1\rangle, |\nu_2\rangle, |\nu_3\rangle$ and the three eigenvalues $m_1, m_2, m_3$, there are three mixing angles $\theta_{12}, \theta_{13}, \theta_{23}$ and three squared mass differences $\Delta m_{12}^2, \Delta m_{13}^2, \Delta m_{23}^2$. Despite the larger number of parameters involved and a higher dimensional Hilbert space, the analysis of the three flavor neutrino oscillations follows the same steps outlined at the beginning of the section (1.1). The transition probabilities have a more intricate structure with respect to the two flavor case, but still follow a recognizable oscillatory behaviour. The only real novelty in three flavors is the appearance of a (Charge-Parity) $CP$-violating phase $\delta_{CP}$ in the mixing matrix (1.33). As the name suggests, a non-trivial phase $\delta_{CP}$ has the effect of producing transition probabilities that are not invariant under a $CP$ transformation. For the sake of completeness we mention that $\delta_{CP}$ is a Dirac phase, as opposed to the Majorana phases, set here to zero for simplicity, and that it is physical, as it cannot be removed.

## 1.2 Flavor Mixing in Quantum Field Theory

The quantum mechanical theory of neutrino oscillations well describes much of the observed experimental evidence. Nevertheless, modern physical theories are constructed in the more general framework of quantum field theory, which stands at the core of modern particle physics. All the physical phenomena, with some notable exceptions, like gravitation, are today understood as emerging from a fundamental field theoretical description. It is therefore appropriate that we seek a quantum field theoretical description of particle mixing as well. In this perspective the naive quantum mechanical results of the previous section represent an approximation, which the quantum field theory should reproduce when the suitable limits are taken. Notwithstanding the importance of understanding the particle mixing phenomena, and in particular neutrino mixing, in this framework, there is currently no universally accepted quantum field theory of particle mixing. Here we will follow the flavor Fock space approach [50–53] and shall be mainly concerned with the mixing of fermion fields.

### 1.2.1 The Flavor Fock Space

Neutrinos are electrically neutral, and thus can in principle be described both as Dirac and Majorana fermions. The latter can be seen as Dirac fields with the additional constraint $\psi^C = \psi$, with $\psi^C$ the charge-conjugated field. Thus we limit our analysis to Dirac fields, referring the reader to other sources for the full treatment of Majorana neutrinos [59, 60]. Free Dirac fields $\psi$ satisfy the Dirac equation

$$\left(i\gamma^\mu \partial_\mu - m\right)\psi = 0\,, \tag{1.34}$$

where $\gamma^\mu$ are the $4 \times 4$ Dirac matrices, $m$ is the fermion mass and $\psi$ is a 4 component spinor. Unless otherwise specified, we employ the Dirac representation of the gamma matrices

$$\gamma^0 = \begin{pmatrix} \mathbb{1} & 0 \\ 0 & -\mathbb{1} \end{pmatrix} \qquad \gamma^j = \begin{pmatrix} 0 & \sigma_j \\ -\sigma_j & 0 \end{pmatrix}\,. \tag{1.35}$$

Here $\mathbb{1}$ is the $2 \times 2$ identity matrix and $\sigma_j$ for $j = 1, 2, 3$ are the Pauli matrices. A complete set of solutions to the eq. (1.34) is represented by the plane waves $u_{\boldsymbol{k},s}(x) = e^{-i(\omega_{\boldsymbol{k}} t - \boldsymbol{k}\cdot\boldsymbol{x})} U_{\boldsymbol{k},s}$ and $v_{\boldsymbol{k},s}(x) = e^{i(\omega_{\boldsymbol{k}} t - \boldsymbol{k}\cdot\boldsymbol{x})} V_{\boldsymbol{k},s}$. Here $s = \pm$ is the spin index[1], $\omega_{\boldsymbol{k}} = \sqrt{\boldsymbol{k}^2 + m^2}$ and the $U, V$ are the momentum space spinors, respectively with positive and negative energy:

$$\begin{aligned}
U_{\boldsymbol{k},+} &= \sqrt{\frac{\omega_{\boldsymbol{k}} + m}{2\omega_{\boldsymbol{k}}}} \begin{pmatrix} 1 \\ 0 \\ \frac{k_3}{\omega_{\boldsymbol{k}}+m} \\ \frac{k_1+ik_2}{\omega_{\boldsymbol{k}}+m} \end{pmatrix} &\qquad U_{\boldsymbol{k},-} &= \sqrt{\frac{\omega_{\boldsymbol{k}} + m}{2\omega_{\boldsymbol{k}}}} \begin{pmatrix} 0 \\ 1 \\ \frac{k_1-ik_2}{\omega_{\boldsymbol{k}}+m} \\ \frac{-k_3}{\omega_{\boldsymbol{k}}+m} \end{pmatrix} \\
V_{\boldsymbol{k},+} &= \sqrt{\frac{\omega_{\boldsymbol{k}} + m}{2\omega_{\boldsymbol{k}}}} \begin{pmatrix} \frac{k_3}{\omega_{\boldsymbol{k}}+m} \\ \frac{k_1+ik_2}{\omega_{\boldsymbol{k}}+m} \\ 1 \\ 0 \end{pmatrix} &\qquad V_{\boldsymbol{k},-} &= \sqrt{\frac{\omega_{\boldsymbol{k}} + m}{2\omega_{\boldsymbol{k}}}} \begin{pmatrix} \frac{k_1-ik_2}{\omega_{\boldsymbol{k}}+m} \\ \frac{-k_3}{\omega_{\boldsymbol{k}}+m} \\ 0 \\ 1 \end{pmatrix}\,.
\end{aligned}$$

[1] $s$ here represents the spin projection on the third axis. Other spin indices, like helicity, can be used as well.

The normalization is chosen so that $U^\dagger_{\boldsymbol{k},s}U_{\boldsymbol{k},r} = V^\dagger_{\boldsymbol{k},s}V_{\boldsymbol{k},r} = \delta_{sr}$. In addition they satisfy

$$\begin{aligned} U^\dagger_{\boldsymbol{k},s}V_{\boldsymbol{k},r} = V^\dagger_{\boldsymbol{k},s}U_{\boldsymbol{k},r} &= 0 \\ \sum_s \left(U_{\boldsymbol{k},s}U^\dagger_{\boldsymbol{k},s} + V_{\boldsymbol{k},s}V^\dagger_{\boldsymbol{k},s}\right) = \sum_s \left(u_{\boldsymbol{k},s}(x)u^\dagger_{\boldsymbol{k},s}(x) + v_{\boldsymbol{k},s}(x)v^\dagger_{\boldsymbol{k},s}(x)\right) &= \mathbb{1}_4 \end{aligned} \quad . \tag{1.36}$$

In the equations above $\mathbb{1}_4$ denotes the $4\times 4$ identity matrix. The second of the (1.36) then states that the set of solutions is complete, not only with respect to the solution space of the Dirac equation (1.34), but also with respect to the space of 4-spinors. The field can now be expanded as

$$\psi = \frac{1}{\sqrt{V}}\sum_{\boldsymbol{k},s}\left(a_{\boldsymbol{k},s}u_{\boldsymbol{k},s}(t) + b^\dagger_{-\boldsymbol{k},s}v_{-\boldsymbol{k},s}(t)\right)e^{i\boldsymbol{k}\cdot\boldsymbol{x}}\,. \tag{1.37}$$

Here the spatial dependence of the modes has been split for convenience as $u_{\boldsymbol{k},s}(x) = u_{\boldsymbol{k},s}(t)e^{i\boldsymbol{k}\cdot\boldsymbol{x}}$, $v_{\boldsymbol{k},s}(x) = v_{\boldsymbol{k},s}(t)e^{-i\boldsymbol{k}\cdot\boldsymbol{x}}$. Notice that we perform the expansion on a finite region of volume $V$; later we will let $V\to\infty$. The operator coefficients are required to satisfy the usual canonical anticommutation relations

$$\{a_{\boldsymbol{k},s}, a^\dagger_{\boldsymbol{q},r}\} = \delta_{\boldsymbol{kq}}\delta_{sr} \qquad \{b_{\boldsymbol{k},s}, b^\dagger_{\boldsymbol{q},r}\} = \delta_{\boldsymbol{kq}}\delta_{sr} \tag{1.38}$$

with all the other commutators vanishing, as a consequence of the equal time canonical relation $\{\psi^A(x), \psi^{B\dagger}(x')\}_{t=t'} = \delta_{AB}\delta^3(\boldsymbol{x}-\boldsymbol{x}')$ valid for all the spinor indices $A, B = 1,2,3,4$.

Consider now two neutrino fields $\psi_1, \psi_2$ with definite masses $m_1, m_2$, each satisfying the Dirac equation for the corresponding mass. One can perform the expansion (1.37) for each $\psi_j$, with $j = 1,2$, provided that the additional label $j$ is placed wherever needed: $m_j, \omega_{\boldsymbol{k};j} = \sqrt{\boldsymbol{k}^2 + m_j^2}, u_{\boldsymbol{k},s;j}(x) = e^{-i(\omega_{\boldsymbol{k};j}t - \boldsymbol{k}\cdot\boldsymbol{x})}U_{\boldsymbol{k},s;j}$ and so on. All the operators with distinct mass labels $j' \neq j$ anticommute. The field expansion of the $\psi_j$ defines the *mass vacuum* $|0_M\rangle$ as the unique state annihilated by all the $a, b$ operators:

$$a_{\boldsymbol{k},s;j}\,|0_M\rangle = 0 \qquad b_{\boldsymbol{k},s;j}\,|0_M\rangle = 0 \quad \forall \boldsymbol{k}, s, j \tag{1.39}$$

and the mass Fock space is built by repeated application of the creation operators $a^\dagger_{\boldsymbol{k},s;j}, b^\dagger_{\boldsymbol{k},s;j}$ on the vacuum. The flavor fields are defined as

$$\begin{aligned} \psi_e(x) &= \cos\theta\psi_1(x) + \sin\theta\psi_2(x) \\ \psi_\mu(x) &= -\sin\theta\psi_1(x) + \cos\theta\psi_2(x) \end{aligned} \tag{1.40}$$

which are the mixing relations translated on the quantum fields. Our duty is now to find a meaningful flavor field expansion starting from the relations (1.40). The right hand side of equations (1.40) corresponds to an $SU(2)$ rotation on the doublet of mass fields. In analogy with ordinary rotations and other transformations in quantum field theory, one can construct a generator of the mixing transformations, defined as

$$\begin{aligned} \psi_e(x) &= G_\theta^{-1}(x)\psi_1(x)G_\theta(x) \\ \psi_\mu(x) &= G_\theta^{-1}(x)\psi_2(x)G_\theta(x)\,. \end{aligned} \tag{1.41}$$

A couple of points need now to be stressed. First, the definition of $G_\theta$ is clearly sensitive to the choice of the mass fields $\psi_1, \psi_2$; for instance, one might well swap $\psi_1$ and $\psi_2$ in eqs. (1.41), and interpret $\psi_e$ as arising from the transformation of $\psi_2$. In general, equations like (1.41) can be written for free fields of any mass $m'_1, m'_2$ and the choice adopted above is only partially justified by the form of eqs. (1.40). Nevertheless, it has been shown [61] that such an ambiguity in the choice of the masses of the free fields is harmless, meaning that no observable quantity is affected by this choice. Therefore we stick to the original definition of eqs. (1.41). Second, the generator $G_\theta(x)$ in principle depends on all the space-time coordinates, but we shall soon see that it depends only on time $t$.

The basic requirements for $G_\theta(x)$ are that (i) it is constructed out of the basic fields $\psi_1, \psi_2$ and their conjugates $\psi_1^\dagger, \psi_2^\dagger$, (ii) that it reproduces the mixing relations (1.40) as per definition (1.41) and (iii) that it reduces to the identity transformation as the mixing angle vanishes $\theta \to 0$. Exploiting the canonical anticommutation relations and the Baker-Campbell-Hausdorff formula [62], it is found that the generator satisfying all the three conditions is

$$G_\theta(t) = e^{\theta \int d^3x \left(\psi_1^\dagger(x)\psi_2(x) - \psi_2^\dagger(x)\psi_1(x)\right)} \,. \tag{1.42}$$

We can recognize in the exponent the Dirac inner product, defined as

$$(\psi, \phi)_t = \int_{x^0=t} d^3x \bar{\psi}\gamma^0\phi = \int_{x^0=t} d^3x \psi^\dagger \phi \,, \tag{1.43}$$

on the spacelike hypersurface $x^0 = t$. In terms of the inner product, the generator is simply

$$G_\theta(t) = e^{\theta[(\psi_1,\psi_2)_t - (\psi_2,\psi_1)_t]} \,. \tag{1.44}$$

This form better lends itself to generalizations. The action of $G_\theta$ on the mass annihilators defines the flavor annihilators as

$$\begin{aligned}
a_{\mathbf{k},s;e}(t) &= G_\theta^{-1}(t) a_{\mathbf{k},s;1} G_\theta(t) = \cos\theta a_{\mathbf{k};s,1} + \sin\theta \left(\mathcal{U}^*_{\mathbf{k},s}(t) a_{\mathbf{k},s;2} + \mathcal{V}_{\mathbf{k},s}(t) b^\dagger_{-\mathbf{k},s;2}\right) \\
a_{\mathbf{k},s;\mu}(t) &= G_\theta^{-1}(t) a_{\mathbf{k},s;2} G_\theta(t) = \cos\theta a_{\mathbf{k};s,2} - \sin\theta \left(\mathcal{U}_{\mathbf{k},s}(t) a_{\mathbf{k},s;1} - \mathcal{V}_{\mathbf{k},s}(t) b^\dagger_{-\mathbf{k},s;1}\right) \\
b_{-\mathbf{k},s;e}(t) &= G_\theta^{-1}(t) b_{-\mathbf{k},s;1} G_\theta(t) = \cos\theta b_{-\mathbf{k};s,1} + \sin\theta \left(\mathcal{U}^*_{\mathbf{k},s}(t) b_{-\mathbf{k},s;2} - \mathcal{V}_{\mathbf{k},s}(t) a^\dagger_{\mathbf{k},s;2}\right) \\
b_{-\mathbf{k},s;\mu}(t) &= G_\theta^{-1}(t) b_{-\mathbf{k},s;2} G_\theta(t) = \cos\theta b_{-\mathbf{k};s,2} - \sin\theta \left(\mathcal{U}_{\mathbf{k},s}(t) b_{-\mathbf{k},s;1} + \mathcal{V}_{\mathbf{k},s}(t) a^\dagger_{\mathbf{k},s;1}\right) \\
&,
\end{aligned} \tag{1.45}$$

where $\mathcal{U}_{\mathbf{k},s}(t) = (u_{\mathbf{k},s;2}, u_{\mathbf{k},s;1})_t = (v_{-\mathbf{k},s;1}, v_{-\mathbf{k},s;2})_t$ and $\mathcal{V}_{\mathbf{k},s}(t) = (u_{\mathbf{k},s;1}, v_{-\mathbf{k},s;2})_t = -(u_{\mathbf{k},s;2}, v_{-\mathbf{k},s;1})_t$. For reasons that will be apparent in a moment, we refer to $\mathcal{U}, \mathcal{V}$ as the *Bogoliubov coefficients* for the mixing transformations. Explicitly they are given by $\mathcal{U}_{\mathbf{k},s}(t) = |\mathcal{U}_\mathbf{k}| e^{i(\omega_{k;2} - \omega_{k;1})t}$ and $\mathcal{V}_{\mathbf{k},s}(t) = |\mathcal{V}_\mathbf{k}| e^{i(\omega_{k;2} + \omega_{k;1})t}$ with

$$\begin{aligned}
|\mathcal{U}_\mathbf{k}| &= \sqrt{\left(\frac{\omega_{\mathbf{k};1} + m_1}{2\omega_{\mathbf{k},1}}\right)\left(\frac{\omega_{\mathbf{k};2} + m_2}{2\omega_{\mathbf{k},2}}\right)} \left(1 + \frac{\mathbf{k}^2}{(\omega_{\mathbf{k};1} + m_1)(\omega_{\mathbf{k};2} + m_2)}\right) \\
|\mathcal{V}_\mathbf{k}| &= \sqrt{\left(\frac{\omega_{\mathbf{k};1} + m_1}{2\omega_{\mathbf{k},1}}\right)\left(\frac{\omega_{\mathbf{k};2} + m_2}{2\omega_{\mathbf{k},2}}\right)} \left(\frac{|\mathbf{k}|}{(\omega_{\mathbf{k};2} + m_2)} - \frac{|\mathbf{k}|}{(\omega_{\mathbf{k};1} + m_1)}\right) \\
&.
\end{aligned} \tag{1.46}$$

The fundamental property of the Bogoliubov coefficients is

$$|\mathcal{U}_\mathbf{k}|^2 + |\mathcal{V}_\mathbf{k}|^2 = 1 \,, \tag{1.47}$$

which ensures that the transformation of the annihnilation operators (1.45) is canonical. The transformation (1.45) has indeed the form of a Bogoliubov (linear canonical) transformation nested into a rotation, as opposed to the simpler transformation law for the fields (1.40).

In accordance with the linearity of the action of the generator $G_\theta(t)$, we ought to interpret the annihilators of eqs. (1.45) as the expansion coefficients of the flavor fields $\psi_e, \psi_\mu$, and precisely with respect to the modes of the corresponding mass fields. This point of view is supported by the observation that

$$a_{\boldsymbol{k},s;e}(t) = (u_{\boldsymbol{k},s;1}, \psi_e)_t \qquad b^\dagger_{\boldsymbol{k},s;e} = (v_{\boldsymbol{k},s;1}, \psi_e)_t \tag{1.48}$$

and similar for $\mu$. We refer to $a_{e(\mu)}, b_{e(\mu)}$ as the flavor annihilation operators. They define a new time-dependent vacuum state, the *flavor vacuum*

$$|0_F(t)\rangle = G_\theta^{-1}(t)\,|0_M\rangle \tag{1.49}$$

annihilated by all the flavor annihilators. Out of the flavor vacuum one constructs the flavor Fock space by repeated application of the flavor creation operators $a^\dagger_{e(\mu)}, b^\dagger_{e(\mu)}$. The relation between the flavor and the mass vacuum is elucidated by computing the inner product

$$\langle 0_M |\, 0_F(t)\rangle = e^{\sum_{\boldsymbol{k}} \log \Gamma(\boldsymbol{k})} \qquad \Gamma(\boldsymbol{k}) = \left(1 - \sin^2\theta |\mathcal{V}_{\boldsymbol{k},s}|^2\right)^2 . \tag{1.50}$$

At finite volume $V < \infty$ the inner product (1.50) is finite and the mixing generator $G_\theta(t)$ turns out to be unitary. On the other hand, in the infinite volume limit $V \to \infty$ the inner product (1.50) vanishes and the mixing generator is no longer unitary. Put otherwise, the flavor Fock space representation is *unitarily inequivalent* to the mass Fock space representation at infinite volume. In addition one finds that the flavor vacua at different times $|0_F(t)\rangle\,, |0_F(t')\rangle$ are orthogonal, implying that the flavor Fock space representations at distinct times are also unitarily inequivalent. As a consequence it is not possible to define the transition probabilities naively from the inner product of the states at different times. In order to define the transition probabilities one notices that the full Lagrangian is invariant under global $U(1)$ transformations and therefore admits the Noether conserved charge

$$Q = \sum_{j=1,2} Q_j(t) = \sum_{j,\boldsymbol{k},s} \left( a^\dagger_{\boldsymbol{k},s;j}(t) a_{\boldsymbol{k},s;j}(t) - b^\dagger_{-\boldsymbol{k},s;j}(t) b_{-\boldsymbol{k},s;j}(t) \right) . \tag{1.51}$$

In analogy one introduces the flavor charges ($\sigma = e, \mu$)

$$Q_\sigma(t) = \sum_{\boldsymbol{k},s} \left( a^\dagger_{\boldsymbol{k},s;\sigma}(t) a_{\boldsymbol{k},s;\sigma}(t) - b^\dagger_{-\boldsymbol{k},s;\sigma}(t) b_{-\boldsymbol{k},s;\sigma}(t) \right) \tag{1.52}$$

which add up to the total conserved charge

$$\sum_{\sigma=e,\mu} Q_\sigma(t) = \sum_{j=1,2} Q_j(t) = Q\,. \tag{1.53}$$

Evidently the expectation value of $Q$ on any definite particle state is constant in time. This motivates the definition

$$\mathcal{P}^{\boldsymbol{k},s}_{\sigma\to\sigma'}(t) = \langle \nu_{\boldsymbol{k},s;\sigma}|\, Q_{\sigma'}(t)\, |\nu_{\boldsymbol{k},s;\sigma}\rangle \ , \tag{1.54}$$

where we have introduced the one-particle states $|\nu_{\boldsymbol{k},s;\sigma}\rangle = a^\dagger_{\boldsymbol{k},s;\sigma}(0)\,|0_F(0)\rangle$. Notice that each of the one particle states is an eigenstate of the total charge with eigenvalue 1, which immediately implies

$$\sum_{\sigma'=e,\mu} \mathcal{P}^{\boldsymbol{k},s}_{\sigma\to\sigma'}(t) = 1 \qquad \forall t, \sigma, \boldsymbol{k}, s \tag{1.55}$$

making the expressions (1.54) into well defined probabilities. After some trivial manipulations the probabilities can be written as

$$\begin{aligned}
\mathcal{P}^{\boldsymbol{k}}_{e\to e}(t) &= \left|\{a_{\boldsymbol{k},s;e}(t), a^{\dagger}_{\boldsymbol{k},s;e}(0)\}\right|^2 + \left|\{b^{\dagger}_{-\boldsymbol{k},s;e}(t), a^{\dagger}_{\boldsymbol{k},s;e}(0)\}\right|^2 \\
\mathcal{P}^{\boldsymbol{k}}_{e\to \mu}(t) &= \left|\{a_{\boldsymbol{k},s;\mu}(t), a^{\dagger}_{\boldsymbol{k},s;e}(0)\}\right|^2 + \left|\{b^{\dagger}_{-\boldsymbol{k},s;\mu}(t), a^{\dagger}_{\boldsymbol{k},s;e}(0)\}\right|^2
\end{aligned} \tag{1.56}$$

where we have dropped the irrelevant $s$ index. Explicitly

$$\begin{aligned}
\mathcal{P}^{\boldsymbol{k}}_{e\to \mu}(t) &= \frac{\sin^2 2\theta}{2}\left[1 - \Re\left(\mathcal{U}^*_{\boldsymbol{k}}(0)\mathcal{U}_{\boldsymbol{k}}(t) + \mathcal{V}^*_{\boldsymbol{k}}(0)\mathcal{V}_{\boldsymbol{k}}(t)\right)\right] \\
&= \sin^2 2\theta \left[|\mathcal{U}_{\boldsymbol{k}}|^2 \sin^2\left(\frac{(\omega_{\boldsymbol{k};2}-\omega_{\boldsymbol{k};1})t}{2}\right) + |\mathcal{V}_{\boldsymbol{k}}|^2 \sin^2\left(\frac{(\omega_{\boldsymbol{k};2}+\omega_{\boldsymbol{k};1})t}{2}\right)\right] \\
&,
\end{aligned} \tag{1.57}$$

and $\mathcal{P}^{\boldsymbol{k}}_{e\to e}(t) = 1 - \mathcal{P}^{\boldsymbol{k}}_{e\to \mu}(t)$. We notice that two oscillating terms appear, with low frequency $\frac{\omega_{\boldsymbol{k},2}-\omega_{\boldsymbol{k},1}}{2}$ and high frequency $\frac{\omega_{\boldsymbol{k},2}+\omega_{\boldsymbol{k},1}}{2}$, modulated by the Bogoliubov coefficients. The last term, in particular, represents an exquisitely field theoretical effect, which is absent in the Pontecorvo oscillation formulae (1.19). That the probabilities (1.57) are a valid generalization of the standard oscillation formulae can be verified in the ultra-relativistic limit $|\boldsymbol{k}| \gg m_1, m_2$, where they effectively reduce to the Pontecorvo formulae (1.19). The transition probabilities of Eq. (1.57) are plotted in Fig. (1.1) for sample values of masses and momenta.

### 1.2.2 The Flavor Vacuum

The hallmark of unitarily inequivalent representations is the different particle content of the corresponding vacua. This notion is familiar from all the known particle creation phenomena, including the Hawking [63] and Parker [64] effects in curved space, the Schwinger [65] and Casimir [66] effect and the BCS [67] vacuum. To uncover the non-trivial structure of the flavor vacuum it is sufficient to exploit its definition (1.49) in terms of the mass vacuum. At time $t = 0$, setting $|0_F\rangle = \prod_{\boldsymbol{k}} |0_F\rangle_{\boldsymbol{k}}$ one explicitly computes that

$$\begin{aligned}
|0_F\rangle_{\boldsymbol{k}} = \prod_{s=\pm 1} \Big[ &\left(1 - \sin^2\theta |\mathcal{V}_{\boldsymbol{k}}|^2\right) + s \sin\theta\cos\theta |\mathcal{V}_{\boldsymbol{k}}| \left(a^{\dagger}_{\boldsymbol{k},s;1} b^{\dagger}_{-\boldsymbol{k},s;2} + a^{\dagger}_{\boldsymbol{k},s;2} b^{\dagger}_{-\boldsymbol{k},s;1}\right) \\
&- s \sin^2\theta |\mathcal{V}_{\boldsymbol{k}}||\mathcal{U}_{\boldsymbol{k}}| \left(a^{\dagger}_{\boldsymbol{k},s;1} b^{\dagger}_{-\boldsymbol{k},s;1} - a^{\dagger}_{\boldsymbol{k},s;2} b^{\dagger}_{-\boldsymbol{k},s;2}\right) + \sin^2\theta |\mathcal{V}_{\boldsymbol{k}}|^2 a^{\dagger}_{\boldsymbol{k},s;1} b^{\dagger}_{-\boldsymbol{k},s;2} a^{\dagger}_{\boldsymbol{k},s;2} b^{\dagger}_{-\boldsymbol{k},s;1} \Big] |0_M\rangle \\
&.
\end{aligned} \tag{1.58}$$

The equation (1.58) shows that the flavor vacuum has the structure of a *condensate* of particle-antiparticle pairs of definite mass. It follows that the number density of particles and antiparticles with definite mass is non-zero in the flavor vacuum:

$$\langle 0_F| a^{\dagger}_{\boldsymbol{k},s;i} a_{\boldsymbol{k},s;i} |0_F\rangle = \langle 0_F| b^{\dagger}_{\boldsymbol{k},s;i} b_{\boldsymbol{k},s;i} |0_F\rangle = \sin^2\theta |\mathcal{V}_{\boldsymbol{k}}|^2 \qquad \forall \boldsymbol{k}, s \text{ and } i = 1,2\,. \tag{1.59}$$

Since the condensate number density is non-vanishing, it can be expected, since particles and antiparticles carry momentum and energy, that also a non-vanishing energy-momentum tensor is associated with the flavor vacuum. This is indeed the case.

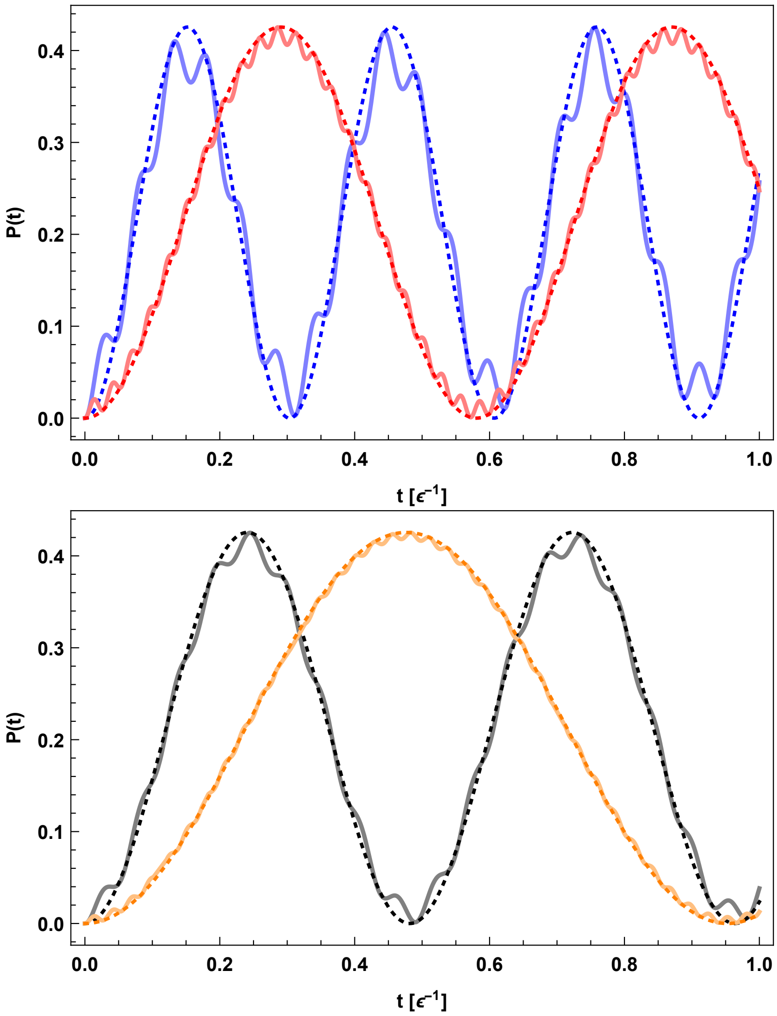


FIGURE 1.1: Two-flavor neutrino oscillation probabilities (Eq. (1.57)) as a function of time $t$. Masses and momenta are expressed in an arbitrary unit of energy $\epsilon$, and time in $\epsilon^{-1}$. Momenta $\boldsymbol{k}$ are assumed to be along the positive third axis. (Upper Panel): the blue lines (light solid for the QFT probability (1.57) and dotted for the Pontecorvo probability (1.19)) correspond to $m_1 = 1, m_2 = 50, k = 50$, the red lines (light solid for the QFT probability (1.57) and dotted for the Pontecorvo probability (1.19)) correspond to $m_1 = 1, m_2 = 50, k = 110$. (Lower Panel): the black lines (light solid for the QFT probability (1.57) and dotted for the Pontecorvo probability (1.19)) correspond to $m_1 = 10, m_2 = 40, k = 50$, the orange lines (light solid for the QFT probability (1.57) and dotted for the Pontecorvo probability (1.19)) correspond to $m_1 = 10, m_2 = 40, k = 110$.

The energy-momentum tensor in flat space is given in terms of the mass fields as

$$T_{\mu\nu}(x) = \frac{i}{2} \sum_{j=1,2} \left( \bar{\psi}_j(x) \gamma_\mu \overleftrightarrow{\partial_\nu} \psi_j(x) \right) , \tag{1.60}$$

where the bilateral derivative is defined as $\overleftrightarrow{\partial_\nu} = \overrightarrow{\partial_\nu} - \overleftarrow{\partial_\nu}$. The customary way to get rid of the ordering ambiguity in (1.60) is to consider the normal ordered tensor, in which all the creation operators stand to the left of the annihilation operators. The normal ordering operation is itself defined with respect to a specific vacuum state. In the current case the natural choice is to consider the energy-momentum tensor normal ordered with respect to the mass vacuum, which we denote $: T_{\mu\nu} :$. Then, by definition,

$$\langle 0_M | : T_{\mu\nu} : | 0_M \rangle = 0 \tag{1.61}$$

that is exactly what one expects for the vacuum state of free fermions with definite mass. The expectation value of the energy-momentum tensor on the *flavor* vacuum is instead non zero, and precisely

$$\begin{aligned} \langle 0_F | : T_{00} : | 0_F \rangle &= 8 \sin^2\theta \int d^3k \, (\omega_{\boldsymbol{k},1} + \omega_{\boldsymbol{k},2}) \, |\mathcal{V}_{\boldsymbol{k}}|^2 \\ \langle 0_F | : T_{0i} : | 0_F \rangle &= 0 = \langle 0_F | : T_{ij} : | 0_F \rangle \qquad \text{for } i, j = 1, 2, 3 \, . \end{aligned} \tag{1.62}$$

Regularizing the first integral by imposing an ultraviolet momentum cutoff $K$, we can write

$$\langle 0_F | : T_{00} : | 0_F \rangle = \frac{\Delta m \sin^2\theta}{2\pi^2} \int_0^K dk k^2 \left( \frac{m_2}{\omega_{k,2}} - \frac{m_1}{\omega_{k,1}} \right) , \tag{1.63}$$

with $\Delta m = m_2 - m_1$. The result (1.62) is obtained by inserting the plane wave expansion of the fields in eq. (1.60) and computing the expectation value after the application of the normal ordering prescription (for details see [34]). Due to its diagonality $\langle 0_F | : T_{\mu\nu} : | 0_F \rangle$ can be interpreted as the *classical* energy-momentum tensor associated with a perfect fluid. In particular, the fluid has a non zero energy density $\rho = \langle 0_F | : T_{00} : | 0_F \rangle$ and vanishing pressure $p = - \langle 0_F | : T_{ii} : | 0_F \rangle = 0$. Then its equation of state reads

$$w = \frac{p}{\rho} = 0 \tag{1.64}$$

which is consistent with the equation of state of cold dark matter. Strictly speaking the result (1.64) has been obtained in flat spacetime, using the solutions of the flat space Dirac equation. Nevertheless it is a clear indication that the condensate associated to flavor mixing may represent a dark matter component. The analysis shall be generalized to curved spacetimes in the following chapters. In conclusion we mention that similar results hold for the quantum field theoretic mixing of boson fields [34], for which the condensate equation of state is akin to that of the cosmological constant $w = -1$ [34].

# Chapter 2

# Neutrino mixing in curved spacetime

The first part of the thesis collects the results obtained in the analysis of neutrino mixing in curved spacetime. The importance of the topic cannot be overestimated, due to the prominent role that neutrinos play in cosmology and astrophysics. Neutrinos are indeed used to extract valuable informations on the cosmos, and, along with electromagnetic and gravitational waves, are a crucial element in multimessenger astronomy [68]. Neutrinos are essential in many astrophysical phenomena, including the core-collapse supernovae [69]. In addition, it is believed that neutrinos have played a key role during the first phases of the universe, in particular by inducing the original baryon asymmetry through the leptogenesis mechanism [70, 71]. For these reasons curved spacetime represents the natural background on which to study neutrino physics. A thorough understanding of the mixing phenomenon in curved space, developed in the framework of quantum field theory, is essential for the study of its cosmological and astrophysical implications. A big effort is therefore devoted to the generalization of the flavor Fock space approach in the semiclassical context of quantum field theory in curved space (section 2.1). There we introduce the formalism needed to compute the oscillation formulae and apply it to various relevant spacetimes. Next we employ the formalism to study the energy-momentum tensor associated to the flavor vacuum in spatially flat FLRW spacetimes (section 2.2). This represents the first attempt at generalizing the important results concerning the flavor vacuum in flat space. In particular, we discuss how fermion mixing can represent a dark matter component within the semiclassical theory.

## 2.1 Mixing and Oscillations

In this section we introduce neutrino mixing in curved space, by generalizing the quantum field theory of neutrino mixing in flat space. The topic of neutrino oscillations in curved space has been discussed in several works , where it was found that gravitational fields may alter both the oscillations in vacuum and in matter [72–74]. Here we wish to go beyond the heuristic treatment of ref. [74], and present a quantum field theoretical approach, based on the field quantization in curved space-time, to evaluate the effects of gravitational fields on neutrino oscillations. We derive oscillation formulae for the flavor fields in curved spacetime and we show that gravitational backgrounds alter both the amplitude and the phase of the oscillations, in accordance with the predictions of quantum field theory in flat space. We then discuss the particle interpretation of the theory, for which the interplay between gravity and mixing entails a remarkable complexity. Not only the unitarily inequivalence between mass and flavor representations, but also the intrinsic ambiguity in the notion of particle in curved space have to be properly taken into account. This motivates us to study how the mixing changes when moving from a mass field representation to another. We show that the local observables, represented by expectation values on flavor states of local operators constructed from the flavor fields, do not depend on the expansion chosen for the mass fields. We demonstrate that the oscillation probabilities, on the other hand, do in general depend on the representation of the mass fields, since they are not a local observable and involve the comparison between particles in different spacetime regions. We then establish the conditions which have to be satisfied in order that the resulting transition probabilities are invariant under changes of mass field representation. Once these aspects have been clarified, the general oscillation formulae are applied to particular metrics of interest. We compute explicitly the oscillation formulae for two examples of spatially flat Friedmann–Lemaitre–Robertson–Walker spacetimes, corresponding to a cosmological constant–dominated and a radiation–dominated universe respectively. In these cases, exact analytical solutions to the Dirac equation are available, and the formalism here introduced can be applied directly. We then give an estimation of the oscillation formulae for neutrinos propagating from the past infinity to the future infinity in a stationary Schwarzschild spacetime. To this end we introduce a method to extract the oscillation formulae on spacetimes with asymptotically flat regions without resorting to the exact solutions of the Dirac equation. We then employ this strategy to compute the formulae on the Schwarzschild black hole spacetime, for neutrinos propagating from the past infinity to the future infinity. The Hawking radiation appears to be naturally embedded in the resulting transition probabilities. Overall, our results generalize those of the previous works [74], and are consistent with the latter when the suitable limits are considered. For simplicity, our analysis is limited to the oscillations in vacuum of two-flavor neutrinos, therefore considering the sole effect of gravity on neutrino oscillations.

### 2.1.1 Mass neutrino fields in curved Space

To deduce the oscillation formulae for neutrinos on a curved spacetime, it is necessary to consider both the effects of curvature and mixing on the (free) mass fields. Let $M$ be a globally hyperbolic spacetime, and let $\tau \in \mathbb{R}$ label a foliation of $M$ by Cauchy surfaces. The limitation to globally hyperbolic spacetimes is necessary to avoid causality issues and allows for a more direct generalization of the flat space results. The foliation by Cauchy complete spatial hypersurfaces, allowed on globally hyperbolic spacetimes, is indeed reminiscent of the foliation induced by a time coordinate on Minowski space. Last, but not least, the foliation makes the introduction of the Hamiltonian formalism, and thus the canonical quantization, more transparent. Consider next the tetrad fields $e_a^{\mu}(x)$, by definition satisfying $\eta^{ab} e_a^{\mu}(x) e_b^{\nu}(x) = g^{\mu\nu}(x)$. Here $\eta^{ab} \equiv diag(1,-1,-1,-1)$ is the Minkowski metric tensor, while $g^{\mu\nu}(x)$ is the contravariant metric $g^{\mu\nu}(x) g_{\nu\rho}(x) = \delta^{\mu}_{\rho}$ on $M$ in a given coordinate system. The massive neutrino fields satisfy the Dirac equations:

$$(i\tilde{\gamma}^{\mu}(x) D_{\mu} - m_i)\psi_i = 0 \tag{2.1}$$

where $\tilde{\gamma}^{\mu}(x) = e_a^{\mu}(x)\gamma^a$, $\gamma^a$ being the usual flat space Dirac matrices, and $D_{\mu} = \partial_{\mu} - \frac{i}{4}\omega_{\mu}^{ab}\sigma_{ab}$. The spin connection is defined as $\omega_{\mu}^{ab} = e_{\nu}^{a}\Gamma_{\rho\mu}^{\nu}e^{\rho b} + e_{\nu}^{a}\partial_{\mu}e^{\nu b}$, whereas $\sigma_{ab}$ are the commutators of flat Dirac matrices $\sigma_{ab} = \frac{i}{2}[\gamma^a, \gamma^b]$. In equation (2.1), the index $i = 1, 2, ..., N$ ranges over the number of neutrino species $N$. For the sake of simplicity we focus on the case $N = 2$, though the generalization to $N = 3$ is straightforward. In general equation (2.1) cannot be solved exactly. Even if one is able to find exact solutions, these do not play the same prominent role as their flat spacetime counterpart. It is well–known, indeed, that the positive frequency solutions of equation (2.1) cannot be defined univocally, and that, consequently, there is no natural (nor unique) particle interpretation for the corresponding Quantum Field Theory [75, 76]. Nevertheless, the canonical quantization of the Dirac field proceeds along the same lines as in Minkowski spacetime.

To perform a field expansion, one must find a set of positive $\zeta_{k,i}$ and negative $\xi_{k,i}$ frequency solutions for each of the equations (2.1). In general the bipartition of the solutions to eq. (2.1) makes sense only locally, while there is no natural global definition of positive and negative frequency modes. Anyway, one is free to choose a set of modes [1] $\{\zeta_{k,i}, \xi_{k,i}\}$ , deemed to be positive/negative frequency modes according to some specified observer, and expand the field with respect to them, provided that they form a complete (and orthonormal) set of solutions under the inner product

$$(a_i, b_i) = \int_{\Sigma(\tau)} \sqrt{-g} d\Sigma_\mu(\tau) \bar{a}_i \tilde{\gamma}^\mu(x) b_i \tag{2.2}$$

with $a_i, b_i$ any solution to equation (2.1) with mass $m_i$ and $\bar{b}_i = b_i^\dagger \gamma^0(x)$. Here $d\Sigma^\mu(\tau) = n^\mu(\tau) dV_\tau$ denotes the volume element on the surface $\tau$ with unit timelike normal $n^\mu(\tau)$. This has to hold separately for each $i = 1, 2$. As it is easy to prove, for $a_i, b_i$ solutions of the (same) Dirac equation, the inner product (2.2) does not depend on the hypersurface chosen for the integration. In particular, it is independent on the foliation by Cauchy hypersurfaces employed. The fields can then be expanded as

$$\psi_i(x) = \sum_{k,s} \left( \gamma_{k,s;i} \zeta_{k,s;i}(x) + \epsilon^\dagger_{k,s;i} \xi_{k,s;i}(x) \right) \tag{2.3}$$

with the operator coefficients $\gamma_{k,s,i}, \epsilon_{k,s,i}$ satisfying the usual canonical anticommutation relations, $k$ momentum index and $s$ helicity index. The annihilators are also required to anticommute for $i \neq j$, and, in particular $\{\gamma_{k,s,i}, \gamma^\dagger_{k,s,j}\} = \delta_{ij}$, $\{\epsilon_{k,s,i}, \epsilon^\dagger_{k,s,j}\} = \delta_{ij}$. In equation (2.3) we prefer to keep any space-time dependence within the modes, for ease of treatment with a general metric. The expansions (2.3) define the mass Hilbert space $\mathcal{H}_m = H_1 \otimes H_2$, which is constructed out of the vacuum $|0_m\rangle = |0_1\rangle \otimes |0_2\rangle$. Here $|0_i\rangle$ is defined, as usual, by $\gamma_{k,s,i} |0_i\rangle = 0 = \epsilon_{k,s,i} |0_i\rangle$ for each $k, s, i$.

As hinted above, the field expansions (2.3) are somewhat arbitrary, as opposed to the flat spacetime case, where there is no ambiguity in the definition of positive and negative frequency modes. Any other basis $\{\tilde{\zeta}_{k,s,i}, \tilde{\xi}_{k,s,i}\}$ can be used to expand the fields $\psi_i = \sum_{k,s} (\tilde{\gamma}_{k,s,i} \tilde{\zeta}_{k,s,i}(x) + \tilde{\epsilon}^\dagger_{k,s,i} \tilde{\xi}_{k,s,i}(x))$. Since both the sets $\{\zeta_{k,s,i}, \xi_{k,s,i}\}$ and $\{\tilde{\zeta}_{k,s,i}, \tilde{\xi}_{k,s,i}\}$ form a basis for the space of solutions of eqs. (2.1), one can write the modes of a set in terms of the other, for each $i$:

$$\begin{aligned} \tilde{\zeta}_{k',s',i} &= \sum_{k,s} (\Gamma^*_{k',s';k,s;i} \zeta_{k,s,i} + \Sigma^*_{k',s';k,s;i} \xi_{k,s,i}) \\ \tilde{\xi}_{k',s',i} &= \sum_{k,s} (\Gamma_{k',s';k,s;i} \xi_{k,s,i} - \Sigma_{k',s';k,s;i} \zeta_{k,s,i}) \end{aligned} \tag{2.4}$$

where

$$\begin{aligned} \Gamma_{k',s';ks;i} &= (\tilde{\zeta}_{k',s',i}, \zeta_{k,s,i}) = (\xi_{k,s,i}, \tilde{\xi}_{k',s',i}) \\ \Sigma_{k',s';ks;i} &= (\tilde{\zeta}_{k',s',i}, \xi_{k,s,i}) = -(\zeta_{k,s,i}, \tilde{\xi}_{k's',i}) \end{aligned}$$

. This is a fermionic Bogoliubov transformation, for which

$$\sum_{q,r} \left( \Gamma^*_{k,s;q,r;i} \Gamma_{k',s';q,r;i} + \Sigma^*_{k,s;q,r;i} \Sigma_{k',s';q,r;i} \right) = \delta_{k,k'} \delta_{s,s'} \tag{2.5}$$

[1]Here the index $k$ refers to a generic set of quantum numbers labelling the modes. The sums $\sum_k$ are understood as integrals if $k$ is a continuous index.

for each $i$. The corresponding relation between the two sets of annihilators is given by

$$\begin{aligned}\tilde{\gamma}_{k,s,i} &= \sum_{k',s'} \left(\Gamma_{k,s;k's';i}\gamma_{k',s',i} + \Sigma_{k,s;k',s';i}\epsilon^{\dagger}_{k',s',i}\right) \\ \tilde{\epsilon}_{k,s,i} &= \sum_{k',s'} \left(\Gamma_{k,s;k',s';i}\epsilon_{k',s',i} - \Sigma_{k,s;k',s';i}\gamma^{\dagger}_{k',s',i}\right) .\end{aligned} \tag{2.6}$$

It is often the case that the Bogoliubov coefficients $\Gamma_{k,s;k',s';i}, \Sigma_{k,s;k',s';i}$ can be written as $\Gamma_{k,s;k',s';i} = \delta_{k,k'}\delta_{s,s'}\Gamma_{k,i}$, $\Sigma_{k,s;k',s';i} = \delta_{k,k'}\delta_{s,s'}\Sigma_{k,i}$, with $\Gamma_{k,i}$ and $\Sigma_{k,i}$ depending on $k$ alone. In this occurrence, they admit the parametrization $\Gamma_{k,i} = e^{i\eta_{k,i}}\cos(\theta_{k,i})$ ,$\Sigma_{k,i} = e^{i\phi_{k,i}}\sin(\theta_{k,i})$, with $\eta_{k,i}, \phi_{k,i}, \theta_{k,i}$ real functions of $k$. We remark that the Bogoliubov transformations (2.6) can be recast in terms of the generators

$$J_i = e^{\sum_{k,k',s,s'}\left[(\lambda^*_{k,k',s,s',i}\gamma^{\dagger}_{k,s,i}\epsilon^{\dagger}_{k's',i} - \lambda_{k,k',s,s',i}\epsilon_{k,s,i}\gamma_{k',s',i})\right]} , \tag{2.7}$$

with $\lambda_{k,k',s,s',i} = Arctan(\frac{\Sigma_{k,s;k',s';i}}{\Gamma_{k,s;k',s';i}})$, as

$$\tilde{\gamma}_{k,s,i} = J_i^{-1}\gamma_{k,s,i}J_i , \qquad \tilde{\epsilon}_{k,s,i} = J_i^{-1}\epsilon_{k,s,i}J_i . \tag{2.8}$$

The maps $J_i : \tilde{\mathcal{H}}_i \to \mathcal{H}_i$ interpolate between the Fock spaces $\mathcal{H}_i$ built from the $\gamma_{k,s,i}, \epsilon_{k,s,i}$ and the Fock space $\tilde{\mathcal{H}}_i$ built from the $\tilde{\gamma}_{k,s,i}, \tilde{\epsilon}_{k,s,i}$. In particular, one has for the vacuum states $|\tilde{0}_i\rangle = J_i^{-1}|0_i\rangle$. As for the untilded representation, the mass Hilbert space in the tilded representation is the tensor product $\tilde{\mathcal{H}}_m = \tilde{\mathcal{H}}_1 \otimes \tilde{\mathcal{H}}_2$. It is convenient to define a unique generator of Bogoliubov transformations $J : \tilde{\mathcal{H}}_m \longrightarrow \mathcal{H}_m$ on $\tilde{\mathcal{H}}_m$ as the tensor product $J = J_1 \otimes J_2$. Then

$$\tilde{\gamma}_{k,s,i} = J^{-1}\gamma_{k,s,i}J , \qquad \tilde{\epsilon}_{k,s,i} = J^{-1}\epsilon_{k,s,i}J \tag{2.9}$$

for $i = 1, 2$. The expansions of the two fields $\psi_1$ and $\psi_2$ must be compatible with each other, i.e., each of the modes $\zeta_{k,s,2}, \xi_{k,s,2}$ must be obtainable from the corresponding modes $\zeta_{k,s,1}, \xi_{k,s,1}$ by the substitution $m_1 \leftrightarrow m_2$, and vice–versa. In the context of mixing, this ensures that the same kind of particle, described by the same set of quantum numbers, is being mixed. This, of course, does not undermine the arbitrariness in the choice of the modes; these can be any complete set of solutions to the Dirac equation, provided that the same choice is made for the two fields.

### 2.1.2 Neutrino mixing and oscillation formulae in curved space-time

Having introduced the quantization of the Dirac mass fields on a generic globally hyperbolic spacetime, we now discuss the mixing transformations and the transition probabilities. These are first worked out in a fixed, but arbitrary, representation of the mass fields. Then the transformation properties under changes of mass representation are discussed. General considerations on the infinitely many unitarily inequivalent representations of the canonical anticommutation relations, which characterize the quantization of mixed fields and of fields in curved space are presented.

#### Oscillation Formulae

As remarked above, the QFT of free Dirac fields in curved space is characterized by infinitely many unitarily inequivalent representations of the canonical anticommutation relations. The phenomenon of mixing, even in Minkowski space, suffers from an analogous ambiguity, in that the flavor and the mass representations are unitarily inequivalent [51–53, 77–82]. The effects of such inequivalence have been analyzed in flat space time [34–38, 83–86] and the possibility to reveal them in experimental setup has been recently proposed [87]. Let us start by fixing the mass field expansions (2.3) and describe the mixing in a given representation of the mass fields. The flavor fields are defined as $\psi_e = \cos(\theta)\psi_1 + \sin(\theta)\psi_2$ and $\psi_\mu = \cos(\theta)\psi_2 - \sin(\theta)\psi_1$ with $\theta$ the (2-flavor) mixing angle. Just like the Bogoliubov transformations (2.9), the rotation to flavor fields can be cast in terms of a generator $\mathcal{I}_\theta(\tau)$. This is given by

$$\mathcal{I}_\theta(\tau) = e^{\theta[(\psi_1,\psi_2)_\tau - (\psi_2,\psi_1)_\tau]} \,. \tag{2.10}$$

where the scalar products $(\psi_i, \psi_j)$ *do* depend on the hypersurface chosen for the integration, since they are solutions to different Dirac equations. The equation (2.10) is the straightforward generalization of eq. (1.44). Then, by definition, the flavor fields are expressed as

$$\psi_e = \mathcal{I}_\theta^{-1}(\tau)\psi_1\mathcal{I}_\theta(\tau) \,, \qquad \psi_\mu = \mathcal{I}_\theta^{-1}(\tau)\psi_2\mathcal{I}_\theta(\tau). \tag{2.11}$$

These equations are formally identical with eqs. (1.41), from which they differ for the definition of the mixing generator. In writing equations (2.10) and (2.11), we are assuming that the usual equal $\tau$ anticommutation relations hold, namely

$$\{\psi_j^A(\tau,\boldsymbol{x}), \psi_j^{\dagger B}(\tau',\boldsymbol{x'})\}_{\tau=\tau'} = \delta^{AB}\delta^3_{\Sigma(\tau)}(\boldsymbol{x},\boldsymbol{x'}), \tag{2.12}$$

where $j = 1,2$, $A, B = 1, ..., 4$ denote the spinor components and the delta function is defined by the property $\int_{\Sigma(\tau)} d^3y f(\tau,\boldsymbol{y})\delta^3_{\Sigma(\tau)}(\boldsymbol{x},\boldsymbol{y}) = f(\tau,\boldsymbol{x})$ for any function $f$, with the integration to be performed over the spatial hypersurface $\Sigma(\tau)$. Notice that the distribution $\delta^3_{\Sigma(\tau)}(\boldsymbol{x},\boldsymbol{x'})$ includes a factor coming from the metric determinant.

If we let the generator (2.10) act on the mass annihilators, we obtain the flavor annihilators for curved space

$$\begin{aligned}\gamma_{k,s,e}(\tau) &= \mathcal{I}_\theta^{-1}(\tau)\gamma_{k,s,1}\mathcal{I}_\theta(\tau) \\ &= \cos(\theta)\gamma_{k,s,1} + \sin(\theta)\sum_{q,r}\left[\Lambda^*_{q,r;k,s}(\tau)\gamma_{q,r,2} + \Xi_{q,r;k,s}(\tau)\epsilon^\dagger_{q,r,2}\right].\end{aligned} \tag{2.13}$$

And similar for $\gamma_{k,s,\mu}(\tau), \epsilon_{k,s,e}(\tau), \epsilon_{k,s,\mu}(\tau)$. The Bogoliubov coefficients are provided by the inner products of the solutions to the *curved space* Dirac equation with mass $m_1$ and $m_2$, that is, $\Lambda_{q,r;k,s}(\tau) = (\zeta_{q,r,2}, \zeta_{k,s,1})_\tau = (\xi_{k,s,1}, \xi_{q,r,2})_\tau$ and $\Xi_{q,r;k,s}(\tau) = (\zeta_{k,s,1}, \xi_{q,r,2})_\tau = -(\zeta_{q,r,2}, \xi_{k,s,1})_\tau$. The mixing coefficients always satisfy

$$\sum_{q,r}\left(\Lambda^*_{k,s;q,r}(\tau)\Lambda_{k',s';q,r}(\tau) + \Xi^*_{k,s;q,r}(\tau)\Xi_{k',s';q,r}(\tau)\right) = \delta_{k,k'}\delta_{s,s'} \,. \tag{2.14}$$

Since the mass expansions are compatible, the mixing coefficients are often diagonal, namely of the form

$$\begin{aligned}\Lambda_{q,r;k,s}(\tau) &= \delta_{q,k}\delta_{r,s}\Lambda_{k,s}(\tau) \\ \Xi_{q,r;k,s}(\tau) &= \delta_{q,k}\delta_{r,s}\Xi_{k,s}(\tau)\end{aligned} \tag{2.15}$$

with $\Lambda_{k,s}(\tau)$, $\Xi_{k,s}(\tau)$ depending on $k$ and $s$ alone [2]. Exceptions to this arise, for instance, when we consider expansions of the mass fields in terms of modes labelled by the energy. In such a case, the mixing coefficients are non–diagonal and different from zero $\Lambda_{\omega,\omega'} \neq 0$ ,$\Xi_{\omega,\omega'} \neq 0$, once $\omega$ is fixed, only for a specific value of $\omega'$, as determined by the mass

[2] The helicity index can always be decoupled by choosing eigenstates of the helicity operator.

difference.

$$|\Lambda_{k,s}(\tau)|^2 + |\Xi_{k,s}(\tau)|^2 = 1 \tag{2.16}$$

for each $k, s, \tau$, and

$$|\Lambda_{\omega;\omega'}(\tau)|^2 + |\Xi_{\omega;\omega'}(\tau)|^2 = 1 \tag{2.17}$$

respectively. Just as in flat space, the mass and the flavor representations are unitarily inequivalent. For each $\tau$ one has a distinct flavor Fock space $\mathcal{H}_f(\tau)$ defined by $\gamma_{e,\mu}(\tau), \epsilon_{e,\mu}(\tau)$. The flavor vacuum $|0_f(\tau)\rangle = \mathcal{I}_\theta^{-1}(\tau)\,|0_m\rangle$ is a condensate of $\psi_1, \psi_2$ particle-antiparticle pairs.

In order to define the transition probabilities, we observe that the total Lagrangian is invariant under $U(1)$ gauge transformations. Therefore the total charge $Q = Q_1 + Q_2 = Q_e + Q_\mu$ is conserved[3] (independent of $\tau$) , where $Q_i = \sum_{k,s}\left(\gamma^\dagger_{k,s,i}\gamma_{k,s,i} - \epsilon^\dagger_{k,s,i}\epsilon_{k,s,i}\right)$ for $i = 1, 2, e, \mu$. It is then meaningful to define the transition probabilities as

$$P^{\rho\to\sigma}_{k,s}(\tau) = \sum_{q,r}\left(\langle \nu_{\rho,k,s}(\tau_0)|Q^{q,r}_\sigma(\tau)|\nu_{\rho,k,s}(\tau_0)\rangle - \langle 0_f(\tau_0)|Q^{q,r}_\sigma(\tau)|0_f(\tau_0)\rangle\right). \tag{2.18}$$

Here $\rho, \sigma = e, \mu$, the state $|\nu_{\rho,k,s}(\tau_0)\rangle = \gamma^\dagger_{k,s,\rho}(\tau_0)\,|0_f(\tau_0)\rangle$ is the state with a single neutrino of flavor $\rho$, momentum $k$ and helicity $s$ on the reference hypersurface $\tau = \tau_0$ . The second term on the rhs of (2.18) is just the implementation of the normal ordering with respect to $|0_f(\tau_0)\rangle$. By construction $P^{e\to e}_{k,s}(\tau) + P^{e\to\mu}_{k,s}(\tau) = 1$ and $P^{\mu\to e}_{k,s}(\tau) + P^{\mu\to\mu}_{k,s}(\tau) = 1$ for each $\tau$. A straightforward calculation yields, in the general case (accounting for both diagonal and non–diagonal mixing coefficients) the result

$$P^{e\to\mu}_{k,s}(\tau) = 2\cos^2(\theta)\sin^2(\theta)\left[1 - \sum_{q,r}\Re\left(\Lambda^*_{k,s;q,r}(\tau_0)\Lambda_{k,s;q,r}(\tau) + \Xi^*_{k,s;q,r}(\tau_0)\Xi_{k,s;q,r}(\tau)\right)\right]. \tag{2.19}$$

Equation (2.19) represents the quantum field theoretic transition probabilities in curved space. This is to be compared with the flat space counterpart (1.57). When equations (2.15) hold, the equation simplifies to

$$P^{e\to\mu}_{k,s}(\tau) = 2\cos^2(\theta)\sin^2(\theta)\left[1 - \Re\left(\Lambda^*_{k,s}(\tau_0)\Lambda_{k,s}(\tau) + \Xi^*_{k,s}(\tau_0)\Xi_{k,s}(\tau)\right)\right]. \tag{2.20}$$

In both cases one has

$$P^{e\to e}_{k,s}(\tau) = 1 - P^{e\to\mu}_{k,s}(\tau). \tag{2.21}$$

### 2.1.3 Mixing on a curved background and gravity-induced ambiguity in the particle interpretation

Up to now, we have worked within a fixed, but arbitrary, representation of the mass fields. By paralleling the flat space argument, we have developed the mixing transformations and derived the oscillation formulae. Nonetheless the quantum field theory in curved space presents an additional difficulty, in that no preferred expansion of the mass fields exists. It is then necessary that we worry about the other possible representations, and determine how the mixing changes when moving from a representation to another. For the definition (2.18) to make sense, we must determine if and how the probabilities vary when the mass representation is changed. We take as a guideline the principle of covariance, so that the *local* physical observables should be independent of the underlying representation. In moving from a given representation $\{\gamma_1, \epsilon_1\}, \{\gamma_2, \epsilon_2\}$ to another $\{\tilde{\gamma}_1, \tilde{\epsilon}_1\}, \{\tilde{\gamma}_2, \tilde{\epsilon}_2\}$, we know how to connect the

[3]This does *not* imply that $Q_e$ and $Q_\mu$ are conserved separately.

mass Fock spaces, namely via the generator (2.9) $J^{-1} : \mathcal{H}_m \to \tilde{\mathcal{H}}_m$. For each mass representation, we can proceed as we did above and build the corresponding flavor annihilators and flavor spaces $\mathcal{H}_f(\tau), \tilde{\mathcal{H}}_f(\tau)$, together with the mixing generators $\mathcal{I}_\theta(\tau) : \mathcal{H}_f(\tau) \to \mathcal{H}_m$, $\tilde{\mathcal{I}}_\theta(\tau) : \tilde{\mathcal{H}}_f(\tau) \to \tilde{\mathcal{H}}_m$. It is useful, at this point, to determine the relations among the mixing coefficients $\Lambda(\tau), \Xi(\tau)$ and $\tilde{\Lambda}(\tau), \tilde{\Xi}(\tau)$ that appear in the explicit form of the two generators $\mathcal{I}_\theta(\tau)$ and $\tilde{\mathcal{I}}_\theta(\tau)$. By definition we have

$$\begin{aligned}
&\tilde{\Lambda}_{q,r;k,s}(\tau) = (\tilde{\zeta}_{q,r;2}, \tilde{\zeta}_{k,s;1})_\tau \\
&= \sum_{q',k',r',s'} \left( \left[ \Gamma^*_{q,r;q',r';2} \zeta_{q',r';2} + \Sigma^*_{q,r;q',r';2} \xi_{q',r';2} \right], \left[ \Gamma^*_{k,s;k',s';1} \zeta_{k',s';1} + \Sigma^*_{k,s;k',s';1} \xi_{k',s';1} \right] \right)_\tau .
\end{aligned}$$

Here the first equality is just the definition of $\tilde{\Lambda}(\tau)$, the second follows from the Bogoliubov transformations (2.6). By using the properties of the inner product (2.2), in the general case (again, accounting for both the diagonal and non–diagonal mixing coefficients), we obtain

$$\begin{aligned}
&\tilde{\Lambda}_{q,r;k,s}(\tau) = \\
&\sum_{q',k',r',s'} \Big[ \Gamma_{q,r;q'r';2} \Gamma^*_{k,s;k',s';1} (\zeta_{q',r';2}, \zeta_{k',s';1})_\tau + \ \Gamma_{q,r;q',r';2} \Sigma^*_{k,s;k',s';1} (\zeta_{q',r';2}, \xi_{k',s';1})_\tau \\
&+ \ \Sigma_{q,r;q'r';2} \Gamma^*_{k,s;k's';1} (\xi_{q',r';2}, \zeta_{k',s';1})_\tau + \ \Sigma_{q,r;q',r';2} \Sigma^*_{k,s;k',s';1} (\xi_{q',r';2}, \xi_{k',s';1})_\tau \Big] ,
\end{aligned} \tag{2.22}$$

and, finally, from the definition of $\Lambda(\tau)$ and $\Xi(\tau)$, we have

$$\begin{aligned}
\tilde{\Lambda}_{q,r;k,s}(\tau) = \sum_{q',k',r',s'} &\Big[ \Gamma_{q,r,q'r';2} \left( \Gamma^*_{k,s;k',s';1} \Lambda_{q',r';k',s'}(\tau) - \Sigma^*_{k,s;k',s';1} \Xi_{q',r';k',s'}(\tau) \right) \\
&+ \Sigma_{q,r;q',r';2} \left( \Gamma^*_{k,s;k',s';1} \Xi^*_{q',r';k's'}(\tau) + \Sigma^*_{k,s;k',s';1} \Lambda^*_{q',r';k',s'}(\tau) \right) \Big] .
\end{aligned} \tag{2.23}$$

Similarly we have

$$\begin{aligned}
\tilde{\Xi}_{q,r;k,s}(\tau) = \sum_{q',k';r',s'} &\Big[ \Gamma_{q,r;q',r';2} \left( \Gamma_{k,s;k',s';1} \Xi_{q',r';k',s'}(\tau) + \Sigma_{k,s;k',s';1} \Lambda_{q',r';k',s'}(\tau) \right) \\
&- \Sigma_{q,r;q',r';2} \left( \Gamma_{k,s;k',s';1} \Lambda^*_{q',r';k',s'}(\tau) - \ \Sigma_{k,s;k',s';1} \Xi^*_{q',r';k',s'}(\tau) \right) \Big] .
\end{aligned} \tag{2.24}$$

When equations (2.15) hold for both the representations $\{q, r\}, \{q', r'\}$, the equations reduce to

$$\begin{aligned}
\tilde{\Lambda}_{q,r}(\tau) \ &= \ \sum_{q',r'} \Big[ \Gamma_{q,r,q'r';2} \left( \Gamma^*_{q,r;q',r';1} \Lambda_{q',r'}(\tau) - \Sigma^*_{q,r;q',r';1} \Xi_{q',r'}(\tau) \right) \\
&+ \ \ \Sigma_{q,r;q',r';2} \left( \Gamma^*_{q,r;q',r';1} \Xi^*_{q',r'}(\tau) + \Sigma^*_{q,r;q',r';1} \Lambda^*_{q',r'}(\tau) \right) \Big] .
\end{aligned} \tag{2.25}$$

and

$$\begin{aligned}\tilde{\Xi}_{q,r}(\tau) &= \sum_{q',r'}\Big[\Gamma_{q,r;q',r';2}\left(\Gamma_{q,r;q',r';1}\Xi_{q',r'}(\tau)+\Sigma_{q,r;q',r';1}\Lambda_{q',r'}(\tau)\right) \\ &- \Sigma_{q,r;q',r';2}\left(\Gamma_{q,r;q',r';1}\Lambda^*_{q',r'}(\tau)-\Sigma_{q,r;q',r';1}\Xi^*_{q',r'}(\tau)\right)\Big]. \end{aligned} \quad (2.26)$$

The equations (2.23, 2.24, 2.25, 2.26) provide an explicit relation between $\mathcal{I}_\theta(\tau)$ and $\tilde{\mathcal{I}}_\theta(\tau)$, and show how the mixing coefficients change, in moving from a mass representation to another, in order to ensure covariance. In particular, the tilded coefficients turn out to be a linear combination of the untilded coefficients weighted by the coefficients of the Bogoliubov transformations between the two mass representations. A slightly modified version of the eqs. (2.23) and (2.24) will be expedient in the calculation of the transition probabilities in a number of interesting cases.

It remains to establish how the flavor operators $\gamma_\rho(\tau), \epsilon_\rho(\tau)$ and the flavor vacuum $|0_f(\tau)\rangle$ transform under a change of mass representation. We focus on the vacuum state $|0_f(\tau)\rangle \in \mathcal{H}_f(\tau)$. First we employ the generator $\mathcal{I}_\theta(\tau) : \mathcal{H}_f(\tau) \to \mathcal{H}_m$ to get the mass vacuum $|0_m\rangle$. Then we apply the generator of Bogoliubov transformations (2.9) $J^{-1}$ : $\mathcal{H}_m \to \tilde{\mathcal{H}}_m$ to obtain $|\tilde{0}_m\rangle$. Finally, the generator of mixing in the tilde representation $\tilde{\mathcal{I}}_\theta^{-1}(\tau) : \tilde{\mathcal{H}}_m \to \tilde{\mathcal{H}}_f(\tau)$ is employed to get $|\tilde{0}_f(\tau)\rangle$. We conclude that the two flavor vacua are related by the transformation

$$|\tilde{0}_f(\tau)\rangle = J_f^{-1}(\tau)|0_f(\tau)\rangle \doteq \tilde{\mathcal{I}}_\theta^{-1}(\tau)J^{-1}\mathcal{I}_\theta(\tau)|0_f(\tau)\rangle \quad (2.27)$$

where we have defined the inverse $J_f^{-1}(\tau)$ for convenience. The flavor operators must then transform as

$$\begin{aligned}\gamma_{k,s,\rho}(\tau) &\to J_f^{-1}(\tau)\gamma_{k,s,\rho}(\tau)J_f(\tau) \\ \epsilon_{k,s,\rho}(\tau) &\to J_f^{-1}(\tau)\epsilon_{k,s,\rho}(\tau)J_f(\tau)\end{aligned} \quad (2.28)$$

and similarly for the creation operators. A diagrammatic exemplification of the generators connecting the various Hilbert spaces is given in Fig. (2.1). Equations (2.27) and (2.28) ensure the invariance of local observables in the form of expectation values $\langle\psi_f(\tau)|\, F(\psi_e(\tau), \psi_\mu(\tau))\, |\psi_f(\tau)\rangle$ with $|\psi_f(\tau)\rangle \in \mathcal{H}_f(\tau)$ and $F(\psi_e(\tau), \psi_\mu(\tau))$ any local operator constructed from the fields $\psi_e(\tau)$, $\psi_\mu(\tau)$.

### 2.1.4 Transition probabilities and the mass representation

The oscillation probabilities are not a local observable, since they involve the comparison between particles at different values of $\tau$, as it is evident from the definition (2.18). In general these quantities *do* depend on the representation of the mass fields, and this is because distinct representations might assign a different meaning to the quantum numbers $k, s$. For example, one might consider two expansions of the mass fields, one in terms of plane waves, labelled by the three–momenta $\{\boldsymbol{k}\}$, and one in terms of localized wave packets, labelled by a suitable set of quantum numbers $\{q\}$. It is clear that the two expansions describe particles with different physical properties; the first describes particles with definite momentum, the second describes particles for which momentum and position are definite to some extent. Therefore the probabilities $P^{\rho\to\sigma}_{k,s}$ and $P^{\rho\to\sigma}_{q,s}$ refer to the oscillations of different particles, and have a different interpretation. It would make no sense, in such a case, to require the equivalence of the two. This, of course, would be true even in flat space.

$$
\begin{tikzcd}[column sep=huge, row sep=huge]
\boldsymbol{\mathcal{H}}_f(\tau) \arrow[r, "\boldsymbol{\mathcal{J}}_\theta(\tau)"] \arrow[d, dotted, "\boldsymbol{J}_f^{-1}(\tau)"'] & \boldsymbol{\mathcal{H}}_m \arrow[d, "\boldsymbol{J}^{-1}"] \\
\widetilde{\boldsymbol{\mathcal{H}}}_f(\tau) \arrow[r, "\tilde{\boldsymbol{\mathcal{J}}}_\theta(\tau)"'] & \widetilde{\boldsymbol{\mathcal{H}}}_m
\end{tikzcd}
$$

FIGURE 2.1: Diagram defining the generator $J_f^{-1}(\tau)$. The diagram is required to commute.

What is meaningful to require, is that the transition probabilities $P_{k,s}^{\rho\to\sigma}$ be the same for each compatible representation, i.e., for each representation that refers to the same kind of particle, and therefore agrees on the meaning of the quantum numbers $k, s$. In mathematical terms, any two such representations shall be connected by diagonal Bogoliubov transformations

$$
\begin{aligned}
\tilde{\zeta}_{k,s,i} &= \Gamma^*_{k,s;i}\zeta_{k,s,i} + \Sigma^*_{k,s;i}\xi_{k,s,i} \\
\tilde{\xi}_{k,s,i} &= \Gamma_{k,s;i}\xi_{k,s,i} - \Sigma_{k,s;i}\zeta_{k,s,i}
\end{aligned}
\tag{2.29}
$$

where it is understood that $\Gamma_{k,s;q,r;i} = \delta_{k,q}\delta_{s,r}\Gamma_{k,s;i}$ and $\Sigma_{k,s;q,r;i} = \delta_{k,q}\delta_{s,r}\Sigma_{k,s;i}$, In this case the transition probabilities $P_{k,s}^{\rho\to\sigma}$ are indeed the same, and this can be proven explicitly, by writing out equation (2.20) for the two representations

$$
P_{k,s}^{e\to\mu}(\tau) = 2\cos^2\theta\sin^2\theta\left[1 - \sum_{q,r}\Re\left(\Lambda^*_{k,s;q,r}(\tau_0)\Lambda_{k,s;q,r}(\tau) + \Xi^*_{k,s;q,r}(\tau_0)\Xi_{k,s;q,r}(\tau)\right)\right]
\tag{2.30}
$$

and

$$
\tilde{P}_{k,s}^{e\to\mu}(\tau) = 2\cos^2\theta\sin^2\theta\left[1 - \sum_{q,r}\Re\left(\tilde{\Lambda}^*_{k,s;q,r}(\tau_0)\tilde{\Lambda}_{k,s;q,r}(\tau) + \tilde{\Xi}^*_{k,s;q,r}(\tau_0)\tilde{\Xi}_{k,s;q,r}(\tau)\right)\right] \, .
\tag{2.31}
$$

With the aid of equations (2.23) , (2.24) and (2.29) we find

$$
\begin{aligned}
&\tilde{\Lambda}^*_{k,s;q,r}(\tau_0)\tilde{\Lambda}_{k,s;q,r}(\tau) + \tilde{\Xi}^*_{k,s;q,r}(\tau_0)\tilde{\Xi}_{k,s;q,r}(\tau) = \\
&\left(\Lambda^*_{k,s;q,r}(\tau_0)\Lambda_{k,s;q,r}(\tau) + \Xi^*_{k,s;q,r}(\tau_0)\Xi_{k,s;q,r}(\tau)\right)\left[|\Gamma_{k,s,2}|^2|\Gamma_{q,r,1}|^2 + |\Gamma_{k,s,2}|^2|\Sigma_{q,r,1}|^2\right] \\
&+ \left(\Lambda_{k,s;q,r}(\tau_0)\Lambda^*_{k,s;q,r}(\tau) + \Xi_{k,s;q,r}(\tau_0)\Xi^*_{k,s;q,r}(\tau)\right)\left[|\Sigma_{k,s,2}|^2|\Gamma_{q,r,1}|^2 + |\Sigma_{k,s,2}|^2|\Sigma_{q,r,1}|^2\right] \, .
\end{aligned}
$$

Each of the terms in the square brackets is real. Considered that

$$\begin{aligned}
\Lambda_{k,s;q,r}(\tau_0)\Lambda^*_{k,s;q,r}(\tau) &= \left(\Lambda^*_{k,s;q,r}(\tau_0)\Lambda_{k,s;q,r}(\tau)\right)^*, \\
\Xi_{k,s;q,r}(\tau_0)\Xi^*_{k,s;q,r}(\tau) &= \left(\Xi^*_{k,s;q,r}(\tau_0)\Xi_{k,s;q,r}(\tau)\right)^*,
\end{aligned} \tag{2.32}$$

and that the Bogoliubov coefficients satisfy $|\Gamma_{k,s,i}|^2 + |\Sigma_{k,s,i}|^2 = 1$ for each $k, s, i$, we finally get

$$\begin{aligned}
&\Re[\tilde{\Lambda}^*_{k,s;q,r}(\tau_0)\tilde{\Lambda}_{k,s;q,r}(\tau) + \tilde{\Xi}^*_{k,s;q,r}(\tau_0)\tilde{\Xi}_{k,s;q,r}(\tau)] = \\
&\Re[\Lambda^*_{k,s;q,r}(\tau_0)\Lambda_{k,s;q,r}(\tau) + \Xi^*_{k,s;q,r}(\tau_0)\Xi_{k,s;q,r}(\tau)],
\end{aligned} \tag{2.33}$$

which proves the invariance of (2.30). In the most general case, as the quantum numbers $k, s$ and $k', s'$ have a different phyiscal meaning, the probabilities $P^{\rho\to\sigma}_{k,s}$ and $\tilde{P}^{\rho\to\sigma}_{k',s'}$ have different interpretations. Different representations of the mass fields do indeed assign a different meaning to such indices, so that the probabilities (2.18) have no invariant meaning. In order to make sense of the probabilities in eqs. (2.18) in the most general case, a representation of the mass fields must be fixed on the grounds of physical relevance. When the underlying spacetime $M$ possesses non trivial symmetries, as time translational invariance or spherical symmetry, there is no doubt that the representation should be fixed so to take them into account. In these cases "good quantum numbers" are suggested by the symmetries themselves (for instance, the energy $\omega$ for stationary metrics, the angular momentum $l, m$ for spherically symmetric spacetimes). In any case, the probabilities in a given mass representation can always be related to the probabilites in any other mass representation with the aid of equations (2.25) and (2.26). As a final remark, we stress that the issue discussed here has nothing to do with the diffeomorphism covariance of the theory. All the probabilities (2.20) are (generally covariant) scalars, as it is evident from the definitions.

### 2.1.5 Neutrino oscillation formulae in FLRW metrics and in presence of a Schwarzschild black hole

In this section we apply the formalism developed above to some cases of interest. After an analysis of the flat space limit, we consider two cosmologically relevant FLRW metrics, corresponding to a cosmological constant–dominated and a radiation–dominated universe respectively. In these cases, exact analytical solutions to the Dirac equation are available, and it is possible to employ equation (2.19) directly. We then introduce a method to extract the oscillation formulae on spacetimes with asymptotically flat regions without resorting to the exact solutions of the Dirac equation. We employ this strategy to compute the formulae on the Schwarzschild black hole spacetime, for neutrinos propagating from the past infinity to the future infinity. We show how the Hawking radiation is naturally embedded in the resulting transition probabilities.

#### Flat spacetime limit

As a first, trivial, application of the formulae (2.20), let us check the flat spacetime limit. We can see at once that the equations (2.20) reduce to the ordinary oscillation formulae. Indeed, in this case, we can choose the cauchy hypersurfaces to be the $t = constant$ surfaces in a given Minkowskian coordinate system, while the modes $\{\zeta_{\boldsymbol{k},s,i}(x), \xi_{\boldsymbol{k},s,i}(x)\}$ are just the plane wave solutions to the flat Dirac equation with definite momentum, so that $\Lambda_{q,r;k,s}(t) \to \mathcal{U}_{q,r;k,s}(t)$ and $\Xi_{q,r;k,s}(t) \to \mathcal{V}_{q,r;k,s}(t)$, where $\mathcal{U}_{q,r;k,s}$ and $\mathcal{V}_{q,r;k,s}$ are the usual mixing coefficients in flat space (1.46). Assuming, without loss of generality, $k$ along the $z$ direction, the helicity indices decouple $\mathcal{U}_{q,r;k,s} = \delta^3(\boldsymbol{k}-\boldsymbol{q})\delta_{r,s}\mathcal{U}_{\boldsymbol{k}}$, $\mathcal{V}_{q,r;k,s} = \delta^3(\boldsymbol{k}-\boldsymbol{q})\delta_{r,s}(-1)^s\mathcal{V}_{\boldsymbol{k}}$. Since $\mathcal{U}_{\boldsymbol{k}}(t) = |\mathcal{U}_{\boldsymbol{k}}|e^{i(\omega_{k,2}-\omega_{k,1})t}$ and $\mathcal{V}_{\boldsymbol{k}}(t) = |\mathcal{V}_{\boldsymbol{k}}|e^{i(\omega_{k,2}+\omega_{k,1})t}$, we get

$$\begin{aligned}&\sum_{k',r',q,r} \Re[\mathcal{U}^*_{k,s;k',r'}(0)\mathcal{U}_{k',r';q,r}(t) + \mathcal{V}^*_{k,s;k',r'}(0)\mathcal{V}_{k',r';q,r}(t)] \\ &= \Re[|\mathcal{U}_{\boldsymbol{k}}|^2 e^{i(\omega_{k,2}-\omega_{k,1})t} + |\mathcal{V}_{\boldsymbol{k}}|^2 e^{i(\omega_{k,2}+\omega_{k,1})t}] \\ &= |\mathcal{U}_{\boldsymbol{k}}|^2\cos[(\omega_{k,2}-\omega_{k,1})t] + |\mathcal{V}_{\boldsymbol{k}}|^2\cos[(\omega_{k,2}+\omega_{k,1})t]. \end{aligned} \tag{2.34}$$

Substituting this result in eqs. (2.20) yields the flat space oscillation formulae, which further reduce to the Pontecorvo oscillation formulae in the quantum mechanical limit ($\mathcal{V}_{\boldsymbol{k}} = 0$). Flat space also offers the possibility to illustrate some points discussed above in the simplest possible context. The plane wave expansion of the Dirac fields is by no means compulsory. One might well expand the mass fields in terms of modes with definite energy and angular momentum $\zeta_{\omega,\kappa_j,m_j;i}$, $\xi_{\omega,\kappa_j,m_j,s;i}$ instead of considering modes with definite cartesian three–momentum $\boldsymbol{k}$. The former shall be suitable combinations of spherical spinors [88]. Interestingly, in such a representation, the mixing coefficients are no longer diagonal. Indeed one has

$$\Lambda_{\omega'\kappa'_j m'_j;\omega\kappa_j m_j}(t) = \delta_{\omega',\sqrt{\omega^2+\Delta m^2}}\delta_{\kappa'_j,\kappa_j}\delta_{m'_j,m_j}|\mathcal{U}_{\omega,\omega'}|e^{i(\omega'-\omega)t} \tag{2.35}$$

with $\Delta m^2 = m_2^2 - m_1^2$ and

$$|\mathcal{U}_{\omega,\omega'}| = \sqrt{\frac{\omega'+m_2}{2\omega'}}\sqrt{\frac{\omega+m_1}{2\omega}}\left(1+\sqrt{\frac{(\omega'-m_2)(\omega-m_1)}{(\omega+m_1)(\omega'+m_2)}}\right), \tag{2.36}$$

and similar for $\Xi$, where the exponential is $e^{i(\omega'+\omega)t}$ and $|\mathcal{U}_{\omega,\omega'}|$ is replaced by

$$|\mathcal{V}_{\omega,\omega'}| = \sqrt{\frac{\omega'+m_2}{2\omega'}}\sqrt{\frac{\omega+m_1}{2\omega}}\left(\sqrt{\frac{\omega'-m_2}{\omega'+m_2}} - \sqrt{\frac{\omega-m_1}{\omega+m_1}}\right). \tag{2.37}$$

Here the quantum number $\kappa_j$ refers to a relativistic generalization of the spin–orbit operator, which enters the Dirac equation in spherical coordinates [88, 89], and takes into account both the orbital and spin angular momentum. The index $m_j$ refers to one component of the total angular momentum $\boldsymbol{J}$, and has not to be confused with the masses $m_i$. Without delving into the details of the calculation, the result of equation (2.35) can be understood as follows. The modes, apart from a normalization constant, are given by

$$\zeta_{\omega,\kappa_j,m_j;i} = e^{-i\omega t}\sqrt{\frac{\omega+m_i}{2\omega r^2}}\begin{pmatrix} P_{\kappa_j}(\lambda_i r)\Omega_{\kappa_j,m_j}(\theta,\phi) \\ \sqrt{\frac{\omega-m_i}{\omega+m_i}}P_{\kappa_j}(\lambda_i r)\Omega_{-\kappa_j,m_j}(\theta,\phi)\end{pmatrix} \tag{2.38}$$

$$\xi_{\omega,\kappa_j,m_j;i} = e^{i\omega t}\sqrt{\frac{\omega+m_i}{2\omega r^2}}\begin{pmatrix} -\sqrt{\frac{\omega-m_i}{\omega+m_i}}P_{\kappa_j}(-\lambda_i r)\Omega_{\kappa_j,m_j}(\theta,\phi) \\ P_{\kappa_j}(-\lambda_i r)\Omega_{-\kappa_j,m_j}(\theta,\phi)\end{pmatrix} \tag{2.39}$$

where $\Omega_{\kappa_j,m_j}(\theta,\phi)$ are spherical spinors, and $P_{\kappa_j}(\lambda_i r)$ are radial functions of the product $\lambda_i r$, with the radial momentum $\lambda_i = \sqrt{\omega^2 - m_i^2}$. These are solutions to the radial part of the Dirac equation, which has the form of a Riccati–Bessel equation [90]. The functions $P_{\kappa_j}(\lambda_i r)$ are combinations of spherical bessel functions $j_n$ of the form $P_{\kappa_j}(\lambda_i r) = r j_{\kappa_j}(\lambda_i r)$. In computing the inner products, the radial integration $\int dr P^*_{\kappa_j;2}(\lambda_2 r)P_{\kappa_j;1}(\lambda_1 r)$ will produce a factor $\delta_{\lambda_2,\pm\lambda_1}$, because of the closure relation satisfied by the spherical Bessel functions. Since

$\lambda_2 = \sqrt{\omega'^2 - m_2^2}$ and $\lambda_1 = \sqrt{\omega^2 - m_1^2}$, this will give rise to the delta factor appearing in (2.35). Notice that $|\mathcal{U}_{\omega,\omega'}|, |\mathcal{V}_{\omega,\omega'}|$ are numerically the same as the usual flat space coefficients $|\mathcal{U}_{\boldsymbol{k}}|, |\mathcal{V}_{\boldsymbol{k}}|$, when $k^2 = \omega^2 - m_1^2 = \omega'^2 - m_2^2$ .This shows why the mixing coefficients $\Lambda$, $\Xi$ are not generally diagonal, and the flexibility of the formalism we have employed. Indeed, the non–diagonal coefficients automatically ensure that the flavor operators $\gamma_{\omega,\rho}$, $\epsilon_{\omega,\rho}$ take into account the mass difference, involving operators with distinct energies $\omega, \omega'$ for the fields $\psi_1$ and $\psi_2$[4]. In flat space, the shift between the two representations is actually of no use. However, in a non–trivial framework, the versatility of the formalism is essential, as there are instances in which the cartesian components of the momentum $k_x, k_y, k_z$ are useless, while the "spherical" quantum numbers $\omega, l, m$ are well defined.

#### Expanding universe with exponential growth of the scale factor

The simplest non–trivial application is to spatially flat Friedmann–Lemaitre–Robertson–Walker (FLRW) spacetimes. The spacetimes within this class are conformally equivalent to Minkowski spacetime, with a conformal factor that depends only on time. In this sense they represent a minimal generalization of Minkowski spacetime, and a perfect ground to test the formalism developed above. More details on the FLRW metrics are given in the appendix B. Consider the metric $ds^2 = dt^2 - a^2(t)(dx^2 + dy^2 + dz^2)$ with an exponential expansion $a(t) = e^{Ht}$, and $H$ a constant with dimensions of energy. This is well–suited to describe a homogeneous, spatially flat and isotropic universe dominated by a cosmological constant. The normalized solutions to the Dirac equation for this metric were derived in [91]. Assuming, without loss of generality, the momentum $k$ to be along the $z$ direction, the helicities decouple as in flat space. Choosing the Cauchy surfaces as the surfaces with $t = constant$, or equivalently with $a(t) = constant$, the mixing coefficients read

$$\begin{aligned}
\Lambda_{k,s;q,r}(t) &= \delta_{s,r} \frac{\delta^3(\boldsymbol{k}-\boldsymbol{q})\pi k e^{-Ht}}{2H\sqrt{\cos(\frac{i\pi m_2}{H})\cos(\frac{i\pi m_1}{H})}} \left[J^*_{v_2}(ku)\, J_{v_1}(ku) + J^*_{v_2-1}(ku)\, J_{v_1-1}(ku)\right] \\
\Xi_{k,s;q,r}(t) &= \delta_{s,r}(-1)^s \frac{\delta^3(\boldsymbol{k}+\boldsymbol{q})\pi k e^{-Ht}}{2H\sqrt{\cos(\frac{i\pi m_2}{H})\cos(\frac{i\pi m_1}{H})}} \left[J^*_{v_1}(ku)\, J_{-v_2}(ku) - J^*_{v_1-1}(ku)\, J_{1-v_2}(ku)\right]
\end{aligned} \tag{2.40}$$

where $J_\alpha$ denotes the $\alpha$ Bessel function (see the appendix A), $u(t) = \frac{e^{-Ht}}{H}$ and $v_j = \frac{1}{2}\left(1 + \frac{2im_j}{H}\right)$ for $j = 1, 2$. Plugging these expressions in equations (2.20), we obtain ($u_0 = u(t_0)$)

$$\begin{aligned}
P^{e\to\mu}_{k,s}(t) &= 2\cos^2(\theta)\sin^2(\theta)\Bigg\{1 - \frac{\pi^2 k^2 e^{-H(t+t_0)}}{4H^2\cos(\frac{i\pi m_2}{H})\cos(\frac{i\pi m_1}{H})} \\
&\times \Re\Bigg[\left[J_{v_2}(ku_0)\, J^*_{v_1}(ku_0) + J_{v_2-1}(ku_0)\, J^*_{v_1-1}(ku_0)\right]\left[J^*_{v_2}(ku)\, J_{v_1}(ku) + J^*_{v_2-1}(ku)\, J_{v_1-1}(ku)\right] \\
&+ \left[J_{v_1}(ku_0)\, J^*_{-v_2}(ku_0) - J_{v_1-1}(ku_0)\, J^*_{1-v_2}(ku_0)\right]\left[J^*_{v_1}(ku) J_{-v_2}(ku) - J^*_{v_1-1}(ku)\, J_{1-v_2}(ku)\right]\Bigg]\Bigg\}
\end{aligned} \tag{2.41}$$

The qualitative behaviour of Eq. (2.41) for sample values of masses and momenta is shown in the left panel of Fig. (2.2). We notice that for small times the oscillations display an interference pattern similar to that of coupled harmonic oscillators. As time is increased, the

[4]In this case the label $\omega$ refers to the energies of the reference mass field, that is $\psi_1$ for $\rho = e$ and $\psi_2$ for $\rho = \mu$. This *must not* be interpreted as the energy of neutrinos with flavor $\rho$, since by definition they have no definite energy. Indeed, the non–diagonality of (2.35) shows that it is impossible to classify flavor neutrinos with a single energy $\omega$.

transition probabilities gradually converge to a flat space–like oscillation and the interference pattern eventually disappears. In the right panel of Fig. (2.2) a qualitative comparison with the Pontecorvo formulae, for different sample values of masses and momenta is shown.

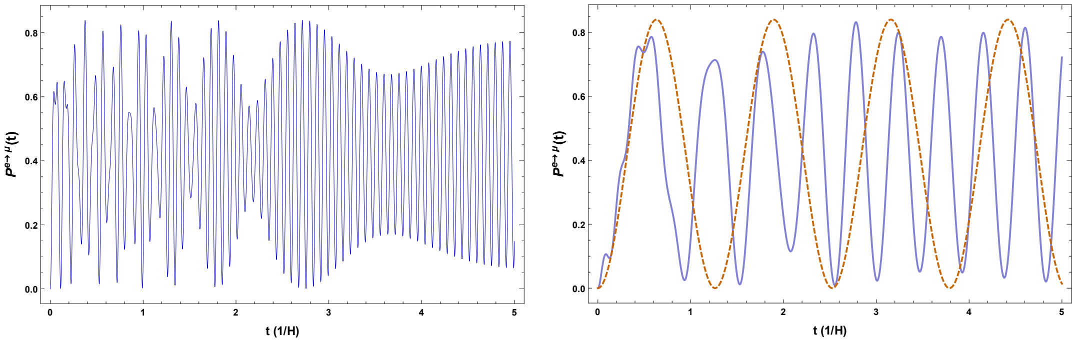


FIGURE 2.2: (color online) Plots of the oscillation formulae from Eq. (2.41) for different sample values of masses and momenta, chosen in order to highlight the qualitative behaviour of Eq. (2.41). Masses and momenta are expressed in units of $H$, time is expressed in units of $H^{-1}$. (Left panel) Plot of the $\nu_e - \nu_\mu$ transition probability Eq. (2.41) as a function of time. Here we have used the sample values $\sin^2(\theta) = 0.3, k = 30, m_1 = 1, m_2 = 80$ and $t_0 = 0$. (Right panel) Plot of the oscillation formulae from Eq. (2.41) (blue solid line) and from the Pontecorvo formulae (orange dashed line) for sample values of masses and momenta. Here we have used $\sin^2(\theta) = 0.3, k = 20, m_1 = 1, m_2 = 15$ and $t_0 = 0$.

### Expanding universe dominated by radiation

Here we consider the FLRW metric for a radiation dominated universe $a(t) = a_0 t^{\frac{1}{2}}$. Notice that since $a(t)$ has to be adimensional, $a_0$ has dimension $[t]^{-\frac{1}{2}} = [m]^{\frac{1}{2}}$. As before, without loss of generality, we assume the neutrino momentum $k$ along the $z$ direction to decouple the helicities, and consider a foliation by the $t = constant$ hypersurfaces. The solutions to the Dirac equation for this metric are again found in [91], and yield the mixing coefficients

$$
\begin{aligned}
\Lambda_{k,s;q,r}(t) &= \delta_{s,r}\delta^3(\boldsymbol{k}-\boldsymbol{q})\frac{1}{\sqrt[4]{4m_1m_2t^2}}e^{-\frac{\pi k^2(m_1+m_2)}{4m_1m_2a_0^2}}\Big\{W^*_{\kappa_2,\frac{1}{4}}(-2im_2t)W_{\kappa_1,\frac{1}{4}}(-2im_1t) \\
&+\frac{4k^2}{m_1m_2a_0^2t}\left[\frac{1}{4}W^*_{\kappa_2,\frac{1}{4}}(-2im_2t)-\frac{1}{8}\left(1+\frac{ik^2}{m_2a_0^2}\right)W^*_{\kappa_2-1,\frac{1}{4}}(-2im_2t)\right] \\
&\times\left[\frac{1}{4}W_{\kappa_1,\frac{1}{4}}(-2im_1t)-\frac{1}{8}\left(1-\frac{ik^2}{m_1a_0^2}\right)W_{\kappa_1-1,\frac{1}{4}}(-2im_1t)\right]\Big\};
\end{aligned}
$$

$$
\begin{aligned}
\Xi_{k,s;q,r}(t) &= \delta_{s,r}(-1)^s\frac{\delta^3(\boldsymbol{k}+\boldsymbol{q})k}{\sqrt[4]{2m_1(2m_2)^3a_0^4t^2}}e^{-\frac{\pi k^2(m_1+m_2)}{4m_1m_2a_0^2}}\Big\{W^*_{\kappa_1,\frac{1}{4}}(-2im_1t)W_{-\kappa_2,\frac{1}{4}}(2im_2t) \\
&+\frac{k^2}{m_1m_2a_0^2t}\left[\frac{1}{4}W^*_{\kappa_1,\frac{1}{4}}(-2im_1t)-\frac{1}{8}\left(1+\frac{ik^2}{m_1a_0^2}\right)W^*_{\kappa_1-1,\frac{1}{4}}(-2im_1t)\right] \\
&\times\left[W_{-\kappa_2,\frac{1}{4}}(2im_2t)+\frac{2im_2a_0^2}{k^2}W_{-\kappa_2+1,\frac{1}{4}}(2im_2t)\right]\Big\}
\end{aligned}
\tag{2.42}
$$

where $W_{\kappa,\mu}(z)$ are the Whittaker functions (see the appendix A) and $\kappa_j = \frac{1}{4}\left(1+\frac{2ik^2}{a_0^2 m_j}\right)$ for $j=1,2$. Insertion in eqs. (2.20) gives the transition probabilities ($t_0, t > 0$)

$$
\begin{aligned}
P^{e\to\mu}_{k,s}(t) &= 2\cos^2(\theta)\sin^2(\theta)\Bigg\{1 - \Re\Bigg[\frac{1}{\sqrt[2]{4m_1m_2t_0t}}e^{-\frac{\pi k^2(m_1+m_2)}{2m_1m_2a_0^2}}\Bigg\{W_{\kappa_2,\frac{1}{4}}(-2im_2t_0)W^*_{\kappa_1,\frac{1}{4}}(-2im_1t_0) \\
&+\frac{4k^2}{m_1m_2a_0^2t_0}\left(\frac{1}{4}W_{\kappa_2,\frac{1}{4}}(-2im_2t_0) - \frac{1}{8}\left(1-\frac{ik^2}{m_2a_0^2}\right)W_{\kappa_2-1,\frac{1}{4}}(-2im_2t_0)\right) \\
&\times\left(\frac{1}{4}W^*_{\kappa_1,\frac{1}{4}}(-2im_1t_0) - \frac{1}{8}\left(1+\frac{ik^2}{m_1a_0^2}\right)W^*_{\kappa_1-1,\frac{1}{4}}(-2im_1t_0)\right)\Bigg\}\Bigg\{W^*_{\kappa_2,\frac{1}{4}}(-2im_2t)W_{\kappa_1,\frac{1}{4}}(-2im_1t) \\
&+\frac{4k^2}{m_1m_2a_0^2t}\left(\frac{1}{4}W^*_{\kappa_2,\frac{1}{4}}(-2im_2t) - \frac{1}{8}\left(1+\frac{ik^2}{m_2a_0^2}\right)W^*_{\kappa_2-1,\frac{1}{4}}(-2im_2t)\right) \\
&\times\left(\frac{1}{4}W_{\kappa_1,\frac{1}{4}}(-2im_1t) - \frac{1}{8}\left(1-\frac{ik^2}{m_1a_0^2}\right)W_{\kappa_1-1,\frac{1}{4}}(-2im_1t)\right)\Bigg\} \\
&+\frac{k^2}{\sqrt[2]{2m_1(2m_2)^3a_0^4t_0t}}e^{-\frac{\pi k^2(m_1+m_2)}{2m_1m_2a_0^2}}\Bigg\{W_{\kappa_1,\frac{1}{4}}(-2im_1t_0)W^*_{-\kappa_2,\frac{1}{4}}(2im_2t_0) \\
&+\frac{k^2}{m_1m_2a_0^2t_0}\left(\frac{1}{4}W_{\kappa_1,\frac{1}{4}}(-2im_1t_0) - \frac{1}{8}\left(1-\frac{ik^2}{m_1a_0^2}\right)W_{\kappa_1-1,\frac{1}{4}}(-2im_1t_0)\right) \\
&\times\left(W^*_{-\kappa_2,\frac{1}{4}}(2im_2t_0) - \frac{2im_2a_0^2}{k^2}W^*_{-\kappa_2+1,\frac{1}{4}}(2im_2t_0)\right)\Bigg\}\Bigg\{W^*_{\kappa_1,\frac{1}{4}}(-2im_1t)W_{-\kappa_2,\frac{1}{4}}(2im_2t) \\
&+\frac{k^2}{m_1m_2a_0^2t}\left(\frac{1}{4}W^*_{\kappa_1,\frac{1}{4}}(-2im_1t) - \frac{1}{8}\left(1+\frac{ik^2}{m_1a_0^2}\right)W^*_{\kappa_1-1,\frac{1}{4}}(-2im_1t)\right) \\
&\times\left(W_{-\kappa_2,\frac{1}{4}}(2im_2t) + \frac{2im_2a_0^2}{k^2}W_{-\kappa_2+1,\frac{1}{4}}(2im_2t)\right)\Bigg\}\Bigg]\Bigg\}
\end{aligned}
\tag{2.43}
$$

The qualitative behaviour of Eq. (2.43) is shown in Fig. (2.3) for sample values of masses and momenta.

### Spacetimes with asymptotically flat regions

The FLRW spacetimes considered above are among the few non–trivial metrics for which the Dirac equation (2.63) can be solved analytically. More often one does not have an exact solution at his disposal, and the implementation of eqs. (2.20) is a complicated task. In many cases of interest, however, the spacetime $M$ admits asymptotically flat regions $\Omega_A, \Omega_B \subset M$, usually in the far past and in the far future. $\Omega_A$ and $\Omega_B$ are separated by a region with non-trivial curvature, where the Dirac equation is usually unsolvable analytically. In $\Omega_A$ and $\Omega_B$ the solutions to the Dirac equation are the flat space modes $\{u^I_{k,s,i}(x), v^I_{k,s,i}(x)\}$ with $I = A, B$, and one has a natural choice for the positive frequency modes. Because of the non-trivial curvature, the two sets of solutions $A, B$ are distinct. When limited to one of the two regions, eqs. (2.20) reduce to the ordinary flat space formulae. When the intermediate curvature region is involved, a direct application of eqs. (2.20) is prohibitive. Nevertheless, if one is able to provide the relation between the two sets $A, B$, in the form of a Bogoliubov transformation, it is possible to derive oscillation formulae for the propagation from $\Omega_A$ to $\Omega_B$. Assume that $\Omega_A = \bigcup_{\tau \leq \tau_A} \Sigma_\tau$ and $\Omega_B = \bigcup_{\tau \geq \tau_B} \Sigma_\tau$ for some values $\tau_B > \tau_A$, and consider $\tau_0 \leq \tau_A$, $\tau \geq \tau_B$. Suppose also that the $B$ modes are given in terms of the $A$ modes

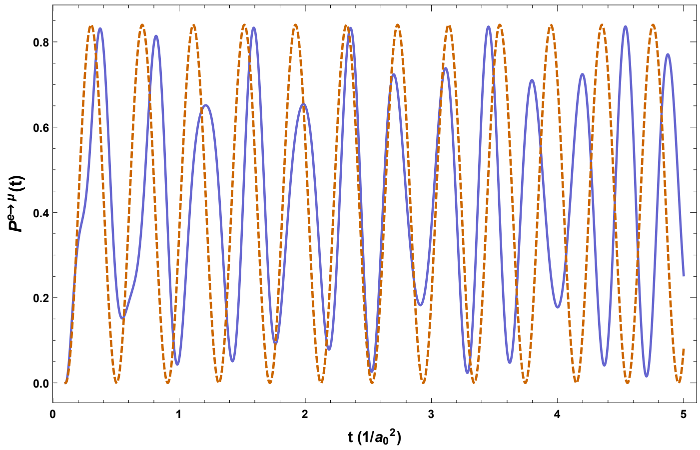


FIGURE 2.3: (color online) Plots of the $\nu_e - \nu_\mu$ transition probability as a function of time as from Eq. (2.43) (blue solid line) and from the Pontecorvo formulae (orange dashed line) for sample values of massed and momenta, chosen in order to highlight the qualitative behaviour of Eq. (2.43). Masses and momenta are expressed in units of $a_0^2$, time is expressed in units of $a_0^{-2}$. We have used the sample values $\sin^2(\theta) = 0.3, k = 5, m_1 = 1, m_2 = 20$ and $t_0 = 0.1$.

as

$$u^B_{k',s',i} = \sum_{k,s}\left(\Gamma^*_{k',s';k,s;i}u^A_{k,s,i} + \Sigma^*_{k',s';k,s;i}v^A_{k,s,i}\right) \tag{2.44}$$

$$v^B_{k's',i} = \sum_{k,s}\left(\Gamma_{k',s';k,s;i}v^A_{k,s,i} - \Sigma_{k',s';k,s;i}u^A_{k,s,i}\right) . \tag{2.45}$$

Here the Bogoliubov coefficients $\Gamma_{k',s';k,s;i}, \Sigma_{k',s';k,s;i}$ are again provided by the inner products $(u_i^A, u_i^B)$, $(u_i^A, v_i^B)$, yet their significance is slightly different from those in (2.4). While equation (2.4) describes a general and arbitrary change of basis, the transformation of equation (2.44) is dictated by the circumstance of having a natural choice for the modes in $\Omega_A$ and $\Omega_B$, with a well–defined physical meaning. Indeed, the Bogoliubov coefficients take into account the effect of the curvature in the intermediate region. Then we can specialize equations (2.23), (2.24) to get

$$\Lambda^B_{q,r;k,s}(\tau) = \sum_{q',k',r',s'}\Big[\Gamma_{q,r;q',r';2}\left(\Gamma^*_{k,s;k',s';1}\Lambda^A_{q',r';k',s'}(\tau) - \Sigma^*_{k,s;k',s';1}\Xi^A_{q',r';k',s'}(\tau)\right)$$
$$+\Sigma_{q,r;q',r';2}\left(\Gamma^*_{k,s;k',s';1}\Xi^{A*}_{q',r';k',s'}(\tau) + \Sigma^*_{k,s;k',s';1}\Lambda^{A*}_{q',r';k',s'}(\tau)\right)\Big] . \tag{2.46}$$

$$\Xi^B_{q,r;k,s}(\tau) = \sum_{q',k',r',s'}\Big[\Gamma_{q,r;q',r';2}\left(\Gamma_{k,s;k',s';1}\Xi^A_{q',r';k',s'}(\tau) + \Sigma_{k,s;k',s';1}\Lambda^A_{q',r';k',s'}(\tau)\right)$$
$$-\Sigma_{q,r;q',r';2}\left(\Gamma_{k,s;k',s';1}\Lambda^{A*}_{q',r';k',s'}(\tau) - \Sigma_{k,s;k',s';1}\Xi^{A*}_{q',r';k',s'}(\tau)\right)\Big] . \tag{2.47}$$

For $\tau < \tau_A$ $\Lambda^A(\tau), \Xi^A(\tau)$ are trivial, and vice-versa, for $\tau > \tau_B$, $\Lambda^B(\tau), \Xi^B(\tau)$ are trivial. Choosing, for instance, the $B$ representation, one would have a trivial expression for $\Lambda^B(\tau), \Xi^B(\tau)$ and one can make use of eqs. (2.46), (2.47) to obtain $\Lambda^B(\tau_0), \Xi^B(\tau_0)$ in terms of $\Lambda^A(\tau_0), \Xi^A(\tau_0)$, which are also trivial. Then one can plug $\Lambda^B(\tau,\tau_0)$ and $\Xi^B(\tau,\tau_0)$ in equation (2.20) to obtain $P^{e\to\mu}_{k,s\to q,r}(\tau)$ for $\tau \geq \tau_B$ and the reference hypersurface $\tau_0 \leq \tau_A$.

### Scwharzschild black hole

As a realization of this scheme, consider the (static) Schwarzschild metric

$$ds^2 = \left(1 - \frac{2GM}{r}\right) dt^2 - \left(1 - \frac{2GM}{r}\right)^{-1} dr^2 - r^2 d\Omega, \tag{2.48}$$

and two sequences of spacelike hypersurfaces[5] $\{\Sigma_n^+\}_{n\in\mathbb{N}}$, $\{\Sigma_n^-\}_{n\in\mathbb{N}}$ approaching, respectively, the future $\mathcal{I}^+$ and the past null infinity $\mathcal{I}^-$ as $n \to \infty$. We require that $\Sigma_n^+$ and $\Sigma_n^-$ be Cauchy surfaces respectively for the causal past $J^-(\mathcal{I}^+)$ of $\mathcal{I}^+$ and the causal future $J^+(\mathcal{I}^-)$of $\mathcal{I}^-$ for each $n$. For $n$ large enough, these surfaces span an approximately flat portion of the Schwarzschild spacetime. On the surfaces $\Sigma_n^-$, as $n$ approaches infinity, we expand the massive fields in terms of the incoming solutions, with frequency defined with respect to the schwarzschild time $t$ and with definite angular momentum,

$$\zeta^{IN}_{\omega,\kappa_j,m_j;i}(t,r,\theta,\phi) \propto e^{-i\omega t}, \qquad \xi^{IN}_{\omega,\kappa_j,m_j;i}(t,r,\theta,\phi) \propto e^{i\omega t}. \tag{2.49}$$

These modes reduce to the flat space solutions (2.38) and (2.39) as $\mathcal{I}^-$ is approached. Omitting the irrelevant angular and spin quantum numbers, as $n \to \infty$, we get

$$\Lambda^{IN}_{\omega;\omega'}(\Sigma_n^-) \to \delta_{\omega',\sqrt{\omega^2+\Delta m^2}} |\mathcal{U}_{\omega,\omega'}| e^{i\varphi^-(\omega,n)} \tag{2.50}$$

$$\Xi^{IN}_{\omega;\omega'}(\Sigma_n^-) \to \delta_{\omega',\sqrt{\omega^2+\Delta m^2}} |\mathcal{V}_{\omega,\omega'}| e^{i\rho^-(\omega,n)} \tag{2.51}$$

with $|\mathcal{U}_{\omega,\omega'}|$ and $|\mathcal{V}_{\omega,\omega'}|$ flat space spherical mixing coefficients as defined in (2.36) and (2.37), and $\varphi^-(\omega,n), \rho^-(\omega,n)$ phase factors depending on $\omega$ and $n$. A similar reasoning can be carried on for the *outgoing* modes emerging at $\mathcal{I}^+$, $\zeta^{OUT}_{\omega,\kappa_j,m_j;i}(t,r,\theta,\phi)$, $\xi^{OUT}_{\omega,\kappa_j,m_j;i}(t,r,\theta,\phi)$, so to yield as $n \to \infty$

$$\Lambda^{OUT}_{\omega;\omega'}(\Sigma_n^+) \to \delta_{\omega',\sqrt{\omega^2+\Delta m^2}} |\mathcal{U}_{\omega,\omega'}| e^{i\varphi^+(\omega,n)} \tag{2.52}$$

$$\Xi^{OUT}_{\omega;\omega'}(\Sigma_n^+) \to \delta_{\omega',\sqrt{\omega^2+\Delta m^2}} |\mathcal{V}_{\omega,\omega'}| e^{i\rho^+(\omega,n)}\,. \tag{2.53}$$

Because of the Black Hole, the $IN$ and $OUT$ modes do not coincide. Fermion creation by the Schwarzschild black hole has been studied, via the tunneling method, in [92]. There it has been shown that the Hawking temperature $T_H = \frac{1}{8\pi GM}$ is recovered for the emission of spin–$\frac{1}{2}$ particles. We then infer that the $IN$ and $OUT$ modes are related by a thermal Bogoliubov transformation at the Hawking temperature $T_H$, corrected for fermions:

$$\zeta^{OUT}_{\omega,\kappa_j,m_j;i} = \sqrt{\frac{e^{\frac{\omega}{k_B T_H}}}{e^{\frac{\omega}{k_B T_H}}+1}}\,\zeta^{IN}_{\omega,\kappa_j,m_j;i} + \sqrt{\frac{1}{e^{\frac{\omega}{k_B T_H}}+1}}\,\xi^{IN}_{\omega,\kappa_j,m_j;i} \tag{2.54}$$

$$\xi^{OUT}_{\omega,\kappa_j,m_j;i} = \sqrt{\frac{e^{\frac{\omega}{k_B T_H}}}{e^{\frac{\omega}{k_B T_H}}+1}}\,\xi^{IN}_{\omega,\kappa_j,m_j;i} - \sqrt{\frac{1}{e^{\frac{\omega}{k_B T_H}}+1}}\,\zeta^{IN}_{\omega,\kappa_j,m_j;i}\,, \tag{2.55}$$

[5] We use here two discrete families of surfaces, but also continuous families would do the trick, as long as the same limiting process is involved ($\Sigma^\pm \to \mathcal{I}^\pm$).

It is understood that these equations hold as long as the spacetime is stationary (eternal black hole). For a body that collapses to a Schwarzschild black hole, as considered in the original paper by Hawking [63], we expect a slightly modified version of the Bogoliubov transformations, comprising non–diagonal thermal coefficients $\Gamma_{\omega,\omega';i}$ and $\Sigma_{\omega,\omega';i}$ with $\omega \neq \omega'$. We pick the ingoing representation to calculate the probabilities (of course, the outgoing representation yields the same result, as the Bogoliubov transformations are diagonal), and employ eqs. (2.46, 2.47) to obtain, with $F_H(\omega) = \frac{1}{e^{\frac{\omega}{k_B T_H}}+1}$,

$$\begin{aligned}
&\Lambda^{IN}_{\omega;\omega'}(\Sigma^+_n) = \\
&\left\{ \sqrt{[1-F_H(\omega)]\,[1-F_H(\omega')]}\Lambda^{OUT}_{\omega;\omega'}(\Sigma^+_n) - \sqrt{F_H(\omega)\,[1-F_H(\omega')]}\Xi^{OUT}_{\omega;\omega'}(\Sigma^+_n) \right. \\
&\left. +\sqrt{F_H(\omega')\,[1-F_H(\omega)]}\left(\Xi^{OUT}_{\omega;\omega'}\right)^*(\Sigma^+_n) + \sqrt{F_H(\omega)F_H(\omega')}\left(\Lambda^{OUT}_{\omega;\omega'}\right)^*(\Sigma^+_n) \right\} \\
&,
\end{aligned} \tag{2.56}$$

Considered that $\Lambda^{OUT}_{\omega;\omega'}(\Sigma^+_n) \to \delta_{\omega',\sqrt{\omega^2+\Delta m^2}}|\mathcal{U}_{\omega,\omega'}|e^{i\varphi^+(\omega,n)}$ and that $\Xi^+_{\omega;\omega'}(\Sigma^+_n)$ converges to $\delta_{\omega',\sqrt{\omega^2+\Delta m^2}}|\mathcal{V}_{\omega,\omega'}|e^{i\rho^+(\omega,n)}$ as $n \to \infty$, we obtain

$$\begin{aligned}
&\Lambda^{IN}_{\omega;\omega'}(\Sigma^+_n) = \delta_{\omega',\sqrt{\omega^2+\Delta m^2}} \times \\
&\left\{ \sqrt{[1-F_H(\omega)]\,[1-F_H(\omega')]}|\mathcal{U}_{\omega;\omega'}|e^{i\varphi^+(\omega,n)} - \sqrt{F_H(\omega)\,[1-F_H(\omega')]}|\mathcal{V}_{\omega;\omega'}|e^{i\rho^+(\omega,n)} \right. \\
&\left. +\sqrt{F_H(\omega')\,[1-F_H(\omega)]}|\mathcal{V}_{\omega;\omega'}|e^{-i\rho^+(\omega,n)} + \sqrt{F_H(\omega)F_H(\omega')}|\mathcal{U}_{\omega,\omega'}|e^{-i\varphi^+(\omega,n)} \right\}
\end{aligned}$$

and

$$\begin{aligned}
&\Xi^{IN}_{\omega;\omega'}(\Sigma^+_n) = \delta_{\omega',\sqrt{\omega^2+\Delta m^2}} \times \\
&\left\{ \sqrt{[1-F_H(\omega)]\,[1-F_H(\omega')]}|\mathcal{V}_{\omega,\omega'}|e^{i\rho^+(\omega,n)} + \sqrt{F_H(\omega)\,[1-F_H(\omega')]}|\mathcal{U}_{\omega,\omega'}|e^{i\varphi^+(\omega,n)} \right. \\
&\left. -\sqrt{F_H(\omega')\,[1-F_H(\omega)]}|\mathcal{U}_{\omega,\omega'}|e^{-i\varphi^+(\omega,n)} + \sqrt{F_H(\omega)F_H(\omega')}|\mathcal{V}_{\omega,\omega'}|e^{-i\rho^+(\omega,n)} \right\}.
\end{aligned}$$

Choosing as reference hypersurface $\Sigma^-_m$ for large $m$, we can now compute the probabilities (2.20) for a neutrino propagating from $\Sigma^-_m$ to $\Sigma^+_n$, i.e. from $\mathcal{I}^-$ to $\mathcal{I}^+$ in the limit $m, n \to \infty$. We find, for $m, n \to \infty$

$$\begin{aligned}
&P^{e\to\mu}_\omega(m,n) \approx 2\cos^2\theta\sin^2\theta \times \\
&\left( 1 - \sqrt{[1-F_H(\omega)]\,[1-F_H(\omega')]}\left[|\mathcal{U}_{\omega;\omega'}|^2\cos(\Delta^-_{\omega;m,n}) + |\mathcal{V}_{\omega;\omega'}|^2\cos(\Phi^-_{\omega;m,n})\right] \right. \\
&+\sqrt{F_H(\omega)\,[1-F_H(\omega')]}|\mathcal{U}_{\omega;\omega'}||\mathcal{V}_{\omega;\omega'}|\left[\cos(\Theta^-_{\omega;m,n}) - \cos(\Psi^-_{\omega;m,n})\right] \\
&+\sqrt{F_H(\omega')\,[1-F_H(\omega)]}|\mathcal{U}_{\omega;\omega'}||\mathcal{V}_{\omega;\omega'}|\left[\cos(\Psi^+_{\omega;m,n}) - \cos(\Theta^+_{\omega;m,n})\right] \\
&\left. -\sqrt{F_H(\omega)F_H(\omega')}\left[|\mathcal{U}_{\omega;\omega'}|^2\cos(\Delta^+_{\omega;m,n}) + |\mathcal{V}_{\omega;\omega'}|^2\cos(\Phi^+_{\omega;m,n})\right] \right).
\end{aligned} \tag{2.57}$$

with the phase differences $\Delta^\pm_{\omega;m,n} = \varphi^+(\omega,n) \pm \varphi^-(\omega,m)$, $\Phi^\pm_{\omega;m,n} = \rho^+(\omega,n) \pm \rho^-(\omega,m)$, $\Psi^\pm_{\omega;m,n} = \rho^+(\omega,n) \pm \varphi^-(\omega,m)$ and $\Theta^\pm_{\omega;m,n} = \varphi^+(\omega,n) \pm \rho^-(\omega,m)$ . In particular, for

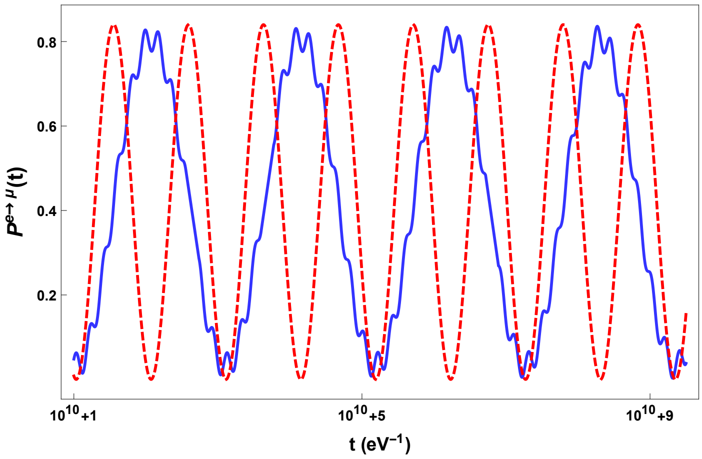


FIGURE 2.4: (color online) Plot of the $\nu_e - \nu_\mu$ transition probability from Eq. (2.57) (blue solid line) and from the Pontecorvo oscillation formulae (red dashed line) for late times and sample values of masses, momenta and Hawking Temperature. The phases in (2.57) have been chosen so as to match the flat space phases for simplicity, $\Delta^{\pm}_{\omega;m,n} \to \frac{\omega_2-\omega_1}{2}(t \pm t_0)$, $\Phi^{\pm}_{\omega;m,n} \to \frac{\omega_2+\omega_1}{2}(t \pm t_0)$, $\Psi^{\pm}_{\omega;m,n} \to \frac{\omega_2}{2}(t \pm t_0) + \frac{\omega_1}{2}(t \mp t_0)$, $\Theta^{\pm}_{\omega;m,n} \to \frac{\omega_2}{2}(t \pm t_0) - \frac{\omega_1}{2}(t \mp t_0)$, where $t$ and $t_0$ denote respectively the future and past hypersurfaces. We have used the sample values $\sin^2(\theta) = 0.3$, $k = 30eV$, $m_1 = 1eV$, $m_2 = 20eV$, $t_0 = 0$, $k_B T_H = 10^{-10}eV$ and $t$ in the range $[10^{10}+1, 10^{10}+9.5]eV^{-1}$.

large energies of the mass fields $\omega, \omega'$, $|\mathcal{V}_{\omega,\omega'}| \to 0$ and $|\mathcal{U}_{\omega,\omega'}| \to 1$, thus

$$P^{e\to\mu}_{\omega}(m,n) \approx 2\cos^2\theta \sin^2\theta \times \left(1 - \sqrt{[1-F_H(\omega)]\,[1-F_H(\omega')]}\cos(\Delta^{-}_{\omega,\kappa_j;m,n}) - \sqrt{F_H(\omega)F_H(\omega')}\cos(\Delta^{+}_{\omega,\kappa_j;m,n})\right), \tag{2.58}$$

where it is understood that $\omega'^2 = \omega^2 + \Delta m^2$. If the limit $T_H \to 0$ is taken in equation (2.58), one obtains, apart from a phase factor, the usual Pontecorvo oscillation formulae. The qualitative behaviour of Eq. (2.57) is displayed in Fig. (2.4). To compute the oscillation formulae on a Schwarzschild background for an arbitrary propagation, since exact analytical solutions are unavailable, one has to resort to approximate solutions to the Dirac equation. In all the applications considered, the oscillation formulae do not depend on the helicity $s$ of neutrinos. However, when additional complications due to frame–dragging and non–conservation of angular momentum arise (see e.g. [93, 94]), the formulae for left-handed and right-handed neutrinos can differ.

### Quantum mechanical limit

It is a general feature of equations (2.20) that when all the quantum field theoretical effects are negligible, the oscillation formulae are modified only for a phase factor. Indeed, when one can neglect $\Xi_{k,s}$ in equation (2.20), one immediately has $|\Lambda^*_{k,s}(\tau)| = 1$, ($|\Lambda_{\omega,\omega'}(\tau)| = 1$ respectively, in the non–diagonal case) for each $\tau$ from equation (2.15). Then the product $\Lambda_{k,s}(\tau_0)^*\Lambda_{k,s}(\tau)$, $(\Lambda_{\omega,\omega'}(\tau_0)^*\Lambda_{\omega,\omega'}(\tau)$ respectively) is just a phase $e^{i\varphi(\tau_0,\tau)}$ and the net effect is a phase shift with respect to the Pontecorvo oscillation formulae, consistently with previous results obtained in a heuristic treatment[74]. Of course, the explicit value of the phase $\varphi(\tau_0, \tau)$ depends on the metric and the surfaces $\tau$ considered, as well as on the mode expansion chosen for the mass fields. When the gravitational fields are weak enough, the phase can be computed by means of geometrical optics considerations [74, 93, 95].

## 2.2 The flavor vacuum in the expanding universe

In the previous section we have introduced the mixing transformation in curved space and discussed the resulting oscillation probabilities. The formalism there developed is also necessary to study the energy-momentum content of the flavor vacuum in curved space. In flat space it has been shown (cfr. chapter 1) that the flavor vacuum has the structure of a condensate with the equation of state of a pressure-less perfect fluid. Here we generalize the analysis to the cosmologically relevant class of spatially flat Friedmann-Lemaître-Robertson-Walker metrics (see the appendix B for more details). We compute the expectation value of the energy-momentum tensor on the curved space flavor vacuum and we show that it resembles the energy-momentum tensor of a perfect fluid. We then apply the general formalism to a specific metric, generalizing the flat space result on the equation of state of the flavor vacuum.

### 2.2.1 The Dirac Equation and its solutions in flat FLRW spacetime

For the reader's convenience we start this section by setting the notation and introducing the class of metrics of interest. We then elaborate on the Dirac equation and discuss the general form of the solution. We will focus on the spatially flat Friedmann-Lemaître-Robertson-Walker spacetime described by the metric

$$g_{\mu\nu} = \text{diag}\Big(1, -C^2(t), -C^2(t), -C^2(t)\Big). \tag{2.59}$$

where $C(t)$ is the scale factor. For our purposes it will be useful to express this metric in terms of the conformal time $\tau$ defined as $d\tau = \frac{dt}{C(t)}$ with range $\tau \in (-\infty, \infty)$ corresponding to $t \in (-\infty, \infty)$. Using $\tau$, the line element reads

$$ds^2 = C^2(\tau)[d\tau^2 - dx^2 - dy^2 - dz^2] \tag{2.60}$$

when expressed in cartesian spatial coordinates and in conformal time $\tau$.

In order to write the Dirac equation, we need to choose a tetrad field $e^A_\mu$ with the property $g_{\mu\nu} = e^A_\mu e^B_\nu \eta_{AB}$. Given the metric of Eq.(2.60) a convenient choice of tetrads is

$$e^A_\mu = C(\tau)\delta^A_\mu \,, \tag{2.61}$$

where the Kronecker symbol $\delta^A_\mu$ signals that the only non-zero component of $e^A$ is the one for which the Lorentz index $A$ and the spacetime index $\mu$ coincide.

Using the tetrads above one can define the generalization of gamma matrices $\gamma^A$ to the case of curved spacetime $\tilde{\gamma}^\mu = e^\mu_A \gamma^A$

Finally, in order to write the Dirac equation, we also need the spin connections $\omega^{AB}_\mu = e^A_\nu \Gamma^\nu_{\sigma\mu} e^{\sigma B} + e^A_\nu \partial_\mu e^{\nu B}$ . The spinorial covariant derivative is defined with the aid of the spin connections as $D_\mu \psi = \partial_\mu \psi + \Gamma_\mu \psi$, $\Gamma_\mu = \frac{1}{8}\omega^{AB}_\mu [\gamma_A, \gamma_B]$. Similarly one defines the action of the covariant derivative on the adjoint spinor $\bar{\psi} = \psi^\dagger \gamma^0$ as

$$D_\mu \bar{\psi} = \partial_\mu \bar{\psi} - \bar{\psi}\Gamma_\mu \,. \tag{2.62}$$

We can now write down the Dirac equation

$$i\tilde{\gamma}^{\mu}(x)D_{\mu}\psi - m\psi = 0\,. \tag{2.63}$$

The above equation can be generated by the Lagrangian

$$\mathcal{L} = \sqrt{-g}\left\{\frac{i}{2}\left[\bar{\psi}\tilde{\gamma}^{\mu}(x)D_{\mu}\psi - D_{\mu}\bar{\psi}\tilde{\gamma}^{\mu}(x)\psi\right] - m\bar{\psi}\psi\right\} \tag{2.64}$$

and we can define the energy-momentum tensor of the spinor field as the variation of the above Lagrangian with respect to $\psi$ and $\bar{\psi}$

$$T_{\mu\nu} = \frac{i}{2}\left\{\bar{\psi}\tilde{\gamma}_{\mu}(x)D_{\nu}\psi + \bar{\psi}\tilde{\gamma}_{\nu}(x)D_{\mu}\psi - D_{\mu}\bar{\psi}\tilde{\gamma}_{\nu}(x)\psi - D_{\nu}\bar{\psi}\tilde{\gamma}_{\mu}(x)\psi\right\}\,. \tag{2.65}$$

In the metric (2.60) the Dirac equation reads

$$\left(i\gamma^{0}\partial_{\tau} + \frac{3i}{2}\frac{\partial_{\tau}C}{C}\gamma^{0} + i\gamma^{j}\partial_{j} - mC\right)\psi = 0\,. \tag{2.66}$$

The spatial dependence of this equation suggests that we look for plane wave solutions $\psi \propto e^{i\boldsymbol{p}\cdot\boldsymbol{x}}$, where the mode label $\boldsymbol{p}$ is a 3-vector that can be thought as the would-be plane wave momentum when $C(t)$ reduces to a constant, and "$\cdot$" denotes the euclidean $3d$ scalar product (see ). We remark that the actual momentum that is istanteneously carried by the mode with label $\boldsymbol{p}$ is the comoving momentum[6] $\frac{\boldsymbol{p}}{C(\tau)}$.

Using the helicity eigenbispinors $\xi_{\lambda}$ defined as

$$\frac{\boldsymbol{\sigma}\cdot\boldsymbol{p}}{p}\xi_{\lambda} = \lambda\xi_{\lambda}\,. \tag{2.67}$$

the solution of (2.66) can be written as the combination of the positive and negative energy solutions in the form

$$u_{\boldsymbol{p},\lambda}(\tau,\boldsymbol{x}) = e^{i\boldsymbol{p}\cdot\boldsymbol{x}}\begin{pmatrix} f_{p}(\tau)\xi_{\lambda}(\hat{p}) \\ g_{p}(\tau)\lambda\xi_{\lambda}(\hat{p})\end{pmatrix} \quad v_{\boldsymbol{p},\lambda}(\tau,\boldsymbol{x}) = e^{i\boldsymbol{p}\cdot\boldsymbol{x}}\begin{pmatrix} g_{p}^{*}(\tau)\xi_{\lambda}(\hat{p}) \\ -f_{p}^{*}(\tau)\lambda\xi_{\lambda}(\hat{p})\end{pmatrix}\,. \tag{2.68}$$

The negative energy solutions are obtained by charge conjugation of the positive energy solutions $v = \mathcal{C}u^{*}$. Inserting Eq.(2.68) in Eq.(2.66), and using the defining property of the helicity bispinors, we can write (2.66) as the system

$$\begin{aligned}
i\partial_{\tau}f_{\boldsymbol{p}} &= \left(mC - \frac{3i}{2}\frac{\partial_{\tau}C}{C}\right)f_{\boldsymbol{p}} + pg_{\boldsymbol{p}} \\
i\partial_{\tau}g_{\boldsymbol{p}} &= \left(-mC - \frac{3i}{2}\frac{\partial_{\tau}C}{C}\right)g_{\boldsymbol{p}} + pf_{\boldsymbol{p}}\,, \\
i\partial_{\tau}f_{p}^{*} &= \left(-mC - \frac{3i}{2}\frac{\partial_{\tau}C}{C}\right)f_{p}^{*} - pg_{p}^{*} \\
i\partial_{\tau}g_{p}^{*} &= \left(mC - \frac{3i}{2}\frac{\partial_{\tau}C}{C}\right)g_{p}^{*} - pf_{p}^{*}\,.
\end{aligned} \tag{2.69}$$

[6] This is most conveniently seen by inserting the plane wave ansatz in Eq. (2.66) and reverting to the coordinate time $t$:

$$\left[i\gamma^{0}\left(\partial_{t} + \frac{3i}{2}\frac{\partial_{t}C}{C}\right) - \frac{\gamma^{j}p_{j}}{C} - m\right]\psi_{\boldsymbol{p}} = 0\,.$$

In this form the equation resembles the Dirac equation in flat space, with a time-dependent potential $\frac{3i}{2}\frac{\partial_{t}C}{C}$ and with the quantity $\frac{p_j}{C}$ playing the role of an instantaneous momentum.

The above equations show that the functions $f, g$ depend only on the modulus $p$ of the 3-momentum. Thus, from now on, we will drop the vector index $\boldsymbol{p}$ in favor of the scalar index $p$. The scalar product between two solutions of the Dirac equation $A, B$ is defined as

$$(A, B)_\tau = \int_{\Sigma_\tau} d^3x \sqrt{-g} \bar{A} \tilde{\gamma}^\tau(x) B \,, \tag{2.70}$$

where the integration is to be carried over a hypersurface $\Sigma_\tau$ of constant conformal time $\tau$. If $A$ and $B$ are solutions of the *same* Dirac equation, the scalar product $(A, B)_\tau$ is independent of $\tau$. This is no longer true if $A$ and $B$ are solutions of distinct Dirac equations. Knowing that the determinant is $g = -C^8$, we can easily compute the scalar product between the solutions (2.68):

$$\begin{aligned}(u_{\boldsymbol{p},\lambda}, u_{\boldsymbol{q},\lambda'})_\tau &= \int_{\Sigma_\tau} d^3x C^3 u^\dagger_{\boldsymbol{p},\lambda} u_{\boldsymbol{q},\lambda'} \\ &= \int_{\Sigma_\tau} d^3x C^3 e^{-i(\boldsymbol{p}-\boldsymbol{q})\cdot \boldsymbol{x}} \xi^\dagger_\lambda \xi_{\lambda'} \left( f^*_p f_q + \lambda\lambda' g^*_p g_q \right) \\ &= (2\pi)^3 C^3 \delta^3(\boldsymbol{p}-\boldsymbol{q}) \delta_{\lambda,\lambda'} \left( |f_p|^2 + |g_p|^2 \right) \,. \end{aligned} \tag{2.71}$$

In the last step we have used the definition of the Dirac delta function and the orthonormality of the helicity bispinors. In a similar way it is easy to show that $(u_{\boldsymbol{p},\lambda}, v_{\boldsymbol{q},\lambda'})_\tau = 0$, $(v_{\boldsymbol{p},\lambda}, u_{\boldsymbol{q},\lambda'})_\tau = 0$ and

$$(v_{\boldsymbol{p},\lambda}, v_{\boldsymbol{q},\lambda'})_\tau = (2\pi)^3 C^3 \delta^3(\boldsymbol{p}-\boldsymbol{q}) \delta_{\lambda,\lambda'} \left( |f_p|^2 + |g_p|^2 \right) \,. \tag{2.72}$$

Eqs.(2.71) and (2.72) suggest that we adopt the following normalization:

$$|f_p|^2 + |g_p|^2 = \frac{1}{(2\pi C)^3} \tag{2.73}$$

in order that the orthonormality of the solutions is satisfied. The set of solutions (2.68) is complete:

$$\begin{aligned}&\sum_\lambda \left( u_{\boldsymbol{p},\lambda} u^\dagger_{\boldsymbol{p},\lambda} + v_{\boldsymbol{p},\lambda} v^\dagger_{\boldsymbol{p},\lambda} \right) \\ &= \sum_\lambda \left[ \begin{pmatrix} f_p \xi_\lambda \\ g_p \lambda \xi_\lambda \end{pmatrix} \begin{pmatrix} f^*_p \xi^\dagger_\lambda & g^*_p \lambda \xi^\dagger_\lambda \end{pmatrix} + \begin{pmatrix} g^*_p \xi_\lambda \\ -f^*_p \lambda \xi_\lambda \end{pmatrix} \begin{pmatrix} g_p \xi^\dagger_\lambda & -f_p \lambda \xi^\dagger_\lambda \end{pmatrix} \right] \\ &= \sum_\lambda \xi_\lambda \xi^\dagger_\lambda \begin{pmatrix} |f_p|^2 + |g_p|^2 & 0 \\ 0 & |f_p|^2 + |g_p|^2 \end{pmatrix} = \frac{1}{(2\pi C)^3} \begin{pmatrix} \mathbb{I} & 0 \\ 0 & \mathbb{I} \end{pmatrix} \,. \end{aligned} \tag{2.74}$$

In the last step we have used the completeness of the helicity basis $\sum_\lambda \xi_\lambda \xi^\dagger_\lambda = \mathbb{I}$, with $\mathbb{I}$ the $2 \times 2$ identity matrix, and the normalization condition (2.73). Eq.(2.74) shows that the set of solutions (2.68) provides a basis not only for the solution space of the Dirac equation, but also for the space of 4-spinors.

The system of equations (2.69) can be further simplified by introducing the functions

$$\phi_p = C^{\frac{3}{2}} f_p \quad \gamma_p = C^{\frac{3}{2}} g_p \tag{2.75}$$

since then the system becomes

$$\begin{aligned}\partial_\tau \phi_p &= -imC\phi_p - ip\gamma_p \\ \partial_\tau \gamma_p &= imC\gamma_p - ip\phi_p \\ \partial_\tau \phi_p^* &= imC\phi_p^* + ip\gamma_p^* \\ \partial_\tau \gamma_p^* &= -imC\gamma_p^* + ip\phi_p^*\end{aligned}$$

and the normalization condition (2.73) becomes

$$|\phi_p|^2 + |\gamma_p|^2 = \frac{1}{(2\pi)^3}\,. \tag{2.76}$$

The first two of Eqs.(2.76) can be combined to give two second order equation for $\phi_p$

$$\partial_\tau^2 \phi_p + \left(im\partial_\tau C + p^2 + m^2 C^2\right)\phi_p = 0\,. \tag{2.77}$$

In the same way, we can obtain a second-order equation for $\phi_p^*$.

Notice that for each $\lambda = \pm 1$, the quantity $\xi_\lambda^\dagger(\hat{p})\sigma_i\xi_\lambda(\hat{p})$ is an odd function of $p_i$, for $i = 1, 2, 3$. In particular, $\xi_\lambda^\dagger(\hat{p})\sigma_i\xi_\lambda(\hat{p})$ changes sign when the momentum is reversed $\boldsymbol{p} \to -\boldsymbol{p}$.
**Proof:** The statement can be proven by direct calculation. Letting $\theta_p$ and $\phi_p$ denote the polar angles of $\hat{p}$, for the $\lambda = +1$ case, we have

$$\begin{aligned}\xi_+^\dagger\sigma_1\xi_+ &= \begin{pmatrix} e^{i\frac{\phi_p}{2}}\cos(\frac{\theta_p}{2}) & e^{-i\frac{\phi_p}{2}}\sin(\frac{\theta_p}{2})\end{pmatrix}\begin{pmatrix}0 & 1\\ 1 & 0\end{pmatrix}\begin{pmatrix} e^{-i\frac{\phi_p}{2}}\cos(\frac{\theta_p}{2}) \\ e^{i\frac{\phi_p}{2}}\sin(\frac{\theta_p}{2})\end{pmatrix} \\ &= \cos(\frac{\theta_p}{2})\sin(\frac{\theta_p}{2})\left(e^{i\phi_p} + e^{-i\phi_p}\right) = \sin(\theta_p)\cos(\phi_p) = \frac{p_1}{p}\end{aligned} \tag{2.78}$$

$$\begin{aligned}\xi_+^\dagger\sigma_2\xi_+ &= \begin{pmatrix} e^{i\frac{\phi_p}{2}}\cos(\frac{\theta_p}{2}) & e^{-i\frac{\phi_p}{2}}\sin(\frac{\theta_p}{2})\end{pmatrix}\begin{pmatrix}0 & -i\\ i & 0\end{pmatrix}\begin{pmatrix} e^{-i\frac{\phi_p}{2}}\cos(\frac{\theta_p}{2}) \\ e^{i\frac{\phi_p}{2}}\sin(\frac{\theta_p}{2})\end{pmatrix} \\ &= \cos(\frac{\theta_p}{2})\sin(\frac{\theta_p}{2})\left(ie^{-i\phi_p} - ie^{i\phi_p}\right) = \sin(\theta_p)\sin(\phi_p) = \frac{p_2}{p}\end{aligned} \tag{2.79}$$

$$\begin{aligned}\xi_+^\dagger\sigma_3\xi_+ &= \begin{pmatrix} e^{i\frac{\phi_p}{2}}\cos(\frac{\theta_p}{2}) & e^{-i\frac{\phi_p}{2}}\sin(\frac{\theta_p}{2})\end{pmatrix}\begin{pmatrix}1 & 0\\ 0 & -1\end{pmatrix}\begin{pmatrix} e^{-i\frac{\phi_p}{2}}\cos(\frac{\theta_p}{2}) \\ e^{i\frac{\phi_p}{2}}\sin(\frac{\theta_p}{2})\end{pmatrix} \\ &= \cos^2(\frac{\theta_p}{2}) - \sin^2(\frac{\theta_p}{2}) = \cos(\theta_p) = \frac{p_3}{p}\end{aligned} \tag{2.80}$$

similarly, for the $\lambda = -1$ case we have

$$\begin{aligned}\xi_-^\dagger\sigma_1\xi_- &= \begin{pmatrix} e^{i\frac{\phi_p}{2}}\sin(\frac{\theta_p}{2}) & -e^{-i\frac{\phi_p}{2}}\cos(\frac{\theta_p}{2})\end{pmatrix}\begin{pmatrix}0 & 1\\ 1 & 0\end{pmatrix}\begin{pmatrix} e^{-i\frac{\phi_p}{2}}\sin(\frac{\theta_p}{2}) \\ -e^{i\frac{\phi_p}{2}}\cos(\frac{\theta_p}{2})\end{pmatrix} \\ &= -\cos(\frac{\theta_p}{2})\sin(\frac{\theta_p}{2})\left(e^{i\phi_p} + e^{-i\phi_p}\right) = -\sin(\theta_p)\cos(\phi_p) = \frac{-p_1}{p}\end{aligned} \tag{2.81}$$

$$\begin{aligned}\xi_-^\dagger\sigma_2\xi_- &= \begin{pmatrix} e^{i\frac{\phi_p}{2}}\sin(\frac{\theta_p}{2}) & -e^{-i\frac{\phi_p}{2}}\cos(\frac{\theta_p}{2})\end{pmatrix}\begin{pmatrix}0 & -i\\ i & 0\end{pmatrix}\begin{pmatrix} e^{-i\frac{\phi_p}{2}}\sin(\frac{\theta_p}{2}) \\ -e^{i\frac{\phi_p}{2}}\cos(\frac{\theta_p}{2})\end{pmatrix} \\ &= -\cos(\frac{\theta_p}{2})\sin(\frac{\theta_p}{2})\left(ie^{-i\phi_p} - ie^{i\phi_p}\right) = -\sin(\theta_p)\sin(\phi_p) = \frac{-p_2}{p}\end{aligned} \tag{2.82}$$

$$
\begin{aligned}
\xi_-^\dagger \sigma_3 \xi_- &= \begin{pmatrix} e^{i\frac{\phi_p}{2}}\sin(\frac{\theta_p}{2}) & -e^{-i\frac{\phi_p}{2}}\cos(\frac{\theta_p}{2}) \end{pmatrix} \begin{pmatrix} 1 & 0 \\ 0 & -1 \end{pmatrix} \begin{pmatrix} e^{-i\frac{\phi_p}{2}}\sin(\frac{\theta_p}{2}) \\ -e^{i\frac{\phi_p}{2}}\cos(\frac{\theta_p}{2}) \end{pmatrix} \\
&= -\cos^2(\frac{\theta_p}{2}) + \sin^2(\frac{\theta_p}{2}) = -\cos(\theta_p) = \frac{-p_3}{p} \,. \qquad (2.83)
\end{aligned}
$$

This result can be summarized in the equation

$$
\xi_\lambda^\dagger \boldsymbol{\sigma} \xi_\lambda = \frac{\lambda \boldsymbol{p}}{p} \,. \qquad (2.84)
$$

### 2.2.2 The Auxiliary Tensor

We here introduce a bilinear form of the solutions of the Dirac Equation, which is convenient for the study of the energy-momentum tensor. Given two solutions $A, B$ of the Dirac equation, we define the auxiliary tensor as

$$
L_{\mu\nu}(A,B) = \bar{A}\tilde{\gamma}_\mu(x) D_\nu B + \bar{A}\tilde{\gamma}_\nu(x) D_\mu B - D_\mu \bar{A}\tilde{\gamma}_\nu(x) B - D_\nu \bar{A}\tilde{\gamma}_\mu(x) B \,. \qquad (2.85)
$$

The tensor (2.85) enjoys a number of useful properties. The first property is obvious from the definition: $L_{\mu\nu}(A,B) = L_{\nu\mu}(A,B)$ for any $A, B$. The second property can be seen at once by comparing the definition (2.85) with the form of the energy-momentum tensor (2.65). Since $T_{\mu\nu}$ is real, we immediately deduce that $L_{\mu\nu}(A,A)$ is pure imaginary for each solution $A$. The third property can be easily deduced by tracing the definition:

$$
L^\mu_\mu(A,B) = g^{\mu\nu} L_{\mu\nu}(A,B) = 2\left(\bar{A}\tilde{\gamma}^\mu(x) D_\mu B - D_\mu \bar{A}\tilde{\gamma}_\mu(x) B\right) = -4im\bar{A}B \qquad (2.86)
$$

where we have used the Dirac equation and its adjoint in the last step. Next we give a more explicit form for $L_{\tau\tau}(A,B)$. We can write

$$
\begin{aligned}
L_{\tau\tau}(A,B) &= 2\left(\bar{A}\tilde{\gamma}_\tau(x) D_\tau B - D_\tau \bar{A}\tilde{\gamma}_\tau(x) B\right) = 2C\left(\bar{A}\gamma^0 \partial_\tau B - \partial_\tau \bar{A}\gamma^0 B\right) \\
&= 2C\left(A^\dagger \partial_\tau B - \partial_\tau A^\dagger B\right) \,. \qquad (2.87)
\end{aligned}
$$

In particular we are interested in the auxiliary tensors $L_{\tau\tau}(u(v), u(v))$ and the traces $L^\mu_\mu(u(v), u(v))$ computed on the solutions (2.68). For the traces we have

$$
\begin{aligned}
L^\mu_\mu(u_{\boldsymbol{p},\lambda}, u_{\boldsymbol{p},\lambda}) &= -4im\bar{u}_{\boldsymbol{p},\lambda} u_{\boldsymbol{p},\lambda} = -4im u^\dagger_{\boldsymbol{p},\lambda}\gamma^0 u_{\boldsymbol{p},\lambda} \\
&= -4im \begin{pmatrix} f_p^* \xi_\lambda^\dagger & g_p^* \lambda \xi_\lambda^\dagger \end{pmatrix} \begin{pmatrix} \mathbb{I} & 0 \\ 0 & -\mathbb{I} \end{pmatrix} \begin{pmatrix} f_p \xi_\lambda \\ g_p \lambda \xi_\lambda \end{pmatrix} \\
&= -4im(|f_p|^2 - |g_p|^2) = -4imC^{-3}\left(|\phi_p|^2 - |\gamma_p|^2\right) \qquad (2.88)
\end{aligned}
$$

$$
\begin{aligned}
L^\mu_\mu(u_{\boldsymbol{p},\lambda}, v_{\boldsymbol{p},\lambda}) &= -4im\bar{u}_{\boldsymbol{p},\lambda} v_{\boldsymbol{p},\lambda} = -4im u^\dagger_{\boldsymbol{p},\lambda}\gamma^0 v_{\boldsymbol{p},\lambda} \\
&= -4im \begin{pmatrix} f_p^* \xi_\lambda^\dagger & g_p^* \lambda \xi_\lambda^\dagger \end{pmatrix} \begin{pmatrix} \mathbb{I} & 0 \\ 0 & -\mathbb{I} \end{pmatrix} \begin{pmatrix} g_p^* \xi_\lambda \\ -f_p^* \lambda \xi_\lambda \end{pmatrix} \\
&= -8im f_p^* g_p^* = -8imC^{-3}\phi_p^* \gamma_p^* \qquad (2.89)
\end{aligned}
$$

$$\begin{aligned}
L^{\mu}_{\mu}(v_{\boldsymbol{p},\lambda}, u_{\boldsymbol{p},\lambda}) &= -4im\bar{v}_{\boldsymbol{p},\lambda} u_{\boldsymbol{p},\lambda} = -4im v^{\dagger}_{\boldsymbol{p},\lambda}\gamma^0 u_{\boldsymbol{p},\lambda} \\
&= -4im \begin{pmatrix} g_p \xi^{\dagger}_{\lambda} & -f_p\lambda\xi^{\dagger}_{\lambda}\end{pmatrix} \begin{pmatrix} \mathbb{I} & 0 \\ 0 & -\mathbb{I}\end{pmatrix} \begin{pmatrix} f_p\xi_{\lambda} \\ g_p\lambda\xi_{\lambda}\end{pmatrix} \\
&= -8imf_p g_p = -8imC^{-3}\phi_p\gamma_p = -\left(L^{\mu}_{\mu}(u_{\boldsymbol{p},\lambda}, v_{\boldsymbol{p},\lambda})\right)^* \qquad (2.90)
\end{aligned}$$

$$\begin{aligned}
L^{\mu}_{\mu}(v_{\boldsymbol{p},\lambda}, v_{\boldsymbol{p},\lambda}) &= -4im\bar{v}_{\boldsymbol{p},\lambda} v_{\boldsymbol{p},\lambda} = -4im v^{\dagger}_{\boldsymbol{p},\lambda}\gamma^0 v_{\boldsymbol{p},\lambda} \\
&= -4im \begin{pmatrix} g_p \xi^{\dagger}_{\lambda} & -f_p\lambda\xi^{\dagger}_{\lambda}\end{pmatrix} \begin{pmatrix} \mathbb{I} & 0 \\ 0 & -\mathbb{I}\end{pmatrix} \begin{pmatrix} g^*_p\xi_{\lambda} \\ -f^*_p\lambda\xi_{\lambda}\end{pmatrix} \\
&= -4im(|g_p|^2 - |f_p|^2) = -4imC^{-3}\left(|\gamma_p|^2 - |\phi_p|^2\right) \\
&= -L^{\mu}_{\mu}(u_{\boldsymbol{p},\lambda}, u_{\boldsymbol{p},\lambda}) \,. \qquad (2.91)
\end{aligned}$$

We then compute the $\tau\tau$ components

$$\begin{aligned}
L_{\tau\tau}(u_{\boldsymbol{p},\lambda}, u_{\boldsymbol{p},\lambda}) &= 2C\left[u^{\dagger}_{\boldsymbol{p},\lambda}\partial_\tau u_{\boldsymbol{p},\lambda} - \partial_\tau u^{\dagger}_{\boldsymbol{p},\lambda} u_{\boldsymbol{p},\lambda}\right] \\
&= 2C\left[\begin{pmatrix} f^*_p\xi^{\dagger}_{\lambda} & g^*_p\lambda\xi^{\dagger}_{\lambda}\end{pmatrix}\begin{pmatrix}\partial_\tau f_p\xi_\lambda \\ \partial_\tau g_p\lambda\xi_\lambda\end{pmatrix} - \begin{pmatrix}\partial_\tau f^*_p\xi^{\dagger}_{\lambda} & \partial_\tau g^*_p\lambda\xi^{\dagger}_{\lambda}\end{pmatrix}\begin{pmatrix} f_p\xi_\lambda \\ g_p\lambda\xi_\lambda\end{pmatrix}\right] \\
&= 2C\left[f^*_p\partial_\tau f_p - \partial_\tau f^*_p f_p + g^*_p\partial_\tau g_p - \partial_\tau g^*_p g_p\right] \\
&= 2C^{-2}\left[\phi^*_p\partial_\tau\phi_p - \partial_\tau\phi^*_p\phi_p + \gamma^*_p\partial_\tau\gamma_p - \partial_\tau\gamma^*_p\gamma_p\right] \qquad (2.92)
\end{aligned}$$

$$\begin{aligned}
&L_{\tau\tau}(u_{\boldsymbol{p},\lambda}, v_{\boldsymbol{p},\lambda}) = 2C\left[u^{\dagger}_{\boldsymbol{p},\lambda}\partial_\tau v_{\boldsymbol{p},\lambda} - \partial_\tau u^{\dagger}_{\boldsymbol{p},\lambda} v_{\boldsymbol{p},\lambda}\right] \\
&= 2C\left[\begin{pmatrix} f^*_p\xi^{\dagger}_{\lambda} & g^*_p\lambda\xi^{\dagger}_{\lambda}\end{pmatrix}\begin{pmatrix}\partial_\tau g^*_p\xi_\lambda \\ -\partial_\tau f^*_p\lambda\xi_\lambda\end{pmatrix} - \begin{pmatrix}\partial_\tau f^*_p\xi^{\dagger}_{\lambda} & \partial_\tau g^*_p\lambda\xi^{\dagger}_{\lambda}\end{pmatrix}\begin{pmatrix} g^*_p\xi_\lambda \\ -f^*_p\lambda\xi_\lambda\end{pmatrix}\right] \\
&= 2C\left[f^*_p\partial_\tau g^*_p - \partial_\tau f^*_p g^*_p - g^*_p\partial_\tau f^*_p + \partial_\tau g^*_p f^*_p\right] \\
&= 4C^{-2}\left[\phi^*_p\partial_\tau\gamma^*_p - \gamma^*_p\partial_\tau\phi^*_p\right] \;; \qquad (2.93)
\end{aligned}$$

$$L_{\tau\tau}(v_{\boldsymbol{p},\lambda}, u_{\boldsymbol{p},\lambda}) = -\left(L_{\tau\tau}(u_{\boldsymbol{p},\lambda}, v_{\boldsymbol{p},\lambda})\right)^* \qquad (2.94)$$

$$L_{\tau\tau}(v_{\boldsymbol{p},\lambda}, v_{\boldsymbol{p},\lambda}) = -L_{\tau\tau}(u_{\boldsymbol{p},\lambda}, u_{\boldsymbol{p},\lambda}) \,. \qquad (2.95)$$

Notice that as a consequence $L_{\tau\tau}(u_{\boldsymbol{p},\lambda}, v_{\boldsymbol{p},\lambda}) = 0$ if and only if $\gamma_p \propto \phi_p$. This is the case, for instance, in Minkowski spacetime, where $\phi_p \propto \gamma_p \propto e^{-i\omega_p t}$. For a general $C$, the proportionality does not hold, and this has dramatic consequences on the vacuum of the theory (eventually leading to particle creation).

In addition one can show that $L_{\tau i}(u(v), u(v))$ is an odd function of the momentum $\boldsymbol{p}$ and that $L_{ij}(u(v), u(v))$ is an odd function with respect to both $p_i$ and $p_j$. The proof requires a lengthy but straightforward calculation:

$$
\begin{aligned}
L_{\tau i}(u_{\boldsymbol{p},\lambda}, u_{\boldsymbol{p},\lambda}) =& \bar{u}_{\boldsymbol{p},\lambda}\tilde{\gamma}_\tau D_i u_{\boldsymbol{p},\lambda} + \bar{u}_{\boldsymbol{p},\lambda}\tilde{\gamma}_i D_\tau u_{\boldsymbol{p},\lambda} - D_i\bar{u}_{\boldsymbol{p},\lambda}\tilde{\gamma}_\tau u_{\boldsymbol{p},\lambda} - D_\tau\bar{u}_{\boldsymbol{p},\lambda}\tilde{\gamma}_i u_{\boldsymbol{p},\lambda} \\
=& \, C u^\dagger_{\boldsymbol{p},\lambda}\left(\partial_i + \frac{1}{8}\omega_i^{A,B}[\gamma_A,\gamma_B]\right)u_{\boldsymbol{p},\lambda} - C u^\dagger_{\boldsymbol{p},\lambda}\gamma^0\gamma^i\partial_\tau u_{\boldsymbol{p},\lambda} \\
&- C\left(\partial_i u^\dagger_{\boldsymbol{p},\lambda}\gamma^0 - u^\dagger_{\boldsymbol{p},\lambda}\frac{\gamma^0}{8}\omega_i^{A,B}[\gamma_A,\gamma_B]\right)\gamma^0 u_{\boldsymbol{p},\lambda} + C\partial_\tau u^\dagger_{\boldsymbol{p},\lambda}\gamma^0\gamma^i u_{\boldsymbol{p},\lambda} \\
=& \, C u^\dagger_{\boldsymbol{p},\lambda}\left(ip_i + \frac{\partial_\tau C}{2C}\begin{pmatrix}0 & \sigma_i\\ \sigma_i & 0\end{pmatrix}\right)u_{\boldsymbol{p},\lambda} - C u^\dagger_{\boldsymbol{p},\lambda}\begin{pmatrix}0 & \sigma_i\\ \sigma_i & 0\end{pmatrix}\partial_\tau u_{\boldsymbol{p},\lambda} \\
&- C u^\dagger_{\boldsymbol{p},\lambda}\left(-ip_i + \frac{\partial_\tau C}{2C}\begin{pmatrix}0 & \sigma_i\\ \sigma_i & 0\end{pmatrix}\right)u_{\boldsymbol{p},\lambda} + C\partial_\tau u^\dagger_{\boldsymbol{p},\lambda}\begin{pmatrix}0 & \sigma_i\\ \sigma_i & 0\end{pmatrix}u_{\boldsymbol{p},\lambda} \\
=& \, 2ip_i C u^\dagger_{\boldsymbol{p},\lambda}u_{\boldsymbol{p},\lambda} + C\left[\partial_\tau u^\dagger_{\boldsymbol{p},\lambda}\begin{pmatrix}0 & \sigma_i\\ \sigma_i & 0\end{pmatrix}u_{\boldsymbol{p},\lambda} - u^\dagger_{\boldsymbol{p},\lambda}\begin{pmatrix}0 & \sigma_i\\ \sigma_i & 0\end{pmatrix}\partial_\tau u_{\boldsymbol{p},\lambda}\right] \\
=& \, 2ip_i C\left[|f_p|^2 + |g_p|^2\right] + C\lambda\left[\partial_\tau f_p^* g_p + \partial_\tau g_p^* f_p - f_p^*\partial_\tau g_p - g_p^*\partial_\tau f_p\right]\xi^\dagger_\lambda\sigma_i\xi_\lambda \\
=& \, p_i\left\{\frac{i}{\pi^3 C^2} + \frac{\lambda}{p}\left[C\left(\partial_\tau f_p^* g_p + \partial_\tau g_p^* f_p - c.c.\right)\right]\right\}\,.
\end{aligned}
\tag{2.96}
$$

In the last step, we have made use of the normalization condition (2.73) and the property (2.84). As it is evident from Eq.(2.96), each $\tilde{\gamma}_i$ factor and each spatial derivative $\partial_i$ brings along a factor $p_i$. Then for each $a, b = u_{\boldsymbol{p},\lambda}, v_{\boldsymbol{p},\lambda}$ one has

$$
L_{\tau i}(a,b) = p_i h_{a,b}(p)\,, \tag{2.97}
$$

with $h_{a,b}(p)$ a function of the modulus $p$ alone. In particular

$$
L_{\tau i}(u_{\boldsymbol{p},\lambda}, v_{\boldsymbol{p},\lambda}) = 0\,. \tag{2.98}
$$

Similarly, for each $a, b = u_{\boldsymbol{p},\lambda}, v_{\boldsymbol{p},\lambda}$

$$
L_{ij}(a,b) = p_i p_j l_{a,b}(p)\,, \tag{2.99}
$$

with $l_{a,b}(p)$ a function of the modulus $p$ alone.

### 2.2.3 Quantization of flavor fields

In the following we adapt the flavor field quantization of the previous sections to the specific case of spatially flat FLRW metrics, computing the energy momentum tensor explicitly.

#### Dirac field

Since the set of solutions (2.68) $\{u_{\boldsymbol{p},\lambda}, v_{\boldsymbol{p},\lambda}\}_{\boldsymbol{p},\lambda}$ is complete, any solution of the (linear) Dirac equation can be written as a linear combination of these modes. In particular, this is true for the Dirac field: $\psi(x) = \sum_\lambda \int d^3p\left(A_{\boldsymbol{p},\boldsymbol{\lambda}} u_{\boldsymbol{p},\lambda} + B^*_{-\boldsymbol{p},\lambda} v_{\boldsymbol{p},\lambda}\right)$. In this equation, the notation $B^*_{-\boldsymbol{p},\lambda}$ is chosen to remark that $v_{\boldsymbol{p},\lambda}$ describes an antiparticle with momentum $-\boldsymbol{p}$. Notice that all the spacetime dependence is in the modes, while the coefficients do not depend on any of the spacetime coordinates.

Quantization is achieved, as usual, by promoting the field, and thus the expansion coefficients to operators

$$\psi(x) = \sum_{\lambda} \int d^3p \left( A_{\boldsymbol{p},\lambda} u_{\boldsymbol{p},\lambda} + B^{\dagger}_{-\boldsymbol{p},\lambda} v_{\boldsymbol{p},\lambda} \right) . \tag{2.100}$$

and imposing the canonical anticommutation relations. The momentum conjugate to $\psi(x)$, according to the Lagrangian (2.64), is $\pi_{\psi}(x) = iC^3 \psi^{\dagger}(x)$ , so that the canonical anticommutation relations to be imposed are

$$\{\psi_A(\tau, \boldsymbol{x}), \pi_{\psi B}(\tau, \boldsymbol{x'})\} = iC^3 \{\psi_A(\tau, \boldsymbol{x}), \psi^{\dagger}_B(\tau, \boldsymbol{x'})\} = i\delta_{AB}\delta^3(\boldsymbol{x} - \boldsymbol{x'}) . \tag{2.101}$$

Here the indices $A, B$ are referred to the spinor components $A, B = 1, 2, 3, 4$. It is easy to show that the relations (2.101) are satisfied if one imposes the following anticommutation relations on the coefficients:

$$\{A_{\boldsymbol{p},\lambda}, A^{\dagger}_{\boldsymbol{q},\lambda'}\} = \{B_{\boldsymbol{p},\lambda}, B^{\dagger}_{\boldsymbol{q},\lambda'}\} = \delta_{\lambda\lambda'}\delta^3(\boldsymbol{p} - \boldsymbol{q}) \tag{2.102}$$

with all the other anticommutators vanishing. Indeed

$$\begin{aligned}
&\{\psi_A(\tau, \boldsymbol{x}), \pi_{\psi B}(\tau, \boldsymbol{x'})\} = \\
&iC^3 \sum_{\lambda,\lambda'} \int d^3p \int d^3q \left[ \{A_{\boldsymbol{p},\lambda}, A^{\dagger}_{\boldsymbol{q},\lambda'}\} \left( u_{\boldsymbol{p},\lambda} u^{\dagger}_{\boldsymbol{q},\lambda'} \right)_{AB} + \{B^{\dagger}_{-\boldsymbol{p},\lambda}, B_{-\boldsymbol{q},\lambda'}\} \left( v_{\boldsymbol{p},\lambda} v^{\dagger}_{\boldsymbol{q},\lambda'} \right)_{AB} \right] \\
&= iC^3 \sum_{\lambda} \int d^3p \left[ \left( u_{\boldsymbol{p},\lambda}(\tau, \boldsymbol{x}) u^{\dagger}_{\boldsymbol{p},\lambda}(\tau, \boldsymbol{x'}) \right)_{AB} + \left( v_{\boldsymbol{p},\lambda}(\tau, \boldsymbol{x}) v^{\dagger}_{\boldsymbol{p},\lambda}(\tau, \boldsymbol{x'}) \right)_{AB} \right] \\
&= iC^3 \sum_{\lambda} \int d^3p e^{i\boldsymbol{p}\cdot(\boldsymbol{x}-\boldsymbol{x'})} \left[ \left( u_{\boldsymbol{p},\lambda}(\tau, \boldsymbol{0}) u^{\dagger}_{\boldsymbol{p},\lambda}(\tau, \boldsymbol{0}) \right)_{AB} + \left( v_{\boldsymbol{p},\lambda}(\tau, \boldsymbol{0}) v^{\dagger}_{\boldsymbol{p},\lambda}(\tau, \boldsymbol{0}) \right)_{AB} \right] \\
&= iC^3 \frac{1}{(2\pi)^3 C^3} \delta_{AB} \int d^3p e^{i\boldsymbol{p}\cdot(\boldsymbol{x}-\boldsymbol{x'})} \\
&= i\delta_{AB}\delta^3(\boldsymbol{x} - \boldsymbol{x'}) .
\end{aligned} \tag{2.103}$$

In the fourth step we have made use of the completeness relation (Eq.(2.74)), writing the $4 \times 4$ identity matrix explicitly as $\delta_{AB}$.

The field expansion (2.100) defines the vacuum state $|0\rangle$ as the state annihilated by all the annihilation operators $A_{\boldsymbol{p},\lambda} |0\rangle = B_{\boldsymbol{p},\lambda} |0\rangle = 0$ , $\forall \boldsymbol{p}, \lambda$. It is important to stress that the definition of the vacuum state depends critically on the choice of the field modes. Specifically, its particle interpretation is tied to the boundary conditions specified on the solutions (2.68). Another kind of field expansion is possible if one assumes a specific time evolution of the modes, as is done within the adiabatic approximation (see, e.g., [64]). Contrary to our field expansion (2.100), the annihilation operators (and thus the vacuum) are thereby endowed with a specific time dependence. The expansion (2.100), instead, does not assume any particular time dependence and is, therefore, more general. The two expansions can be made to coincide at a given time. The quantized energy-momentum tensor is obtained by inserting the field expansion in the definition (2.65):

$$
\begin{aligned}
T_{\mu\nu} &= \frac{i}{2}\sum_{\lambda,\lambda'}\int d^3p \int d^3q \Big\{ \left(A^\dagger_{\boldsymbol{p},\lambda}\bar{u}_{\boldsymbol{p},\lambda} + B_{-\boldsymbol{p},\lambda}\bar{v}_{\boldsymbol{p},\lambda}\right)\tilde{\gamma}_\mu D_\nu \left(A_{\boldsymbol{q},\lambda'}u_{\boldsymbol{q},\lambda'} + B^\dagger_{-\boldsymbol{q},\lambda'}v_{\boldsymbol{q},\lambda'}\right) \\
&+ \left(A^\dagger_{\boldsymbol{p},\lambda}\bar{u}_{\boldsymbol{p},\lambda} + B_{-\boldsymbol{p},\lambda}\bar{v}_{\boldsymbol{p},\lambda}\right)\tilde{\gamma}_\nu D_\mu \left(A_{\boldsymbol{q},\lambda'}u_{\boldsymbol{q},\lambda'} + B^\dagger_{-\boldsymbol{q},\lambda'}v_{\boldsymbol{q},\lambda'}\right) \\
&- D_\mu \left(A^\dagger_{\boldsymbol{p},\lambda}\bar{u}_{\boldsymbol{p},\lambda} + B_{-\boldsymbol{p},\lambda}\bar{v}_{\boldsymbol{p},\lambda}\right)\tilde{\gamma}_\nu \left(A_{\boldsymbol{q},\lambda'}u_{\boldsymbol{q},\lambda'} + B^\dagger_{-\boldsymbol{q},\lambda'}v_{\boldsymbol{q},\lambda'}\right) \\
&- D_\nu \left(A^\dagger_{\boldsymbol{p},\lambda}\bar{u}_{\boldsymbol{p},\lambda} + B_{-\boldsymbol{p},\lambda}\bar{v}_{\boldsymbol{p},\lambda}\right)\tilde{\gamma}_\mu \left(A_{\boldsymbol{q},\lambda'}u_{\boldsymbol{q},\lambda'} + B^\dagger_{-\boldsymbol{q},\lambda'}v_{\boldsymbol{q},\lambda'}\right) \Big\} \\
&= \frac{i}{2}\sum_{\lambda,\lambda'}\int d^3p \int d^3q \{ A^\dagger_{\boldsymbol{p},\lambda}A_{\boldsymbol{q},\lambda'}L_{\mu\nu}(u_{\boldsymbol{p},\lambda}, u_{\boldsymbol{q},\lambda'}) + A^\dagger_{\boldsymbol{p},\lambda}B^\dagger_{-\boldsymbol{q},\lambda'}L_{\mu\nu}(u_{\boldsymbol{p},\lambda}, v_{\boldsymbol{q},\lambda'}) \\
&\quad + B_{-\boldsymbol{p},\lambda}A_{\boldsymbol{q},\lambda'}L_{\mu\nu}(v_{\boldsymbol{p},\lambda}, u_{\boldsymbol{q},\lambda'}) + B_{-\boldsymbol{p},\lambda}B^\dagger_{-\boldsymbol{q},\lambda'}L_{\mu\nu}(v_{\boldsymbol{p},\lambda}, v_{\boldsymbol{q},\lambda'})\}\,, 
\end{aligned} \tag{2.104}
$$

where we have used the definition (2.85) of $L_{\mu\nu}$. The Hamiltonian density corresponds to the component $T^\tau_\tau$ of the above equation. It follows immediately that the vacuum is not an eigenstate of the Hamiltonian unless $L^\tau_\tau(v_{\boldsymbol{p},\lambda}, u_{\boldsymbol{q},\lambda'}) = 0$, due to the $A^\dagger_{\boldsymbol{p},\lambda}B^\dagger_{-\boldsymbol{q},\lambda'}$ term. In particular, the vacuum is unstable under the creation of particle-antiparticle pairs with opposite momentum, a result known from the previous analyses. This is a reflection of the non-invariance under time translations. On the other hand, from the relation: $L_{\tau i}(u_{\boldsymbol{p},\lambda}, v_{\boldsymbol{p},\lambda}) = 0$ (cfr. Eq.(2.98)), it is clear that the vacuum respects the residual translational symmetry in the spatial coordinates, i.e. $\boldsymbol{P}\,|0\rangle = 0$.

### The flavor fields

Up to now, our considerations have been restricted to a single Dirac field of definite mass. To introduce the flavor fields, we follow the procedure outlined in the previous sections and start by introducing two Dirac fields with distinct masses $m_1, m_2$. We consider two flavors for simplicity but the analysis can be easily generalized to three flavors. The theory of two free massive Dirac fields is just the product of two copies of the theory for a single Dirac field. All the relations discussed above remain valid, provided we assign a new index $j = 1, 2$ to all the quantities involved $\psi_j, m_j, A_{\boldsymbol{p},\lambda;j}, u_{\boldsymbol{p},\lambda;j}$ and so on. All the previous relations are index-wise valid for $j = 1, 2$. The mass vacuum that we now denote explicitly as $|0_M\rangle$ is annihilated by all the annihilators for each index $j$. The total energy-momentum tensor is simply the sum of two copies of Eq.(2.104), one for each $j$. We also require that each mode of the field 1 is related to the corresponding mode of the field 2, with the same labels $\boldsymbol{p}, \lambda$ by the substitution $m_1 \to m_2$, and vice-versa.

The flavor fields are then introduced via the rotation

$$
\begin{aligned}
\psi_e(x) &= \cos(\theta)\psi_1(x) + \sin(\theta)\psi_2(x) \\
\psi_\mu(x) &= \cos(\theta)\psi_2(x) - \sin(\theta)\psi_1(x)\,,
\end{aligned} \tag{2.105}
$$

where $\theta$ is the two-flavor mixing angle. At the quantum level, the rotation is employed by the mixing generator

$$
\mathcal{I}_\theta(\tau) = exp\left\{\theta\left[(\psi_1, \psi_2)_\tau - (\psi_2, \psi_1)_\tau\right]\right\}\,. \tag{2.106}
$$

Here $(\psi_2, \psi_1)_\tau$ stands for the scalar product at the $\tau$ hypersurface (recall that for fields of distinct masses the product *does* depend on $\tau$). The flavor fields are then

$$\begin{aligned} \psi_e(x) &= \mathcal{I}_\theta^{-1}\psi_1(x)\mathcal{I}_\theta \\ \psi_\mu(x) &= \mathcal{I}_\theta^{-1}\psi_2(x)\mathcal{I}_\theta \, . \end{aligned} \tag{2.107}$$

The action of the generator also defines the flavor annihilators ($A_{\mathbf{p},\lambda;e} = \mathcal{I}_\theta^{-1}A_{\mathbf{p},\lambda;1}\mathcal{I}_\theta$ and similar) and the flavor vacuum, as

$$|0_F\rangle = \mathcal{I}_\theta^{-1}\,|0_M\rangle \ . \tag{2.108}$$

Notice that, contrary to the mass vacuum, the flavor vacuum has an explicit $\tau$ dependence. The terminology 'flavor vacuum' is justified in that this state is annihilated by all the flavor annihilators.

### 2.2.4 VEV of the energy-momentum tensor on the flavor vacuum

We are specifically interested in the contributions that flavor mixing induces on the energy-momentum tensor. More precisely, we ask what is the expectation value of the energy-momentum tensor on the state corresponding to the absence of flavor neutrinos at a given time $|O_F(\tau_0)\rangle$. We stress that in this calculation, we assume a fixed but arbitrary expansion of the mass fields, and therefore a fixed but arbitrary choice of the mass vacuum. The effect of a change in the mass representation on the flavor fields is known from the previous sections, and once the result is computed for a given representation, one can implement the adequate transformations to get the result in other mass representations. Likewise, we keep the time $\tau_0$ arbitrary and distinct from the time argument $\tau$ of the energy-momentum tensor. The quantity we wish to compute is then

$$\mathbb{T}_{\mu\nu} = \langle 0_F(\tau_0)|\, T_{\mu\nu}\, |0_F(\tau_0)\rangle \ , \tag{2.109}$$

where $T_{\mu\nu}$ is given by Eq.(2.104). Explicitly

$$\begin{aligned} T_{\mu\nu} &= \frac{i}{2}\sum_{j=1,2}\sum_{\lambda,\lambda'}\int d^3p \int d^3q \{A^\dagger_{\mathbf{p},\lambda;j}A_{\mathbf{q},\lambda';j}L_{\mu\nu}(u_{\mathbf{p},\lambda;j}, u_{\mathbf{q},\lambda';j}) \\ &+ A^\dagger_{\mathbf{p},\lambda;j}B^\dagger_{-\mathbf{q},\lambda';j}L_{\mu\nu}(u_{\mathbf{p},\lambda;j}, v_{\mathbf{q},\lambda';j}) + B_{-\mathbf{p},\lambda;j}A_{\mathbf{q},\lambda';j}L_{\mu\nu}(v_{\mathbf{p},\lambda;j}, u_{\mathbf{q},\lambda';j}) \\ &+ B_{-\mathbf{p},\lambda;j}B^\dagger_{-\mathbf{q},\lambda';j}L_{\mu\nu}(v_{\mathbf{p},\lambda;j}, v_{\mathbf{q},\lambda';j})\} \, . \end{aligned} \tag{2.110}$$

We remark that the only sensible definition for the energy-momentum tensor is the one (2.104) in terms of the fields with definite mass. Let us analyze the typical term in equation (2.109). It has the form

$$\langle 0_F(\tau_0)|\, A^\dagger_{\mathbf{p},\lambda;1}A_{\mathbf{q},\lambda';1}\, |0_F(\tau_0)\rangle \ . \tag{2.111}$$

Using the definition of the flavor vacuum this equals

$$\begin{aligned} &\langle 0_M|\, \mathcal{I}_\theta(\tau_0)A^\dagger_{\mathbf{p},\lambda;1}A_{\mathbf{q},\lambda';1}\mathcal{I}_\theta^{-1}(\tau_0)\, |0_M\rangle = \\ &\langle 0_M|\, \mathcal{I}_\theta(\tau_0)A^\dagger_{\mathbf{p},\lambda;1}\mathcal{I}_\theta^{-1}(\tau_0)\mathcal{I}_\theta(\tau_0)A_{\mathbf{q},\lambda';1}\mathcal{I}_\theta^{-1}(\tau_0)\, |0_M\rangle = \\ &\langle 0_M|\, \mathcal{I}_{-\theta}^{-1}(\tau_0)A^\dagger_{\mathbf{p},\lambda;1}\mathcal{I}_{-\theta}(\tau_0)\mathcal{I}_{-\theta}^{-1}(\tau_0)A_{\mathbf{q},\lambda';1}\mathcal{I}_{-\theta}(\tau_0)\, |0_M\rangle \ , \end{aligned} \tag{2.112}$$

where we have used that (eq. 2.106) $\mathcal{I}_\theta^{-1} = \mathcal{I}_{-\theta}$. Now the operator $\mathcal{I}_{-\theta}^{-1}(\tau_0)A_{\mathbf{p},\lambda;1}\mathcal{I}_{-\theta}(\tau_0)$ is just the mass annihilator transformed according to a mixing transformation with angle $-\theta$.

Knowing the transformation rule in terms of $\theta$ we can easily write down the transformed operators:

$$
\begin{aligned}
\mathcal{I}^{-1}_{-\theta}(\tau_0)A_{\boldsymbol{p},\lambda;1}\mathcal{I}_{-\theta}(\tau_0) &= \cos(\theta)A_{\boldsymbol{p},\lambda;1} - \sin(\theta)\left(\Lambda^*_{\boldsymbol{p}}(\tau_0)A_{\boldsymbol{p},\lambda;2} + \Xi_{\boldsymbol{p}}(\tau_0)B^\dagger_{-\boldsymbol{p},\lambda;2}\right) \\
\mathcal{I}^{-1}_{-\theta}(\tau_0)A_{\boldsymbol{p},\lambda;2}\mathcal{I}_{-\theta}(\tau_0) &= \cos(\theta)A_{\boldsymbol{p},\lambda;2} + \sin(\theta)\left(\Lambda_{\boldsymbol{p}}(\tau_0)A_{\boldsymbol{p},\lambda;1} - \Xi_{\boldsymbol{p}}(\tau_0)B^\dagger_{-\boldsymbol{p},\lambda;1}\right) \\
\mathcal{I}^{-1}_{-\theta}(\tau_0)B_{-\boldsymbol{p},\lambda;1}\mathcal{I}_{-\theta}(\tau_0) &= \cos(\theta)B_{-\boldsymbol{p},\lambda;1} - \sin(\theta)\left(\Lambda^*_{\boldsymbol{p}}(\tau_0)B_{-\boldsymbol{p},\lambda;2} - \Xi_{\boldsymbol{p}}(\tau_0)A^\dagger_{\boldsymbol{p},\lambda;2}\right) \\
\mathcal{I}^{-1}_{-\theta}(\tau_0)B_{-\boldsymbol{p},\lambda;2}\mathcal{I}_{-\theta}(\tau_0) &= \cos(\theta)B_{-\boldsymbol{p},\lambda;2} + \sin(\theta)\left(\Lambda_{\boldsymbol{p}}(\tau_0)B_{-\boldsymbol{p},\lambda;1} + \Xi_{\boldsymbol{p}}(\tau_0)A^\dagger_{\boldsymbol{p},\lambda;1}\right)
\end{aligned}
\tag{2.113}
$$

while the transformation rule for the adjoint operators can be obtained by considering the adjoint equations. The Bogoliubov coefficients are defined as the inner products

$$
\begin{aligned}
\delta^3(\mathbf{0})\Lambda_{\boldsymbol{p}}(\tau) &= \left(u_{\boldsymbol{p},\lambda;2}, u_{\boldsymbol{p},\lambda;1}\right)_\tau = \left(v_{\boldsymbol{p},\lambda;1}, v_{\boldsymbol{p},\lambda;2}\right)_\tau \\
\delta^3(\mathbf{0})\Xi_{\boldsymbol{p}}(\tau) &= \left(u_{\boldsymbol{p},\lambda;1}, v_{\boldsymbol{p},\lambda;2}\right)_\tau = -\left(u_{\boldsymbol{p},\lambda;2}, v_{\boldsymbol{p},\lambda;1}\right)_\tau ,
\end{aligned}
\tag{2.114}
$$

where the notation anticipates that they don't depend on $\lambda$ (we will see that they actually depend only on the modulus of the momentum $p$). The $\delta^3(\mathbf{0})$ factor is a reminiscence of the more general expressions involving distinct momenta $\Lambda_{\boldsymbol{p},\boldsymbol{q}} \propto \delta^3(\boldsymbol{p}-\boldsymbol{q})$ . The delta factor is absorbed by a corresponding momentum integration in the Eqs.(2.113), leaving only the finite coefficients defined via Eq.(2.114). These coefficients satisfy $|\Lambda_{\boldsymbol{p}}|^2 + |\Xi_{\boldsymbol{p}}|^2 = 1$ for all $\boldsymbol{p}, \tau$. With the aid of Eqs.(2.113), we can evaluate all the expectation values appearing in Eq.(2.109):

$$
\begin{aligned}
\langle 0_F(\tau_0)|\, A^\dagger_{\boldsymbol{p},\lambda;j}A_{\boldsymbol{q};\lambda';j}\,|0_F(\tau_0)\rangle &= \sin^2\theta|\Xi_{\boldsymbol{p}}(\tau_0)|^2\delta_{\lambda\lambda'}\delta^3(\boldsymbol{p}-\boldsymbol{q}) \ , \quad \forall j \\
\langle 0_F(\tau_0)|\, B^\dagger_{-\boldsymbol{p},\lambda;j}B_{-\boldsymbol{q};\lambda';j}\,|0_F(\tau_0)\rangle &= \sin^2\theta|\Xi_{\boldsymbol{p}}(\tau_0)|^2\delta_{\lambda\lambda'}\delta^3(\boldsymbol{p}-\boldsymbol{q}) \ , \quad \forall j \\
\langle 0_F(\tau_0)|\, A^\dagger_{\boldsymbol{p},\lambda;1}B^\dagger_{-\boldsymbol{q};\lambda';1}\,|0_F(\tau_0)\rangle &= \sin^2\theta\,\Xi^*_{\boldsymbol{p}}(\tau_0)\Lambda_{\boldsymbol{p}}(\tau_0)\delta_{\lambda\lambda'}\delta^3(\boldsymbol{p}-\boldsymbol{q}) \\
\langle 0_F(\tau_0)|\, A^\dagger_{\boldsymbol{p},\lambda;2}B^\dagger_{-\boldsymbol{q};\lambda';2}\,|0_F(\tau_0)\rangle &= -\sin^2\theta\,\Xi^*_{\boldsymbol{p}}(\tau_0)\Lambda^*_{\boldsymbol{p}}(\tau_0)\delta_{\lambda\lambda'}\delta^3(\boldsymbol{p}-\boldsymbol{q}) \\
\langle 0_F(\tau_0)|\, B_{-\boldsymbol{p},\lambda;1}A_{\boldsymbol{q};\lambda';1}\,|0_F(\tau_0)\rangle &= \sin^2\theta\,\Xi_{\boldsymbol{p}}(\tau_0)\Lambda^*_{\boldsymbol{p}}(\tau_0)\delta_{\lambda\lambda'}\delta^3(\boldsymbol{p}-\boldsymbol{q}) \\
\langle 0_F(\tau_0)|\, B_{-\boldsymbol{p},\lambda;2}A_{\boldsymbol{q};\lambda';2}\,|0_F(\tau_0)\rangle &= -\sin^2\theta\,\Xi_{\boldsymbol{p}}(\tau_0)\Lambda_{\boldsymbol{p}}(\tau_0)\delta_{\lambda\lambda'}\delta^3(\boldsymbol{p}-\boldsymbol{q}) \ .
\end{aligned}
\tag{2.115}
$$

We can now give the result:

$$
\mathbb{T}_{\mu\nu} = \mathbb{T}^{(MIX)}_{\mu\nu} + \mathbb{T}^{(N)}_{\mu\nu} \tag{2.116}
$$

$$
\begin{aligned}
\mathbb{T}^{(MIX)}_{\mu\nu} &= \frac{i}{2}\sin^2\theta\sum_\lambda\int d^3p\{|\Xi_{\boldsymbol{p}}(\tau_0)|^2\sum_{j=1,2}\left(L_{\mu\nu}(u_{\boldsymbol{p},\lambda;j}, u_{\boldsymbol{p},\lambda;j}) - L_{\mu\nu}(v_{\boldsymbol{p},\lambda;j}, v_{\boldsymbol{p},\lambda;j})\right) \\
&+ \Xi^*_{\boldsymbol{p}}(\tau_0)\Lambda_{\boldsymbol{p}}(\tau_0)L_{\mu\nu}(u_{\boldsymbol{p},\lambda;1}, v_{\boldsymbol{p},\lambda;1}) + \Xi_{\boldsymbol{p}}(\tau_0)\Lambda^*_{\boldsymbol{p}}(\tau_0)L_{\mu\nu}(v_{\boldsymbol{p},\lambda;1}, u_{\boldsymbol{p},\lambda;1}) \\
&- \Xi^*_{\boldsymbol{p}}(\tau_0)\Lambda^*_{\boldsymbol{p}}(\tau_0)L_{\mu\nu}(u_{\boldsymbol{p},\lambda;2}, v_{\boldsymbol{p},\lambda;2}) - \Xi_{\boldsymbol{p}}(\tau_0)\Lambda_{\boldsymbol{p}}(\tau_0)L_{\mu\nu}(v_{\boldsymbol{p},\lambda;2}, u_{\boldsymbol{p},\lambda;2})\}
\end{aligned}
\tag{2.117}
$$

$$
\mathbb{T}^{(N)}_{\mu\nu} = \frac{i}{2}\sum_\lambda\sum_{j=1,2}\int d^3p L_{\mu\nu}(v_{\boldsymbol{p},\lambda;j}, v_{\boldsymbol{p},\lambda;j}) \ . \tag{2.118}
$$

The last term comes from applying the anticommutator relation $\left\{B^\dagger_{-\boldsymbol{p},\lambda;j}, B_{-\boldsymbol{q},\lambda';j}\right\} = \delta_{\lambda\lambda'}\delta^3(\boldsymbol{p}-\boldsymbol{q})$ to the $BB^\dagger$ term. While the remaining terms, regrouped under the symbol $\mathbb{T}^{(MIX)}_{\mu\nu}$ show an explicit dependence on $\sin^2\theta$, and are therefore zero in absence of mixing, the last term is present independently of mixing. Indeed, it is easy to check that $\mathbb{T}^{(N)}_{\mu\nu}$ represents the expectation value of the energy-momentum tensor on the *mass* vacuum:

$$\mathbb{T}^{(N)}_{\mu\nu} = \langle 0_M | T_{\mu\nu} | 0_M \rangle \ . \tag{2.119}$$

The origin of this term is an ordering ambiguity in the energy-momentum tensor of the quantized fields. To understand its significance, let us consider the flat space limit, where $v_{\boldsymbol{p},\lambda;j} \propto e^{i\omega_{p;j}t}$ with $\omega_{p;j} = \sqrt{p^2 + m_j^2}$. The auxiliary tensor becomes

$$L_{\mu\nu}(A,B) = \bar{A}\gamma_\mu \partial_\nu B + \bar{A}\gamma_\nu \partial_\mu B - \partial_\mu \bar{A}\gamma_\nu B - \partial_\nu \bar{A}\gamma_\mu B \tag{2.120}$$

where both the Dirac matrices and the derivatives are the ordinary flat space ones. In particular one has

$$L_{00}(v_{\boldsymbol{p},\lambda;j}, v_{\boldsymbol{p},\lambda;j}) = 2(v^\dagger_{\boldsymbol{p},\lambda;j}\partial_t v_{\boldsymbol{p},\lambda;j} - \partial_t v^\dagger_{\boldsymbol{p},\lambda;j} v_{\boldsymbol{p},\lambda;j}) = 4i\omega_{p;j} v^\dagger_{\boldsymbol{p},\lambda;j} v_{\boldsymbol{p},\lambda;j} = 4i\omega_{p;j} \ , \tag{2.121}$$

where we have made use of the normalization $v^\dagger_{\boldsymbol{p},\lambda;j} v_{\boldsymbol{p},\lambda;j} = 1$. Then

$$\mathbb{T}^{(N)}_{00} = -2\sum_\lambda \sum_{j=1,2} \int d^3p \ \omega_{p;j} \qquad (< 0) \ . \tag{2.122}$$

We can see that $\mathbb{T}^{(N)}_{00}$ corresponds to the diverging negative energy that is removed by the normal ordering prescription in flat space. In order that the energy-momentum tensor $T_{\mu\nu}$ approaches the normal-ordered flat-space expression in the limit, one must subtract $\mathbb{T}^{(N)}_{\mu\nu}$. Then we define a renormalized energy-momentum tensor by

$$T^r_{\mu\nu} = T_{\mu\nu} - \mathbb{T}^{(N)}_{\mu\nu} \tag{2.123}$$

and whose expectation value is

$$\langle 0_F(\tau_0) | T^r_{\mu\nu} | 0_F(\tau_0) \rangle = \mathbb{T}^{(MIX)}_{\mu\nu} \ . \tag{2.124}$$

The requirement that the energy momentum tensor reduces to its normal ordered form in the flat space limit is one of the axioms outlined by Wald [96], and is necessary for the definition of a proper energy momentum tensor. We now derive the general properties of the Bogoliubov coefficients, and we show that $\mathbb{T}^{(MIX)}_{\mu\nu}$ behaves as a perfect fluid, determining the functional expression of $\mathbb{T}_{\tau\tau}$ and $\mathbb{T}^\mu_\mu$.

**General properties of the Bogoliubov Coefficients**

Much can still be said without specifying the precise metric, i.e., without providing an explicit form for the scale factor $C$. Plugging the solutions (2.68) in the definition (2.114) we compute

$$\begin{aligned} \delta^3(\mathbf{0})\Lambda_{\boldsymbol{p}}(\tau) &= (u_{\boldsymbol{p},\lambda;2}, u_{\boldsymbol{p},\lambda;1}) = C^3 \int_{\Sigma_\tau} d^3x u^\dagger_{\boldsymbol{p},\lambda;2}(\tau,\boldsymbol{x}) u_{\boldsymbol{p},\lambda;1}(\tau,\boldsymbol{x}) \\ &= C^3 \int_{\Sigma_\tau} d^3x \begin{pmatrix} f^*_{p;2}\xi^\dagger_\lambda & g^*_{p;2}\lambda\xi^\dagger_\lambda \end{pmatrix} \begin{pmatrix} f_{p;1}\xi_\lambda \\ g_{p;1}\lambda\xi_\lambda \end{pmatrix} \\ &= \delta^3(\mathbf{0})(2\pi)^3 C^3 \left( f^*_{p;2} f_{p;1} + g^*_{p;2} g_{p;1} \right) \end{aligned}$$

that implies

$$\Lambda_p(\tau) = (2\pi C)^3 \left( f^*_{p;2} f_{p;1} + g^*_{p;2} g_{p;1} \right) , \tag{2.125}$$

where we have switched to the notation $\Lambda_p$ to highlight that it depends only upon the modulus $p$. In a similar way

$$\begin{aligned}
\delta^3(\mathbf{0})\Xi_{\boldsymbol{p}}(\tau) &= (u_{\boldsymbol{p},\lambda;1}, v_{\boldsymbol{p},\lambda;2}) = C^3 \int_{\Sigma_\tau} d^3x u^\dagger_{\boldsymbol{p},\lambda;1}(\tau,\boldsymbol{x}) v_{\boldsymbol{p},\lambda;2}(\tau,\boldsymbol{x}) \\
&= C^3 \int_{\Sigma_\tau} d^3x \begin{pmatrix} f^*_{p;1}\xi^\dagger_\lambda & g^*_{p;1}\lambda\xi^\dagger_\lambda \end{pmatrix} \begin{pmatrix} g^*_{p;2}\xi_\lambda \\ -f^*_{p;2}\lambda\xi_\lambda \end{pmatrix} \\
&= \delta^3(\mathbf{0})(2\pi)^3 C^3 \left( f^*_{p;1} g^*_{p;2} - g^*_{p;1} f^*_{p;2} \right)
\end{aligned}$$

and then

$$\Xi_p(\tau) = (2\pi C)^3 \left( f^*_{p;1} g^*_{p;2} - g^*_{p;1} f^*_{p;2} \right) . \tag{2.126}$$

From Eqs.(2.125) and (2.126) we can verify that

$$\begin{aligned}
&|\Lambda_p(\tau)|^2 + |\Xi_p(\tau)|^2 \\
&= (2\pi C)^6 \left( |f_{p;2}|^2 |f_{p;1}|^2 + |g_{p;2}|^2 |g_{p;1}|^2 + f_{p;2} f^*_{p;1} g^*_{p;2} g_{p;1} + f^*_{p;2} f_{p;1} g_{p;2} g^*_{p;1} \right) \\
&+ (2\pi C)^6 \left( |f_{p;1}|^2 |g_{p;2}|^2 + |g_{p;1}|^2 |f_{p;2}|^2 - f_{p;1} g_{p;2} g^*_{p;1} f^*_{p;2} - f^*_{p;1} g^*_{p;2} g_{p;1} f_{p;2} \right) \\
&= (2\pi C)^6 \left( |f_{p;1}|^2 + |g_{p;1}|^2 \right) \left( |f_{p;2}|^2 + |g_{p;2}|^2 \right) = 1 ,
\end{aligned} \tag{2.127}$$

where in the last step we have made use of the normalization condition (2.73). We conclude this subsection by expressing the Bogoliubov coefficients in terms of the reduced functions $\phi_p, \gamma_p$:

$$\begin{aligned}
\Lambda_p(\tau) &= (2\pi)^3 \left( \phi^*_{p;2} \phi_{p;1} + \gamma^*_{p;2} \gamma_{p;1} \right) \\
\Xi_p(\tau) &= (2\pi)^3 \left( \phi^*_{p;1} \gamma^*_{p;2} - \gamma^*_{p;1} \phi^*_{p;2} \right) .
\end{aligned} \tag{2.128}$$

**Diagonality of the energy-momentum tensor**

Using the result (Eq.(2.128)), we can prove that $\mathbb{T}_{\mu\nu}$ is non-zero only when $\mu = \nu$. This result has the important consequence that $\mathbb{T}^\mu_\nu$ can be interpreted as the energy-momentum tensor of a perfect fluid.

We start by proving that $\mathbb{T}_{\tau i} = 0$ for $i = 1, 2, 3$. According to eq. (2.116) we have

$$\begin{aligned}
\mathbb{T}_{\tau i} &= \frac{i}{2} \sin^2\theta \sum_\lambda \int d^3p \{ |\Xi_p(\tau_0)|^2 \sum_{j=1,2} \left( L_{\tau i}(u_{\boldsymbol{p},\lambda;j}, u_{\boldsymbol{p},\lambda;j}) - L_{\tau i}(v_{\boldsymbol{p},\lambda;j}, v_{\boldsymbol{p},\lambda;j}) \right) \\
&+ \Xi^*_p(\tau_0)\Lambda_p(\tau_0) L_{\tau i}(u_{\boldsymbol{p},\lambda;1}, v_{\boldsymbol{p},\lambda;1}) + \Xi_p(\tau_0)\Lambda^*_p(\tau_0) L_{\tau i}(v_{\boldsymbol{p},\lambda;1}, u_{\boldsymbol{p},\lambda;1}) \\
&- \Xi^*_p(\tau_0)\Lambda^*_p(\tau_0) L_{\tau i}(u_{\boldsymbol{p},\lambda;2}, v_{\boldsymbol{p},\lambda;2}) - \Xi_p(\tau_0)\Lambda_p(\tau_0) L_{\tau i}(v_{\boldsymbol{p},\lambda;2}, u_{\boldsymbol{p},\lambda;2}) \} \\
&+ \frac{i}{2} \sum_\lambda \sum_{j=1,2} \int d^3p L_{\tau i}(v_{\boldsymbol{p},\lambda;j}, v_{\boldsymbol{p},\lambda;j}) .
\end{aligned}$$

Due to the property given in Eq.(2.97), we can always write $L_{\tau i}(a,b) = p_i h_{a,b}(p)$ , each of the terms in the integrand of Eq. (2.116) is of the form $p_i \mathcal{F}(p)$ , with $\mathcal{F}(p)$ a function of $p$ only. We therefore have an odd function of $p_i$ integrated over an even domain $p_i \in (-\infty, +\infty)$ and the integral vanishes:

$$\mathbb{T}_{\tau i} = 0\,. \tag{2.129}$$

The situation is similar for $\mathbb{T}_{ij}$ with $i \neq j$ and $i,j = 1,2,3$. In this case (see Eq.(2.99)), namely, $L_{ij}(a,b) = p_i p_j l_{a,b}(p)$, implies that each term under the integral sign is of the form $p_i p_j \mathcal{G}(p)$ with $\mathcal{G}(p)$ a function of $p$ alone. It is clear that also in this case, the integral over the even domain $(p_i, p_j) \in (-\infty, +\infty) \times (-\infty, +\infty)$ vanishes, yielding $\mathbb{T}_{ij} = 0$ for $i \neq j$. Notice that the same conclusion does not apply to $\mathbb{T}_{ii}$, since in this case the integrand is an even function $p_i^2 \mathcal{A}(p)$ of $p_i$. It is easy to verify that $\mathbb{T}_{ii}$ is the same for each $i = 1,2,3$, consistently with the isotropy of the underlying metric. Due to the manifest diagonality and isotropy of the energy-momentum tensor, there are really only two independent components of $\mathbb{T}_{\mu\nu}$, i.e. $\mathbb{T}_{\tau\tau}$ and $\mathbb{T}_{ii}$ for a given $i$. Alternatively one can consider the $\mathbb{T}_{\tau\tau}$ component and the trace $\mathbb{T}^{\mu}_{\mu}$, as by definition

$$\mathbb{T}^{\mu}_{\mu} \;=\; g^{\mu\nu}\mathbb{T}_{\mu\nu} = C^{-2}\mathbb{T}_{\tau\tau} - 3C^{-2}\mathbb{T}_{ii}$$

and then

$$\mathbb{T}_{ii} \;=\; \frac{\mathbb{T}_{\tau\tau} - C^2\mathbb{T}^{\mu}_{\mu}}{3}\,, \tag{2.130}$$

where no sum is intended over the index $i$ and we have used the isotropy of $\mathbb{T}_{\mu\nu}$.

It is worth stressing that, as evident from the definition and the expression of the auxiliary tensor, $\mathbb{T}_{\mu\nu}$ depends only on the time coordinate $\tau$ and parametrically on the arbitrary fixed time $\tau_0$.

We conclude the section by giving the explicit functional form of $\mathbb{T}_{\tau\tau}$ and $\mathbb{T}^{\mu}_{\mu}$. From Eqs.(2.116) and (2.128) we have

$$\begin{aligned}
&\mathbb{T}_{\tau\tau}\left[\phi_{p;j}, \gamma_{p;j}\right] = \\
&2iC^{-2}\sin^2\theta \sum_{\lambda} \int d^3p \{(2\pi)^6[|\phi_{p;1}(\tau_0)|^2|\gamma_{p;2}(\tau_0)|^2 + |\gamma_{p;1}(\tau_0)|^2|\phi_{p;2}(\tau_0)|^2 \\
&-\phi_{p;1}(\tau_0)\gamma_{p;2}(\tau_0)\gamma^*_{p;1}(\tau_0)\phi^*_{p;2}(\tau_0) - \phi_{p;2}(\tau_0)\gamma_{p;1}(\tau_0)\gamma^*_{p;2}(\tau_0)\phi^*_{p;1}(\tau_0)] \\
&\times \sum_{j=1,2}\left(\phi^*_{p;j}\partial_\tau\phi_{p;j} + \gamma^*_{p;j}\partial_\tau\gamma_{p;j} - \partial_\tau\phi^*_{p;j}\phi_{p;j} - \partial_\tau\gamma^*_{p;j}\gamma_{p;j}\right) \\
&+ 2i(2\pi)^6\Im[(\phi_{p;1}(\tau_0)\gamma_{p;2}(\tau_0) - \gamma_{p;1}(\tau_0)\phi_{p;2}(\tau_0))\left(\phi^*_{p;2}(\tau_0)\phi_{p;1}(\tau_0) + \gamma^*_{p;2}(\tau_0)\gamma_{p;1}(\tau_0)\right) \\
&\times\left(\phi^*_{p;1}\partial_\tau\gamma^*_{p;1} - \gamma^*_{p;1}\partial_\tau\phi^*_{p;1}\right)] \\
&- 2i(2\pi)^6\Im[(\phi_{p;1}(\tau_0)\gamma_{p;2}(\tau_0) - \gamma_{p;1}(\tau_0)\phi_{p;2}(\tau_0))\left(\phi_{p;2}(\tau_0)\phi^*_{p;1}(\tau_0) + \gamma_{p;2}(\tau_0)\gamma^*_{p;1}(\tau_0)\right) \\
&\times\left(\phi^*_{p;2}\partial_\tau\gamma^*_{p;2} - \gamma^*_{p;2}\partial_\tau\phi^*_{p;2}\right)]\} \\
&-iC^{-2}\sum_{\lambda}\sum_{j=1,2}\int d^3p\left[\phi^*_{p;j}\partial_\tau\phi_{p;j} + \gamma^*_{p;j}\partial_\tau\gamma_{p;j} - \partial_\tau\phi^*_{p;j}\phi_{p;j} - \partial_\tau\gamma^*_{p;j}\gamma_{p;j}\right]\,.
\end{aligned}$$

Similarly

$$
\begin{aligned}
&\mathbb{T}^{\mu}_{\mu}\left[\phi_{p;j},\gamma_{p;j}\right] = \\
&4iC^{-3}\sin^2\theta\sum_{\lambda}\int d^3p\{(2\pi)^6[|\phi_{p;1}(\tau_0)|^2|\gamma_{p;2}(\tau_0)|^2+|\gamma_{p;1}(\tau_0)|^2|\phi_{p;2}(\tau_0)|^2 \\
&-\phi_{p;1}(\tau_0)\gamma_{p;2}(\tau_0)\gamma^*_{p;1}(\tau_0)\phi^*_{p;2}(\tau_0)-\phi_{p;2}(\tau_0)\gamma_{p;1}(\tau_0)\gamma^*_{p;2}(\tau_0)\phi^*_{p;1}(\tau_0)]\times \\
&-i\sum_{j=1,2}m_j\left(|\phi_{p;j}|^2-|\gamma_{p;j}|^2\right) \\
&+2i(2\pi)^6\Im[\left(\phi_{p;1}(\tau_0)\gamma_{p;2}(\tau_0)-\gamma_{p;1}(\tau_0)\phi_{p;2}(\tau_0)\right)\left(\phi^*_{p;2}(\tau_0)\phi_{p;1}(\tau_0)+\gamma^*_{p;2}(\tau_0)\gamma_{p;1}(\tau_0)\right) \\
&\times\left(-im_1\phi^*_{p;1}\gamma^*_{p;1}\right)] \\
&-2i(2\pi)^6\Im[\left(\phi_{p;1}(\tau_0)\gamma_{p;2}(\tau_0)-\gamma_{p;1}(\tau_0)\phi_{p;2}(\tau_0)\right)\left(\phi_{p;2}(\tau_0)\phi^*_{p;1}(\tau_0)+\gamma_{p;2}(\tau_0)\gamma^*_{p;1}(\tau_0)\right) \\
&\times\left(-im_2\phi^*_{p;2}\gamma^*_{p;2}\right)]\} \\
&-2C^{-3}\sum_{\lambda}\sum_{j=1,2}\int d^3p\, m_j\left(|\phi_{p;j}|^2-|\gamma_{p;j}|^2\right)\,. \qquad (2.131)
\end{aligned}
$$

These results are definitely more compact if we keep the Bogoliubov coefficients implicit. Indeed we can write

$$
\begin{aligned}
&\mathbb{T}_{\tau\tau}\left[\phi_{p;j},\gamma_{p;j}\right] = 2iC^{-2}\sin^2\theta\sum_{\lambda}\int d^3p\{|\Xi_p(\tau_0)|^2 \\
&\times\sum_{j=1,2}\left(\phi^*_{p;j}\partial_\tau\phi_{p;j}+\gamma^*_{p;j}\partial_\tau\gamma_{p;j}-\partial_\tau\phi^*_{p;j}\phi_{p;j}-\partial_\tau\gamma^*_{p;j}\gamma_{p;j}\right) \\
&+2i\Im[\Xi^*_p(\tau_0)\Lambda_p(\tau_0)\left(\phi^*_{p;1}\partial_\tau\gamma^*_{p;1}-\gamma^*_{p;1}\partial_\tau\phi^*_{p;1}\right) \\
&-\Xi^*_p(\tau_0)\Lambda^*_p(\tau_0)\left(\phi^*_{p;2}\partial_\tau\gamma^*_{p;2}-\gamma^*_{p;2}\partial_\tau\phi^*_{p;2}\right)]\} \\
&-iC^{-2}\sum_{\lambda}\sum_{j=1,2}\int d^3p\left[\phi^*_{p;j}\partial_\tau\phi_{p;j}+\gamma^*_{p;j}\partial_\tau\gamma_{p;j}-\partial_\tau\phi^*_{p;j}\phi_{p;j}-\partial_\tau\gamma^*_{p;j}\gamma_{p;j}\right]\,,
\end{aligned}
\qquad (2.132)
$$

and

$$
\begin{aligned}
\mathbb{T}^{\mu}_{\mu}\left[\phi_{p;j},\gamma_{p;j}\right] &= 4iC^{-3}\sin^2\theta\sum_{\lambda}\int d^3p\{-i|\Xi_p(\tau_0)|^2\sum_{j=1,2}m_j\left(|\phi_{p;j}|^2-|\gamma_{p;j}|^2\right) \\
&+ 2i\Im\left[im_2\Xi^*_p(\tau_0)\Lambda^*_p(\tau_0)\phi^*_{p;2}\gamma^*_{p;2}-im_1\Xi^*_p(\tau_0)\Lambda_p(\tau_0)\phi^*_{p;1}\gamma^*_{p;1}\right]\} \\
&- 2C^{-3}\sum_{\lambda}\sum_{j=1,2}m_j\int d^3p\left(|\phi_{p;j}|^2-|\gamma_{p;j}|^2\right)\,. \qquad (2.133)
\end{aligned}
$$

In all the equations above the last term, which bears no proportionality to $\sin^2\theta$, is referred to $\mathbb{T}^{(N)}_{\mu\nu}$, and is reported only for completeness. Note that both the $\tau\tau$ component (2.132) and the trace (2.133) can also be seen as functionals of $\{\phi_p,\partial_\tau\phi_p\}$. In fact from Eqs.(2.76) we have

$$
\begin{aligned}
\gamma_p(\eta) &= \frac{i}{p}\left(\partial_\eta\phi_p(\eta)+imC(\eta)\phi_p(\eta)\right) \\
\partial_\eta\gamma_p(\eta) &= \frac{i}{p}\left(\partial^2_\eta\phi_p(\eta)+im\partial_\eta C(\eta)\phi_p(\eta)+imC(\eta)\partial_\eta\phi_p(\eta)\right)\,, \qquad (2.134)
\end{aligned}
$$

which can be substituted in the expressions above for $\mathbb{T}_{\mu\nu}$. From the diagonality of $\mathbb{T}_{\mu\nu}$ one can also prove that it is covariantly conserved (see Appendix C).

### 2.2.5 Applications: exponential expansion

In this section, we assume a specific evolution of the scale factor $C$ and compute the corresponding expectation value of the energy-momentum tensor on the flavor vacuum. In doing so, we are neglecting the back-reaction due to the flavor fields, i.e., the modifications induced on the metric by the energy-momentum tensor of Eq. (2.109). The computation based on a fixed background metric is undoubtedly an approximation, but it is useful to get an insight into the kind of contribution that emerges from the flavor vacuum. The self-consistent way to deal with $\mathbb{T}_{\mu\nu}$ is to insert Eq. (2.109), together with all the relevant matter terms, on the right-hand side of the Einstein equations and then solve simultaneously for the scale factor $C$ and the Dirac modes. This kind of calculation will be performed elsewhere. For the moment we assume that the right hand side of the Einstein field equations is dominated by other source terms which force a specific background metric.

#### Positive energy solutions

Here, in particular, we study the energy momentum-tensor corresponding to an exponential evolution of the scale factor $C(t) = e^{H_0 t}$, with $H_0$ a constant with dimensions of mass. The advantage of this choice stands in the possibility to solve the Dirac equation analytically. Transforming to conformal time we have

$$\tau = -\frac{1}{H_0} e^{-H_0 t} \,, \qquad C = -\frac{1}{H_0 \tau} \,. \tag{2.135}$$

Notice that the conformal time $\tau$ is always negative. Inserting Eq. (2.135) in Eq. (2.77) we obtain

$$\tau^2 \partial_\tau^2 \phi_p + \left( p^2 \tau^2 + \frac{im}{H_0} + \frac{m^2}{H_0^2} \right) \phi_p = 0 \,, \tag{2.136}$$

or, introducing the positive variable $s = -p\tau$

$$s^2 \partial_s^2 \phi_p + \left( s^2 + \frac{im}{H_0} + \frac{m^2}{H_0^2} \right) \phi_p = 0 \,. \tag{2.137}$$

This is a Bessel-like equation, whose general solution can be written as

$$\phi_p(s) = s^{\frac{1}{2}} \left( C_1 J_\nu(s) + C_2 J_{-\nu}(s) \right) \,, \qquad \nu = \frac{1}{2} \left( 1 - \frac{2im}{H_0} \right) \tag{2.138}$$

with $J_\nu(s)$ denoting the Bessel function of order $\nu$ and $C_1, C_2$ arbitrary complex constants. In order to specify the solution we need to impose some kind of boundary conditions, which in turn determine the positive energy solutions. We require that the modes of Eq. (2.138) be positive energy with respect to $\partial_\tau$ at early times, i.e. for $\tau \to -\infty$ (where $C \to 0$). With this choice the mass vacuum corresponds to the absence of massive neutrinos at early times. As $\tau \to -\infty$ the mass terms can be neglected, and equation (2.136) becomes

$$\partial_\tau^2 \phi_p + p^2 \phi_p = 0 \,. \tag{2.139}$$

The positive energy solution with respect to $\partial_\tau$ is evidently $\phi_p^+ \propto e^{-ip\tau}$, or, in terms of the $s$ variable, $\phi_p^+(s) \propto e^{is}$. We then impose the requirement $\lim_{s\to+\infty} \phi_p(s) \propto e^{is}$ . Recalling that $s$ is a positive real variable, we can employ the large argument expansion of the Bessel functions (see [90] and the appendix A)

$$J_\nu(s) \simeq \sqrt{\frac{2}{\pi s}} \cos\left(s - \frac{\nu\pi}{2} - \frac{\pi}{4}\right) \quad for \quad s \to +\infty \tag{2.140}$$

In this way, we show that the combination satisfying the requirement is given by

$$\phi_p(s) = N_p s^{\frac{1}{2}} \left(J_\nu(s) - i e^{\frac{\pi m}{H_0}} J_{-\nu}(s)\right) \simeq N_p \sqrt{\frac{2}{\pi}} (-i e^{\frac{\pi m}{2H_0}}) \cosh\left(\frac{\pi m}{H_0}\right) e^{is}, \tag{2.141}$$

where $N_p$ is a normalization constant and the last equivalence holds in the limit $s \to +\infty$. Inserting Eq.(2.141) in the first of the Eqs.(2.134), we deduce

$$\gamma_p(s) = N_p s^{\frac{1}{2}} \left(-i J_{\nu-1}(s) + e^{\frac{\pi m}{H_0}} J_{1-\nu}(s)\right) \tag{2.142}$$

where we have made use of the differential relations satisfied by the Bessel functions [90]. In order to fix $N_p$ we impose the normalization condition (2.76) in the $s \to +\infty$ limit. Using the large argument expansion once again, we obtain $|N_p|^2 = \frac{1}{32\pi^2 \cosh^2\left(\frac{\pi m}{H_0}\right)} e^{-\frac{\pi m}{H_0}}$. Finally, choosing $N_p$ real, we can write the positive energy solutions as

$$\begin{aligned} \phi_p(s) &= \frac{1}{4\pi} \frac{e^{-\frac{\pi m}{2H_0}}}{\cosh\left(\frac{\pi m}{H_0}\right)} \sqrt{\frac{s}{2}} \left(J_\nu(s) - i e^{\frac{\pi m}{H_0}} J_{-\nu}(s)\right) \\ \gamma_p(s) &= \frac{1}{4\pi} \frac{e^{-\frac{\pi m}{2H_0}}}{\cosh\left(\frac{\pi m}{H_0}\right)} \sqrt{\frac{s}{2}} \left(-i J_{\nu-1}(s) + e^{\frac{\pi m}{H_0}} J_{1-\nu}(s)\right) \end{aligned} \tag{2.143}$$

with $\nu = \frac{1}{2}\left(1 - \frac{2im}{H_0}\right)$ and $s = -p\tau$.

### Bogoliubov Coefficients

We have two sets of solutions $\phi_{p,j}, \gamma_{p,j}$, one for each value of the mass $m_j$, with $j = 1,2$ from the equations (2.143). The compatibility requirement then implies that each of the $\phi_{p,j}, \gamma_{p,j}$ has the same form for $j = 1,2$, except that one has $m_j$ wherever the mass appears, including the function index $\nu_j = \frac{1}{2}\left(1 - \frac{2im_j}{H_0}\right)$. We can compute the Bogoliubov coefficients $(\Lambda_p(\tau), \Xi_p(\tau))$ straight away from Eqs.(2.128):

$$\begin{aligned} \Lambda_p(\tau) &= \frac{\pi s}{4} \frac{e^{-\frac{\pi}{2H_0}(m_1+m_2)}}{\cosh\left(\frac{\pi m_1}{H_0}\right)\cosh\left(\frac{\pi m_2}{H_0}\right)} \\ &\times \Big\{ J^*_{\nu_2}(s) J_{\nu_1}(s) + J^*_{\nu_2-1}(s) J_{\nu_1-1}(s) + i e^{\frac{\pi m_1}{H_0}} \left[J^*_{\nu_2-1}(s) J_{1-\nu_1}(s) - J^*_{\nu_2}(s) J_{-\nu_1}(s)\right] \\ &+ i e^{\frac{\pi m_2}{H_0}} \left[J^*_{-\nu_2}(s) J_{\nu_1}(s) - J^*_{1-\nu_2}(s) J_{\nu_1-1}(s)\right] \\ &+ e^{\frac{\pi}{H_0}(m_1+m_2)} \left[J^*_{-\nu_2}(s) J_{-\nu_1}(s) + J^*_{1-\nu_2}(s) J_{1-\nu_1}(s)\right] \Big\}; \end{aligned}$$

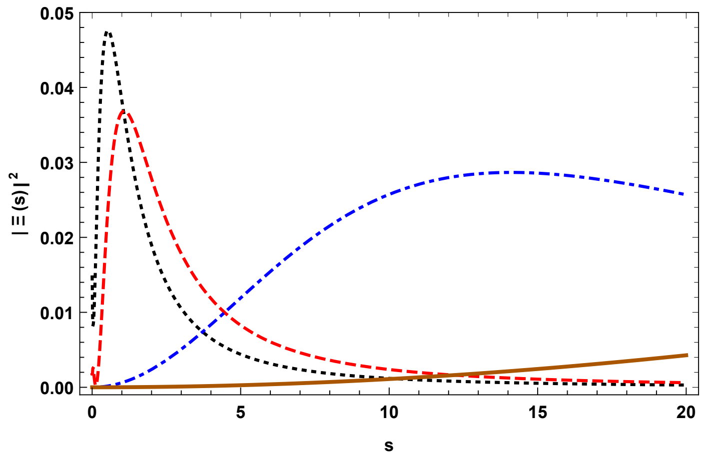


FIGURE 2.5: Squared modulus of the Bogoliubov coefficient $|\Xi_p|^2$ as a function of $s$ for sample values of the masses (all in units of $H_0$): (black dotted line) $m_1 = 0.7$, $m_2 = 1.4$ , (red dashed line) $m_1 = 1, m_2 = 2$, (blue dotdashed line) $m_1 = 10, m_2 = 20$, (dark orange solid line), $m_1 = 100$, $m_2 = 300$. The momentum dependence is implicit in $s = -p\tau$.

$$
\begin{aligned}
\Xi_p(\tau) \quad &= \frac{\pi s}{4} \frac{e^{-\frac{\pi}{2H_0}(m_1+m_2)}}{\cosh\left(\frac{\pi m_1}{H_0}\right)\cosh\left(\frac{\pi m_2}{H_0}\right)} \\
\times \quad & \left\{ i\left[J^*_{\nu_1}(s)J^*_{\nu_2-1}(s) - J^*_{\nu_1-1}(s)J^*_{\nu_2}(s)\right] + e^{\frac{\pi m_2}{H_0}}\left[J^*_{\nu_1}(s)J^*_{1-\nu_2}(s) + J^*_{\nu_1-1}(s)J^*_{-\nu_2}(s)\right]\right. \\
- \quad & e^{\frac{\pi m_1}{H_0}}\left[J^*_{-\nu_1}(s)J^*_{\nu_2-1}(s) + J^*_{1-\nu_1}(s)J^*_{\nu_2}(s)\right] \\
+ \quad & \left. ie^{\frac{\pi}{H_0}(m_1+m_2)}\left[J^*_{-\nu_1}(s)J^*_{1-\nu_2}(s) - J^*_{1-\nu_1}(s)J^*_{-\nu_2}(s)\right]\right\}
\end{aligned} \tag{2.144}
$$

To give an idea of the behaviour of the Bogoliubov coefficients we have plotted $|\Xi_p(s)|^2$ as a function of $s$ for sample values of $m_1, m_2$ in figure (2.5). We shall be particularly interested in the late time expression of the Bogoliubov coefficients, namely for $s \to 0^+$ (the corresponding limit is $\tau \to 0^-$, or $t \to +\infty$). For its determination we make use of the small argument expansion of the Bessel functions $J_\nu(s) \simeq \left(\frac{s}{2}\right)^\nu \frac{1}{\Gamma(1+\nu)}$ with $\Gamma$ denoting the Euler gamma function. From the Eqs.(2.144), it is easy to find that at the leading order for $s \to 0^+$ one has

$$
\begin{aligned}
\Lambda_p(s) &\simeq \frac{\pi}{2} \frac{e^{-\frac{\pi}{2H_0}(m_1+m_2)}}{\cosh\left(\frac{\pi m_1}{H_0}\right)\cosh\left(\frac{\pi m_2}{H_0}\right)}\left[\frac{e^{i\left(\frac{m_2-m_1}{H_0}\right)\log\left(\frac{s}{2}\right)}}{\Gamma^*(\nu_2)\Gamma(\nu_1)} + e^{\frac{\pi}{H_0}(m_1+m_2)}\frac{e^{-i\left(\frac{m_2-m_1}{H_0}\right)\log\left(\frac{s}{2}\right)}}{\Gamma^*(1-\nu_2)\Gamma(1-\nu_1)}\right] \\
\Xi_p(s) &\simeq \frac{\pi}{2} \frac{e^{-\frac{\pi}{2H_0}(m_1+m_2)}}{\cosh\left(\frac{\pi m_1}{H_0}\right)\cosh\left(\frac{\pi m_2}{H_0}\right)}\left[\frac{e^{\frac{\pi m_2}{H_0}}e^{-i\left(\frac{m_2-m_1}{H_0}\right)\log\left(\frac{s}{2}\right)}}{\Gamma^*(\nu_1)\Gamma^*(1-\nu_2)} - \frac{e^{\frac{\pi m_1}{H_0}}e^{i\left(\frac{m_2-m_1}{H_0}\right)\log\left(\frac{s}{2}\right)}}{\Gamma^*(1-\nu_1)\Gamma^*(\nu_2)}\right]
\end{aligned} \tag{2.145}
$$

**Explicit form of the energy-momentum tensor**

Keeping in mind the results of the previous sections, it is sufficient to compute the $\tau\tau$ component and the trace in order to fully determine $\mathbb{T}_{\mu\nu}$. Inserting the solutions (2.143) in the

Eq.(2.132) we find, after a lengthy but straightforward calculation:

$$
\begin{aligned}
\mathbb{T}^{(MIX)}_{\tau\tau}(\tau) &= i\sin^2\theta \sum_\lambda \int d^3p |\Xi_p(\tau_0)|^2 \left(\frac{H_0^2 p^2 \tau^3}{16\pi^2}\right) \sum_{j=1,2} \frac{e^{-\frac{\pi m_j}{H_0}}}{\cosh^2\left(\frac{\pi m_j}{H_0}\right)} \\
&\times \Bigg\{ \left[ 2(J^*_{\nu_j} J_{\nu_j-1} - J^*_{\nu_j-1} J_{\nu}) + \frac{\nu_j^* - \nu_j}{s} |J_{\nu_j}|^2 + \frac{\nu_j - \nu_j^*}{s} |J_{\nu_j-1}|^2 \right] + \\
& ie^{\frac{\pi m_j}{H_0}} \Bigg[ 2\left( J^*_{\nu_j} J_{1-\nu_j} + J^*_{-\nu_j} J_{\nu_j-1} + J^*_{\nu_j-1} J_{-\nu_j} + J^*_{1-\nu_j} J_{\nu_j} \right) + \frac{\nu_j - \nu_j^*}{s} J^*_{\nu_j} J_{-\nu_j} \\
&+ \frac{\nu_j^* - \nu_j}{s} J^*_{-\nu_j} J_{\nu_j} + \frac{\nu_j - \nu_j^*}{s} J^*_{\nu_j-1} J_{1-\nu_j} + \frac{\nu_j^* - \nu_j}{s} J^*_{1-\nu_j} J_{\nu_j-1} \Bigg] \\
&+ e^{\frac{2\pi m_j}{H_0}} \left[ 2(J^*_{1-\nu_j} J_{-\nu_j} - J^*_{-\nu_j} J_{1-\nu_j}) + \frac{\nu_j^* - \nu_j}{s} |J_{-\nu_j}|^2 + \frac{\nu_j - \nu_j^*}{s} |J_{1-\nu_j}|^2 \right] \Bigg\} \\
&+ \frac{i}{2}\sin^2\theta \sum_\lambda \int d^3p \Bigg\{ \Xi^*_p(\tau_0) \Lambda_p(\tau_0) \left( \frac{H_0^2 p^2 \tau^3 e^{-\frac{\pi m_1}{H_0}}}{8\pi^2 \cosh^2\left(\frac{\pi m_1}{H_0}\right)} \right) \\
&\times \Bigg[ \left( -i(J^*_{\nu_1})^2 - i(J^*_{\nu_1-1})^2 + i\frac{2\nu_1^* - 1}{s} J^*_{\nu_1} J^*_{\nu_1-1} \right) \\
&+ e^{\frac{\pi m_1}{H_0}} \left( 2(J^*_{\nu_1} J^*_{-\nu_1} - J^*_{\nu_1-1} J^*_{1-\nu_1}) + \frac{2\nu_1^* - 1}{s} J^*_{\nu_1} J^*_{1-\nu_1} + \frac{1 - 2\nu_1^*}{s} J^*_{-\nu_1} J^*_{\nu_1-1} \right) \\
&+ ie^{\frac{2\pi m_1}{H_0}} \left( (J^*_{-\nu_1})^2 + (J^*_{1-\nu_1})^2 + \frac{2\nu_1^* - 1}{s} J^*_{-\nu_1} J^*_{1-\nu_1} \right) \Bigg] - c.c. \Bigg\} \\
&- \frac{i}{2}\sin^2\theta \sum_\lambda \int d^3p \Bigg\{ \Xi^*_p(\tau_0) \Lambda^*_p(\tau_0) \left( \frac{H_0^2 p^2 \tau^3 e^{-\frac{\pi m_2}{H_0}}}{8\pi^2 \cosh^2\left(\frac{\pi m_2}{H_0}\right)} \right) \\
&\times \Bigg[ \left( -i(J^*_{\nu_2})^2 - i(J^*_{\nu_2-1})^2 + i\frac{2\nu_2^* - 1}{s} J^*_{\nu_2} J^*_{\nu_2-1} \right) \\
&+ e^{\frac{\pi m_2}{H_0}} \left( 2(J^*_{\nu_2} J^*_{-\nu_2} - J^*_{\nu_2-1} J^*_{1-\nu_2}) + \frac{2\nu_2^* - 1}{s} J^*_{\nu_2} J^*_{1-\nu_2} + \frac{1 - 2\nu_2^*}{s} J^*_{-\nu_2} J^*_{\nu_2-1} \right) \\
&+ ie^{\frac{2\pi m_2}{H_0}} \left( (J^*_{-\nu_2})^2 + (J^*_{1-\nu_2})^2 + \frac{2\nu_2^* - 1}{s} J^*_{-\nu_2} J^*_{1-\nu_2} \right) \Bigg] - c.c. \Bigg\}
\end{aligned}
$$

In the above equation we have left the Bogoliubov coefficients implicit and the argument of the Bessel functions $s = -p\tau$ has been omitted for a better visualization. We recall that the helicity sum is over $\lambda = \pm 1$ and that in general $\tau \neq \tau_0$. An analogous calculation can be performed for the trace:

$$
\begin{aligned}
&\mathbb{T}_{\mu}^{\mu(MIX)} = \\
&i\sin^2\theta \sum_{\lambda}\int d^3p |\Xi_p(\tau_0)|^2 \left(\frac{iH_0^3\tau^3 s}{8\pi^2}\right)\sum_{j=1,2}\left(\frac{m_j e^{\frac{-\pi m_j}{H_0}}}{\cosh^2\left(\frac{\pi m_j}{H_0}\right)}\right)\Bigg\{|J_{\nu_j}|^2-|J_{\nu_j-1}|^2 \\
&+ie^{\frac{\pi m_j}{H_0}}\left(J^*_{-\nu_j}J_{\nu_j}-J^*_{\nu_j}J_{-\nu_j}+J^*_{1-\nu_j}J_{\nu_j-1}-J^*_{\nu_j-1}J_{1-\nu_j}\right)+e^{\frac{2\pi m_j}{H_0}}\left(|J_{-\nu_j}|^2-|J_{1-\nu_j}|^2\right)\Bigg\} \\
&+\frac{i}{2}\sin^2\theta\sum_{\lambda}\int d^3p\Bigg\{\Xi_p^*(\tau_0)\Lambda_p(\tau_0)\left(\frac{im_1 sH_0^3\tau^3 e^{-\frac{\pi m_1}{H_0}}}{4\pi^2\cosh^2\left(\frac{\pi m_1}{H_0}\right)}\right)\Bigg[iJ^*_{\nu_1}J^*_{\nu_1-1}+e^{\frac{\pi m_1}{H_0}}J^*_{\nu_1}J^*_{1-\nu_1} \\
&-e^{\frac{\pi m_1}{H_0}}J^*_{-\nu_1}J^*_{\nu_1-1}+ie^{\frac{2\pi m_1}{H_0}}J^*_{-\nu_1}J^*_{1-\nu_1}\Bigg]-c.c\Bigg\} \\
&-\frac{i}{2}\sin^2\theta\sum_{\lambda}\int d^3p\Bigg\{\Xi_p^*(\tau_0)\Lambda_p^*(\tau_0)\left(\frac{im_2 sH_0^3\tau^3 e^{-\frac{\pi m_2}{H_0}}}{4\pi^2\cosh^2\left(\frac{\pi m_2}{H_0}\right)}\right)\Bigg[iJ^*_{\nu_2}J^*_{\nu_2-1}+e^{\frac{\pi m_2}{H_0}}J^*_{\nu_2}J^*_{1-\nu_2} \\
&-e^{\frac{\pi m_2}{H_0}}J^*_{-\nu_2}J^*_{\nu_2-1}+ie^{\frac{2\pi m_2}{H_0}}J^*_{-\nu_2}J^*_{1-\nu_2}\Bigg]-c.c\Bigg\} \quad . \qquad (2.146)
\end{aligned}
$$

We are particularly interested in the late time ($\tau \to 0^-$) expression of the above equations. According to the definition (2.109), these represent the contribution of the flavor vacuum state, defined at an earlier time $\tau_0 < \tau$, to the energy-momentum tensor at late times. We then perform the small argument expansion $J_\nu(-p\tau) \simeq \left(\frac{-p\tau}{2}\right)^\nu \frac{1}{\Gamma(1+\nu)}$ for all the Bessel functions appearing in Eqs. (2.146) and (2.146), and keep only the terms of lowest order in the variable $\tau$. At order $\tau$, the $\tau\tau$ component is found to be

$$
\begin{aligned}
\mathbb{T}_{\tau\tau}^{(MIX)(1)}(\tau) &\simeq i\sin^2\theta\sum_{\lambda}\int d^3p|\Xi_p(\tau_0)|^2\left(i\frac{H_0\tau}{2\pi^3}\right)\sum_{j=1,2}m_j\tanh\left(\frac{\pi m_j}{H_0}\right) \\
&+ \frac{i}{2}\sin^2\theta\sum_{\lambda}\int d^3p\left[\Xi_p^*(\tau_0)\Lambda_p(\tau_0)\left(\frac{-im_1H_0\tau}{2\pi^3\cosh\left(\frac{\pi m_1}{H_0}\right)}\right)-c.c.\right] \\
&- \frac{i}{2}\sin^2\theta\sum_{\lambda}\int d^3p\left[\Xi_p^*(\tau_0)\Lambda_p^*(\tau_0)\left(\frac{-im_2H_0\tau}{2\pi^3\cosh\left(\frac{\pi m_2}{H_0}\right)}\right)-c.c.\right] \\
&. \qquad (2.147)
\end{aligned}
$$

The corresponding lowest order in the trace is $\propto \tau^3$. To see why this is the case, recall that by definition

$$
\mathbb{T}_{\mu}^{\mu} = C^{-2}\mathbb{T}_{\tau\tau} - C^{-2}\sum_{l=1}^{3}\mathbb{T}_{ll} = H_0^2\tau^2\mathbb{T}_{\tau\tau} - H_0^2\tau^2\sum_{l=1}^{3}\mathbb{T}_{ll}\,, \qquad (2.148)
$$

so that in correspondence with $\mathbb{T}_{\tau\tau} \propto \tau$ one has $\mathbb{T}^{\mu}_{\mu} \propto \tau^3$. To this order the trace is

$$\begin{aligned}
\mathbb{T}^{\mu\ (MIX)\ (1)}_{\mu} \simeq & \; i \sin^2\theta \sum_{\lambda} \int d^3p |\Xi_p(\tau_0)|^2 \left(\frac{iH_0^3\tau^3}{2\pi^3}\right) \sum_{j=1,2} m_j \tanh\left(\frac{\pi m_j}{H_0}\right) \\
+ & \; \frac{i}{2}\sin^2\theta \sum_{\lambda}\int d^3p \left[\Xi^*_p(\tau_0)\Lambda_p(\tau_0)\left(\frac{-im_1 H_0^3\tau^3}{2\pi^3\cosh\left(\frac{\pi m_1}{H_0}\right)}\right) - c.c.\right] \\
- & \; \frac{i}{2}\sin^2\theta \sum_{\lambda}\int d^3p \left[\Xi^*_p(\tau_0)\Lambda^*_p(\tau_0)\left(\frac{-im_2 H_0^3\tau^3}{2\pi^3\cosh\left(\frac{\pi m_2}{H_0}\right)}\right) - c.c.\right] \\
. &
\end{aligned}$$

Inserting Eqs. (2.147) and (2.149) in Eq. (2.130), we can deduce the important result $\mathbb{T}^{(MIX)(1)}_{ii} = 0$ , $\forall i$ . In other words, at first order in $\tau$, the spatial components of the energy-momentum tensor vanish. Then the equation of state reads, at lowest order in $\tau$:

$$w^{(1)} = \frac{\mathbb{T}^{i\ (MIX)(1)}_{i}}{\mathbb{T}^{\tau\ (MIX)(1)}_{\tau}} = 0\,, \tag{2.149}$$

i. e., *the energy-momentum tensor associated to the flavor vacuum satisfies, at late times ($\tau \to 0^-$), the equation of state of a pressure-less perfect fluid.* It is important to stress that this result does not depend on the value of the momentum integrals, and therefore is independent of any regularization. Moreover, as it is evident from (2.149) it holds for any choice of the reference time $\tau_0$.

**Regularization**

All the momentum integrals in the expression for the energy-momentum tensor, both for the general case and the for the late time approximation, are to be performed over the whole of $\mathbb{R}^3$ and are formally divergent. To extract a finite result, we need some form of regularization. The most immediate way to regularize the momentum integrations is to introduce an ultraviolet momentum cut-off $\mathcal{K}$. Usually, the cut-off is chosen in correspondence with a 'new physics' energy scale, beyond which the 'low energy' quantum field theory description breaks down. In our case, $\mathcal{K}$ ought to be related to the scale at which the semiclassical approximation breaks down, i. e., at the quantum gravity scale $\mathcal{K} \simeq M_{pl}$ which is of the order of the Planck mass $M_{pl}$. However, we can expect the cut-off to be at a much lower scale for what concerns the proper mixing term. Indeed, at very high energies, the mass difference between the neutrino states becomes negligible, and the oscillation frequency $\propto \frac{1}{p}$ approaches zero, implying that there is no oscillation. The same result also holds in quantum field theory, where the mixing Bogoliubov coefficient $\Xi_p$ generally approaches zero at high energies (therefore yielding no contribution to the energy-momentum tensor.). The heuristic argument above provides a physical reason to adopt the cut-off regularization and also justifies the adoption of a cut-off scale $\mathcal{K} \ll M_{pl}$, at least for what concerns the mixing.

Before proceeding we need to clarify that the cut-off must be imposed upon the comoving momentum $\boldsymbol{p}_{PHYS} = \frac{\boldsymbol{p}}{C}$ . rather than the mode label $p$.

The imposition of a cut-off $\mathcal{K}_0$ on $p_{PHYS}$ then translates into a sort of 'comoving' cutoff for the mode label $p$

$$p_{CUTOFF} = \mathcal{K}_0 C = \frac{-\mathcal{K}_0}{H_0\tau} = \mathcal{K}(\tau)\,, \tag{2.150}$$

which is strictly positive (recall that $\tau < 0$). For the late time energy-momentum tensor, in the approximation in which $\tau_0 < \tau$ is also at late times $\tau_0 \to 0^-$, we can give a simple

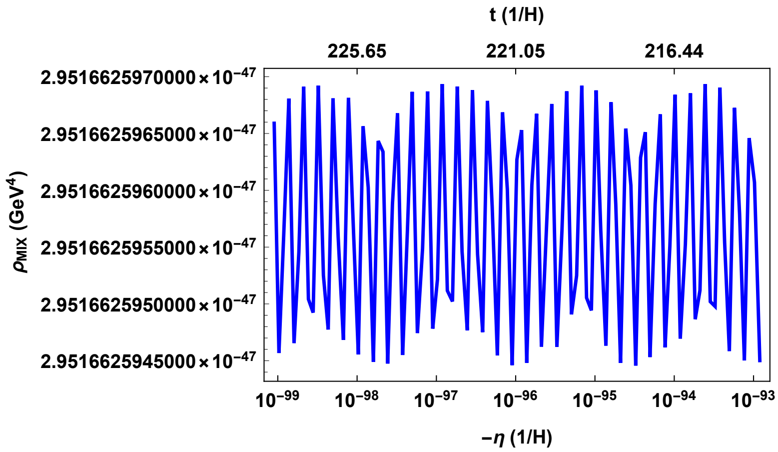


FIGURE 2.6: Logarithmic scale plot of the energy density $\rho_{MIX} = \mathbb{T}_{\tau}^{\tau(MIX)}$ from Eq. (2.151) as a function of conformal time $\tau$ for sample values of the parameters. The corresponding coordinate time $t$ is reported above. We have used a cut-off $\mathcal{K}_0 = 246$ GeV of the order of the electroweak scale, neutrino masses $m_1 = 15.25H_0$ , $m_2 = 22.25H_0$ and the expansion rate $H_0 = 10^{-3}$eV.

analytical form of the regularized integrals. Performing the integrals in Eqs. (2.147) and (2.149), with the comoving cut-off of Eq. (2.150), we obtain

$$
\begin{aligned}
\frac{\mathbb{T}^{(MIX)\,(1)}_{\tau\tau}}{\mathcal{K}^3(\tau)} &= \frac{-\sin^2\theta H_0\tau}{3\pi^2}\Bigg[\frac{e^{\frac{\pi(m_2-m_1)}{H_0}}+e^{-\frac{\pi(m_2-m_1)}{H_0}}}{\cosh\left(\frac{\pi m_1}{H_0}\right)\cosh\left(\frac{\pi m_2}{H_0}\right)}\left(m_1\tanh\left(\frac{\pi m_1}{H_0}\right)+m_2\tanh\left(\frac{\pi m_2}{H_0}\right)\right)\\
&-2\frac{m_1\tanh\left(\frac{\pi m_2}{H_0}\right)}{\cosh^2\left(\frac{\pi m_1}{H_0}\right)}-2\frac{m_2\tanh\left(\frac{\pi m_1}{H_0}\right)}{\cosh^2\left(\frac{\pi m_2}{H_0}\right)}\Bigg]+\sin^2\theta H_0\tau\Bigg[\left(\frac{m_1\tanh\left(\frac{\pi m_1}{H_0}\right)+m_2\tanh\left(\frac{\pi m_2}{H_0}\right)}{\cosh^2\left(\frac{\pi m_1}{H_0}\right)\cosh^2\left(\frac{\pi m_2}{H_0}\right)}\right)\\
&\times\left(\frac{1}{\Gamma(\nu_1)\Gamma^*(\nu_2)}\right)^2\left(\frac{1}{3+2i\frac{m_2-m_1}{H_0}}\right)\left(\frac{-\mathcal{K}(\tau)\tau_0}{2}\right)^{\frac{2i(m_2-m_1)}{H_0}}+c.c.\Bigg]\\
&+\Bigg\{\Bigg[\left(\frac{-im_1H_0\tau e^{\frac{-\pi m_1}{H_0}}}{2\cosh^3\left(\frac{\pi m_1}{H_0}\right)\cosh^2\left(\frac{\pi m_2}{H_0}\right)}\right)\left(\frac{1}{\Gamma(\nu_1)\Gamma^*(\nu_2)}\right)^2\left(\frac{1}{3+2i\frac{m_2-m_1}{H_0}}\right)\left(\frac{-\mathcal{K}(\tau)\tau_0}{2}\right)^{\frac{2i(m_2-m_1)}{H_0}}\\
&-\left(\frac{-im_1H_0\tau e^{\frac{-\pi m_1}{H_0}}}{2\cosh^3\left(\frac{\pi m_1}{H_0}\right)\cosh^2\left(\frac{\pi m_2}{H_0}\right)}\right)\left(\frac{1}{\Gamma^*(\nu_1)\Gamma(\nu_2)}\right)^2\left(\frac{1}{3-2i\frac{m_2-m_1}{H_0}}\right)\left(\frac{-\mathcal{K}(\tau)\tau_0}{2}\right)^{\frac{-2i(m_2-m_1)}{H_0}}\Bigg]\\
&-c.c.\Bigg\}\times i\sin^2\theta\\
&-\Bigg\{\Bigg[\left(\frac{-im_2H_0\tau e^{\frac{-\pi m_2}{H_0}}}{2\cosh^3\left(\frac{\pi m_2}{H_0}\right)\cosh^2\left(\frac{\pi m_1}{H_0}\right)}\right)\left(\frac{1}{\Gamma(\nu_1)\Gamma^*(\nu_2)}\right)^2\left(\frac{1}{3+2i\frac{m_2-m_1}{H_0}}\right)\left(\frac{-\mathcal{K}(\tau)\tau_0}{2}\right)^{\frac{2i(m_2-m_1)}{H_0}}\\
&-\left(\frac{-im_2H_0\tau e^{\frac{-\pi m_2}{H_0}}}{2\cosh^3\left(\frac{\pi m_2}{H_0}\right)\cosh^2\left(\frac{\pi m_1}{H_0}\right)}\right)\left(\frac{1}{\Gamma^*(\nu_1)\Gamma(\nu_2)}\right)^2\left(\frac{1}{3-2i\frac{m_2-m_1}{H_0}}\right)\left(\frac{-\mathcal{K}(\tau)\tau_0}{2}\right)^{\frac{-2i(m_2-m_1)}{H_0}}\Bigg]\\
&-c.c.\Bigg\}\times i\sin^2\theta
\end{aligned}
\tag{2.151}
$$

The trace can be deduced immediately from Eq. (2.151) by simply multiplying by the factor $C^{-2}$, since the pressure is zero for the late time energy momentum tensor (see Eq. (2.149)). A visual indication of the physical content of Eq. (2.151) is provided in Figure (2.6), where the mixing energy density $\mathbb{T}_{\tau}^{\tau\ (MIX)}$ from equation (2.151) is plotted against conformal time $\tau$ for sample values of the parameters. We notice that $\rho_{MIX}$, for the parameters and the range considered in Figure (2), is nearly constant, except for tiny oscillations of relative magnitude $\delta\rho_{MIX}/\rho_{MIX} \simeq 10^{-9}$. The oscillations come from the imaginary exponentials in Eq. (2.151). Such a simple evolution pattern can be expected to disappear when other time ranges are considered, and the full expression from Eq. (2.146) is employed, entailing a much more intricate time evolution. The results obtained in this work indicate that the vacuum energy associate to neutrino mixing in curved space might represent a dark matter component. Notice that for a momentum cutoff of the order of the electroweak scale $\mathcal{K}_0 = 246$ GeV, for neutrino masses $m_1, m_2$ such that $\Delta m_{12}^2 \simeq 10^{-5}\text{eV}^2$ and for a value of $H_0 \simeq 10^{-3}\text{eV}$, we obtain an energy density $\mathbb{T}_{\tau}^{\tau(MIX)}$ which is compatible with the upper bound on the dark matter content of the universe. A value of $H_0 \simeq 10^{-3}\text{eV}$ might have been reached during the very early phases ($t < 1$ s) of the Universe.

## 2.3 Concluding Remarks

As we have seen, the application of the formalism developed in this chapter is not limited to the study of neutrino oscillations in gravitational backgrounds, for which the influence of curved spacetime on matter is taken into account. The formalism also serves as a basis to investigate the effects that neutrino mixing has on the spacetime geometry, as exemplified in the last sections. Much still remains to be done in this direction, and future works will be devoted to a deeper study of the topics introduced here. These include a self-consistent calculation of the energy-momentum tensor in spatially flat FLRW metrics, that requires the simultaneous resolution of the Einstein field equations and of the Dirac equation. Such a calculation would allow to investigate scenarios in which neutrino mixing, through the condensate structure of the flavor vacuum, is the primary source for the Einstein field equations. Pertaining to the dark matter-like behaviour of the flavor vacuum, it is certainly worth analyzing neutrino mixing on metrics that are adequate for the description of galaxies. In addition, the mixing of boson fields in curved space, along the same lines, may be important in supersymmetric contexts.

# Chapter 3

# Axions and axionlike particles

In the previous chapter we have developed the quantum field theory of neutrino mixing in curved space and have shown that the flavor vacuum may act as a dark matter component. Other explanations for dark matter rely on new particles beyond the standard model. The common feature of these models is the tiny interactions among the new particles and the standard model fields, required to fit the dark matter behaviour. Among them *axion* and *axionlike* particle models are the most promising. Axions were indeed originally introduced to solve another long-standing issue in the standard model, known as the strong $CP$ problem. The capability to solve this puzzle, together with the naturally small interactions with the standard model fields, provides a solid theoretical motivation for their introduction. Axionlike particle is a common denomination for axion-inspired particle models, which generally deviate from the original axion proposal in many respects. Despite the strong theoretical motivations and a large number of experiments, no clear evidence of axions and axionlike particles has been found up to now. In this context we introduce two new detection strategies for axions and axionlike particles. In doing so we interlace seemingly unrelated topics, using tools and notions from non-relativistic quantum mechanics, like entanglement and quantum interferometry, to gain information on fundamental particle physics beyond the standard model. Section 3.1 presents a brief introduction to axions and axionlike particles, with a particular emphasis on the axion-fermion interactions. The latter constitute the basis for the analyses of sections 3.2 and 3.3, where we present new axion detection mechanisms based on the entanglement and on neutron interferometry respectively.

## 3.1 Axions and Axion Interactions

The standard model of particles is able to explain a wide range of phenomena involving fundamental particles and their interactions. In spite of its success, it certainly does not represent the definitive theory of elementary particles. Several phenomena, including particle mixing [48, 49, 97–99] and the quantum features of gravitation [100], are beyond the standard model. Among the shortcomings of the theory is the so–called *strong CP problem* in Quantum Chromodynamics (QCD) [44, 58, 101]. The QCD Lagrangian features a gluon–gluon interaction term that in principle allows for an arbitrary violation of CP (Charge-Parity) symmetry

$$\mathcal{L}_\Theta = -\Theta \left(\frac{\alpha_s}{8\pi}\right) \mathrm{Tr}\left(G_{\mu\nu}\tilde{G}^{\mu\nu}\right) \ . \tag{3.1}$$

Here $\alpha_s$ is the strong coupling and the trace is computed on the product of the gluon field $G^a_{\mu\nu}$ and its dual $\tilde{G}^a_{\mu\nu}$. The parameter $\Theta$ is not constrained by any QCD argument, so that an arbitrary CP symmetry violation is possible. Nonetheless no such violation is observed in strong processes [44, 58, 101–103]. One of the consequences of the CP violating term would be a relatively large neutron electric dipole moment, which the recent experiments constrain below $3 \times 10^{-26} e\,\mathrm{cm}$ (see [104] and, for a more recent result [105]). Analogous bounds on the electric dipole moment of atoms and molecules [106, 107] pose a further constraint on the magnitude of the CP violating term. To remedy this inconsistency, R. Peccei and H. Quinn introduced a new global symmetry $U_{PQ}(1)$ (called Peccei–Quinn symmetry) that is spontaneously broken [44, 101] at low energies. As shown by Frank Wilczek and Steven Weinberg [102, 103], this gives rise to a new particle, named the axion, which is the pseudo–Nambu–Goldstone boson of the broken $U_{PQ}(1)$ symmetry [108]. The new pseudoscalar field $a$ couples to gluons, modifying the $\Theta$ term as

$$\mathcal{L}_\Theta = \left(\frac{a}{f_A} - \Theta\right)\left(\frac{\alpha_s}{8\pi}\right) \mathrm{Tr}\left(G_{\mu\nu}\tilde{G}^{\mu\nu}\right) . \tag{3.2}$$

The quantity $f_A$ is known as the axion decay constant and sets the energy scale of the $PQ$ symmetry breaking. The symmetry breaking potential for $a$ is such that the minimum is at $a = \Theta f_A$, so to cancel the $\Theta$ term of Eq. (3.1). The new field then provides a dynamical solution to the puzzle, by shifting the effective $\Theta$ term and suppressing the $CP$ violation. The energy scale at which the symmetry breaking occurs $f_A$, appears in the low energy phenomena and plays a role analogous to the pion decay constant $f_\pi$. It determines, according to the model considered, both the axion mass $m_a \propto \frac{1}{f_A}$ and the effective couplings with the standard matter. In the original proposal $f_A$ was thought to be close to the electroweak scale [44, 102, 103], a hypotesis that was later ruled out by the experiments. In the subsequent years alternative axion models were devised, notably the KSVZ model [109, 110], featuring heavy quarks carrying a Peccei–Quinn (PQ) charge, and the DFSZ model [111, 112], in which the ordinary quarks and additional Higgs doublets carry the PQ charge. They provide a reference for two large classes of axion models (*hadronic* and *GUT* axions). Today the axion decay costant is estimated to be very large $f_A > 10^9$GeV, so that the QCD axions (both hadronic and GUT) have to be very light $m_a \sim 10^{-6} - 10^{-2}$eV and very weakly interacting [58]. These aspects make axions a natural candidate for dark matter.

Motivated by the search for dark matter components, a number of Axion–like–particles (ALPs) has been introduced. They can deviate significantly from the original Peccei–Quinn proposal, and are not necessarily tied to the solution of the strong CP problem, but share the fundamental nature of axions as (pseudo-)scalar fields and generally interact weakly with the standard model particles. In these models the relation between the coupling constant and the mass of the ALP can differ from the direct proportionality that characterizes the PQ axions. They range from masses $m_a \sim 10^{-22}$ eV, characteristic of the ultra–light axions [113, 114], up to masses of 1 TeV for the heavy GUT axions [115]. Axions and ALPs are, to date, one of the most credible explanations for dark matter [116–119].

Given the solid theoretical arguments behind their introduction, several experiments have been designed to prove the existence of ALPs. Perhaps unsurprisingly, considered their extremely small interaction rates, the experimental search for ALPs has proven to be very challenging. Many experiments take advantage of the axion–photon coupling. Among them, searches for polarization anomalies in the light propagating through a magnetic field (PVLAS) [120], “light shining through a wall” experiments (OSQAR, ALPS) [121–123], detection via the Primakoff effect (CAST) [124], and haloscope experiments (ADMX) [125]. More recently other approaches based on geometric phases [126] and QFT effects in the axion–photon mixing [77] were also suggested. Astrophysical observations and terrestrial experiments over the decades have restricted the allowed regions in parameter space, and additional constraints might emerge from the analysis of the axion–nucleon and axion–lepton interactions, as suggested for instance in [127]. Experiments based on the axion–fermion interaction have also been proposed (QUAX) [128]. Despite this, no evidence for the existence of the ALPs has been found up to now.

### 3.1.1 Axion Interactions

Axions and axionlike particles are (pseudo-)scalar bosons and their free Lagrangian density at low energy (below $f_A$) is that of a massive Klein-Gordon field:

$$\mathcal{L}_a = \frac{1}{2}\left(\partial^\mu a \partial_\mu a - m_a^2 a^2\right) \ . \tag{3.3}$$

The (pseudo-)scalar nature of the field is determined by its transformation under parity $\boldsymbol{x} \to -\boldsymbol{x}$. In the following we shall limit ourselves to the pseudoscalar models, these being the most studied and including the original axion. Hence all the interactions considered shall have the form of a Yukawa-like coupling between the ALP and a pseudoscalar form constructed out of the other fields.

As noted above axions and more generally ALPs interact very weakly with the Standard Model fields. Besides the gluon coupling (3.2), they interact with the electromagnetic field via the two-photon vertex

$$\mathcal{L}_{a\gamma\gamma} = -\frac{g_{a\gamma\gamma}}{4} a F^{\mu\nu}\tilde{F}_{\mu\nu} \ , \tag{3.4}$$

where the electromagnetic tensor $F_{\mu\nu}$ and its dual $\tilde{F}^{\mu\nu} = \epsilon^{\mu\nu\rho\sigma}F_{\rho\sigma}$ appear. This interaction is responsible for the axion-photon mixing phenomenon [77, 126, 129] and provides the theoretical basis for many axion detection experiments. Most of the current searches do indeed constraint the axion-photon coupling $g_{a\gamma\gamma}$. In addition, axions and ALPs can mediate an interaction between the standard model fermions. The coupling of axions with fermions is described by a Yukawa pseudoscalar vertex [130, 131]. If $\psi_1$ and$\psi_2$ are the fermion fields, the interaction term reads

$$\mathcal{L}_{a\psi\psi} = -\sum_{j=1,2} i g_{pj} a \bar{\psi}_j \gamma_5 \psi_j \tag{3.5}$$

where $\gamma_5$ is the product of Dirac matrices $i\gamma^0\gamma^1\gamma^2\gamma^3$ and $g_{pj}$ are the effective axion–fermion coupling constants, which depend critically on the fermions considered and the underlying axion (or ALP) model. Since the couplings are expected to be small, i.e. $g_{pj} \ll 1$, the scattering amplitudes are well approximated by the leading order in the perturbative expansion. For the scattering $\psi_1(p_1)\psi_2(p_2) \to \psi_1(p_1^{'})\psi_2(p_2^{'})$ we have

$$iA = \bar{u}_1^{s_1^{'}}(p_1^{'}) g_{p1}\gamma_5 u_1^{s_1}(p_1) \frac{i}{q^2-m^2} \bar{u}_1^{s_2^{'}}(p_2^{'}) g_{p2}\gamma_5 u_2^{s_2}(p_2) \tag{3.6}$$

where the pseudoscalar free propagator with momentum $q = p_1^{'} - p_1 = p_2 - p_2^{'}$ appears, and $m$ is the axion mass. Here $u_i^{s_i}(p_i)$ are the solutions of the free Dirac equation in momentum space, for the i-th fermion with momentum $p_i$ and spin projection $s_i$:

$$u_i^{s_i}(p_i) = \sqrt{\frac{\omega_i + M_i}{2\omega_i}} \begin{pmatrix} \phi_{s_i} \\ \frac{\boldsymbol{\sigma}\cdot\boldsymbol{p}_i}{\omega_i+M_i}\phi_{s_i} \end{pmatrix} \tag{3.7}$$

with $M_i$ mass of the $i$-th fermion, $\omega_i = \sqrt{\boldsymbol{p}_i^2 + M_i^2}$ energy of the $i$-th fermion and $\phi_{s_i}$ normalized two–component spinors. In the non–relativistic limit $\omega_i \approx M_i$, these become

$$u_i^{s_i}(p_i) \approx \begin{pmatrix} \phi_{s_i} \\ \frac{\boldsymbol{\sigma}\cdot\boldsymbol{p}_i}{2M_i}\phi_{s_i} \end{pmatrix} \ . \tag{3.8}$$

Inserting equations (3.8) in equation (3.6), one obtains the scattering amplitude for non–relativistic fermions

$$A \approx \frac{g_{p_1} g_{p_2}}{\boldsymbol{q}^2 + m^2} \frac{\left(\phi^\dagger_{s'_1} \left(\boldsymbol{\sigma} \cdot \boldsymbol{q}\right) \phi_{s_1}\right) \left(\phi^\dagger_{s'_2} \left(\boldsymbol{\sigma} \cdot \boldsymbol{q}\right) \phi_{s_2}\right)}{4 M_1 M_2} . \tag{3.9}$$

By Fourier transforming the amplitude (3.9) into real space, one finds the two–body potential due to axion exchange [130]

$$\begin{aligned} V(\boldsymbol{r}) &= -\frac{g_{p_1} g_{p_2} e^{-mr}}{16\pi M_1 M_2} \left[ \boldsymbol{\sigma}_1 \cdot \boldsymbol{\sigma}_2 \left( \frac{m}{r^2} + \frac{1}{r^3} + \frac{4}{3}\pi\delta^3(\boldsymbol{r}) \right) \right. \\ & \left. \qquad - \left(\boldsymbol{\sigma}_1 \cdot \hat{\boldsymbol{r}}\right) \left(\boldsymbol{\sigma}_2 \cdot \hat{\boldsymbol{r}}\right) \left( \frac{m^2}{r} + \frac{3m}{r^2} + \frac{3}{r^3} \right) \right] , \end{aligned} \tag{3.10}$$

where $r$ ($\hat{\boldsymbol{r}}$) stands for the modulus (the unit vector) of the relative distance between the fermions and $\delta^3(\boldsymbol{r})$ is the Dirac delta, while $\boldsymbol{\sigma}_i$ is the three–dimensional vector of Pauli operators defined on the $i$–th fermion. For two identical non–relativistic fermions one has $M_1 = M_2 = M$ and $g_{p_1} = g_{p_2} = g_p$, yielding the interaction Hamiltonian

$$\begin{aligned} H_p &= -\frac{g_p^2 e^{-mr}}{16\pi M^2} \left[ \boldsymbol{\sigma}_1 \cdot \boldsymbol{\sigma}_2 \left( \frac{m}{r^2} + \frac{1}{r^3} + \frac{4}{3}\pi\delta^3(\boldsymbol{r}) \right) \right. \\ & \left. \qquad - \left(\boldsymbol{\sigma}_1 \cdot \hat{\boldsymbol{r}}\right) \left(\boldsymbol{\sigma}_2 \cdot \hat{\boldsymbol{r}}\right) \left( \frac{m^2}{r} + \frac{3m}{r^2} + \frac{3}{r^3} \right) \right] . \end{aligned} \tag{3.11}$$

In the following we will always consider $r$ large enough that the contact term proportional to $\delta^3(\boldsymbol{r})$ can be neglected. Assuming, without loss of generality, that $\hat{\boldsymbol{r}}$ coincides with the $z$–direction, we obtain

$$H_p = - \frac{g_p^2 e^{-mr}}{16\pi M^2 r^3} \left[ m^2 r^2 \, \sigma_1^z \sigma_2^z + (mr + 1)\, \mathcal{O} \right] \tag{3.12}$$

where the operator $\mathcal{O}$ is defined as $\mathcal{O} = 2\sigma_1^z\sigma_2^z - \sigma_1^x\sigma_2^x - \sigma_1^y\sigma_2^y$. The equation (3.12) is the interaction, due to axion exchange, between two identical non–relativistic fermions. The form of eq. (3.12) is well suited to describe the two particle interaction, but is not sufficiently general to describe many particle interactions. The more general expression (3.11) has to be used in this case. Disregarding the $\delta$ term we can rewrite the equation (3.11) more compactly as

$$H_p = \frac{\mathcal{A}\mathcal{B} e^{-mr}}{r^3} \left[ K^{(a)}(r) \sigma_1^r \sigma_2^r - K^{(b)}(r) \boldsymbol{\sigma}_1 \cdot \boldsymbol{\sigma}_2 \right] . \tag{3.13}$$

Here $\mathcal{A} = \frac{g^2\alpha}{16M^2}$ is related to the magnetic dipole-dipole interaction, $\mathcal{B} = \frac{g_p^2}{\pi\alpha g^2}$ quantifies the relative strength of the axion-mediated interaction, $g$ denotes the fermion $g$-factor and $\alpha \simeq \frac{1}{137}$ is the fine structure constant. The functions $K^{(a)}(r) = m^2r^2 + 3mr + 3$ and $K^{(b)}(r) = mr + 1$ are dimensionless in natural units ($c = 1 = \hbar$). Finally $\sigma_j^r$ denotes the projection on $\hat{\boldsymbol{r}}$ of the Pauli vector of the $j$-th fermion $\sigma_j^r = \boldsymbol{\sigma}_j \cdot \hat{\boldsymbol{r}}$.

## 3.2 Axionlike particles and Entanglement

Having introduced ALPs and their interactions, we now proceed to study their effect on the dynamics of the standard model fermions. In this section, in particular, we study the entanglement generated by the axion-mediated interaction on a pair of identical non-relativistic fermions. We find that the entanglement properties of the two-fermion state bear a signature of the axion-mediated interaction. Therefore a measurement of such properties might provide an indirect evidence for the existence of ALPs and constitute the basis for a novel detection strategy.

### 3.2.1 Dynamics of entanglement

Inasmuch as we wish to analyze the entanglement between two fermions generated by the axion–mediated interaction (3.12), we first need to establish whether the latter can actually induce entanglement in a fermionic system. More precisely, considering two fermions interacting through the Hamiltonian $H_p$ of eq. (3.12) and initially prepared in a fully separable (non–entangled) state, we need to determine whether their state develops a non-vanishing entanglement under the action of $H_p$. There exist precise conditions that a Hamiltonian operator has to fulfill in order to produce entanglement: 1) a non completely degenerate spectrum and 2) the impossibility to be reduced to the sum of local terms acting separately on every single object [132–134]. It is immediate to verify that the Hamiltonian in eq. (3.12) satisfies both the requirements, and shall therefore induce entanglement on the two fermion system. This fact can be used to reveal axions and ALPs through the analysis of the entanglement properties of the two fermion state.

Therefore we focus on a system of two identical spin–$\frac{1}{2}$ fermions (for instance electrons or neutrons) and study the time evolution of its entanglement properties. We write the state of the system as

$$\Psi(\boldsymbol{r}_1,\boldsymbol{r}_2,s_1,s_2;t) = R(\boldsymbol{R},\boldsymbol{r};t)\psi(s_1,s_2;t) \tag{3.14}$$

where the spatial wave–function $R$ depends on the center of mass position $\boldsymbol{R}$ and the relative position of the two fermions $\boldsymbol{r} = \boldsymbol{r}_1 - \boldsymbol{r}_2$, while the spin wave–function $\psi(s_1,s_2;t)$ is a state vector in the product space $H_1^{spin} \otimes H_2^{spin}$ of the spin Hilbert spaces associated to the two particles. In order to simplify the analysis, we assume, as a first approximation, that the spatial wave–function $R$ is sharply peaked at a given value of the distance $r = |\boldsymbol{r}_1 - \boldsymbol{r}_2|$, and so remains during the time interval of interest. We then consider the distance $r$ in eq. (3.12) as a parameter, and the Hamiltonian $H_p$ as an operator acting on the spin state alone. Of course, the full wave–function $\Psi$ must be antisymmetric under particle exchange. Since we shall consider symmetric spin states $\psi(s_1,s_2;t)$, the spatial wave–function $R(\boldsymbol{R},\boldsymbol{r};t)$ must be antysimmetric.

At $t = 0$ we assume that the spin state of the whole system is fully separable, i.e. that it can be written as the tensor product of two states, each defined in the Hilbert space of a single fermion. In other words we have that, at $t = 0$, the state of the system can be written as

$$\begin{aligned} |\psi(0)\rangle &= |\varphi(0)\rangle_1 \otimes |\varphi(0)\rangle_2 \\ |\varphi(0)\rangle_i &= \cos(\theta)\,|\uparrow\rangle_i + e^{\imath\phi}\sin(\theta)\,|\downarrow\rangle_i \end{aligned} \tag{3.15}$$

where we have dropped the spin arguments $s_1, s_2$ and have switched to a more convenient Dirac notation. Here $|\uparrow\rangle_i$ and $|\downarrow\rangle_i$ denote the eigenstates of the magnetic moment along the direction joining the two fermions ($z$-direction). Being the state of Eq. (3.15) separable, the entanglement vanishes for $t = 0$.

If the two fermions were to interact with each other only through axions, a non–vanishing entanglement would directly signal their presence, but this is not the case. The two fermions generally interact with each other through several channels, and any of these is potentially a source of entanglement, depending on the distance $r$ and on the states that one considers. As we are interested in highlighting the entanglement due to axions, these interactions produce an unwanted contribution that has to be minimized in order to successfully reveal the axion–induced entanglement. Then we must devise a setting in which these additional sources of entanglement are suppressed or at least significantly reduced.

The strong and weak nuclear interactions have a very limited range. Assuming, in our setup, a relative distance large enough ($r > 10^{-12}$m), we can neglect them altogether. Gravitational and electrostatic (if the fermions have a non–vanishing electric charge) interactions persist at any distance. Nonetheless, their action on the evolution of the spin state cannot induce entanglement and amounts to a global phase factor. This is because, as previously stated, a fundamental requirement for the interaction to induce entanglement in a system is that the spectrum of the associated Hamiltonian is not fully degenerate. Particles such as electrons, protons, or neutrons are characterized by precise values of charge and mass that do not depend on their spin states. Consequently, any state depending exclusively on the spin of the particles, like those we are considering, will react to gravitational and electrostatic interactions in the same way. Then these interactions shall be represented by fully degenerate Hamiltonians on the Hilbert space of the two-fermion system, and will not generate any entanglement. The situation would clearly be different if the relative distance $\boldsymbol{r}$ were considered as a degree of freedom and not as a mere parameter. In that case the spatial part of the wavefunctions would enter the dynamics, and both gravitational and electrostatic interactions would be able to generate entanglement.

Another unwanted entanglement source is the dipole–dipole magnetic interaction, whose Hamiltonian reads

$$H_\mu = -\frac{1}{4\pi r^3}\frac{g^2 {q_e}^2}{16\, M^2}\mathcal{O}\,, \tag{3.16}$$

where $g$ is the g–factor and $q_e$ is the charge of the electron. As done in Eq. (3.12), we have dropped a contact term proportional to $\delta^3(\boldsymbol{r})$ in Eq. (3.16), assuming that $r$ is large enough. Being associated with the exchange of massless photons, this interaction is not confined at short–range and it is sensible to the different spin states in a way that cannot be reduced to the action of local operators. Hence its contribution to the entanglement is different from zero. However, in the following we will show that, by properly setting the time interval of the entanglement measurement, the contribution to entanglement due to the dipole–dipole magnetic interaction can be neglected and the entanglement reduces to the axion contribution alone.

Starting from the initial state $|\psi(0)\rangle$, the state at $t > 0$ can be obtained as $|\psi(t)\rangle = U(t)\,|\psi(0)\rangle$, where the time evolution operator $U(t)$ is unitary, since we consider our system to be closed (we neglect any other interaction with the surrounding world). $U(t)$ can be written as $U(t) = \exp[-it(H_T)]$, where the total Hamiltonian $H_T$ is the sum of the magnenetic $(H_\mu)$ and the axion term $(H_p)$, i.e. $H_T = H_p + H_\mu$, and reads

$$H_T \;=\; -\frac{\mathcal{A}}{r^3}\left[\mathcal{O} + \mathcal{B}e^{-mr}\left(m^2r^2\,\sigma_1^z\sigma_2^z + \mathcal{O}\left(mr+1\right)\right)\right]. \tag{3.17}$$

Notice that the form of the evolution operator $U(t) = e^{-iH_T t}$ presupposes a time-independent Hamiltonian operator. This condition is verified as long as the relative distance $r$ does not vary sensibly during the interaction. Since the operator $U(t)$ is unitary for any time $t \geq 0$, the state $|\psi(t)\rangle$ remains a pure state, although in general, differently from $|\psi(0)\rangle$, it is not separable, and thus entangled. The amount of entanglement between the two fermions in $|\psi(t)\rangle$ can be quantified using different measures. Here we consider the 2–Renyi entropy [135–138], that has the advantage, with respect to the other entropy–based entanglement measures, to be associated, at least in some experimental devices, to experimentally accessible quantities [139–143]. The 2–Renyi entropy is defined as $S_2 = -\ln(\mathcal{P}(\rho_i(t)))$, where

$\rho_i(t) = \mathrm{Tr}_{\mathrm{j}\neq\mathrm{i}}(|\psi(t)\rangle\langle\psi(t)|)$ is the reduced density matrix obtained projecting $|\psi(t)\rangle$ on the Hilbert space defined on one of the two femions and $\mathcal{P}(\rho_i(t)) = \mathrm{Tr}\rho_i^2(t)$ is the purity of $\rho_i(t)$. Clearly, when the state is separable the reduced density matrix corresponds to a pure state $\mathcal{P}(\rho_i(t)) = 1$ and the 2-Renyi entropy vanishes. In our system the 2-Renyi entropy reads

$$S_2(t) = -\ln\left[1 - \frac{\sin^4(2\theta)}{2}\sin^2(\Gamma t)\right] \tag{3.18}$$

where $\Gamma = \frac{6\mathcal{A}}{r^3}\left[1 + \frac{\mathcal{B}}{3}e^{-rm}\left(3 + 3rm + r^2m^2\right)\right]$. For the explicit calculation, see the appendix D. As we can see from the expression of $\Gamma$, the entanglement derives from both the dipole–dipole magnetic interaction (due to $\frac{6\mathcal{A}}{r^3}$) and from the presence of the axions (due to the term $\frac{2\mathcal{A}}{r^3}\left[\mathcal{B}e^{-rm}\left(3 + 3rm + r^2m^2\right)\right]$ ). Given the form of the 2–Renyi entropy (3.18), there exist certain times at which the entanglement is only due to the axion–mediated interaction. Indeed, by setting $t = nt^*$, with $n$ a positive integer and $t^* = \frac{\pi r^3}{6\mathcal{A}}$, we obtain:

$$\begin{aligned} S_2(nt^*) &= -\ln\left\{1 - \frac{\sin^4(2\theta)}{2}\sin^2\left[n\pi\left(1 + \frac{\mathcal{B}}{3}e^{-mr}(3 + 3mr + m^2r^2)\right)\right]\right\} \\ &\simeq \frac{\sin^4(2\theta)}{2}n^2\pi^2\mathcal{B}^2e^{-2mr}\left(1 + mr + \frac{m^2r^2}{3}\right)^2 . \end{aligned} \tag{3.19}$$

In equation (3.19), the dependence on the dipole–dipole magnetic interaction has disappeared. Recalling that $\mathcal{B} \propto g_p^2$, we can see at once that if there is no axion–mediated interaction ($g_p \to 0$), the 2-Renyi entropy, and thus the entanglement, vanishes. More precisely, as $g_p \ll 1$, the last line of eq. (3.19) shows that the entropy is proportional to $\mathcal{B}^2$ and then to $g_p^4$. In the case in which a non–zero entanglement is detected, in correspondence with the times $t = nt^*$, one can conclude that the former is a consequence of the axion–induced interaction alone. This would constitute an indirect proof of the existence of axions.

For a numerical analysis of the 2-Renyi entropy (3.19), we focus on ALPs in the mass range $10^{-3} - 1$ eV. These have been considered in the refs. [144–148], where experimental constraints have been obtained on the coupling constant $g_p$ as a function of the ALP mass, both for protons and neutrons. In Fig. 3.1 we consider two neutrons at a distance $r = 1\,\mathrm{nm}$ apart, and initial state given by Eq. (3.15) with $\theta = \pi/4$ and $\phi = 0$. We set, for each value of the mass in the range $10^{-3} - 1$ eV, the coupling constant $g_p$ equal to the threshold value $g_{threshold}$ obtained from the experimental analyses in the refs. [144–148]. In particular: for the black dot–dashed line, we set $g_p = g_{CP}$, where $g_{CP}$ is the threshold from effective Casimir pressure measurements [144], and sample values are $g_{CP} = 0.0327$ for $m = 10^{-3}$eV, $g_{CP} = 0.0348$ for $m = 0.05$eV, $g_{CP} = 0.0674$ for $m = 1$eV; for the red solid line we set $g_p = g_{CF}$, where $g_{CF}$ is the threshold from measurements of the difference of Casimir forces [148], and sample values are $g_{CF} = 0.007$ for $m = 10^{-3}$eV, $g_{CF} = 0.012$ for $m = 0.05eV$, $g_{CF} = 0.066$ for $m = 1$eV; for the blue dashed line we set $g_p = g_{IE}$, where $g_{IE}$ is the threshold from isoelectronic experiments [146], and sample values are $g_{IE} = 0.0036$ for $m = 10^{-3}$eV, $g_{IE} = 0.006$ for $m = 0.05$eV, $g_{IE} = 0.07$ for $m = 1$eV. For the three cases, the 2-Renyi entropy $S_2(t^*)$ at $t = t^*$ is shown in the upper panel of Fig. 3.1. All the lines depicted in the figure show a very similar behavior. At constant distance, larger axion masses imply a stronger damping by the Yukawa factor $e^{-mr}$. Increasing the mass one eventually arrives at a value for which the Yukawa damping starts to be relevant. From this point on, a further increment of the mass of the axions will suppress the entanglement exponentially.

To our knowledge, for ALPs in the mass range $10^{-3} - 1$eV, the values reported in

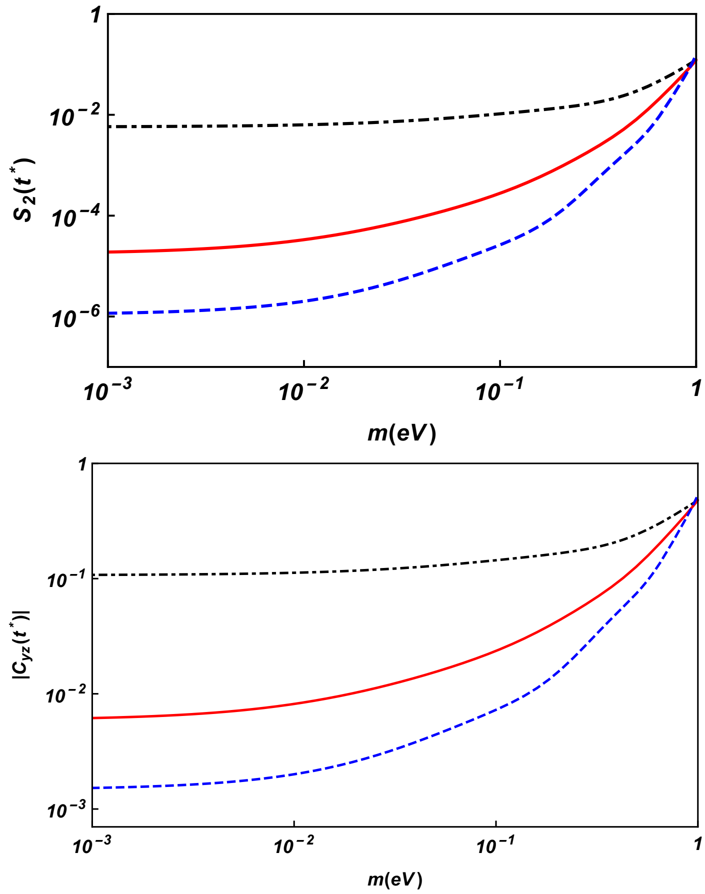


FIGURE 3.1: (color online) Plot of the 2–Renyi entropies (upper panel) and of the Witnesses $C_{yz}$ (lower panel) at $t = t^*$, i.e. for $n = 1$, between two neutrons as function of the axions mass $m$ at distance $r = 1\,\text{nm}$. In the plots we have considered two neutrons at a distance $r = 1\,\text{nm}$ apart, and initial state given by Eq. (3.15) with $\theta = \pi/4$ and $\phi = 0$. We set, for each value of the mass in the range $10^{-3} - 1$ eV, the coupling constant $g_p$ equal to the threshold value $g_{threshold}$ obtained from the experimental analyses in the refs. [144–148]. In particular: for the black dot–dashed line we set $g_p = g_{CP}$, where $g_{CP}$ is the threshold from effective Casimir pressure measurements [144], and sample values are $g_{CP} = 0.0327$ for $m = 10^{-3}$eV, $g_{CP} = 0.0348$ for $m = 0.05$eV, $g_{CP} = 0.0674$ for $m = 1$eV; for the red solid line we set $g_p = g_{CF}$, where $g_{CF}$ is the threshold from measurements of the difference of Casimir forces [148], and sample values are $g_{CF} = 0.007$ for $m = 10^{-3}$eV, $g_{CF} = 0.012$ for $m = 0.05$eV, $g_{CF} = 0.066$ for $m = 1$eV; for the blue dashed line we set $g_p = g_{IE}$, where $g_{IE}$ is the threshold from isoelectronic experiments [146], and sample values are $g_{IE} = 0.0036$ for $m = 10^{-3}$eV, $g_{IE} = 0.006$ for $m = 0.05$eV, $g_{IE} = 0.07$ for $m = 1$eV.

refs. [144–148] represent the strongest model–independent constraints on axion–nucleon interactions from laboratory experiments. For this class of ALPs, as the figure 3.1 shows, the 2-Renyi entropy is significantly different from zero, so that the laboratory constraints might be strengthened by several orders of magnitude from entanglement measurements. Of course, the so obtained constraints would be model–independent, since no specific axion or ALP model has been assumed. On the other hand, for QCD axion models there exist several constraints from astrophysical sources, primarily from supernovae [149], neutron star cooling [150] and Black Hole superradiance [151]. The indicative bound set by supernovae $g^2_{aNN} \sim 10^{-19}$ renders our method unviable for QCD axions, at least for present day technologies. For general ALPs, since mass and coupling constants are essentially unrelated, and the latter can in principle assume any value, our approach can strengthen the current laboratory constraints, with the only limitations presented by the experimental sensitivities and coherence time. It is worth to note that the idea, here presented, to use entanglement to test theories of fundamental physics is in line with several recent works, see for example Ref. [152–154] that suggest exploiting the entanglement as a probe for the quantum nature of the gravity. In fact, in these papers, the spatial wave function has a non trivial evolution, and consequently, gravitational interactions can induce entanglement.

### 3.2.2 The entanglement witness

In the upper panel of Fig. (3.1), we plot the entanglement entropy between two neutrons as a function of the axions mass, at distance $r = 1$nm and for ALPs with coupling constants $g_p$ constrained by the analysis of Refs. [144], [148] and [146]. Notice that a direct measurement of the 2–Renyi entropy is in general not easy to accomplish. To overcome this difficulty we can make use of an entanglement witness, which is a quantity strictly related to the family of states and to the dynamics of the system under analysis, whose value is able to signal the presence of entanglement. Let us set to zero the phase $\phi$ of the initial state in eq. (3.15). In this case, the entanglement witness can be identified with the two–spins correlation functions

$$C_{yz} = \langle\psi(t)|\, \sigma_1^y \sigma_2^z \,|\psi(t)\rangle \equiv \langle\psi(t)|\, \sigma_1^z \sigma_2^y \,|\psi(t)\rangle \,. \tag{3.20}$$

For any choice of $\phi$, one can find a different correlation function playing the same role. It is straightforward to show that, for any time greater than zero, the correlation function $C_{yz}$ is given by $C_{yz}(t) = -\sin(2\theta)\sin(\Gamma t)$. This function, for any $\theta \neq \frac{k\pi}{2}$ with $k$ integer, vanishes only when the entanglement is zero. For $t = nt^* = \frac{n\pi r^3}{6\mathcal{A}}$, the correlation function $C_{yz}$ depends only on the interaction between axions and fermions and reduces to

$$\begin{aligned} C_{yz}(nt^*) &= -\sin(2\theta)\sin\left[n\pi\left(1+\frac{\mathcal{B}}{3}e^{-mr}(3+3mr+m^2r^2)\right)\right] \\ &\simeq (-1)^{n+1}\sin(2\theta)n\pi\mathcal{B}e^{-rm}\left(1+rm+\frac{r^2m^2}{3}\right) \,. \end{aligned} \tag{3.21}$$

Therefore, a measurement of this quantity could provide an indirect evidence of the existence of axions.

From eq. (3.21), we can see that the entanglement witness, for $n\pi\mathcal{B} \ll 1$, has a dependence on the interaction strength proportional to $g_p^2$ rather than to $g_p^4$ making the signal larger (indeed $\mathcal{B} = \frac{4g_p^2}{\alpha g^2}$). In fact, the entanglement witness of our system assumes values larger than the entropy, making the detection of the axion and of the ALPs much more viable. This is shown in the lower panel of Fig. (3.1), where plots of the entanglement witness for $t = t^*$ are reported, and compared with those of the 2-Renyi entropy in correspondence with the same parameters.

## 3.3 Interferometry and Axionlike Particles

We have seen in the previous section that the axion-mediated interaction between two fermions is able to generate an entanglement which is in principle measurable. A fortiori the same interaction must induce observable effects on a system of *many* fermions. In this section we consider, as a prototype for such a system, a beam of neutrons. We then devise a neutron interferometry setup in order to reveal the axion-mediated interaction. In the context of neutron physics, interferometry has proven to be a formidable tool in investigating particle interactions and their quantum properties. Neutron interferometry is indeed a subject of study in its own right [155] and has granted us the chance to verify many theoretical predictions related to the quantum theory. These include the Sagnac effect [156], the geometric phase [157–159], wave–particle duality and the change of sign in the spin $1/2$ wave–function after a $2\pi$ rotation [155]. Other experiments, oriented to searches for non-Newtonian gravity at short distances and to the observation of relativistic proper time effects, related to a gravitational redshift, may be set up with neutron interferometry [155]. Here we use such a versatile tool, as neutron interferometry, to extract informations on the neutron–neutron interactions. In particular, we aim at revealing the axion–induced interaction and propose an alternative approach to the detection of ALPs for future experiments. We show that the axion–mediated interactions between neutrons sum up to give an additional magnetic term, whose presence affects the phase of the neutrons and produces an extra phase difference in interferometric experiments. We consider an idealized interferometric setup in which a collimated neutron beam is split into two sub–beams that are later let interfere with each other. Each of the sub–beams is subject to an external magnetic field of equal strength but different direction. In particular, if one of the two magnetic fields is set in the direction of propagation of the relative sub-beam and the other is orthogonal to the propagation, the neutrons will gain a path-dependent phase factor that can be easily detected by an interferometer. The experimental parameters are fixed in such a way that the interference pattern is only due to the magnetic and axion–induced interactions. We show how to isolate the axion contribution by appropriately choosing the neutron path and we set an arm length such that the contribution to the phase difference given by the dipole-dipole interaction is an integer multiple of $2\pi$. In this way, we obtain a phase difference depending only on the axion–induced interaction. The setting considered here is oversimplified in order to illustrate the basic idea. Many of the approximations employed can be lifted, and the basic geometry modified, in order to get a more realistic and efficient experimental setup. This shall be the object of future studies.

### 3.3.1 The effective magnetic field

Just as we did for the analysis of entanglement, we will assume that the neutron velocities are non-relativistic and analyze the interaction Hamiltonian (3.13) within the context of ordinary quantum mechanics. The state of the single neutron shall be taken to be the product of a spatial and a spin wavefunction. Since we are interested in the evolution of the neutron state, it is our duty to write down the appropriate Schroedinger equation. To this end we need to take into account all the possible interactions between neutrons. The gravitational interaction is easily seen to be irrelevant, due to the smallness of the masses involved. Moreover, as we did in the previous section, we shall assume an average relative distance $r > 10^{-12}$m, so that the short–range nuclear interactions can also be ignored. With this assumption the only other relevant interaction is the magnetic one between the neutron dipoles. The two–neutron interaction Hamiltonian, comprising the magnetic and the axion–mediated interaction can thus be written as

$$H = -\frac{\mathcal{A}}{r^3}\Big[\left(3-\mathcal{B}e^{-mr}K^{(a)}(r)\right)\sigma_1^r\sigma_2^r-\left(1-\mathcal{B}e^{-mr}K^{(b)}(r)\right)\boldsymbol{\sigma}_1\cdot\boldsymbol{\sigma}_2\Big]\,. \tag{3.22}$$

The two–neutron interaction can easily be generalized to an arbitrary number of neutrons. Our starting point is the total two–body Hamiltonian of eq. (3.22), with a notation suitable for an arbitrary number of neutrons:

$$H_{ij} = -\frac{\mathcal{A}}{r_{ij}^3}\left[\left(3 - \mathcal{B}e^{-mr_{ij}}K^{(a)}(r_{ij})\right)\sigma_i^{r_{ij}}\sigma_j^{r_{ij}} - \left(1 - \mathcal{B}e^{-mr_{ij}}K^{(b)}(r_{ij})\right)\boldsymbol{\sigma}_i\cdot\boldsymbol{\sigma}_j\right].$$

In the case of two particles it is natural to choose one of the spatial axes so to coincide with the line joining the two $\hat{\boldsymbol{r}}$, see e.g. eq. (3.11). For a generic number of particles there are many such directions $\hat{\boldsymbol{r}}_{ij}$, one for each pair, and thus one has to express eq. (3.23) with respect to an arbitrary, but fixed, spatial triple $\hat{\boldsymbol{x}}, \hat{\boldsymbol{y}}, \hat{\boldsymbol{z}}$. Hence, for each pair $i, j$, we introduce the projections $R_{ij}^u = \hat{\boldsymbol{r}}_{ij}\cdot\hat{\boldsymbol{u}}$, with $u = x, y, z$. In terms of the polar angles $\theta_{ij}, \phi_{ij}$, the projections can explicitly be written as $R_{ij}^x = \sin(\theta_{ij})\cos(\phi_{ij})$, $R_{ij}^y = \sin(\theta_{ij})\sin(\phi_{ij})$ and $R_{ij}^z = \sin(\theta_{ij})$. The operators $\sigma_i^r$ are then obviously equal to

$$\sigma_i^{r_{ij}} = R_{ij}^x\sigma_i^x + R_{ij}^y\sigma_i^y + R_{ij}^z\sigma_i^z\,. \tag{3.23}$$

The notation $\sigma_i^{r_{ij}}$ is used to remark that while these operators act only upon the space of the $i$-th particle, their form depends on the specific pair $i, j$ considered. Writing the projections explicitly, equation (3.22) becomes

$$\begin{aligned}H_{ij} = &-\frac{\mathcal{A}}{r_{ij}^3}\left(1 - \mathcal{B}e^{-mr_{ij}}K^{(b)}(r_{ij})\right)\boldsymbol{\sigma}_i\cdot\boldsymbol{\sigma}_j - \frac{\mathcal{A}}{r_{ij}^3}\left(3 - \mathcal{B}e^{-mr_{ij}}K^{(a)}(r_{ij})\right)\\ &\times\Big[(R_{ij}^x)^2\sigma_i^x\sigma_j^x + (R_{ij}^y)^2\sigma_i^y\sigma_j^y + (R_{ij}^z)^2\sigma_i^z\sigma_j^z + R_{ij}^xR_{ij}^y\left(\sigma_i^x\sigma_j^y + \sigma_i^y\sigma_j^x\right)\\ &+R_{ij}^xR_{ij}^z\left(\sigma_i^x\sigma_j^z + \sigma_i^z\sigma_j^x\right) + R_{ij}^yR_{ij}^z\left(\sigma_i^y\sigma_j^z + \sigma_i^z\sigma_j^y\right)\Big]\,.\end{aligned} \tag{3.24}$$

Then, the total interaction Hamiltonian is simply

$$H = \frac{1}{2}\sum_{i,j} H_{ij} \tag{3.25}$$

where the sum runs over all the neutron pairs $i \neq j$ and the factor $\frac{1}{2}$ accounts for double counting.

To go further, we express (3.24) in a more compact way. Setting $C(\boldsymbol{r})$ and $D(\boldsymbol{r})$ as

$$C(\boldsymbol{r}) = \frac{\mathcal{A}}{r^3}\left(1 - \mathcal{B}e^{-mr}K^{(b)}(r)\right), \tag{3.26}$$

$$D(\boldsymbol{r}) = \frac{\mathcal{A}}{r^3}\left(3 - \mathcal{B}e^{-mr}K^{(a)}(r)\right), \tag{3.27}$$

we can introduce the symmetric matrix $K^{uv}(\boldsymbol{r})$

$$K^{uv}(\boldsymbol{r}) = C(\boldsymbol{r})\delta^{uv} - D(\boldsymbol{r})R^u(\boldsymbol{r})R^v(\boldsymbol{r})\,. \tag{3.28}$$

where $u, v = x, y, z$. Here $\delta^{uv}$ is the Kronecker symbol and $R^u(\boldsymbol{r}) = \hat{\boldsymbol{r}}\cdot\hat{\boldsymbol{u}}$ (notice that $R_{ij}^u = R^u(\boldsymbol{r}_j - \boldsymbol{r}_i)$). The interaction Hamiltonian can then be written as

$$H = \frac{1}{2}\sum_{i\neq j}\sum_{u,v} K^{uv}(\boldsymbol{r}_j - \boldsymbol{r}_i)\sigma_i^u\sigma_j^v. \tag{3.29}$$

From eq. (3.29) it is easy to see that the analysis of the evolution of the $n$–neutron state with a generic $n$, interacting via $H$ is in principle a complicated many–body problem, which hardly admits an analytical treatment if no further assumptions are made. In the present context, however, we are not interested in correlations and collective effects, and are concerned only with the evolution of the single neutron state. For this reason it is convenient to encode the interaction with all the other nucleons in an effective one–particle potential, by resorting to a mean field approach. Given a neutron at position $\boldsymbol{r}_i$ and Pauli operator $\boldsymbol{\sigma}_i$, the instantaneous interaction Hamiltonian due to the other neutrons is $H_i = \sum_{u,v}\sum_{j\neq i} K^{uv}(\boldsymbol{r_{ij}})\sigma_j^u\sigma_i^v$ , where the sum runs over all the other neutrons $j$. To obtain an effective local potential for the single neutron, this equation is replaced with its expectation value on the state of the other nucleons. In doing so, the single particle Hamiltonian $H$ acquires a very neat interpretation in terms of an effective magnetic field due to the other neutrons. Indeed, setting

$$\mu \boldsymbol{B_i}(\boldsymbol{r_i}) = -\sum_u\sum_j K^{uv}(\boldsymbol{r_{ij}})\langle\sigma_j^u\rangle\,, \tag{3.30}$$

we recover the usual term of a spin interacting with a magnetic field $H_i = -\mu\left(\boldsymbol{B_i}(\boldsymbol{r_i})\right)\cdot\boldsymbol{\sigma}$. Once the effective magnetic field is computed for a particular spatial–spin configuration, one simply plugs the one–particle operator in the Schroedinger equation in order to study the evolution of the single neutron state.

### 3.3.2 Neutron interferometry and ALPS

In the foregoing we shall consider collimated neutron beams. For cold neutrons, collimation and a small beam width of the order of 10 ¯m can be obtained by any of the means described in ref. [160], i.e. by use of collimation slits, reflected beams or neutron waveguides. The neutron flux and its intensity depend on the neutron source (typical intensities at the detector are in the range $I = 10^4 - 10^8\ n/s$) and, of course, on the collimation device, which cuts off a part of the incoming neutron flux. We will also assume that only neutrons around a given value of the kinetic energy $K$ are selected, for instance by use of a monochromator. In its trip from the collimation device to the detector, the neutron beam experiences an angular spread whose entity depends on the collimation device and on the collimator–detector distance. Very small angle spreads can be obtained for reflected beams [160]. We can generally consider that the beam is distributed with cylindrical symmetry around the beam axis $\hat{\boldsymbol{y}}$, and, assuming that it is sufficiently thin, we model the beam as a monodimensional system. As a first instance, we also neglect the losses due to propagation and consider the beam intensity as a constant. None of these assumptions is essential for our analysis, but they ensure the simplest possible setting. The complications due to a finite beam width $w$ and a non-constant intensity have certainly to be taken into account in order to attain a more realistic scenario, and will be dealt with in future works.

#### The setup

Given these preliminaries, we now discuss an idealized setup aimed at revealing the axion–mediated interaction among neutrons. A beam of cold or ultra–cold neutrons, whose source **SRC** might be an appropriate reactor, is conveyed to an external apparatus **EXT** which has the purpose of rendering the beam as monochromatic as possible (e.g. using monochromators) and also serves as a collimator, making the beam as thin and linear as possible. The beam then goes through a beam splitter **BS** which splits the beam into two sub–beams $I$ and $II$. Then each of the sub–beams enters a Stern–Gerlach like apparatus that selects two different spin polarizations $\boldsymbol{P}_I$ and $\boldsymbol{P}_{II}$ (the upper case indices $J = I, II$ and roman numerals are used to denote the specific sub–beam). The average polarizations are maintained by two constant

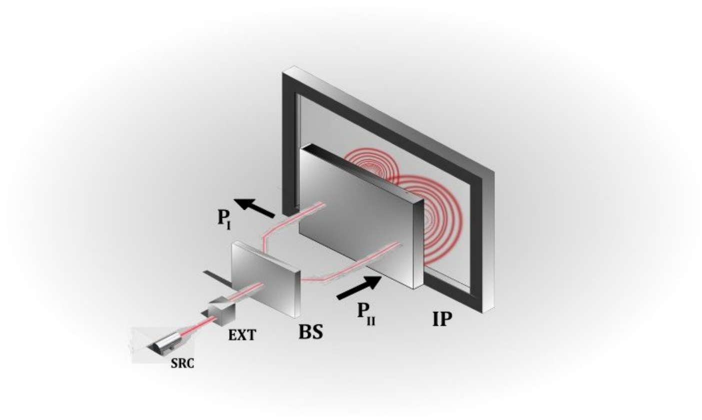


FIGURE 3.2: (color online) Schematic diagram of the interferometric apparatus. The beam from the neutron source **SRC** is conveyed to an external apparatus **EXT** consisting of a collimation device and a monochromator. The collimated and monochromatic beam is then conveyed to a beam splitter **BS** which splits the beam into two subbeams with different average spin polarizations $\boldsymbol{P}_I$ and $\boldsymbol{P}_{II}$. Finally the two subbeams interfere at the interference plane **IP**.

and uniform magnetic fields $\boldsymbol{B^0_I}$ and $\boldsymbol{B^0_{II}}$ surrounding the sub–beams $I$ and $II$ of the same strength but with distinct direction, i.e. $\boldsymbol{B^0_J} = B_0\boldsymbol{P_J}$.

The setup is schematically pictured in fig. (3.2). The fractional intensities of the subbeams with respect to the initial beam $I_0$, namely $\chi_I = \frac{I_I}{I_0}$ and $\chi_{II} = \frac{I_{II}}{I_0}$ should be as close as possible $\chi_I \simeq \chi_{II}$. The intensities regulate the average distance between successive neutrons in the two subbeams $d_I$ and $d_{II}$, in the following way. Assuming a perfectly linear beam and an average distance $d$, in a time $dt$ the number of neutrons passing through a given point on the line of propagation $dN$ is evidently

$$dN = \frac{\bar{v}dt}{d} \tag{3.31}$$

where $\bar{v}$ is the average neutron velocity in the direction of propagation. Then

$$\frac{dN}{dt} = I = \frac{\bar{v}}{d} \tag{3.32}$$

which of course means that the higher is the intensity, the smaller is the average distance between two consecutive neutrons. Therefore $d_I = \frac{\bar{v}}{I_I}$ and $d_{II} = \frac{\bar{v}}{I_{II}}$ (where we have assumed the same average velocity in both subbeams). Considering constant intensities $I_J$ and constant average neutron velocities $\bar{v}_J$, the average distances themselves $d_J$ are constant, resulting in a time–independent one particle Hamiltonian $H$, and if $\chi_I \simeq \chi_{II}$, $d_I \simeq d_{II}$. The $d_J$ should be in any case large enough to neglect the effects of nuclear interactions $d_J > 10^{-12}$m. For simplicity, from now on, we assume that all the nearest neighbour distances within sub–beam $J$ are constant and equal to $d_J$.

The two polarized sub–beams then go through two optical paths of the same length to the interference plane **IP**, where the interference pattern is observed.

### Evaluation of effective magnetic fields

Let $\hat{\boldsymbol{y}}_J$ denote the direction of propagation in sub–beam $J$. Choosing $\boldsymbol{P}_I$ to be orthogonal to $\hat{\boldsymbol{y}}_I$ and $\boldsymbol{P}_{II}$ parallel to $\hat{\boldsymbol{y}}_{II}$, from eq. (3.30), we can find the expression of the magnetic field acting on a single neutron spin. Indeed, according to our assumptions, the two sub–beams can be approximated as a one–dimensional regular chain, in which the distance between neighboring neutrons is constant (at least on average) and equal to $d_J$. Let us first consider the contribution of the closest $2n$ neighboring neutrons to the effective magnetic field acting on the single neutron. In the two sub–beams we have

$$(\mu \boldsymbol{B})_{nI} = \sum_{l=1}^{n} [-2C(ld_I)\boldsymbol{P}_I] \ ; \tag{3.33}$$

$$(\mu \boldsymbol{B})_{nII} = \sum_{l=1}^{n} 2\left[D(ld_{II}) - C(ld_{II})\right] \boldsymbol{P_{II}} \ . \tag{3.34}$$

From eqs. (3.26) and (3.27) we see that each term in the two sums that define the magnetic fields are porportional to $d^{-3}$. This implies that the sums in equations (3.33) and (3.34) converge rapidly to their limiting value ($n \to \infty$), as neutrons farther away give smaller and smaller contributions. Therefore, in the evaluation of the magnetic fields, we can consider the $n \to \infty$ limit as a good approximation, since neutrons at distance $nd_J$ give a vanishing contribution for large $n$. Assuming the $n \to \infty$ limit the effective magnetic fields can be computed straightforwardly. Indeed it is easy to see that

$$\begin{aligned}
\sum_{l=1}^{\infty} C(ld) &= \frac{\mathcal{A}}{d^2}\left[\frac{\zeta(3)}{d} - \frac{\mathcal{B}}{d}\mathrm{Li}_3(e^{-md}) - \mathcal{B}m\mathrm{Li}_2(e^{-md})\right] \ ; \\
\sum_{l=1}^{\infty} D(ld) &= \frac{3\mathcal{A}}{d^3}\zeta(3) + \frac{\mathcal{A}\mathcal{B}m^2}{d}\log(1-e^{-md}) - \frac{3\mathcal{A}\mathcal{B}m}{d^2}\mathrm{Li}_2(e^{-md}) - \frac{3\mathcal{A}\mathcal{B}}{d^3}\mathrm{Li}_3(e^{-md}) \\
&,
\end{aligned} \tag{3.35}$$

where $\zeta(s)$ stands for the Riemann zeta function while $\mathrm{Li}_s(z) = \sum_{n=1}^{\infty} \frac{z^n}{n^s}$ is the Polylogarythm function (see [161] and the appendix A). Exploiting these results the effective magnetic fields can thus be written as ($\mu \boldsymbol{B_J} = \mu B_J \boldsymbol{P_J}$)

$$\begin{aligned}
\mu B_I &= -\frac{2\mathcal{A}\zeta(3)}{d_I^3} + \frac{2\mathcal{A}\mathcal{B}}{d_I^3}\mathrm{Li}_3(e^{-md_I}) + \frac{2\mathcal{A}\mathcal{B}m}{d_I^2}\mathrm{Li}_2(e^{-md_I}) \\
\mu B_{II} &= \frac{4\mathcal{A}\zeta(3)}{d_{II}^3} - \frac{4\mathcal{A}\mathcal{B}}{d_{II}^3}\mathrm{Li}_3(e^{-md_{II}}) - \frac{4\mathcal{A}\mathcal{B}m}{d_{II}^2}\mathrm{Li}_2(e^{-md_{II}}) + \frac{2\mathcal{A}\mathcal{B}m^2}{d_{II}}\log(1-e^{-md_{II}}) \\
&.
\end{aligned} \tag{3.36}$$

**Evolution of the Neutron state and phase difference**

The evolution of the neutron state $\psi_J$, for both subbeams ($J = I, II$), is governed by the Schroedinger equation

$$i\partial_t \psi_J = \left(-\frac{\nabla^2}{2M} + M\right)\psi_J - \boldsymbol{\sigma}\cdot\left[\mu(\boldsymbol{B_J} + \boldsymbol{B_J^0})\right]\psi_J \tag{3.37}$$

where $\psi_J$ is the product of a spatial wave-function (a plane wave $f(t)e^{i\boldsymbol{k}\cdot\boldsymbol{x}}$ if the beam is perfectly monochromatic) and a spin function. It is convenient to write the spinor for each sub–beam in the basis defined by the corresponding polarization, namely $\boldsymbol{\sigma}\cdot\boldsymbol{P_J}\,|\uparrow_J\rangle = |\uparrow_J\rangle$ and $\boldsymbol{\sigma}\cdot\boldsymbol{P_J}\,|\downarrow_J\rangle = -\,|\downarrow_J\rangle$. We assume that as soon as the neutron leaves **BS**, it is found in the up state for the corresponding sub–beam; at this instant we set $t = 0$.

If $y$ denotes the coordinate along the propagation axis, with $y = 0$ at the beginning of the optical path, thereby setting $t = 0$, we have $\psi_J(t) = f(t)e^{iky}\,|\uparrow_J\rangle$ where $f(t)$ is a function to be determined. Assuming $f(t) = e^{-i\omega_J t}$ and substituting in eq. (3.37) gives $\omega_J = \frac{k^2}{2M} + M - \mu B_J - \mu B_0$. Then the total phase accumulated in a time $t$ for a neutron in subbeam $J$ is equal to

$$\phi_J(t) = \arg\left(\langle\psi_J(0)|\psi_J(t)\rangle\right) = -\left(\frac{k^2}{2M} + M - \mu(B_J + \mu B_0)\right)t. \tag{3.38}$$

It follows that the phase difference between the two subbeams at the interference plane is, after a time $t$,

$$\Delta\phi(t) = \phi_{II}(t) - \phi_I(t) = \mu\left(B_{II} - B_I\right)t \tag{3.39}$$

which can be computed immediately with the aid of eqs. (3.36). Assuming $d_I = d_{II} = d$, the phase difference can be compactly expressed as

$$\Delta\phi(t) = \left[G_m(d) + G_a(d)\right]t\,, \tag{3.40}$$

with $G_m(d)$ coming from the dipole–dipole interaction and $G_a(d)$ from the axion–mediated interaction. These are

$$\begin{aligned} G_m(d) &= \frac{6\mathcal{A}}{d^3}\zeta(3) \\ G_a(d) &= -\frac{6\mathcal{A}\mathcal{B}}{d^3}\mathrm{Li}_3(e^{-md}) - \frac{6\mathcal{A}\mathcal{B}m}{d^2}\mathrm{Li}_2(e^{-md}) + \frac{2\mathcal{A}\mathcal{B}m^2}{d}\log(1-e^{-md})\,. \end{aligned}$$

where the $n \to \infty$ limit is understood. To the phase difference $\Delta\phi(t)$ one must in principle add a possible phase shift $\Delta\phi_{BS}$ due to the operations conducted in the beam splitter and in the Stern–Gerlach like apparatus, which for our purposes should be as small as possible.

To isolate the axion contribution in the phase difference, one can set the beam path (and then the evolution time $t$) in such a way that the first term, due to dipole-dipole interactions, is an integer multiple of $2\pi$, since this phase difference is indistinguishable from a vanishing phase difference. These times, for each integer $k$, are clearly given by $T_k = \frac{2k\pi}{G_m(d)} = \frac{k\pi d^3}{3\mathcal{A}\zeta(3)}$, and the phase difference, evaluated at $T_k$, reads

$$\Delta\phi(T_k) = \left\{\frac{k\pi\mathcal{B}}{3\zeta(3)}\left[2m^2d^2\log(1-e^{-md}) - 6md\mathrm{Li}_2(e^{-md}) - 6\mathrm{Li}_3(e^{-md})\right]\right\}_{\mathrm{mod}\,2\pi} \tag{3.41}$$

Notice that this phase is non–zero only in presence of ALPs, since it vanishes for $\mathcal{B} = 0$.

### 3.3.3 Numerical Analysis

In this section we provide a numerical analysis of the phase difference and discuss the main results. As it is evident from eq. (3.41), the phase difference, evaluated at the $k$-th recurrence time $T_k$, is proportional to the parameter $\mathcal{B} \propto g_p^2$. In the range of ALP masses $m \in [10^{-6} - 1]$eV, and inter–neutron distances $d \in [10^{-11} - 10^6]$m, the phase depends only weakly on the parameters $m, d$, while keeping a relatively strong dependence on the coupling. In fig. (3.3) we plot the phase difference, modulo $2\pi$, evaluated at the minimum recurrence time $T_1$ for several values of the coupling constant $g_p$ in the mass range $[10^{-3}, 1]$ eV. The couplings are chosen compatibly with the model–independent constraints from several experimental analyses [144, 146, 148]. For $m < 0.1$eV we see that the phase difference is essentially the same for $d = 10^{-8}$m and $d = 10^{-6}$m, showing that the dependence on the distance becomes relevant only when the product $md$ is quite high (right tail of the curves in the inset of (3.3)). This obviously traces back to the Yukawa damping factor $e^{-md}$ which accompanies the axion–mediated interaction, and can be clearly seen from

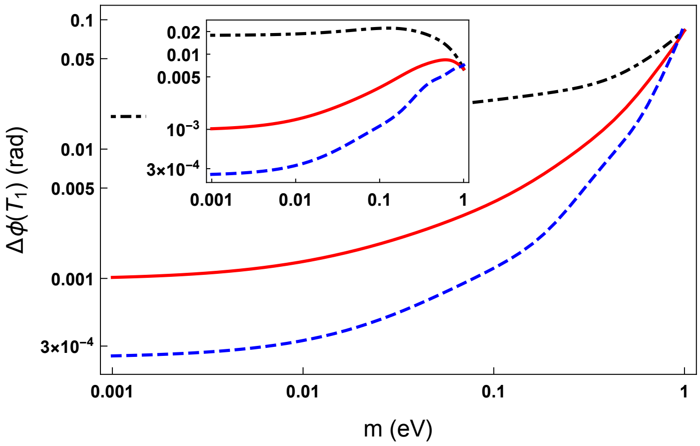


FIGURE 3.3: (color online) Logarithmic scale plot of the phase difference $|\Delta\phi(T_1)|$ (Eq. (3.41)) modulo $2\pi$ for several values of the coupling constant in the ALP mass range $[10^{-3}, 1]$ eV for an inter–neutron distance $d = 10^{-8}$m ($d = 10^{-6}$m in the inset). In particular: (black dot–dashed line) $g_p = g_{CP}$, where $g_{CP}$ is the threshold from effective Casimir pressure measurements [144] and sample values are $g_{CP} = 0.0327$ for $m = 10^{-3}$eV, $g_{CP} = 0.0348$ for $m = 0.05$eV, $g_{CP} = 0.0674$ for $m = 1$eV; (red solid line) $g_p = g_{CF}$, where $g_{CF}$ is the threshold from measurements of the difference of Casimir forces [148] and sample values are $g_{CF} = 0.007$ for $m = 10^{-3}$eV, $g_{CF} = 0.012$ for $m = 0.05$eV, $g_{CF} = 0.066$ for $m = 1$eV; (blue dashed line) $g_p = g_{IE}$, where $g_{IE}$ is the threshold from isoelectronic experiments [146], and sample values are $g_{IE} = 0.0036$ for $m = 10^{-3}$eV, $g_{IE} = 0.006$ for $m = 0.05$eV, $g_{IE} = 0.07$ for $m = 1$eV.

Eq.(3.41) when $md \to 0$: $\Delta\phi(T_k) \simeq \left[-\frac{2k\pi\mathcal{B}}{\zeta(3)}\mathrm{Li}_3(1)\right]_{\mathrm{mod}\,2\pi}$, implying that when $md \ll 1$, the phase difference essentially depends only upon the coupling $g_p$ (via the parameter $\mathcal{B}$).

A similar conclusion can be drawn from fig. (3.4). Here the damping is evident for $d = 10^{-6}$m (lower panel). Fig. (3.4) also shows clearly the $g_p^2$ dependence of the phase difference and an extremely weak dependence on the ALP mass in the ranges considered. The results presented in the figure are in the spirit of a model–independent analysis, which in principle applies to any ALP which experiences an interaction with neutrons. Since masses and couplings vary sensibly from a model to another, we choose a relatively wide range of parameters, with $(m, g_p) \in [10^{-6}, 1]\mathrm{eV} \times [10^{-6}, 10^{-1}]$. For inter–neutron distances $d <$ 1¯m the phase difference is essentially independent on the ALP mass, being sensible to the coupling constant alone. This means that while the mass range considered can be enlarged to include lower and lower masses without affecting the results, the possibility to measure the phase difference at lower coupling constants is limited by the sensibility achievable in the experiment. It should be remarked that when the inter–neutron distance $d$ is small enough, one can evaluate the phase difference at the $k$-th recurrence time with a high $k$, while keeping the propagation time reasonable. This has the effect of bringing along a multiplicative $k$ factor in the phase difference, see eq. (3.41), which in principle may render it observable at lower values of the coupling constant. For instance, at $d = 10^{-9}$m one can choose $k \simeq 4000$ while still keeping $T_k < 1$s. The observability of the phase difference is limited by the finite precision achievable in the experiment, and from the elements over which one has only a poor control. The first obvious limitation comes from the need for a recurrence time $T$ in order to isolate the axion contribution to the phase difference. This time cannot be arbitrarily long, because of the finite neutron lifetime $\tau_n \simeq 880$s and especially because of

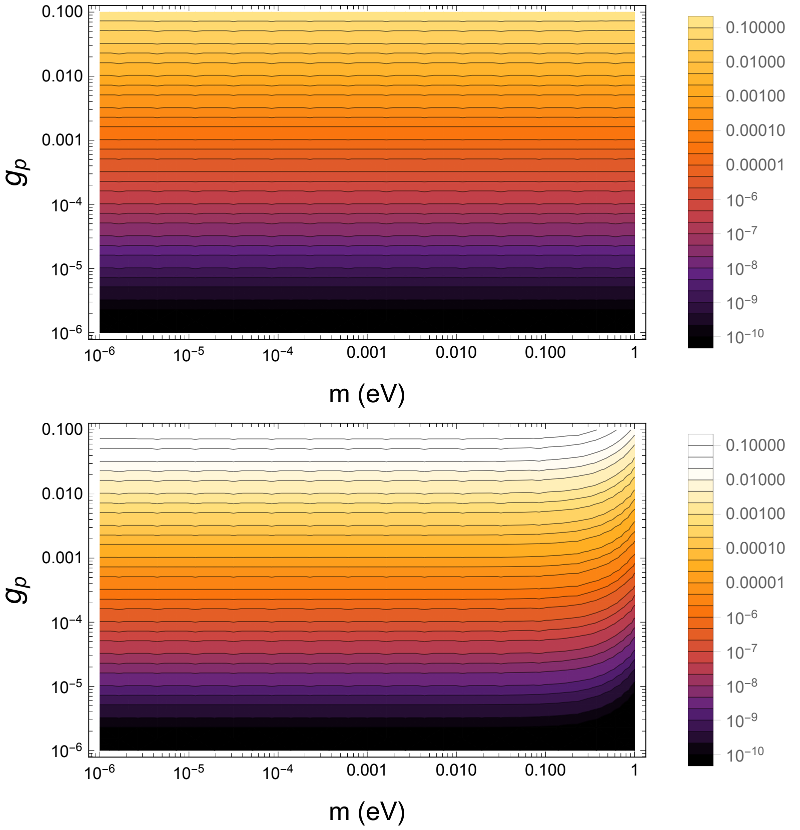


FIGURE 3.4: (color online) Contour plots of the phase difference $|\Delta\phi(T_1)|$, modulo $2\pi$, in the mass–coupling plane for $d = 10^{-9}m$ (upper panel) and $d = 10^{-6}m$ (lower panel) in the range $(m, g_p) \in [10^{-6}, 1]\text{eV} \times [10^{-6}, 10^{-1}]$. The Yukawa damping is visible in the lower panel at the right end of the plot, where curves corresponding to lower values of the phase difference are pushed up vertically.

a finite coherence length (and therefore a finite coherence time) which may be the result of unwanted interactions with the environment. Recurrence times of the order of the second can be obtained for $d \simeq 10^{-8}$ m. At the opposite end stands the issue of time resolution. A recurrence time too small would imply an extremely fast oscillation of the phase difference, rendering its analysis uneasy. This is not really a problem, unless very small inter–neutron distances $d < 10^{-11}$m are considered. The minimum recurrence time $T$ also has an obvious impact on the size of the interferometric apparatus needed. If $v$ denotes the average neutron velocity, the arm length must be at least $L = vT$. If $T \simeq$ s and $L$ must be of the order of meters, the average neutron velocity cannot exceed a few $\text{m/s}$. For this reason ultra cold neutrons are to be preferred, as they can have velocities as small as $5\ \text{m/s}$ [162]. The second important limitation comes from the total neutron flux available, and therefore the available beam intensity $I$. Because of the several devices involved in the preparation of the beam (collimator, monochromator and so on) the flux loss may be significant. A relatively high intensity of the beam, on the other hand, is essential for a sufficiently small inter–neutron distance. In turn, a small $d$ guarantees a reasonable recurrence time. If the neutron velocity is of the order of $v \simeq 1\ \text{m/s}$, a distance $d \simeq 10^{-8}$m is obtained in correspondence with an intensity $I \simeq 10^8\text{n/s}$. This is reasonable, given that pulsed neutron beams can reach intensities of the order $I \simeq 10^{10} n/s$ [163].

### The parameter space

Here we briefly discuss our choice of parameters. We point out that the parameter space we consider is ruled out by astrophysical arguments but is compatible with the theoretical analyses on the Casimir effect and fifth force experiments [144, 146, 148, 164]. We stress that the former are strongly model dependent and rely on a great deal of assumptions on the underlying physics.

We remark that the ALPs we consider are not necessarily QCD Axions but pseudoscalar particles which have properties similar to the axion and that the relation $g_{af} = (C_{af} m_f)/f_a$ which holds for QCD axions is not necessarily verified for a generic ALP, like those we are analyzing. Therefore no conclusion on $f_a$ and on the relation $g_{af} = (C_{af} m_f)/f_a$ can a priori be drawn.

Collider experiments study the existence of heavy ALPs with $m > 100$ MeV [165, 166]. Our proposal is not appropriate for this kind of ALPs, since the phase difference in equation (3.41) is exponentially suppressed,independently of the coupling constant, because of the Yukawa factor $e^{-md}$, even for small distances.

The constraints on axion-like particles from pion decays are relevant for axion masses of the order of $10 - 100$MeV [167]. These values lie outside the range of masses that we can probe. Moreover this kind of experiments is sensitive to the axion-photon coupling and the meson-axion mixing angle but give no direct constraint on the axion-nucleon couplings.

We point out that the experiments (Light shining through a wall [168], CAST [168] ,SUMICO [168] , SN1987a [149, 169], LEP [170], LHC [171, 172], Meson decays [167]), study the axion-photon interaction and constrain the related coupling constant $g_{a\gamma\gamma}$ but provide no direct and model independent constraints on $g_p$. The strategy we propose, which instead focuses on the fermion-fermion interaction mediated by the ALPs, may allow to cover a new parameter space, and eventually test some ALP models, like those considered in the references [144, 146, 148, 164].

# Chapter 4

# Phenomenology of flavor mixing and neutrino interactions

In the first part of the thesis we have discussed the quantum field theory of neutrino mixing in curved space and have shown how the condensate structure of the flavor vacuum may contribute to the dark components of the universe. The effects on flavor mixing due to quantum field theory, either in flat or curved space, are however extremely hard to be experimentally detected, in virtue of their smallness and the poor control over the system. The same holds for the gravitational interaction among neutrinos, especially because of the tiny masses involved $m_\nu \simeq 10^{-3}$eV. Currently these phenomena cannot be accessed directly. Yet it is possible to *simulate* the original system and replicate its physics in a controlled environment. Atomic physics provides the natural framework to simulate otherwise inaccessible physical systems, thanks to the careful handling of the interactions and of the physical background. The next two sections take advantage of versatile atomic systems, namely ultracold Rydberg atoms and trapped ions, in order to simulate, respectively, the quantum field theory effects in neutrino mixing and the neutrino-neutrino gravitational interactions. The last section is devoted to neutrino interactions with matter, in an effort to go beyond the simple MSW treatment. There we discuss how matter leads to dissipative effects and can represent a source of decoherence for neutrinos.

## 4.1 Probing quantum field theory and dark-matter-like effects with Rydberg atoms

A test of the contribution of the condensate of mixed fermions, like neutrinos, to the dark matter, is extremely hard to be achieved. This is because the condensate energy is relevant only at cosmological scales and also because the fermions involved are, usually, difficult to control. Then, it would be of great interest to individuate an analogous physical system that could be, in principle, controlled in laboratory. Here, we identify such a system with an ensemble of independent Rydberg atoms [173] interacting with a laser light. They are atoms whose outermost electron is in a large principal quantum number ($n$) excited state. They owe their name to the fact that their energy levels closely resemble those of the hydrogen atom, up to a corrective factor called *quantum defect* $\delta_l$. Namely, for $n \gg 1$ one has $E_{n,l} = -\frac{Ry}{(n-\delta_l)^2}$, where $Ry \approx 13,6\ eV$ is the Rydberg constant and $\delta_l$ depends both on the atomic species considered and the orbital quantum number. Typically $\delta_l$ is significant only at low angular momentum $l \leq 4$ [174–176]. For neutral alkali atoms, like Cs and Rb, the total electronic spin is $s = \frac{1}{2}$, which makes them good candidates for the simulation of a fermionic system.

The formal analogy between Rydberg atoms and neutrino mixing allows to study some features expected for mixing fermions by means of the analysis of Rydberg atoms. Hence, we analyze the mixing of Rydberg atoms in the framework of Quantum Field Theory (QFT). We show that the QFT formalism of oscillating Rydberg atoms is formally equivalent to that of two flavor fermion mixing and thus must produce the same condensate structure. We prove that the energy of the physical vacuum has, indeed, the equation of state of the dark matter. We compute the additional energy density originating from the condensate structure and its contribution to the thermal capacity of the gas. The study of the thermal capacity of Rydberg atoms could open a new way to the research and to the understanding of the dark components of the universe. The eventual detection of a small deviation from the expected profile of the thermal capacity of such atoms should demonstrate the existence of the condensate and should prove that a component of the dark matter is represented by quantum vacuum energy. Moreover, we show QFT corrections to the oscillation formulas describing the transitions between ground and excited states. Also this correction could be, in principle tested in laboratory.

### 4.1.1 QFT of Rydberg atoms

In this section we prove the formal equivalence between the QFT formalism describing an ensemble of independent Rydberg atoms interacting with a laser light, and the QFT of two flavor fermion mixing. This analogy can be used to study many aspects of particle mixing that are predicted theoretically, but hardly visible from an experimental point of view.

Let us start describing the atomic system that we will consider. We take into account an ensemble of Rydberg atoms at a very low density, that allows us to neglect all the interactions among them, and temperature low enough to permit us to discard all the finite temperature effects. The whole set interacts with a laser light with Rabi frequency $\Omega(t)$ and detuning $\Delta(t)$, coupling two levels of the atoms that we name $g$ and $e$ with related fields $\phi_g$ and $\phi_e$, and with $E_g < E_e$.

With these assumptions the total Hamiltonian describing the system can be seen as the sum of one–particle operators each one of them describing a single atom. The single atom Hamiltonian can be split in two contributions, one corresponding to the center of mass Hamiltonian $H_{CM}$ and the second corresponding to the outer electron $H_E$. With these assumptions, the electronic Hamiltonian, in the rotating wave approximation, is given by [177, 178]

$$H_E = \sum_n \int d^3x (E_n - \Delta_n(t))\phi_n^\dagger(x)\phi_n(x) + \hbar\Omega(t) \int d^3x(\phi_g^\dagger(x)\phi_e(x) + \phi_e^\dagger(x)\phi_g(x)) \,, \tag{4.1}$$

where $n$ is $g$ or $e$ and $\Delta_n(t) = \Delta(t)\,\delta_{ne}$. Moreover, we assume that the center of mass Hamiltonian $H_{CM}$ is that of free Dirac fields

$$H_{CM} = \sum_n \int d^3x \left(\frac{i}{2}\bar{\phi}_n\,\gamma^0 \overleftrightarrow{\partial}_0 \phi_n + \frac{i}{2}\bar{\phi}_n \gamma^j \overleftrightarrow{\partial}_j \phi_n + m\bar{\phi}_n\phi_n\right) \tag{4.2}$$

with $m$ the mass of the atom considered. Let us focus on the electronic part of the Hamiltonian. By setting $\varepsilon_n = E_n - \hbar\Delta_n(t)$, we can equivalently write

$$H_E = \int d^3x\, \bar{\psi}(x)\, \boldsymbol{M}\, \psi(x) \tag{4.3}$$

where $\bar{\psi}(x) = \begin{pmatrix}\bar{\phi}_g(x) & \bar{\phi}_e(x)\end{pmatrix}$ is a doublet of Dirac fields and $\boldsymbol{M}$ is the $8 \times 8$ matrix

$$\boldsymbol{M} = \begin{pmatrix} \varepsilon_g \mathbb{1}_4 & \hbar\Omega(t)\mathbb{1}_4 \\ \hbar\Omega(t)\mathbb{1}_4 & \varepsilon_e \mathbb{1}_4 \end{pmatrix}. \tag{4.4}$$

with $\mathbb{1}_4$ the $4 \times 4$ identity matrix. $\boldsymbol{M}$ is analogous to the two–flavor mass matrix which characterizes the mixing of kaons, $B^0$, $D^0$ [97, 98, 179, 180], neutrinos [48, 49] (in two flavor mixing case), the neutron-antineutron mixing [181] and the axion-photon mixing [182].

It is straightforward to see that the Hamiltonian in eq. (4.3) can be diagonalized by a $SU(2)$ rotation

$$\begin{pmatrix} \phi_g(x) \\ \phi_e(x) \end{pmatrix} = \begin{pmatrix} \cos\theta & \sin\theta \\ -\sin\theta & \cos\theta \end{pmatrix} \begin{pmatrix} \phi_1(x) \\ \phi_2(x) \end{pmatrix} \tag{4.5}$$

where $\phi_i(x)$ (with $i = 1, 2$) are free fields and $\theta$ is the mixing angle given by $\theta = \frac{1}{2}\arctan\left(\frac{-2\hbar\Omega(t)}{\varepsilon_e - \varepsilon_g}\right)$. It is understood that each of the matrix elements in (4.5) acts trivially on the spinor space, being multiplied by the $4\times 4$ identity matrix $\mathbb{1}_4$. The electron Hamiltonian is now given by

$$H_E = \int d^3x (\varepsilon_1 \phi_1^\dagger(x)\phi_1(x) + \varepsilon_2 \phi_2^\dagger(x)\phi_2(x)) \,, \tag{4.6}$$

where

$$\varepsilon_i = \frac{\varepsilon_g + \varepsilon_e}{2} + \frac{(-1)^i}{2}\sqrt{(\varepsilon_g - \varepsilon_e)^2 + 4\hbar^2\Omega^2(t)}. \tag{4.7}$$

with $i = 1, 2$. It is clear that the rotation in eq. (4.5) turns the total Hamiltonian $H = H_{CM} + H_E$ into the sum of two free Dirac Hamiltonians with masses $m_1 = m + \varepsilon_1$ and $m_2 = m + \varepsilon_2$. Hence the atomic fields $\phi_i(x)$ admit a free field expansion

$$\phi_i(x) = \sum_r \int \frac{d^3\boldsymbol{k}}{(2\pi)^{\frac{3}{2}}} \left[ u^r_{\boldsymbol{k},i} a^r_{\boldsymbol{k},i}(t) + v^r_{-\boldsymbol{k},i} b^{r\dagger}_{-\boldsymbol{k},i}(t) \right] e^{i\boldsymbol{k}\cdot\boldsymbol{x}} \tag{4.8}$$

with $u^r_{\boldsymbol{k},i}$, and $v^r_{\boldsymbol{k},i}$, solutions of Dirac equation for the fields $\phi_i$, with effective masses $m_i = m + \varepsilon_i$. The annihilators and creators undergo a trivial evolution $a_{\boldsymbol{k},i}(t) = a_{\boldsymbol{k},i} e^{-i\omega_{\boldsymbol{k},i} t}$, with $\omega_{\boldsymbol{k},i} = \sqrt{\boldsymbol{k}^2 + m_i^2}$. Introducing eq. (4.8) in the expression for the Dirac Hamiltonian, the total Hamiltonian $H = H_E + H_{CM}$ becomes

$$H = \sum_{i,r} \int d^3\boldsymbol{k}\, \omega_{\boldsymbol{k},i} (a^{r\dagger}_{\boldsymbol{k},i} a^r_{\boldsymbol{k},i} + b^{r\dagger}_{-\boldsymbol{k},i} b^r_{-\boldsymbol{k},i}) \,. \tag{4.9}$$

The diagonalization of the total Hamiltonian, by means of a rotation, and the subsequent quantization of the free fields $\phi_1, \phi_2$ of eq. (4.8), show a close analogy with the 2–flavor mixing of neutrinos (see [77, 183] and chapter 1). The correspondence between the QFT of Rydberg atoms and the QFT of neutrino mixing is further established by the introduction of the mixing generator. Indeed, the transformations in eqs. (4.5) can be recast in terms of the mixing generator $\Xi_\theta(t)$ as $\phi_g(x) = \Xi_\theta^{-1}(t)\phi_1(x)\Xi_\theta(t)$, and similarly for $\phi_e(x)$. The mixing generator is given by

$$\Xi_\theta(t) = \exp\left[\theta \int d^3\boldsymbol{x} \left(\phi_1^\dagger(x)\phi_2(x) - \phi_2^\dagger(x)\phi_1(x)\right)\right] \,. \tag{4.10}$$

This operator preserves the canonical anticommutation relations and, at finite volume, is unitary and satisfies $\Xi_\theta^{-1}(t) = \Xi_{-\theta}(t) = \Xi_\theta^\dagger(t)$. The generator $\Xi_\theta$ is analogous to the generator $G_\theta$ of eq. (1.42) for neutrinos.

The action of the generator on the creation and annihilation operators is equivalent to a Bogoliubov transformation nested into a rotation, with coefficients $\Upsilon_{\boldsymbol{k}} \equiv (-1)^r\, u^{r\dagger}_{\boldsymbol{k},1} v^r_{-\boldsymbol{k},2} = -(-1)^r\, u^{r\dagger}_{\boldsymbol{k},2} v^r_{-\boldsymbol{k},1}$ and $\Sigma_{\boldsymbol{k}} \equiv u^{r\dagger}_{\boldsymbol{k},1} u^r_{\boldsymbol{k},2} = v^{r\dagger}_{-\boldsymbol{k},1} v^r_{-\boldsymbol{k},2}$. Explicitly, we have

$$|\Upsilon_{\boldsymbol{k}}| = \frac{(\omega_{k,1} + m_1) - (\omega_{k,2} + m_2)}{2\sqrt{\omega_{k,1}\omega_{k,2}(\omega_{k,1} + m_1)(\omega_{k,2} + m_2)}}\, |\boldsymbol{k}| \tag{4.11}$$

and $\Sigma_{\boldsymbol{k}} = \sqrt{1 - \Upsilon_{\boldsymbol{k}}^2}$.

Here the Bogoliubov coefficient $\Upsilon_{\boldsymbol{k}}$ plays the same role as $\mathcal{V}_{\boldsymbol{k}}$ of eqs. (1.45) and (1.46). The generator $\Xi_\theta(t)$ connects the representations associated with the "flavor" fields $\phi_g, \phi_e$ and the "mass" fields $\phi_1, \phi_2$. In particular, the vacua in the two representations are related by means of the transformation $|0(\theta,t)\rangle \doteq \Xi_\theta^{-1}(t)\,|0\rangle$ and, in the infinite volume limit, the two representations are unitarily inequivalent [34–38, 51–53, 77–86]. The vacuum $|0(\theta,t)\rangle$ has the structure of a condensate of particles with definite mass, whose density is equal to $\langle 0(\theta,t)|\, a^\dagger_{\boldsymbol{k},i} a_{\boldsymbol{k},i}\, |0(\theta,t)\rangle = \sin^2\theta |\Upsilon_{\boldsymbol{k}}|^2\ \forall i$. Namely, $\sin^2\theta|\Upsilon_{\boldsymbol{k}}|^2$ represents the average number density of the atoms with momentum $\boldsymbol{k}$ in the condensate.

### 4.1.2 QFT effects in Rydberg atoms

As we have seen, the QFT describing an ensemble of independent Rydberg atoms interacting with a laser light is formally equivalent to the one associated to the two flavor neutrino mixing. For neutrinos it has been shown that the fermion mixing leads to a non trivial contribution to the vacuum energy [35–38, 83–85], with an equation of state similar to that of the dark matter. Then, by using the formal analogy, we show that the vacuum energy of the Rydberg atoms behaves as a dark matter component. Such a contribution can, in principle be tested in laboratory by analyzing the specific heat of the system. Moreover, QFT predicts a correction to the Rabi oscillations of the atoms forecast by the non–relativistic quantum mechanics.

#### Dark matter–like Thermal capacity

The expectation value of the energy momentum tensor $T^{\mu\nu}(x)$ of free Rydberg atoms on the vacuum for mixed fields $|0(\theta,t)\rangle$, is $\Theta^{\mu\nu}(x) \equiv \langle 0(\theta,t)|\ :T^{\mu\nu}(x):\ |0(\theta,t)\rangle$. Here : ... :, represents the normal ordering with respect to the vacuum for free fields $|0\rangle$. The off–diagonal components of $\Theta^{\mu\nu}(x)$ vanish, then the condensate induced by the mixing is similar to a perfect fluid. The energy density and pressure of fermion condensates can be defined as $\rho = g^{00}\Theta_{00}$ and $p = -g^{jj}\Theta_{jj}$ (no summation on the index $j$ is intended), respectively. For mixed fermions one has zero pressure, $p = 0$, and the state equation reduces to $w = p/\rho = 0$, which is analogous to that of cold dark matter. We stress that the analogy between the condensate of Rydberg atoms and the actual cold dark matter is merely formal. The energy density of the condensate is (compare with eq. (1.63))

$$\rho \;=\; \frac{\Delta\varepsilon \sin^2\theta}{2\pi^2}\int_0^K dk k^2 \left(\frac{m_2}{\omega_{k,2}} - \frac{m_1}{\omega_{k,1}}\right), \tag{4.12}$$

with $\Delta\varepsilon = \varepsilon_2 - \varepsilon_1$ and $K$ is the cut-off on the momenta. Explicitly, we have

$$\rho = \frac{\Delta\varepsilon \sin^2\theta}{2\pi^2}\sum_i (-1)^i \left[K m_i \omega_{K,i} - m_i^3 \ln\left(\frac{K+\omega_{K,i}}{m_i}\right)\right]. \tag{4.13}$$

Such expression of the energy is valid only at very low temperature of the Rydberg system since we are neglecting the finite temperature effects. Integrating over the whole space occupied by the condensate one obtains the associated contribution to the energy $U$ and deriving with respect to the temperature $T$ one can evaluate the contribution of the condensate to the thermal capacity of the system. Having neglected the finite temperature effects, $U$ results to be independent on the temperature.

However, a first approximation of the temperature effects can be obtained by introducing a temperature dependent cut–off. Indeed, increasing the temperature, the average energy increases and, hence, higher momuntum states are populated. Therefore it is reasonable that the cut–off has to increase with $T$. In the simplest case of a linear dependence of the the cut–off $K$ on the temperature, $K(T) = aT + K(0)$, the contribution to the specific heat at constant volume by the vacuum energy of the mixed atoms is

$$c_\rho(T) = a\frac{V(m_2 - m_1)\sin^2\theta\, K(T)^2}{\pi^2\sqrt{(m_1^2 + K(T)^2)(m_2^2 + K(T)^2)}} \tag{4.14}$$

$$\times\left(m_2\sqrt{m_1^2 + K(T)^2} - m_1\sqrt{m_2^2 + K(T)^2}\right). \tag{4.15}$$

where $V$ is the volume of the gas of Rydberg atoms. We observe several unconventional aspects for this contribution to the thermal capacity. The main one is that it is proportional to the volume of the condensate and not to the number of atoms inside. This is due to the fact that, being associated to the vacuum energy of the condensate, it is related to the pairs of *virtual* Rydberg atoms that are continuosly created and annihilated out of the vacuum. The number of such pairs is proportional to the volume occupied by the condensate and is independent on the number of *real* Rydberg atoms in the system. As a consequence, being the pressure of the condensate equal to zero, from the first principle of Thermodynamics $dU = TdS$, also the entropy turns out to be related to $V$. Indeed, this is a quantum field theoretic contribution to the entropy [184] which can show counterintuitive behavior. The contribution to the thermal capacity in eq. (4.14) has to be added to the ordinary terms, among which the one of a fermi gas with two Rabi coupled components.

### QFT Rabi oscillation

The QFT of particle mixing predicts corrections to the oscillation formulae (see chapter 1). In virtue of the analogy we have established, similar corrections are to be expected in the oscillation formulae of Rydberg atoms interacting with a laser light.

By definition, the charge operators for ground and excited Rydberg fields, are

$$:Q_n(t):\equiv \int d^3\boldsymbol{x}\, \phi_n^\dagger(x)\phi_n(x) \tag{4.16}$$

$$= \sum_r \int d^3\mathbf{k}\, \left(\alpha^{r\dagger}_{\mathbf{k},n}(t)\alpha^r_{\mathbf{k},n}(t) - \beta^{r\dagger}_{-\mathbf{k},n}(t)\beta^r_{-\mathbf{k},n}(t)\right) \tag{4.17}$$

where $:\ldots:$ denotes normal ordering with respect to $|0(\theta,t)\rangle$. The oscillation formulae describing the transitions between ground and excited states (in the Heisenberg representation) are given by

$$Q^{\boldsymbol{k}}_{n\to m}(t) = \langle\phi_n(\boldsymbol{x},0)|:Q_m(t):|\phi_n(\boldsymbol{x},0)\rangle, \tag{4.18}$$

Explicitly, we have $Q^{\boldsymbol{k}}_{g\to g}(t) = 1 - Q^{\boldsymbol{k}}_{g\to e}(t)$ and

$$Q^{\boldsymbol{k}}_{g\to e}(t) = \sin^2(2\theta)\left[|\Sigma_{\boldsymbol{k}}|^2\sin^2\left(\omega_k^- t\right) + |\Upsilon_{\boldsymbol{k}}|^2\sin^2\left(\omega_k^+ t\right)\right]. \tag{4.19}$$

where $\omega_k^\pm = \frac{\omega_{k,2}\pm\omega_{k,1}}{2}$. Eq. (4.19) shows the presence of a high frequency oscillation term proportional to $|\Upsilon_{\mathbf{k}}|^2$ and a correction to the amplitude of the QM oscillation formulae proportional to $|\Sigma_{\mathbf{k}}|^2$. The QFT corrections to the oscillation formulae could be, in principle, tested experimentally.

## 4.2 Neutrino gravitational interactions and trapped ions

Besides the interaction with the background gravitational field, neutrinos in principle experience gravitational interactions among themselves. In their simplest form, these are Newtonian two–body interactions, whose strength is proportional to the square of the neutrino mass $m_\nu^2$. Given the weakness of the gravitational interaction and the small mass involved $m_\nu \sim 10^{-3}$eV, no significant effect arises in ordinary contexts. On the contrary in extremely dense media, due to the huge number of neutrinos and the narrow inter-particle distances, the gravitational interaction may be relevant.

Recently, the effects of gravity on neutral mixed particles have been analyzed in a quantum mechanical context [132, 185]. Moreover, gravity has been also considered as a source of decoherence in flavor oscillations [186–188] and the effects of decoherence for mixed particles on fundamental symmetries of nature have been recently studied [189–196]. It has been shown that gravity can affect the frequency of oscillations [132, 185] and leads to many interesting effects like the CPT-symmetry violation in particle mixing [189–195]. Effects of quantum field theory in curved space–time on mixed neutrinos have been also analyzed ([197] and chapter 2). The phenomena mentioned above are difficult to reveal experimentally, due to the elusive nature of neutrinos and the short lifetime of composite particles (as pertaining to meson mixing).

Another particularly thriving field of research is represented by the study of trapped ions. Trapped ions are among the most promising systems for practical quantum computing and many quantum technological applications have been developed by using such systems. An ion trap is a combination of electric or magnetic fields used to capture ions realizing a system well isolated from the external environment. Therefore it is characterized by long lifetimes and coherence [198, 199], strong ion-ion interactions [200], and the existence of cycling transitions between internal states of ions that allows to realize both measurement and laser cooling. Trapped ions, besides being one of the leading technology platforms for large-scale quantum computing, allow the simulation of quantum models of strongly interacting quantum matter and enable the investigation of those quantum dynamics that remain so far unexplored due their inescapable complexity [201, 202]. Not only strongly interacting quantum matter, but also phenomena pertaining to high energy physics can be simulated with ion traps [203] and more generally in atomic systems [204].

In this section, we show that trapped ions can also simulate the gravity effect on mixed neutral particles and thus reproduce, in table top experiments, analogues of phenomena that may have characterized the first stages of the evolution of the Universe.

In particular, we analyze the analogies between a self-interacting system of mixing particles and an ensemble of Doppler cooled ions loaded in a magnetic trap. We note that an effective spin-$1/2$ long range Ising model can describe both Doppler cooled ions held in a segmented ion trap [200, 205–208] and the dynamics of a gravitationally self-interacting system made of oscillating neutrinos, as introduced in Ref. [132]. In that paper, it has been studied an ensemble of $N$ mixed self–interacting neutral particles as a closed system and it has been shown that the self–gravity effects induce a $CPT$ violation and a modification of the oscillation formulae for systems like neutrinos. The emerging entanglement and the $CPT$ violation are extremely small for systems like neutrinos or neutrons, yet such effects might play a crucial role in dense matter and during the early stages of the universe.

Here, we consider different interaction potentials and we analyze the oscillation formulae and the $T$-symmetry violation for traps loaded with 4, 6 and 8 ions. We start by analyzing the case with 4 ions, first in a single harmonic trap and then in three independent wells, in which the inner ions are confined in an a-nharmonic potential and coupled strongly. Then we consider 6 ions confined in a single strongly an-harmonic well, and 8 ions loaded in individual harmonic traps.

We show that trapped ions reproduce the expected corrections to the flavor transitions and the $CPT$ violation induced by gravity on flavor fields. We show that the $T$ violation for confined ions is the analogue of the $CPT$ violation for flavor mixed fields and we find that $T$ violation depends on the number of trapped ions, as predicted for $CPT$ violation in the flavor mixing case. Our numerical results show that such violations, together with the new oscillation formulae are all detectable in the present experiments on ion traps. Reproducing the effects predicted for neutrinos in atomic systems could open new scenarios for the study of fundamental physics; it could be of high relevance in the understanding of the evolution of the universe and possibly lead to the discovery of new phenomena.

### 4.2.1 Oscillations of N gravitationally interacting particles

In this section we report the main results obtained for oscillating and gravitationally interacting particles [132]. The mixing relations for two flavor fields $n_A$ and $n_B$ are

$$\begin{aligned} |n_A\rangle &= \cos(\theta)\,|m_1\rangle + e^{\imath\phi}\sin(\theta)\,|m_2\rangle \ ; \\ |n_B\rangle &= -e^{-\imath\phi}\sin(\theta)\,|m_1\rangle + \cos(\theta)\,|m_2\rangle \ , \end{aligned} \tag{4.20}$$

where $n_A = \nu_e$ and $n_B = \nu_\mu$ for neutrinos, $\theta$ is the mixing angle, $\phi$ is the Majorana phase which is zero in the case of Dirac fermions [54] and $|m_i\rangle$ are the states with definite masses $m_i$.

Denoting with $E$ the energy of the mixed particles travelling through the space, and assuming $m_i \ll E$, the Hamiltonian of mixed fields can be written as (compare with (1.23))

$$H = \omega_0\,\sigma^z \ ; \qquad \omega_0 = \frac{c^2}{4E}(m_1^2 - m_2^2)\,, \tag{4.21}$$

where $\sigma^z = |m_1\rangle\langle m_1| - |m_2\rangle\langle m_2|$, and we neglected the terms proportional to the identity.

Considering the validity of the equivalence principle between inertial and gravitational mass, and representing the gravitational interaction with the Newtonian potential, the Hamiltonian of $N$ mixed particles interacting gravitationally becomes

$$H^{(N)} = \sum_i \omega_i \sigma_i^{(z)} + \frac{1}{2}\sum_{i,j}\Omega_{i,j}\sigma_i^{(z)}\cdot\sigma_j^{(z)}\,, \tag{4.22}$$

where $\omega_i = \omega_0 + \sum_j g_{i,j}(m_1^2 - m_2^2)$ with $\omega_0$ given in Eq.(4.21), $\Omega_{i,j} = g_{i,j}(m_1 - m_2)^2$ with $g_{i,j} = \frac{G}{4d_{i,j}}$, $\Omega_{i,i} = 0$ and $d_{i,j}$ relative distance between the $i$-th and the $j$-th fields that, for sake of simplicity is assumed constant during the evolution.

Assuming that at time $t=0$ the system is described by a fully separable state and that the first $M$ particles are created in the state $|n_A\rangle$ and the rest is in the state $|n_B\rangle$, then the initial state is $|\psi^{(N)}(0)\rangle = \otimes_{\alpha=1}^{M}|n_A\rangle_\alpha \otimes_{\beta=M+1}^{N-M}|n_B\rangle_\beta$. For $t > 0$, since the system is closed, one has the pure state $|\psi^{(N)}(t)\rangle = U(t)\,|\psi^{(N)}(0)\rangle$, where the unitary evolution operator is $U(t) = \exp(-\imath t H^{(N)})$. The reduced density matrix on the selected $k$-th particle is

$$\begin{aligned} \rho_k(t) &= \frac{1}{2}\left(\mathbb{1} + \sum_\alpha \langle\psi^{(N)}(0)|U^\dagger(t)\sigma_k^\alpha U(t)|\psi^{(N)}(0)\rangle\,\sigma_k^\alpha\right) \\ &= \frac{1}{2}\begin{pmatrix} 1 + \zeta_k\cos(2\theta) & \zeta_k e^{-\imath\phi}\sin(2\theta)a_k^*(t) \\ \zeta_k e^{\imath\phi}\sin(2\theta)a_k(t) & 1 - \zeta_k\cos(2\theta) \end{pmatrix}, \end{aligned}$$

where the index $\alpha$ runs over the ensemble $\{x, y, z\}$, the function $\zeta_k$ is equal to $+1$ for $k \leq M$, and to $-1$ for $k > M$, and $a_k(t)$ is given by

$$a_k(t) = e^{\imath 2\omega_k t}\prod_{j=1}^{N}\left(\cos(2\Omega_{k,j}t) + \imath\zeta_k \cos(2\theta)\sin(2\Omega_{k,j}t)\right). \tag{4.23}$$

The total entanglement that any single particle shares with the rest of the system is quantified by 2–Renyi entropy defined as $S_2 = -\ln(\mathcal{P}(\rho_i(t)))$, where

$$\mathcal{P}(\rho_k(t)) = Tr(\rho_k^2(t)) = 1 - \sin^2(2\theta)\left(1 - |a_k(t)|^2\right), \tag{4.24}$$

is the purity. Since $\Omega_{i,j}$ are not invariant under the change of fields, one has $|a_k(t=0)|^2 = 1$ and $|a_k(t)|^2 < 1$, $\forall t > 0$. Therefore, for $t > 0$, any single particle is entangled with the rest of the system.

Considering two copies of the $N$-particle system such that in the first copy one has $M = N$ and in the second one has $M = 0$, the oscillation probabilities (obtained considering the average over all the elements of the system) are

$$\begin{aligned} P_{n_A \to n_B}(t) &= \frac{1}{2}\sin^2(2\theta)\left(1 - \frac{1}{N}\sum_{k=1}^{N}\Re(a_k^{(A)}(t))\right); \\ P_{n_B \to n_A}(t) &= \frac{1}{2}\sin^2(2\theta)\left(1 - \frac{1}{N}\sum_{k=1}^{N}\Re(a_k^{(B)}(t))\right). \end{aligned} \tag{4.25}$$

Note that the $CP$-symmetry is preserved, indeed $\Delta_{CP}(t) = P_{n_A \to n_B}(t) - P_{\overline{n}_A \to \overline{n}_B}(t) = 0$, where $\overline{n}_\sigma$ ($\sigma = A, B$) is the antiparticle state. On the contrary since, $a_k^{(A)}(t) \neq a_k^{(B)}(t)$, the $T$-symmetry is violated. In fact we have $\Delta_T(t) = P_{n_A \to n_B}(t) - P_{n_B \to n_A}(t) \neq 0$. Assuming $\Omega_{i,j}t \ll 1$ the expression of $a_k(t)$ simplifies and becomes equal to $a_k(t) \simeq e^{\imath\omega_k t}\left(1 \pm 2\imath\cos(2\theta)\sum_{j=1}^{N}\Omega_{k,j}t\right)$, where the sign $+$ is for $a_k^{(A)}(t)$ and the sign $-$ is for $a_k^{(B)}(t)$. Then $\Delta_T$ becomes

$$\Delta_T(t) = \sin^2(2\theta)\cos(2\theta)\frac{2t}{N}\sum_{k,j=1}^{N}\sin(2\omega_k t)\Omega_{k,j}. \tag{4.26}$$

Being $\Delta_{CP} \neq \Delta_T$, also the $CPT$ symmetry is violated. Denoting with $F = \frac{1}{N}\sum_{k=1}^{N} f_k$ the average of $f_k$, which are defined as $f_k = \frac{\sin(2\omega_k t)}{N}\sum_j \Omega_{k,j}$, one can express $\Delta_T$ in terms of average values of relative distances among the particles in the system as

$$\Delta_T = \sin^2(2\theta)\cos(2\theta)2NtF. \tag{4.27}$$

This relation shows the explicit dependence of $\Delta_T$ on the number of particles of the system. Similar results are obtained for all the configurations in which, $n_A - n_B \sim N$ at $t = 0$. If $n_A \sim n_B$ at $t = 0$, one has $\Delta_T \propto \sqrt{N}$.

Notice that, the phenomena described above are difficult to be directly detected, due to the smallness of the gravitational coupling for neutrinos. For example, for two neutrinos at the distance of $d = 10^{-15}$m, with $\Delta m^2 = 10^{-5}\text{eV}^2$, one has the following value of the gravitational interaction term: $\Omega \simeq 10^{-54}$eV. This has to be compared with the free oscillation term $\omega$ that, for neutrinos with energy of order of 1MeV, is about $10^{-11}$eV. Despite the smallness of the gravitational interaction term, its effect becomes relevant for a large number of neutrinos. In fact, as it is evident from Eq.(4.22), the free term grows as $N$, while the gravitational interaction term grows as $N^2$. This effect could be relevant in very dense systems like the first stages of the universe or in compact objects. To give an estimate of $N$ in astrophysical object, we consider that in the solar core about one neutrino for each two protons is produced per second. This implies that about $10^{38}$ neutrinos are produced per second and $\frac{\Delta T}{t} \in \left(-10^{-1} - 10^{-1}\right)\frac{t}{sec^2}$. This phenomenon is very difficult to be analyzed directly. These circumstances warrant the need for a simulation to experimentally reveal the mutual gravitational interaction of mixed particles. Here we propose that a possible simulation can be achieved with trapped ions, as we will discuss in the following section.

### 4.2.2 Trapped ions as gravitationally interacting particles

Let us now consider cooled ions held in a segmented ion trap and exposed to a magnetic field gradient in order to realize effective spin $1/2$ models. The effective spin-spin interactions induced by the magnetic field are of Ising type and can be adjusted by tailoring the axial trapping potential. In particular, if the ions are sufficiently cold, such that the ion motion can be neglected, the effective system of $N$ spins is described by the Ising Hamiltonian [209]

$$\bar{H}^{(z)}_{\text{Ising}} = \frac{\hbar}{2}\sum_{i=1}^{N}\overline{\omega}_i\sigma_i^z - \frac{\hbar}{2}\sum_{i,j}J_{ij}\sigma_i^z\sigma_j^z \tag{4.28}$$

where $\overline{\omega}_i$ are the resonance frequencies of the atomic spins, depending on the external magnetic field $B\left(x_{0,j}\right)$ at the equilibrium position of the ion $x_{0,j}$. The spin-spin couplings $J_{ij}$ depend on the trapping potential and on the spatial derivative of the spin resonance frequency, that is determined by the magnetic field gradient. They are given by

$$J_{ij} = \frac{\hbar}{2}\frac{\partial\overline{\omega}_i}{\partial x_i}\bigg|_{x_{0,i}}\frac{\partial\overline{\omega}_j}{\partial x_j}\bigg|_{x_{0,j}}\left(A^{-1}\right)_{ij} \tag{4.29}$$

where $A$ is the Hessian matrix of the potential energy function $V\left(x_1,\cdots x_N\right)$

$$A_{ij} = \frac{\partial^2 V\left(x_1,\cdots x_N\right)}{\partial x_i\partial x_j}\bigg|_{x_\ell = x_{0,\ell},\forall\ell} \tag{4.30}$$

that confines the ions in the position $x_j$. In addition, the magnetic gradient allows for the addressing of individual spins with a microwave field, which can be used to manipulate the spin dynamics.

By comparing the Hamiltonians (4.22) and (4.28), we see that they are formally identical, with the obvious correspondence $\omega_i \leftrightarrow \frac{\overline{\omega}_i}{2}$ , $J_{ij} \leftrightarrow -\Omega_{i,j}$. Hence the resonance frequencies of the atomic spins $\overline{\omega}_i$ play the role of $\omega_i$ in Eq.(4.22), apart from a factor $1/2$, and the spin-spin couplings $J_{ij}$ correspond to the gravitational couplings $\Omega_{i,j}$ except for a sign. Thus the results presented for mixed particle systems can be reproduced with trapped ions. In order to replicate the gravitationally-interacting neutrinos as faithfully as possible, the parameters $\overline{\omega}_i$ and $J_{ij}$ must be chosen so that $\overline{\omega}_i \gg J_{ij}$. It is clear, from the discussion of the previous section, that the original ratio between the gravitational interaction and the free oscillation term, which is of order of $10^{-40}$, cannot be reached with trapped ions. We point out, however that it is the smallness of this ratio which renders the phenomenon of neutrino self interaction hard to be observed. Therefore, in order to reveal the presence of such an effect, it is desirable a ratio that is not too small. Physically this would correspond to neutrinos with high energy and small relative distance (cfr. Eq.(4.21)).

In the following, we consider ions trapped both in anharmonic and harmonic potential and we show that a $T$ violation can be detected in both cases. We remark that, for our purposes, there are no substantial differences between the anharmonic and harmonic traps, since the only relevant parameters are $\overline{\omega}_i$ and $J_{ij}$. There are many ways to implement Ising-type interactions and the parameters $\overline{\omega}_i$ and $J_{ij}$ can be chosen in a very wide range. In the present paper, we choose these parameters in order to highlight the effects predicted for gravitation self interaction of neutrinos and make them experimentally accessible in the analogue, here represented by trapped ions.

It is clear, however, that the analogy fails when the antiparticles are involved. This is because one does not have the $CP$ conjugate of the system at his disposal in the case of trapped ions. If one could hypothetically reproduce the $CP$ conjugate of the system, and the only interaction within the system were the one of Eq. (4.28), all the results, including the $CP$ symmetry would be recovered. In any case, since the oscillation probability are not dependent on the $CP$ violating Majorana phase, there is no reason to believe that the $CP$ conjugate oscillations differ from Eq. (4.25). Then we can infer that the trapped ion system is also $CP$ invariant. In this sense, we can assume that $\Delta_{CP} = 0$. Since the $T$ violation can be tested in this setup, and in the neutrino mixing case it induces a $CPT$ symmetry violation, trapped ions can be used to indirectly test the $CPT$ violation predicted for neutrinos gravitationally interacting.

We now proceed with a numerical analysis, considering different potential shapes, and we analyze the oscillation formulae and the $T$ violation resulting for the cases in which the trap is loaded with 4 ions (with both harmonic and anharmonic potentials) or 6 ions (with anharmonic trapping potential) and the case in which 8 ions are loaded in individual harmonic traps. The initial state of the ion ensemble is assumed to be factorizable as the direct product of single ion states. We consider two possible initial single ion states, written as superposition of spin up $|\uparrow\rangle$ and down $|\downarrow\rangle$:

$$\begin{aligned} |A\rangle &= \cos(\theta)\,|\uparrow\rangle + e^{\imath\phi}\sin(\theta)\,|\downarrow\rangle \\ |B\rangle &= -e^{-\imath\phi}\sin(\theta)\,|\uparrow\rangle + \cos(\theta)\,|\downarrow\rangle\ . \end{aligned} \tag{4.31}$$

Notice that both the states of Eq. (4.31) are pure. A standard method to prepare the states as in Eq. (4.31) is to perform rotations on the Bloch sphere for individual ions.

We start by studying a trap with harmonic potential loaded with 4 ions. The potential is chosen in correspondence with that of figure (2A) in the reference [202]. The values for the frequencies of the atomic spins splitting and for the coupling constants are reported in Appendix A of the same work: $\Delta\omega_i/2\pi(\mathrm{MHz}) = -11.8;\ \ -3.7;\ \ 3.9;\ \ 12$ and $J_{ij}(\,\mathrm{Hz})$: $J_{1,2} = J_{3,4} = 479$; $J_{1,3} = J_{2,4} = 349$; $J_{1,4} = 273$; $J_{2,3} = 457$.

Plots of the transition probability $P_{B\to A}$ as a function of time are shown in Figs.(4.1) and the results for the violation of the $T$-symmetry $\Delta_T$ as a function of time for such a system are reported in Fig. 4.2. For the oscillation probabilities (Fig. 4.1) we use the time range $[10^{-7} - 10^{-6}]$ s, while the $T$-asymmetries are plotted in the range $[10^{-6} - 10^{-4}]$ s because the magnitude of the oscillations is larger here, and therefore they are more visible.

Next we analyze three different anharmonic wells loaded with 4 strongly coupled ions. These simulate a non–uniform distribution of neutrinos in space. To investigate a realistic experimental set-up of this configuration, we use the following values of resonance frequencies of the atomic spins splitting: $\Delta\omega_i/2\pi(\mathrm{MHz}) = -30.7;\ \ -2.3;\ \ 2.4;\ \ 30.9$ , and the following values of the coupling constant $J_{ij}(\,\mathrm{Hz})$: $J_{1,2} = 2.1$; $J_{1,3} = 1.8$; $J_{1,4} = 0.4$; $J_{2,3} = 123.8$, with $J_{3,4} = J_{2,4}$ [202].

The plots show that, apart from specific singular values of the angle $\theta$, as for example $\theta = \pi/4$, for which $\Delta T$ vanishes accordingly with eq.(8), the violation of the $T$-symmetry, and then of the $CPT$ symmetry, is large enough to be detected with the current technologies. Notice that the time intervals considered ($t \in [10^{-7} - 10^{-4}]$ seconds), are well below the coherence time usually characterizing the experiments with trapped ions.

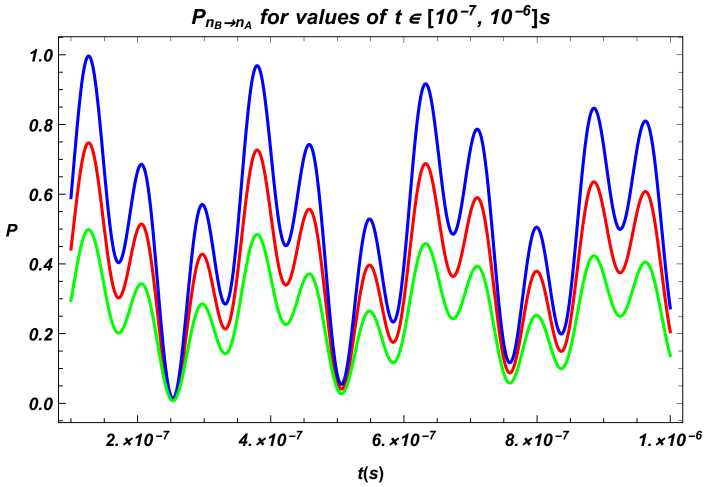


FIGURE 4.1: *(Color online) Plots of $P_{B\to A}(t)$, for $\theta = \pi/3$ (the red line), $\theta = \pi/4$ (the blue line), $\theta = \pi/8$ (the green line). In the plots, we consider $n = 4$ trapped ions in a harmonic potential, and the following values of the resonance frequencies of the atomic spins splitting $\Delta\omega_i/2\pi(\mathrm{MHz}) = -11.8;\ -3.7;\ 3.9;\ 12$ and of the coupling constants $J_{ij}(\mathrm{Hz})$: $J_{1,2} = J_{3,4} = 479$; $J_{1,3} = J_{2,4} = 349$; $J_{1,4} = 273$; $J_{2,3} = 457$.*

It would be interesting to study how the system evolves at longer timescales, since from Eq.(4.27) we aspect $\Delta T$ growing with time $t$. However, the evolution time cannot exceed the coherence time, and this fact prevents the analysis of the systems at larger time scales.

With today's technologies of trapped ions we can also simulate larger systems. However an increment of the number of ions implies a reduction of the coherence time and beyond this time the simulation of gravitational interacting mixed particles no longer reproduces the original system faithfully. Keeping the total number of ions sufficiently small, like $n = 6$, the coherence time is still quite large. Then, we take into account a system made by $n = 6$ ions trapped in a single well with $\Delta\omega_i/2\pi(\mathrm{MHz}) = -32.01;\ -9.9;\ -3.0;\ 3.2;\ 10.0;\ 32.3$ , and $J_{ij}(\mathrm{Hz})$: $J_{1,2} = 27.9$; $J_{1,3} = 19.5$; $J_{1,4} = 16.7$; $J_{1,5} = 16.7$; $J_{1,6} = 1.4$; $J_{2,3} = 411.8$; $J_{2,4} = 319.7$; $J_{2,5} = 300.3$; $J_{2,6} = 16.5$; and $J_{3,4} = 348.3$; $J_{3,5} = 319.2$; $J_{3,6} = 16.4$; $J_{4,5} = 410.9$; $J_{4,6} = 19.1$; $J_{5,6} = 27.3$, and $J_{i,j} = J_{j,i}$ [202]. Considering the same initial states of the previous case, we have the oscillation probabilities shown in fig. 4.5 and the $T$-symmetry violation shown in fig. 4.6. Also here we use different scales for the oscillation probabilities (Fig. 4.3) $[10^{-7} - 10^{-6}]$ s, and the $T$-asymmetries $[10^{-6} - 10^{-4}]$ s, to better highlight the latter.

Our final application is with $n = 8$ ions held in individual harmonic traps. We consider $Yb^{+}$ ions, with the same qubit splitting $\Delta\omega_i = 20\pi$MHz for each ion, corresponding to the typical Zeeman splitting of the $S_{1/2}, F = 1$ level [210], and only nearest neighbour interactions between the ions 1 and 2, 3 and 4, 5 and 6, 7 and 8, with coupling $J = 3$KHz, as discussed in the reference [210]. The same initial states for the ions are assumed. In the figures (4.7) and (4.8) we plot respectively the oscillation probabilities and the $T$-violation for this system.

It should be noted that the general prediction of Eq. (4.27) of the dependence of the $T$ asymmetry on the total particle number $N$ is confirmed by the plots shown above. The 6 ions asymmetry of fig. 4.6 (given the different couplings) at $t_1 = 10^{-6}s$ is slightly bigger than the 4 ions asymmetry of fig. 4.4 at the same time $t_1$ and, due to Eq. (4.27), we expect that a larger number of ions implies a larger $T$ asymmetry, as also shown in the plots of fig. 4.8

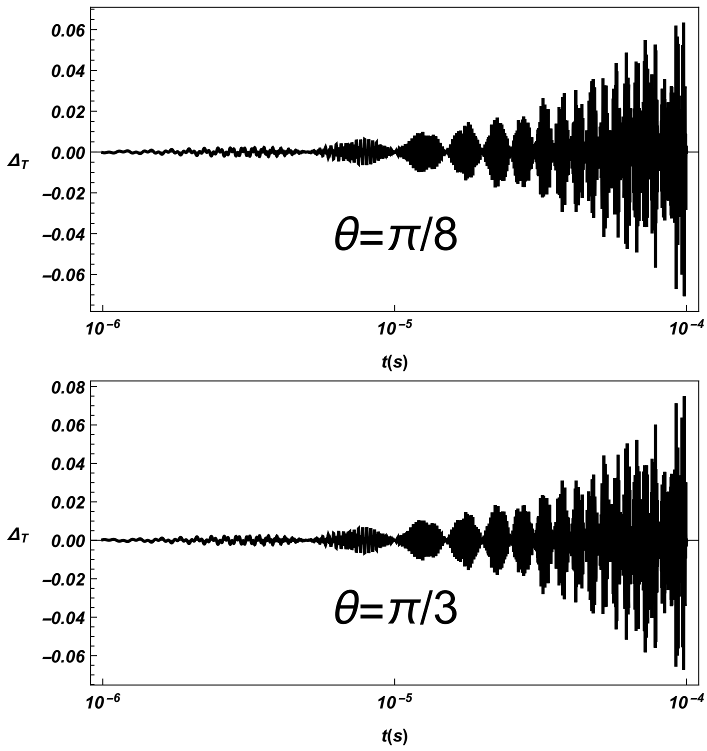


FIGURE 4.2: Plots of $\Delta_T(t)$ for different choices of $\theta$ for a set-up with $n = 4$ trapped ions, and the same parameters as figure (4.1). Here we use a different time scale in order to better highlight the $T$-Violation.

with $n = 8$ ions trapped in individual harmonic traps.

In any case, a limited number of ions is to be preferred, since despite a larger signal, the coherence time is reduced when a large number of ions is considered. The plots obtained show that the oscillation formulae and the $CPT$ violation predicted for gravitationally interacting neutrinos can be tested with ions trapped in many potentials. Indeed, comparing the parameters of original system (we considered the solar core with $\omega \sim 10^{-11} eV$, $\Omega \sim 10^{-54} eV$ and $N \sim 10^{38}$) with those of the simulations, and looking at the results shown in figs.(4.4), (4.6) and (4.8), we see that the small number of ions is compensated by the larger ratio between the interaction term and free oscillation term, so to give a comparable $\Delta_T$.

In order to detect the effects described in the paper, it is necessary to prepare and detect the state of the ions with sufficiently high fidelity. In the case of ions in anharmonic traps we consider, the required resolution is of order of 1%, while for ions trapped in the harmonic potentials we consider, the resolution required is of order 10%. These resolutions can be easily attained in experiments [211].

### 4.2.3 Concluding remarks

The gravitational self-interaction in particle mixing systems leads to new oscillation formulae and to the $CPT$ violation. The corrections to the flavor transitions and the expected $CPT$ symmetry breaking are negligible in the present epoch and therefore they are very hard to be revealed. However, they are proportional to the number of elements of the system and to its density, so that these effects could affect extremely dense systems with a large number of particles, such as some galactic objects and the primordial stages of the universe. Moreover, the

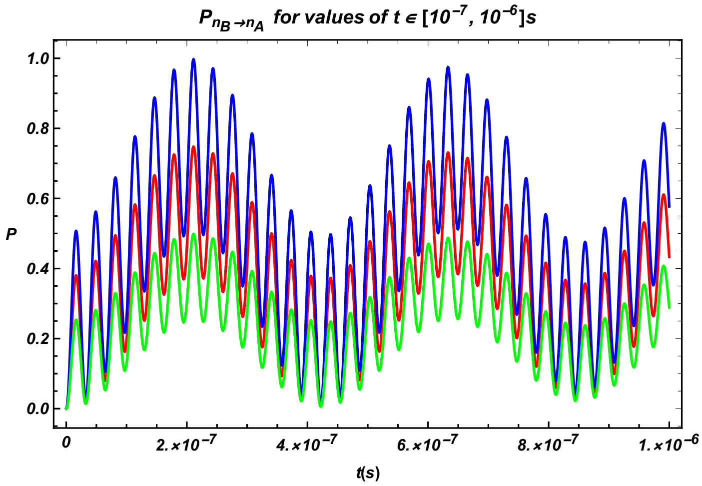


FIGURE 4.3: *(Color online) Plots of* $P_{B\to A}(t)$, *for* $\theta = \pi/3$ *(the red line),* $\theta = \pi/4$ *(the blue line),* $\theta = \pi/8$ *(the green line). In the plots, we consider* $n = 4$ *trapped ions in an anharmonic potential, and the following values of the resonance frequencies of the atomic spins splitting* $\Delta\omega_i/2\pi(\mathrm{MHz}) = -30.7; \quad -2.3; \quad 2.4; \quad 30.9$ *, and of the coupling constant* $J_{ij}(\,\mathrm{Hz})$*:* $J_{1,2} = 2.1$; $J_{1,3} = 1.8$*;* $J_{1,4} = 0.4$; $J_{2,3} = 123.8$, *with* $J_{3,4} = J_{2,4}$.

mechanism leading to $CPT$ violation is not only limited to gravitational interaction. Therefore, the possibility of testing these processes is of great importance for the understanding of fundamental physics.

In this section we have shown the analogies between the effective system of $N$ spins described by the Ising Hamiltonian and the phenomenon of the gravitational self interaction in mixed particle systems. We have shown that cooled ions held in many potential traps can simulate the mutual interaction in mixed neutrino system and allow to reveal the expected new oscillation formulae and the $CPT$ violation for this phenomenon. We considered the case with $N = 4$ ions and coupling in three independent wells and the case of 6 ions confined in a single strongly an-harmonic well. We have shown that the $T$ violation for trapped ions, corresponding to the $CPT$ violation for flavor mixed particles, grows with the size of the system $N$. Moreover, we analyzed the system with $N = 8$ ions held in individual harmonic traps and have shown that in this case the $T$ violation is even larger than in the previous cases, both for the greater number of trapped ions and for the larger value of the coupling constants as compared to the anharmonic cases. Our numerical results show that such violations, together with the new oscillation formulae are all detectable in the present experiments on ion traps. Finally, note that in our approach we have chosen the couplings $J_{ij}$ and the frequencies $\bar{\omega}_i$ in order to maximize the $T$–violation. By lowering the interaction, and therefore the couplings and the frequencies, it is possible to slow down and highlight the oscillations. The potentials can always be tuned according to whether one is interested in highlighting the $T$ asymmetry or the oscillation formulae. As a last remark, we point out that trapped ions are not the only system capable of simulating gravitationally self–interacting neutrinos. The Ising like Hamiltonian of Eq. (4.22) might be reproduced by other atomic systems (as for instance Rydberg atoms), and future investigations shall be devoted to the analysis of these possibilities.

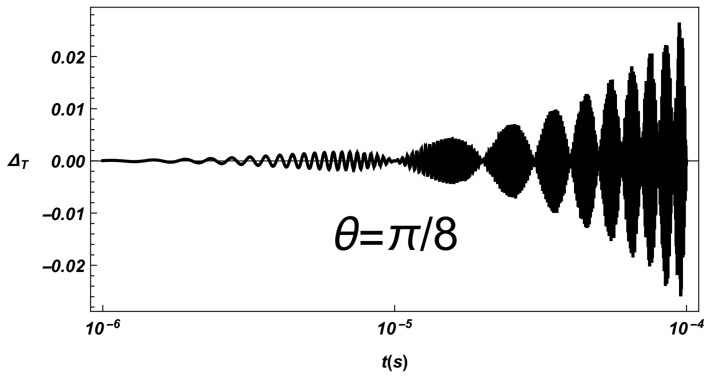


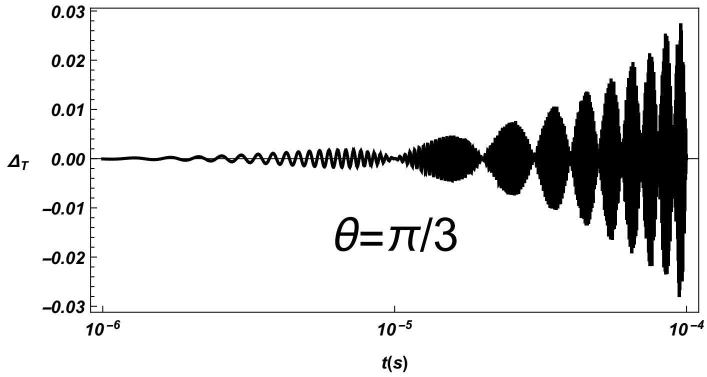


FIGURE 4.4: Plots of $\Delta_T(t)$ for different choices of $\theta$ for a set-up with $n = 4$ trapped ions, and the same parameters as figure (4.3). Here we use a different time scale in order to better highlight the $T$-Violation.

## 4.3 Neutrino-matter interactions beyond the MSW effect

As discussed in the previous sections, neutrinos are notoriously elusive particles with an extremely low interaction rate [212], which oscillate among three different flavors [48, 49, 194, 213–218]. They only participate in weak and gravitational interactions, but the latter can be neglected, for all practical purposes, in virtue of their small mass [218] ( except for very peculiar situations (see [132] and section 4.2)). Indeed, the primary modification induced by matter on neutrino oscillations, known as the MSW effect (see [55, 57] and chapter 1) is entirely due to the weak interactions of neutrinos with the electrons and nucleons of the environment. The MSW effect is, in essence, an effective theory, since all the interactions are comprised in an effective position–dependent potential acting differently on the individual neutrino flavors and hence affecting the oscillation probabilities. However, there is one major shortcoming in adopting such an effective field approach to neutrino–matter interactions, and it is the complete loss of insight on the dissipative aspects of these interactions. Indeed, the unitary evolution driven by the effective potentials $V_\alpha(\boldsymbol{x})$ always preserves the purity of neutrino states. While this is reasonable for neutrino oscillations in a low-density medium, for the interactions in a denser one, a loss of coherence due to collisions with the particles in the medium is to be expected.

Decoherence effects in neutrino oscillations have been thoroughly studied from both a phenomenological and a theoretical standpoint. To include such effects, the neutrino is usually modeled as an open system in which the action of a dissipative dynamics is discussed on quite general grounds [189, 191–193, 219–229]. Exploiting this approach it has been shown that the decoherence leads to modified oscillation formulae [189, 191–193, 221–223] that can shed some light on the fundamental nature of neutrinos [195, 196]. The main problem is that

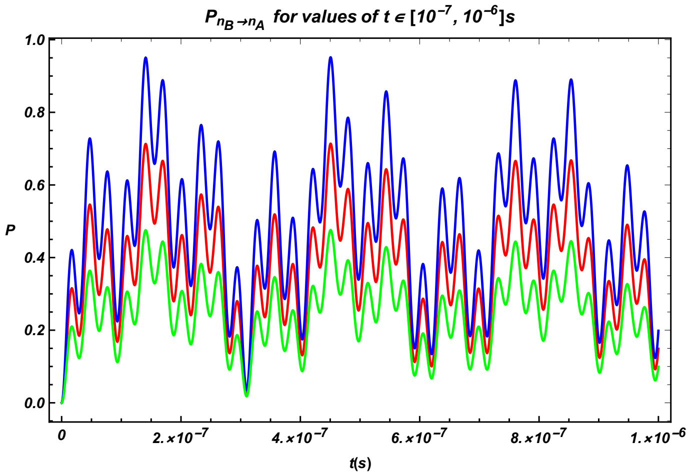


FIGURE 4.5: *(Color online) Plots of $P_{n_B \to n_A}(t)$, for $\theta = \pi/3$ (the red line), $\theta = \pi/4$ (the blue line), $\theta = \pi/8$ (the green line). In the plots, we consider $n = 6$ trapped ions in an anharmonic potential, and the following values of the resonance frequencies of the atomic spins splitting $\Delta\omega_i/2\pi(\mathrm{MHz}) = -32.01;\ -9.9;\ -3.0;\ 3.2;\ 10.0;\ 32.3$, and of the coupling constant $J_{ij}(\mathrm{Hz})$: $J_{1,2} = 27.9$; $J_{1,3} = 19.5$; $J_{1,4} = 16.7$; $J_{1,5} = 16.7$; $J_{1,6} = 1.4$; $J_{2,3} = 411.8$; $J_{2,4} = 319.7$; $J_{2,5} = 300.3$; $J_{2,6} = 16.5$; $J_{3,4} = 348.3$; $J_{3,5} = 319.2$; $J_{3,6} = 16.4$; $J_{4,5} = 410.9$; $J_{4,6} = 19.1$; $J_{5,6} = 27.3$, and $J_{i,j} = J_{j,i}$.*

the dissipative dynamics of neutrinos depends on several external parameters, that are not determined within the theory, hence making the comparison with the experiments extremely hard.

Here, we present a novel approach to neutrino oscillations in matter, in which the loss of coherence due to the collisions with the particles in the medium is explicitly taken into account. We consider oscillations in a dense medium, i.e. in a medium where the electronic density strongly suppresses the flavor oscillations and we provide a theory which goes beyond the effective matter potential, and give a quantitative account of the quantum decoherence induced by the interactions with the environment. To this end, one needs to resolve the details of the single scattering events and estimate the loss of coherence due to the latter. Therefore, our considerations are in principle valid for the propagation of neutrinos in any environment, regardless of the frequency of collisions. This includes also the regimes in which, actually, the neutrino evolution is analyzed in terms of effective damping of the oscillations [230], by means of a Boltzmann–like collision integral [231] and through a kinetic equation for neutrinos [232–234].

We show how the purity of the neutrino state is degraded as an effect of its interactions with the environment that can be interpreted as the quantum decoherence arising from a dissipative Markovian evolution. This provides a microscopic qualitative and quantitative explanation to the phenomenology of decoherent neutrino oscillations as analyzed in previous works. Such a phenomenon can be of particular interest, not only for a deeper understanding of neutrino oscillations in the matter but also for its phenomenological implications. In this picture, we obtain new oscillation formulae with respect to the MSW formulae that show corrections at high neutrino energies and/or high medium density and which reduce to the latter when the scattering probability is negligible. In the end we present a numerical analysis for ultra high energy neutrinos propagating through the Earth and we analyze the related $CP$ and $CPT$ violations.

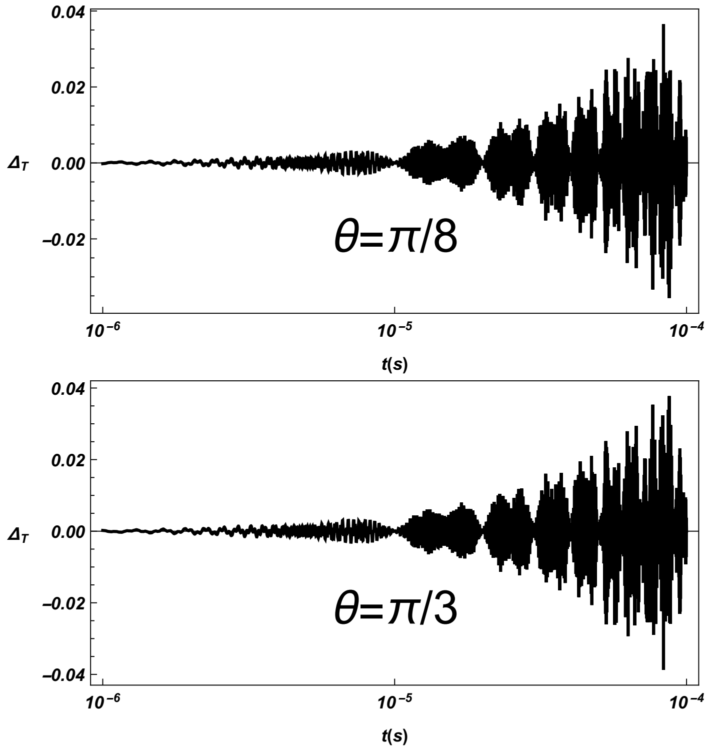


FIGURE 4.6: Plots of $\Delta_T(t)$ for different choices of $\theta$ for a set-up with $n = 6$ trapped ions. The same parameters as figure (4.5) are used. We used a different timescale to better highlight the $T$-violation.

### 4.3.1 Neutrino-Lepton Interactions

To begin with, let us discuss the salient assumptions of our analysis. At first, for the sake of simplicity, we focus on the case of a neutrino with two possible flavor states $\nu_e, \nu_\mu$ propagating in matter. This assumption is not crucial, and the approach that we use can be easily generalized to the more realistic three flavors case. Yet this would render the calculations more involved and would add no relevant physical insights to the discussion. For this reason we prefer to limit ourselves, in the present work, to the two–flavor mixing. The second assumption is that the number of neutrinos remains unchanged in time. This means that we are neglecting *all* processes involving the emission or absorption of neutrinos, as muon decay $\mu^- \to e^- + \bar{\nu}_e + \nu_\mu$ so that it still makes sense to speak about the oscillations of a single neutrino. Moreover, we consider that the interaction with the nucleons of the medium can be neglected, and retain the purely leptonic interactions with electrons $e^-$ and muons $\mu^-$ only. Neutrino–nucleon and neutrino–nuclei interactions would indeed lead to more involved calculations, obscuring the essential physical insights that can already be grasped in our simpler setting. In addition, as far as processes involving the emission or absorption of neutrinos can be neglected, the interaction of nucleons and nuclei with neutrinos is the same for all flavors, so that the oscillations are unaffected. Finally, we assume that collisions always involve a single neutrino and a single charged lepton so that $n$–body interactions with $n > 2$, whose cross-section is usually much smaller than those with $n = 2$, can be neglected.

Summarizing, all the reactions we consider must then have the form

$$\nu_\alpha + l \leftrightarrow \nu_\beta + l' \qquad \bar{\nu}_\alpha + l \leftrightarrow \bar{\nu}_\beta + l' \tag{4.32}$$

where $\alpha, \beta, l, l' = e, \mu$ and the bar denotes antineutrinos. The form of Eq. (4.32) includes all

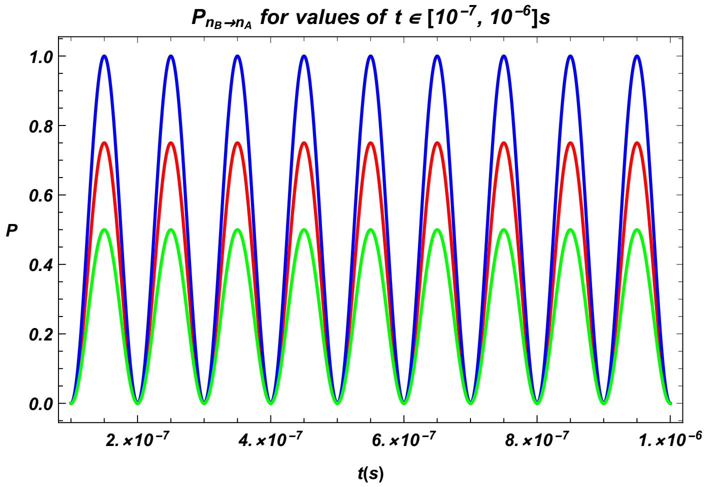


FIGURE 4.7: *(Color online) Plots of* $P_{n_B \to n_A}(t)$*, for* $\theta = \pi/3$ *(the red line),* $\theta = \pi/4$ *(the blue line),* $\theta = \pi/8$ *(the green line). In the plots, we consider* $n = 8$ *trapped ions in individual harmonic traps all with the same atomic splitting* $\Delta\omega_i = 20\pi\mathrm{MHz}$ *and only nearest neighbour interactions between the ions 1 and 2, 3 and 4, 5 and 6, 7 and 8, with the same coupling* $J = 3\mathrm{KHz}$*, as presented in the reference [210].*

the scatterings $(\nu_\alpha, \bar{\nu}_\alpha) + l \leftrightarrow (\nu_\alpha, \bar{\nu}_\alpha) + l$, and two additional reactions, one for neutrinos and one for antineutrinos. These are

$$\nu_e + \mu^- \leftrightarrow \nu_\mu + e^- \qquad \bar{\nu}_e + e^- \leftrightarrow \bar{\nu}_\mu + \mu^- \tag{4.33}$$

and they are, apart from scatterings, the only processes of the form (4.32) which respect lepton number conservation. In the mediums we shall be treating, the interactions of neutrinos with muons can usually be neglected, both due to the muon instability and a negligible muon density (compared to the electron density).

Depending on the neutrino energy $E_\nu$, and to a lesser extent on the medium density, we can distinguish two different regimes. When low energy neutrinos are considered, a large number of constituents of the medium participates in the weak interaction, and the forward scattering amplitudes due to them add up coherently [55, 235]. Their collective action amounts to a (flavor–dependent) neutrino refractive index $n_\alpha(\boldsymbol{x})$, which can also be understood in terms of an average potential term in the neutrino hamiltonian (see [54] and chapter 1)

$$V_\alpha(\boldsymbol{x}, t) = \pm\delta_{\alpha e}\sqrt{2}G_F N_e(\boldsymbol{x}, t)\,. \tag{4.34}$$

Here $\delta_{ae}$ is the Kronecker delta, $G_F$ is the Fermi constant and $N_e(\boldsymbol{x}, t)$ is the electron number density of the medium. In Eq. (4.34) the (minus) plus sign is reserved for (anti–) neutrinos. The coherent phenomenon described by Eq. (4.34) is the source of the MSW effect [55, 57]. This pure neutrino picture breaks down as the neutrino energy $E_\nu$ or the medium density $N_e$ are increased. Indeed, since the total cross-section for neutrino–lepton scattering grows linearly with the energy[1] [212] $\sigma_{\nu l} \propto E_\nu$, the number of scattering events grows, and the evolution is no longer coherent. In most of the cases of interest, even at comparably high neutrino energies $E_\nu \sim 1TeV$, the cross-section remains so small that only a few scattering events can take place during the neutrino propagation. This can be seen immediately by

[1]Actually the proportionality $\sigma_{\nu l} \propto E_\nu$ does not hold in all the reference frames. However, the total cross section is proportional to the Lorentz invariant quantity $s = (p_\nu + p_l)^2$, so that it is always a monotonically increasing function of the neutrino energy.

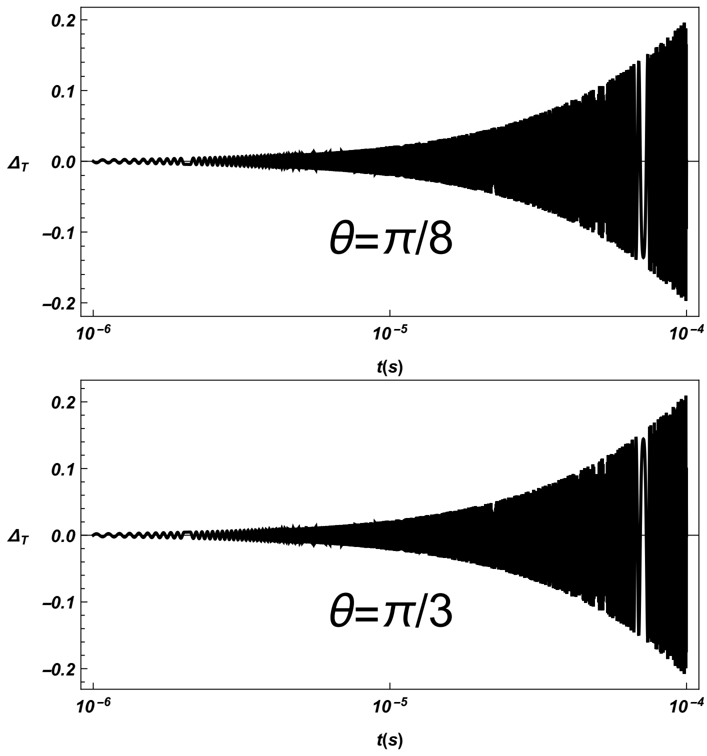


FIGURE 4.8: Plots of $\Delta_T(t)$ for different choices of $\theta$ for a set-up with $n = 8$ trapped ions. The same parameters as figure (4.7) are used. We used a different timescale to better highlight the $T$-violation.

evaluating the neutrino mean free path $l = (N_e\sigma)^{-1}$ for the density profiles $N_e$ of interest. On this basis, one usually discards the second-order effects altogether, and only retains the matter potential of Eq. (4.34). The major drawback in doing so is that the neutrino evolution remains unitary, just as in the vacuum, so that no dissipative effects occur. In order to encompass the dissipative effects due to neutrino–matter interactions, we shall analyze the effect of collisions on the neutrino propagation.

### 4.3.2 Neutrino propagation with collisions: general scheme

In our computation we neglect all the processes implying the emission or absorption of neutrinos and therefore we consider a constant total number of neutrinos. We neglect the interaction with nucleons and we consider only the leptonic interactions with electrons and muons. We consider the system made by the neutrino and the charged lepton that take part in the scattering process as an isolated system. This leads a unitary global evolution of the two particle system, due to the scattering. We note that the total system evolves unitarily, while the neutrino evolution is dissipative.

The neutrino propagation in matter can be characterized by two evolution operators, $U_0(t)$ and $U_W$. The first, associated to the mixing Hamiltonian and the matter potential of Eq. (4.34), acts on the neutrino degrees of freedom alone, and corresponds to the unitary evolution before and after the collisions. The second describes the collision processes, and couples the neutrino with a charged lepton of the medium. The crucial point is that the collisions occur in a narrow spacetime region, in which the effect of $U_0(t)$ can be neglected, so that we can schematize the neutrino propagation as a sequence of (nearly) instantaneous collisions spaced out by intervals of coherent evolution.

In principle, neutrinos may take part in an arbitrary number of collisions. Then, once that the initial neutrino state is specified $\rho_\nu(t_0)$, we define the initial state $\rho(t_0)$ of the system (neutrino + medium) as[2]

$$\rho(t_0) = \rho_\nu(t_0) \otimes \left( \bigotimes_{k=1}^{\infty} \rho_k(t_0) \right) \tag{4.35}$$

where each $\rho_k(t_0)$ denotes the initial state of a single lepton in the medium. We limit our analysis to the interactions of neutrinos with leptons, and we neglect the probability for a neutrino to interact with a free muon in the medium (since the muons are unstable and the muon density is usually negligible with respect to the electron density) with respect to the one with an electron. Therefore, all $\rho_k(t_0)$ describe electronic states.

Having defined the initial state, as a first step, one simply evolves the density matrix according to the evolution operator $U_0(t)$ up to a time right before the first scattering $t_{I_1}$, to obtain $\rho(t_{I_1})$. From this, the density matrix of the system right after the scattering $\rho(t_{F_1})$ is related to the density matrix right before the scattering $\rho(t_{I_1})$ via

$$\rho(t_{F_1}) = U_{W_1} \rho(t_{I_1}) U^\dagger_{W_1} \,. \tag{4.36}$$

where $U_{W_k}$ couple the degrees of freedom of the neutrino and the $k$-th lepton of the medium. After the scattering event, the density matrix evolves again under the action of $U_0(t)$. These steps are repeated as many times as the number of collisions that occur, each time coupling the neutrino with a different charged lepton. At each time $t$ the neutrino state can be recovered by tracing out the charged lepton degrees of freedom $\rho_\nu(t) = Tr_l(\rho(t))$. It is worth to note that, while the evolution of the complete density matrix (neutrino plus charged leptonic states) is unitary, the evolution of the reduced density matrix associated to the sole neutrino is not. This implies that differentiating $\rho_\nu(t)$ with respect to time, one obtains, along with the Hamiltonian, further dissipative terms that induce decoherence effects.

At the end of the process, the neutrino density matrix can generally be written as

$$\rho_\nu(t) = \sum_{n=0}^{\infty} P_n(t) \rho_\nu^{(n)}(t) \,, \tag{4.37}$$

where $P_n(t)$ is the probability that after a time $t$, $n$ scattering events, involving the same neutrino, have taken place, and $\rho_\nu^{(n)}(t)$ is the associated density matrix. If the medium is homogenous, the probability of having a scattering, at any time, is independent of $t$ and $n$, so that $P_n(t)$ is a Poisson distribution[3] $P_n(t) = \frac{1}{n!}(\Gamma t)^n e^{-\Gamma t}$. Since the instants $\{t_1, ..., t_n\}, 0 \leq t_i \leq t$ at which the collisions occur are randomly distributed in the interval $[0, t]$, the density matrix $\rho_\nu^{(n)}(t)$ for $n$ collisions involves a statistical average

$$\rho_\nu^{(n)}(t) = \int_{t_1=0}^{t} \int_{t_n > t_{n-1} ... > t_2 > t_1}^{t} dt_1 ... dt_n R_n(t_1, ..., t_n) \eta_\nu(t; t_1, ..., t_n). \tag{4.38}$$

In equation (4.38), $\eta_\nu(t; t_1, ..., t_n)$ is the neutrino density matrix at time $t$, after $n$ collisions

[2] We remark that this is not the most general form for the state of the medium $\rho_{Medium}$, which is a generic many–particle state. Nevertheless the knowledge of the exact state of the medium is irrelevant to the purpose of determining the neutrino propagation and the associated decoherence. The only quantity related to $\rho_{Medium}$ which is relevant at this level is represented by the electron density $N_e(x)$. Complications related with the exact form of $\rho_{Medium}$ (for instance as a Fermi-Dirac distribution) are deferred to later works.

[3] A homogeneous medium has a uniform electron density $N_e$, indipendent of the position $\boldsymbol{x}$ within the medium. The collision rate $\Gamma = N_e \sigma_T$ depends only on the electron density $N_e$ and on the neutrino energy $E$, and since the latter do not change during the propagation, the former is a constant. Also, the collisions occur independently from each other, so that the probability of having a collision at a given time $t$ does not depend on the previous scattering events. These properties are compatible with a Poisson distribution.

occurring exactly at the times $\{t_1, ..., t_n\}$ while $R_n(t_1, ..., t_n)$ stands for the joint probability distribution of the $n$ collisions occurring at the times $\{t_1, ..., t_n\}$, with normalization

$$\int_{t_1=0}^{t} \int_{t_n>t_{n-1}...>t_2>t_1}^{t} dt_1...dt_n R_n(t_1, ..., t_n) = 1 \tag{4.39}$$

corresponding to the certainty that $n$ collisions occur in the interval $[0, t]$.

As it can be seen from the above discussion, the determination of the neutrino density matrix with growing $n$ becomes soon intractable analytically, and, in the general case, for a large number of collisions some approximation must be invoked. Nevertheless, for a very large set of physical situations of interest the probability of having 2 or more collisions is extremely small and can be neglected. To give an idea, for electronic densities of the order of $N_e = N_A cm^{-3}$, with $N_A$ the Avogadro's number, and neutrino energies $E \sim 1$ GeV, the interaction rate $\Gamma = N_e \sigma_T$, where $\sigma_T$ is the total cross section, is as low as $\Gamma \sim 10^{-7} s^{-1}$. In this case eq. (4.37) simplifies to

$$\rho_\nu(t) = (1 - P_1(t))\rho_\nu^{(0)}(t) + P_1(t)\rho_\nu^{(1)}(t) \tag{4.40}$$

### 4.3.3 Neutrino–Lepton Scattering: Hamiltonian and Evolution operator

In this section we derive the evolution operator describing the scattering. We first establish the general form of the scattering Hamiltonian on the basis of the possible reactions. We compare the scattering matrix obtained via quantum field theoretical calculations with the scattering matrix that would be produced by a quantum mechanical interaction Hamiltonian. Computing the scattering amplitudes allows us to derive the components of the scattering Hamiltonian. For the computation of the evolution operator, we observe that it has the same symmetries as the Hamiltonian, and then use both its expression in terms of the Hamiltonian and its probabilistic interpretation in order to find its precise form. In the following we consider only the forward scattering of the neutrinos, and we assume that the 4-momentum transfer, in all the reactions considered, is negligible with respect to the mass of the weak bosons $m_W, m_Z$.

Due to the assumptions made, both the neutrino and the charged lepton taking part in the reactions of Eq. (4.32) can be thought of as two–level systems. The neutrino (antineutrino) can be either in the electronic $|\nu_e\rangle$ ($|\bar{\nu}_e\rangle$) or in the muonic $|\nu_\mu\rangle$ ($|\bar{\nu}_\mu\rangle$) state, while, similarly, we can regard the electron $|e\rangle$ and the muon $|\mu\rangle$ respectively as the ground and excited state of the charged lepton $|l\rangle$. Since all the processes of Eq. (4.32) involve a neutrino (or an antineutrino) and a charged lepton in both the initial and final state, a useful basis in which the processes can be described is given by

$$|\nu_l, l'\rangle \doteq |\nu_l\rangle \otimes |l'\rangle \ , \tag{4.41}$$

with $l, l' = e, \mu$. The lepton states $|l'\rangle$ are obviously referred to the particular charged lepton of the medium that takes part in the interaction. A couple of comments are in order. For our purposes the exact spacetime dependence of the states of Eq. (4.41) is irrelevant, as long as they are sharply peaked around a given 4–momentum. The essential requirement is that they contain all the kinematical information needed to characterize the reactions of Eq. (4.32). Within our assumptions, this amounts to specifying the neutrino energy $E_\nu$ and the charged lepton spin projection (as the neutrino helicity is fixed[4]. The generic state is then written

$$|\nu_l, l'\rangle_{E_\nu}^{(h)} \ , \tag{4.42}$$

[4]Only left–handed neutrinos and right–handed antineutrinos participate in the weak interaction processes [212].

where $E_\nu$ is the neutrino energy and $h = \pm 1$ is the charged lepton spin projection. In principle one might choose any reference frame to study the reactions, and then the states of Eq. (4.42) would be characterized by the neutrino and the charged lepton 4–momenta $p^\mu_{(\nu)}, p^\mu_{(l)}$ in this frame. One should then enforce the total 4–momentum conservation for each of the processes in Eq. (4.32) by suitably defining the inner products between the states. However, it is much more convenient to work in the rest frame of the medium, which simplifies extremely both the kinematics and the notation. Denoting by $p^\mu_\alpha, p^\mu_l$ (with $\alpha = \nu_e, \nu_\mu$ and $l = e, \mu$) respectively the 4-momentum of the incoming neutrino and of the target charged lepton, we have that the latter is at rest in the chosen frame, so that $p^\mu_l \equiv (m_l, 0, 0, 0)$, with $m_l$ its mass. The assumption that the target charged lepton is at rest in the medium rest frame requires that the temperature of the medium be negligible with respect to the neutrino energy.

Choosing the third spatial axis to coincide with the direction of motion of the incoming neutrino, its momentum reads $p^\mu_\alpha \equiv (E_\alpha, 0, 0, p_\alpha)$, with $p_\alpha \simeq E_\alpha$. Among the reactions of Eq. (4.32) we can distinguish elastic scattering, where the initial and the final charged lepton are the same $l = l'$, and quasi–elastic scattering, where the charged lepton is converted to another kind $l \neq l'$. For the elastic scattering one can enforce the hypothesis of vanishing 4-momentum transfer, so that the neutrino preserves both its initial energy and its initial direction of motion. This hypothesis is in line with the derivation of the MSW effect, and corresponds to the requirement that the medium remains unaltered by the interaction with neutrinos. The condition is $q^\mu = p^\mu_\beta - p^\mu_\alpha \simeq 0$, where $p^\mu_\beta$ is the 4-momentum of the outgoing neutrino and $p^\mu_\alpha$ is the 4-momentum of the incoming neutrino. This means that the outgoing neutrino is emitted within a small solid angle $\delta\Omega$ around the direction of the incoming neutrino. This also implies a vanishing change in the neutrino energy, so that the 4-momentum of the outgoing neutrino is

$$p^\mu_\beta \simeq p^\mu_\alpha \equiv (E_\alpha, 0, 0, p_\alpha) \, . \tag{4.43}$$

In addition, since the 3-momentum is retained by the neutrino $\boldsymbol{p}_\alpha = \boldsymbol{p}_\beta$, by conservation of the total 3-momentum, the spatial momentum of the outgoing charged lepton is zero $\boldsymbol{p}_{l'} \simeq 0$. This in turn implies that the 4-momentum of the outgoing charged lepton is

$$p^\mu_{l'} \simeq (m_{l'}, 0, 0, 0) \, . \tag{4.44}$$

It is obvious that within these assumptions the neutrino energy and the charged lepton spin projection suffice to determine the kinematics of the reaction completely.

On the other hand, for the quasi–elastic reactions it is not kinematically possible to have both a vanishing 4-momentum transfer and forward scattering. The only requirement we can impose is that the neutrino is forward scattered, i.e. that it preserves its original direction of motion. The kinematics in the rest frame of the medium are worked out in detail in the appendix (E). The crucial point is that the incoming neutrino necessarily transfers (or receives) a part of its energy to (from) the medium $E_\alpha \neq E_\beta$. The states of equation (4.42) are still sufficient to describe the reaction, but we need at least two sets $|\nu_l, l'\rangle^{(h)}_{E_\alpha}, |\nu_l, l'\rangle^{(h)}_{E_\beta}$ corresponding to distinct neutrino energies.

If one relaxes the assumptions of vanishing 4-momentum transfer and small scattering angle, the parameters $E_\nu, h$ no longer suffice to specify the states of Eq. (4.41), and the complete kinematics of the reaction must be encoded in the states. We defer these complications to later studies, and, from now on, we shall always work in the 8–dimensional Hilbert space $\mathcal{H}^{(h)}_{E_\alpha} \oplus \mathcal{H}^{(h)}_{E_\beta}$ spanned by the vectors of Eq. (4.42) corresponding to the initial neutrino energy $E_{(\alpha)}$ in the rest frame of the medium and the charged lepton spin projection $h$. The final neutrino energy is uniquely determined both for the elastic reactions ($E_\beta = E_\alpha$) and the quasi-elastic reactions ($E_\beta \neq E_\alpha$) (see the appendix (E)). The situation for the anti–neutrinos, whose states we denote $|\bar{\nu}_l, l'\rangle^{(h)}_{E_\alpha}$, is analogous.

Having established which states are relevant for our analysis, we can now determine the explicit forms of $U_0$ and $U_{W_k}$ on the basis states of Eq. (4.42). The operator $U_0$ determines the evolution of the neutrino states between two successive collisions and can be put in the following form

$$U_0(t) = e^{-\imath(H_M + H_{MSW})t} \,. \tag{4.45}$$

The first Hamiltonian term is that of mixing, which is responsible for the neutrino oscillations. Dropping terms proportional to the identity, it can be written as [132]

$$H_M = -\omega_0 \left(\cos 2\theta \sigma_\nu^z - \sin 2\theta \sigma_\nu^x\right) \otimes \mathbb{1}_l \tag{4.46}$$

where $\omega_0 = \frac{\Delta m^2}{4E_\nu}$, $\theta$ is the two–flavor mixing angle and $\Delta m^2 = m_2^2 - m_1^2$ is the squared neutrino mass difference. The subscripts $\nu$ and $l$ refer to the neutrino and the lepton subspaces, so that $\sigma_\nu^j$ ($\sigma_l^j$) denotes the $j$-th Pauli operator on the neutrino (leptonic) subspace. The Hamiltonian (4.46) obviously depends on the neutrino energy $E_\nu$ via $\omega_0$, so that we have two copies $H_{M,E_\alpha}, H_{M,E_\beta}$ of $H_M$, one for each energy subspace. The Hamiltonian in Eq. (4.46), assuming no CP violating phase, is valid for both neutrinos and antineutrinos. The second term is the MSW matter potential of Eq. (4.34), which can be written as

$$H_{MSW} = \pm \frac{\sqrt{2}}{2} G_F N_e \sigma_\nu^z \otimes \mathbb{1}_l \,. \tag{4.47}$$

The factor $\frac{1}{2}$ in Eq. (4.47) comes from the subtraction of a term proportional to the identity, namely $\pm\frac{\sqrt{2}}{2} G_F N_e \mathbb{1}_\nu \otimes \mathbb{1}_l$ (compare with equation 9.14 in Ref. [54]) and the (minus) plus has to be chosen for (anti–)neutrinos. Since neither the mixing Hamiltonian $H_M$, nor the the matter potential $H_{MSW}$ change the neutrino energy, the $U_0$ operator can be written in the 8-dimensional basis as

$$\mathcal{U}_0(t) = \begin{pmatrix} U_{0\alpha}(t) & 0 \\ 0 & U_{0\beta}(t) \end{pmatrix} , \tag{4.48}$$

where $U_{0\alpha}(t), U_{0\beta}(t)$ are the $4 \times 4$ matrices given by Eq. (4.45) corresponding respectively to the neutrino energies $E_\alpha, E_\beta$.

On the other hand, concerning the collisions, the operators $U_{W_k}$ can be written as

$$U_{W_k} = e^{-\imath H_W \tau} \tag{4.49}$$

where $\tau$ is the time scale of the scattering process and $H_W$ is the Hamiltonian governing the collision. Notice that Eq. (4.49) that describes contribution of the scattering processes (quadratic in the interaction Hamiltonian) has the form of a unitary evolution operator. As a consequence, the time-derivative of the density matrix contains a commutator of $H_W$ and the density matrix, instead of the standard anti-commutator, that appears in the kinetic approach to neutrino oscillations. We point out that this seeming contradiction arises because Eq. (4.49) refers to the evolution of the complete density matrix of the neutrino plus charged lepton state and not to the neutrino alone. This means that Eq. (4.49) describes the evolution of both the physical system (the neutrino) and the reservoir (the charged lepton). For this reason, at this level, the evolution of the total state is unitary. Moreover, equation (4.49) is meant to describe the single scattering event, meaning that no information on the collision rate, related to the cross section, is contained within it. The collision rate, which of course, depends quadratically on the interaction Hamiltonian, is instead encoded in the probabilities $P_n(t)$ of Eq. (4.37). On the contrary, in the kinematic approach to neutrino oscillations, the evolution of the reduced density matrix, associated to neutrinos alone, is considered. This implies a non–unitary evolution which takes the form described in the refs. [232–234] and the presence of anti–commutators in place of the commutator deriving from Eq. (4.49). We remark that the comparison between our approach and the ones presented in [232–234] must be done at the level of the *reduced* density matrix and not for the evolution of the complete density matrix which is instead necessarily unitary. In terms of the reduced density matrix associated only to the neutrino, the two approaches are compatible. Taking into account all the possible processes involving a neutrino and a charged leptonic state in Eqs. (4.32) and (4.33), $H_W$ can be written as

$$H_W^{(h)} = \begin{pmatrix} \alpha_1^{(h)} & 0 & 0 & 0 & 0 & 0 & 0 & 0 \\ 0 & \alpha_2^{(h)} & 0 & 0 & 0 & 0 & 0 & 0 \\ 0 & 0 & \alpha_3^{(h)} & 0 & 0 & \beta^{(h)} & 0 & 0 \\ 0 & 0 & 0 & \alpha_4^{(h)} & 0 & 0 & 0 & 0 \\ 0 & 0 & 0 & 0 & \alpha_5^{(h)} & 0 & 0 & 0 \\ 0 & 0 & \beta^{(h)*} & 0 & 0 & \alpha_6^{(h)} & 0 & 0 \\ 0 & 0 & 0 & 0 & 0 & 0 & \alpha_7^{(h)} & 0 \\ 0 & 0 & 0 & 0 & 0 & 0 & 0 & \alpha_8^{(h)} \end{pmatrix},$$

$$\bar{H}_W^{(h)} = \begin{pmatrix} \bar{\alpha}_1^{(h)} & 0 & 0 & 0 & 0 & 0 & 0 & \gamma^{(h)} \\ 0 & \bar{\alpha}_2^{(h)} & 0 & 0 & 0 & 0 & 0 & 0 \\ 0 & 0 & \bar{\alpha}_3^{(h)} & 0 & 0 & 0 & 0 & 0 \\ 0 & 0 & 0 & \bar{\alpha}_4^{(h)} & 0 & 0 & 0 & 0 \\ 0 & 0 & 0 & 0 & \bar{\alpha}_5^{(h)} & 0 & 0 & 0 \\ 0 & 0 & 0 & 0 & 0 & \bar{\alpha}_6^{(h)} & 0 & 0 \\ 0 & 0 & 0 & 0 & 0 & 0 & \bar{\alpha}_7^{(h)} & 0 \\ \gamma^{(h)*} & 0 & 0 & 0 & 0 & 0 & 0 & \bar{\alpha}_8^{(h)} \end{pmatrix}.$$

Here $\bar{H}_W$ is the Hamiltonian for the antineutrinos, the quantities $\alpha, \bar{\alpha}, \beta, \gamma$ are parameters to be determined and the apex $h$ refers to the charged lepton spin projection. The asterisk denotes complex conjugation. The following convention is adopted

$$\begin{aligned} |\nu_e, e\rangle_{E_\alpha}^{(h)} &\to \boldsymbol{e}_1\,, & |\nu_e, \mu\rangle_{E_\alpha}^{(h)} &\to \boldsymbol{e}_2 \\ |\nu_\mu, e\rangle_{E_\alpha}^{(h)} &\to \boldsymbol{e}_3\,, & |\nu_\mu, \mu\rangle_{E_\alpha}^{(h)} &\to \boldsymbol{e}_4 \\ |\nu_e, e\rangle_{E_\beta}^{(h)} &\to \boldsymbol{e}_5\,, & |\nu_e, \mu\rangle_{E_\beta}^{(h)} &\to \boldsymbol{e}_6 \\ |\nu_\mu, e\rangle_{E_\beta}^{(h)} &\to \boldsymbol{e}_7\,, & |\nu_\mu, \mu\rangle_{E_\beta}^{(h)} &\to \boldsymbol{e}_8 \end{aligned}$$

where $\boldsymbol{e}_j$ is the basis vector with a 1 in the $j$-th position and 0 elsewhere, and similarly for the antineutrinos.

In order to fix these quantities, we need to analyze the field theoretical amplitude for the reactions of Eq. (4.32). The Hamiltonian and the related evolution operators of Eq. (4.49) are intended with respect to the basis states of Eq. (4.42) formed by the neutrino and the specific charged lepton (the $k - th$) taking part in the collision. Assuming that the field theoretical 2-particle states $|p_1, p_2\rangle$ are normalized as $\langle p_1, p_2 | p_1', p_2'\rangle = (2\pi)^3 \delta^3(\boldsymbol{p}_1' - \boldsymbol{p}_1)(2\pi)^3(\boldsymbol{p}_2' -$

$\boldsymbol{p_2}\rangle$ , the scattering amplitude reads [58]

$$\langle p_1', p_2'|S|p_1, p_2\rangle = I - \imath\delta^4(p_1 + p_2 - p_1' - p_2')\frac{(2\pi)^4 M(p,p')}{\sqrt{16E_1E_2E_1'E_2'}} \tag{4.50}$$

where $I$ is the identity and $M(p,p')$ is the Lorentz-invariant amplitude for the process. The matrix elements of the interaction Hamiltonian can be deduced by comparing Eq. (4.50) with the scattering matrix that would be produced by an interaction potential (see for instance [236]), which to first order reads

$$\langle f|\, S\,|i\rangle = I - 2\pi i\delta(E_f - E_i)\,\langle f|\, H_I\,|i\rangle\ . \tag{4.51}$$

Here $|i\rangle$ , $|f\rangle$ denote the initial and final states, $E_i, E_f$ the total initial and final energy and $H_I$ is the interaction Hamiltonian. Comparing Eqs. (4.50) and (4.51) we find

$$\langle f|H_I|i\rangle = (2\pi)^3\delta^3(\boldsymbol{p_1'} + \boldsymbol{p_2'} - \boldsymbol{p_1} - \boldsymbol{p_2})\frac{M(p,p')}{\sqrt{16E_1E_2E_1'E_2'}}. \tag{4.52}$$

The Eq. (4.52) yields the matrix elements of the interaction Hamiltonian on the field theoretical states $|p_1, p_2\rangle$. To go further we need the matrix elements of the interaction Hamiltonian on the states of Eq. (4.42) which are normalized to unity. This is fundamental if one wishes to obtain the transition probability to a definite final state and thus derive a well–defined quantum mechanical operator $H_I$. To renormalize the two particle states, we follow Ref. [237] and enclose the system in a box with large volume $V$. As we only consider states which satisfy 4-momentum conservation, as the states of Eq. (4.42) automatically do, the Dirac delta in (4.52) is just $\delta^3(0) = \frac{V}{2\pi^3}$. In addition, the singular normalization of the 2-particle states becomes

$$\langle p_1, p_2|p_1', p_2'\rangle = V^2\delta_{\boldsymbol{p_1},\boldsymbol{p_1'}}\delta_{\boldsymbol{p_2},\boldsymbol{p_2'}} \tag{4.53}$$

where now $\delta_{\boldsymbol{p},\boldsymbol{q}}$ is a Kronecker delta. The two particle states are then normalized to unity if all of them are multiplied by $\frac{1}{V}$. To find the normalized matrix elements we just divide Eq.(4.52) by $V^2$, so to obtain

$$\langle f|\, H_I^{(norm)}\,|i\rangle = \frac{M(p,p')}{V\sqrt{16E_1E_2E_1'E_2'}}\ . \tag{4.54}$$

The Lorentz-invariant amplitude $M(p,p')$ for the reactions of Eq. (4.32) can be computed employing the Feynman rules for the electroweak interaction. The amplitudse are explicitly calculated in the appendix (E).

We show the derivation of $\alpha_1^{(+)}$ explicitly, but all the parameters of $H_W$ and $\bar{H}_W$ can be computed in a similar fashion. To find $\alpha_1^{(+)}$ we take $|f\rangle \equiv |i\rangle = |\nu_e, e\rangle_{E_\nu}^{(+)}$ where we have taken into account that this reaction does not change the neutrino energy $E_\alpha = E_\beta = E_\nu$. Inserting the amplitude from Eq.(E.8) in Eq. (4.54), we deduce

$$\begin{aligned}\alpha_1^{(+)} &= \frac{-8\sqrt{2}G_F E_\nu m_e\left(\sin^2\theta_W + \frac{1}{2}\right)}{4V\sqrt{E_\nu^2 m_e^2}} \\ &= -\frac{2\sqrt{2}G_F}{V}\left(\sin^2\theta_w + \frac{1}{2}\right)\ .\end{aligned}$$

By the same steps we can fix all the parameters appearing in the scattering Hamiltonian. We quote the result for the reader's convenience.

$$\begin{aligned}
\alpha_1^{(+)} &= \alpha_4^{(+)} = \alpha_5^{(+)} = \alpha_8^{(+)} = -\frac{2\sqrt{2}G_F}{V}\left(\sin^2\theta_W + \frac{1}{2}\right) \\
\alpha_2^{(+)} &= \alpha_2^{(+)} = \alpha_6^{(+)} = \alpha_7^{(+)} = -\frac{2\sqrt{2}G_F}{V}\left(\sin^2\theta_W - \frac{1}{2}\right) \\
\beta^{(+)} &= \frac{4G_F}{V}\frac{m_e}{\sqrt{m_e^2+m_\mu^2}} \\
\alpha_j^{(-)} &= -\frac{2\sqrt{2}G_F}{V}\sin^2\theta_W \quad \forall\, j = 1, ..., 8 \\
\beta^{(-)} &= 0 \\
\bar{\alpha}_1^{(+)} &= \bar{\alpha}_4^{(+)} = \bar{\alpha}_5^{(+)} = \bar{\alpha}_8^{(+)} = \frac{2\sqrt{2}G_F}{V}\left(\frac{3}{2} - \sin^2\theta_W\right) \\
\bar{\alpha}_2^{(+)} &= \bar{\alpha}_3^{(+)} = \bar{\alpha}_6^{(+)} = \bar{\alpha}_7^{(+)} = \frac{2\sqrt{2}G_F}{V} \\
\gamma^{(+)} &= \frac{4G_F}{V}\frac{m_e}{\sqrt{m_e^2+m_\mu^2}} \\
\bar{\alpha}_1^{(-)} &= \bar{\alpha}_4^{(-)} = \bar{\alpha}_5^{(-)} = \bar{\alpha}_8^{(-)} = -\frac{2\sqrt{2}G_F}{V}\sin^2\theta_W \\
\bar{\alpha}_2^{(+)} &= \bar{\alpha}_3^{(+)} = \bar{\alpha}_6^{(+)} = \bar{\alpha}_7^{(+)} = 0 \\
\gamma^{(-)} &= 0\,.
\end{aligned} \tag{4.55}$$

The scattering Hamiltonian shall be expedient in the determination of the corresponding evolution operator. Notice that, the former still contains the undetermined, and in principle arbitrary, normalization volume $V$ while the latter is still characterized by the unknown time $\tau$. To get rid of the interacting volume $V$ and time $\tau$ it is convenient to work directly with the time evolution operator.

Naturally, $U_W$ is a unitary $8 \times 8$ matrix on the basis states of Eq. (4.42). Exactly as it happens for the Hamiltonians, because of the different weak processes occurring we have two distinct operators, one for neutrinos $U_W$ and one for antineutrinos $\bar{U}_W$. From Eq. (4.55), it is clear that the only non–zero elements are those on the main diagonal $U_{W,jj}, \bar{U}_{W,jj}$ with $j = 1, ..., 8$ and the elements $U_{W,36}, U_{W,63}, \bar{U}_{W,18}, \bar{U}_{W,81}$. In order to fix the evolution operator, we start by splitting the scattering Hamiltonian conveniently. Defining $\alpha_\pm^{(+)} = \frac{\alpha_1^{(+)} \pm \alpha_2^{(+)}}{2}$, we can write

$$H_W = \alpha_+^{(+)}\mathbb{1} + K_W^{(+)}\,; \quad K_W^{(+)} = \begin{pmatrix}
\alpha_-^{(+)} & 0 & 0 & 0 & 0 & 0 & 0 & 0 \\
0 & \alpha_-^{(+)} & 0 & 0 & 0 & 0 & 0 & 0 \\
0 & 0 & \alpha_-^{(+)} & 0 & 0 & \beta^{(+)} & 0 & 0 \\
0 & 0 & 0 & \alpha_-^{(+)} & 0 & 0 & 0 & 0 \\
0 & 0 & 0 & 0 & \alpha_-^{(+)} & 0 & 0 & 0 \\
0 & 0 & \beta^{(+)} & 0 & 0 & \alpha_-^{(+)} & 0 & 0 \\
0 & 0 & 0 & 0 & 0 & 0 & \alpha_-^{(+)} & 0 \\
0 & 0 & 0 & 0 & 0 & 0 & 0 & \alpha_-^{(+)}
\end{pmatrix}, \tag{4.56}$$

By exponentiating $U_W = e^{-iH_W\tau}$, it follows that $U_W^{(+)} = e^{-i\alpha_+^{(+)}\tau} V_W^{(+)}$, where

$$V_W^{(+)} = \begin{pmatrix} e^{-i\phi} & 0 & 0 & 0 & 0 & 0 & 0 & 0 \\ 0 & e^{-i\phi} & 0 & 0 & 0 & 0 & 0 & 0 \\ 0 & 0 & e^{i\phi}\cos\beta^{(+)}\tau & 0 & 0 & -ie^{i\phi}\sin\beta^{(+)}\tau & 0 & 0 \\ 0 & 0 & 0 & e^{-i\phi} & 0 & 0 & 0 & 0 \\ 0 & 0 & 0 & 0 & e^{-i\phi} & 0 & 0 & 0 \\ 0 & 0 & -ie^{i\phi}\sin\beta^{(+)}\tau & 0 & 0 & e^{i\phi}\cos\beta^{(+)}\tau & 0 & 0 \\ 0 & 0 & 0 & 0 & 0 & 0 & e^{-i\phi} & 0 \\ 0 & 0 & 0 & 0 & 0 & 0 & 0 & e^{-i\phi} \end{pmatrix}, \tag{4.57}$$

and $\phi = \alpha_-^{(+)}\tau$. The global phase factor $e^{-i\alpha_+^{(+)}\tau}$ does not affect any observable of interest and then it can be discarded. Evidently $\sin^2\beta^{(+)}\tau$ is the probability, once the scattering occurs, that given the initial state $|\nu_\mu, e\rangle_{E_\alpha}^{(+)}$, the final state is $|\nu_e, \mu\rangle_{E_\beta}^{(+)}$. According to Fermi's golden rule, the transition probability from state $|i\rangle$ to state $f$ is proportional to the squared modulus of the matrix element $|\langle f|\, H_I\, |i\rangle\,|^2$ of the interaction Hamiltonian. Then the relative transition probability from the initial state $|\nu_\mu, e\rangle_{E_\alpha}^{(+)}$ to the final state $|\nu_e, \mu\rangle_{E_\beta}^{(+)}$ is given by

$$\sin^2\beta^{(+)}\tau = \frac{|H_{W,36}^{(+)}|^2}{|H_{W,33}^{(+)}|^2 + |H_{W,36}^{(+)}|^2} = \frac{|\beta^{(+)}|^2}{|\alpha_2^{(+)}|^2 + |\beta^{(+)}|^2}\,. \tag{4.58}$$

Substituting the values derived in Eq.(4.55), we obtain

$$\sin\beta^{(+)}\tau = \sqrt{\frac{2m_e^2}{(m_e^2+m_\mu^2)\left[\left(\sin^4\theta_W - \sin^2\theta_W + \frac{1}{4}\right) + \frac{2m_e^2}{m_e^2+m_\mu^2}\right]}}$$

and then

$$\beta^{(+)}\tau = \arcsin\left(\sqrt{\frac{2m_e^2}{(m_e^2+m_\mu^2)\left(\sin^4\theta_W - \sin^2\theta_W + \frac{1}{4}\right) + 2m_e^2}}\right)\,. \tag{4.59}$$

The Eq.(4.59) also allows for an immediate determination of the phase factor $\phi$. Indeed

$$\begin{aligned}\phi &= \alpha_-^{(+)}\tau = \frac{\alpha_-^{(+)}}{\beta^{(+)}}\beta^{(+)}\tau = \\ &- \frac{\sqrt{2}}{4}\sqrt{1+\frac{m_\mu^2}{m_e^2}}\arcsin\left(\sqrt{\frac{2m_e^2}{(m_e^2+m_\mu^2)\left(\sin^4\theta_W - \sin^2\theta_W + \frac{1}{4}\right) + 2m_e^2}}\right)\end{aligned} \tag{4.60}$$

The same analysis carried over for $U_W^{(+)}$ can also be performed for the opposite charged lepton spin projection and for the antineutrino. In particular, given the matrix elements of Eq.(4.55), $U_W^{(-)}$ is just a phase factor times the identity matrix. For $\bar{U}_W^{(+)}$ one arrives at the form $\bar{U}_W^{(+)} = e^{-i\bar{\alpha}_+^{(+)}\tau}\bar{V}_W^{(+)}$ with

$$\bar{V}_W^{(+)} = \begin{pmatrix} e^{-i\bar{\phi}}\cos\gamma^{(+)}\tau & 0 & 0 & 0 & 0 & 0 & 0 & -ie^{i\bar{\phi}}\sin\gamma^{(+)}\tau \\ 0 & e^{-i\bar{\phi}} & 0 & 0 & 0 & 0 & 0 & 0 \\ 0 & 0 & e^{-i\bar{\phi}} & 0 & 0 & 0 & 0 & 0 \\ 0 & 0 & 0 & e^{-i\bar{\phi}} & 0 & 0 & 0 & 0 \\ 0 & 0 & 0 & 0 & e^{-i\bar{\phi}} & 0 & 0 & 0 \\ 0 & 0 & 0 & 0 & 0 & e^{-i\bar{\phi}} & 0 & 0 \\ 0 & 0 & 0 & 0 & 0 & 0 & e^{-i\bar{\phi}} & 0 \\ -ie^{i\bar{\phi}}\sin\gamma^{(+)}\tau & 0 & 0 & 0 & 0 & 0 & 0 & e^{-i\bar{\phi}}\cos\gamma^{(+)}\tau \end{pmatrix}, \tag{4.61}$$

where $\bar{\phi} = \bar{\alpha}_-^{(+)}$. The relative transition probability is fixed, also in this case, by inspecting the ratio of the matrix elements of the Hamiltonian:

$$\gamma^{(+)}\tau = \arcsin\left(\sqrt{\frac{2m_e^2}{(m_e^2+m_\mu^2)\left(\sin^4\theta_W - 3\sin^2\theta_W + \frac{9}{4}\right) + 2m_e^2}}\right). \tag{4.62}$$

### 4.3.4 Results

The analysis carried over in the previous sections provides the tools necessary to determine the evolution of the neutrino state for the propagation in a dense medium, under the assumptions of a sufficiently high energy $E_\nu > 1GeV$ and purely leptonic interactions. For an arbitrary medium, with a non–constant density profile, the evaluation of the density matrix and the related quantities of interest is an extremely complicated numerical task. However, when a constant density profile is assumed, some predictions can be provided analytically.

#### Oscillations for high electron density and/or high neutrino energy case

Accordingly with the MSW theory, the mixing angle in matter $\theta_m$ predicted from the effective potential of Eq.(4.34) satisfies the relation

$$\sin 2\theta_m = \frac{\omega_0 \sin 2\theta}{\sqrt{(\omega_0\cos 2\theta \pm \frac{G_F N_e}{\sqrt{2}})^2 + \omega_0^2\sin^2 2\theta}}, \tag{4.63}$$

where $\theta$ is the mixing angle in vacuum. When $G_F N_e \gg \omega_0$ the equation above becomes, to the leading order

$$\sin 2\theta_m \simeq \epsilon \sin 2\theta \tag{4.64}$$

where $\epsilon = \frac{\sqrt{2}\omega_0}{G_F N_e}$. Then, at high density and/or high neutrino energy, the matter potential inhibits the oscillations, whose probability is proportional to $\sin 2\theta_m$, with the mixing angle falling down with growing energy and density ($\theta_m \propto \frac{1}{N_e E}$).

By contrast, when the scattering is taken into account, neutrinos still have a non–zero transition probability due to the reactions in Eq. (4.33). This point is exemplified in fig. (4.9), where the transition probabilities $P_{\nu_\beta\to\nu_\alpha}(t) = Tr(\rho_{\nu_\beta}(t)\rho_{\nu_\alpha}(0))$ for neutrinos and antineutrinos in a constant high density environment is shown. In this regime the neutrino density matrix attains a simple explicit form. Due to the absence of muons in the medium, and since the oscillations are inhibited by the matter potential, an electron neutrino cannot ever transform in a muon neutrino. Thus, the density matrix of an initial electron neutrino at time $t$ is simply $\rho_{\nu_e}(t) = \rho_{\nu_e}(0)$. If instead the neutrino starts off as a muon neutrino, it can transform into an electron neutrino due to the reactions of Eq. (4.33), but, for what we have just said, it can never go back to its initial state. We can exploit this fact to give an exact prediction of the oscillation probability in this regime. In fact, accordingly with the unitary evolution operators that we have discussed in Sec. 4.3.3, at each single scattering with an electron, the muon neutrino has a probability $|U^{(+)}_{W,33}|^2$ of persisting in the muon state if the target electron has positive spin projection and a probability $|U^{(-)}_{W,33}|^2 = 1$ if the electron has negative spin projection. For an unpolarized medium, we expect that about a half of the electrons shall have a positive spin projection and a half a negative spin projection. At each scattering, the probability that the neutrino remains in the muonic state is then, $P_{\nu_\mu \leftrightarrow \nu_\mu} = \frac{|U^{(+)}_{W,33}|^2+1}{2}$. Clearly the transition probability for a single scattering is given by $P_{\nu_\mu \to \nu_e} = 1 - P_{\nu_\mu \leftrightarrow \nu_\mu} = \frac{|U^{(+)}_{W,36}|^2}{2}$. Therefore, since after a transition into an electron neutrino, it cannot transform back to the muon state, the probability that at time $t$ the neutrino is still in a muon state $(P_{\nu_\mu \leftrightarrow \nu_\mu}(t))$ is equal to

$$P_{\nu_\mu \leftrightarrow \nu_\mu}(t) = \sum_{k=0}^{\infty} P_k(t) \left( \frac{1 + |U_{W,33}|^2}{2} \right)^k \tag{4.65}$$

Here $P_k(t)$ is the probability that, after a time $t$, the neutrino had $k$ scattering processes. Now $P_k(t)$ can be derived from the Poisson distribution with expectation value $\lambda$, where $\lambda$ is the average number of collisions occurring in a time $t$. Denoting by $\sigma_T$ the total cross section for all the reactions of Eq. (4.32), the neutrino mean free path is $l_F = \frac{1}{N_e \sigma_T}$. The average number of collisions is simply the ratio between the distance covered by the neutrino $z$ (that coincide with $t$ assuming $c = 1$) and the neutrino mean free path $\lambda = \frac{t}{l_F} = N_e \sigma_T t$. Thus $P_k(t) = \frac{1}{k!}(N_e \sigma_T t)^k e^{-N_e \sigma_T t}$ and the probability in Eq. (4.65) $P_{\nu_\mu \leftrightarrow \nu_\mu}(t)$ becomes

$$\begin{aligned} P_{\nu_\mu \leftrightarrow \nu_\mu}(t) &= \sum_{k=0}^{\infty} \frac{1}{k!} \left( \frac{N_e \sigma_T t \left(1 + |U_{W,33}|^2\right)}{2} \right)^k e^{-N_e \sigma_T t} \\ &= e^{-(1-|U_{W,33}|^2) \frac{N_e \sigma_T t}{2}} \end{aligned} \tag{4.66}$$

Where in the final expression of Eq. (4.66) we have recognized the Taylor expansion of the exponential. From Eq. (4.66) we immediately deduce the transition probability

$$P_{\nu_\mu \to \nu_e}(t) = 1 - e^{-(1-|U_{W,33}|^2) \frac{N_e \sigma_T t}{2}} . \tag{4.67}$$

In the same way it is possible to prove that, while a muon anti-neutrino with high energy/in high density medium does not oscillate, for an electron anti-neutrino the oscillation probability becomes

$$P_{\bar{\nu}_\mu \to \bar{\nu}_e}(t) = 1 - e^{-(1-|\bar{U}_{W,11}|^2) \frac{N_e \sigma_T t}{2}} . \tag{4.68}$$

Eq. (4.67) and Eq. (4.68) are new oscillation formulae for neutrinos and anti-neutrinos propagating through dense matter and represent the main analytical result of our paper.

We remark that in the high density/high energy limit, i. e. for $G_F N_e \gg \omega_0$ and for the kind of reactions considered, our results are compatible with those obtained via the kinetic equation approach (see for example [231]). In order to show that, we consider Eq. (4.3) of the reference [231]. It can be schematically written as

$$\partial_t \rho_{\mathbf{p}} = -i\sqrt{2} G_F N_e \left[ G, \rho_{\mathbf{p}} \right] + C[\rho_{\mathbf{p}}] , \tag{4.69}$$

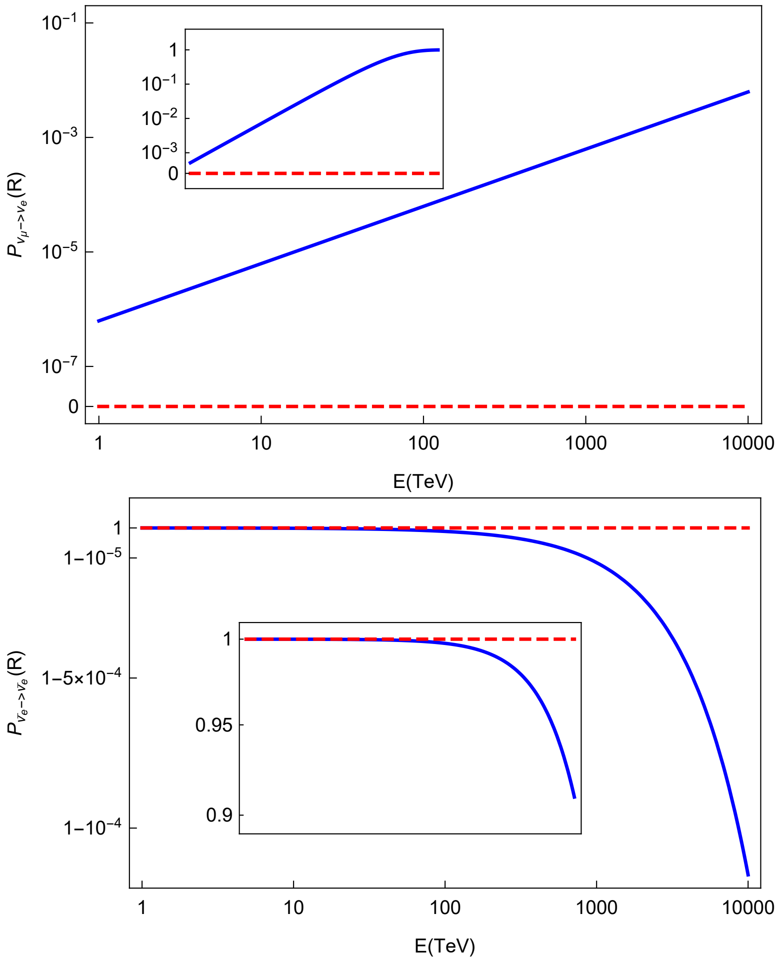


FIGURE 4.9: (color online) Upper Panel – Plot of the $\nu_\mu \to \nu_e$ transition probability as a function of the neutrino energy $E$, for an initial muon neutrino. Lower Panel – Plot of the $\bar{\nu}_e \to \bar{\nu}_e$ survival probability as a function of the antineutrino energy $E$, for an initial electron antineutrino. In both the two plots we consider a travelling lenght equal to the diameter of the Earth. The blue solid line represents our results, while the red dashed line is obtained accordingly with the MSW Theory. For simplicity we have assumed a constant electron density $N_e = 4.069 N_A \text{cm}^{-3}$ obtained as a weighted mean from the earth density profile of the preliminary reference earth model [238]. In the inset the same transition probabilities are plotted for a neutrino travelling through a diametral trajectory in the Sun's Core, with average electron density $N_e = 6.4 \times 10^{26} \text{cm}^{-3}$ and $R_{Core} = 348000$ km corresponding to a quarter of the Sun's diameter.

where $C[\rho_{\boldsymbol{p}}]$ takes into account all the possible collisions with the particles in the medium and is given by

$$C[\rho_{\boldsymbol{p}}] = \frac{1}{2}\int d^3p \Bigg[ W(p',p)(1-\rho_{\boldsymbol{p}})G\rho_{\boldsymbol{p'}}G - W(p,p')\rho_{\boldsymbol{p}}G(1-\rho_{\boldsymbol{p'}})G$$
$$+W(-p',p)(1-\rho_{\boldsymbol{p}})G(1-\bar{\rho}_{\boldsymbol{p'}})G - W(p,-p')\rho_{\boldsymbol{p}}G\bar{\rho}_{\boldsymbol{p'}}G \Bigg].$$

Out of all the terms, the first and the second are respectively gain and loss term due to transitions from and to other states, while the third and the fourth describe neutrino pair production and annihilation processes. We neglect the latter in our tractation right from the offset, because we are interested in generalizing the MSW effect, and thus consider only reactions that preserve the number of neutrinos. In addition,the flavor preserving reactions, as per our assumptions, affect all the flavor states only for an irrelevant common phase factor (since there is no momentum change). In our setting, once the initial neutrino energy is fixed, only two momenta are involved $p_{\nu_\alpha}, p_{\nu_\beta}$, so that the collision term only connects the states $\rho_{p_{\nu_\alpha}}$ and $\rho_{p_{\nu_\beta}}$. Moreover the only possible flavor changing transition is $\nu_\mu + e^- \to \nu_e + \mu^-$, (because there are no free muons in the medium by assumption), so that the collision term actually can only connect the states $\rho_{p_{\nu_\mu}}$ and $\rho_{p_{\nu_e}}$, with the momenta related by momentum conservation. This implies that the time variation due to collisions is

$$\partial_t \rho_{p_{\nu_\mu}}(t) = -W(p_{\nu_\mu}, p_{\nu_e})(1-\rho_{p_{\nu_\mu}}(t))\rho_{p_{\nu_e}} \tag{4.70}$$

and similar, but with the opposite sign, for $\rho_{\nu_e}$. Here $W(p_{\nu_\mu}, p_{\nu_e})$ is the transition rate for the reaction $\nu_\mu + e^- \to \nu_e + \mu^-$, which for the kinematics considered is the same rate appearing in Eq. (4.66). Finally the refractive terms (the commutator term of Eq. (4.69) ) and the free oscillation term have the only effect, when combined, to inhibit the oscillations in this regime. Then the time evolution of the muon neutrino state and the related oscillation probabilities resulting from Eq. (4.70) coincide with the ones found above with our method. Whereas this discussion proves that our method and the kinetic equation approach lead to comparable results for the approximation considered, it is worth noting that the two approaches do not necessarily agree in other circumstances.

**Decoherence**

The charged lepton that is involved in the scattering process with the neutrino actually belongs to a thermal bath and soon after the scattering event, it starts to interact with the other particles in the medium. Therefore, after the scattering, any information on the individual charged lepton state that emerges from the scattering is lost, whereas the neutrino state keeps evolving under the action of the mixing Hamiltonian. These considerations can be made into a quantitative statement about the neutrino state. For the sake of simplicity, let us take into account the case that we have considered in the previous subsection, i.e. when the high electronic density/high neutrino energy condition holds. In such a case, as we have seen, due to the lack of oscillations, the density matrix of an electron neutrino does not change in time and also its purity is unaffected.

A completely different scenario appears when we consider a muon neutrino. In such a case, due to the absence of oscillation between two successive scattering processes, the purity can be written as a function of the oscillation probabilities i.e.

$$\begin{aligned} \mathrm{Tr}(\rho_\mu^2(t)) &= \left(P^2_{\nu_\mu\leftrightarrow\nu_\mu}(t) + P^2_{\nu_\mu\leftrightarrow\nu_e}(t)\right) \\ &= 1 - 2P_{\nu_\mu\leftrightarrow\nu_\mu}(t)P_{\nu_\mu\leftrightarrow\nu_e}(t) \\ &\leq 1 \end{aligned} \tag{4.71}$$

That is, in general, lesser than one and reaches its minimum (equivalently, the impurity $1 - \mathrm{Tr}(\rho_\mu^2(t))$ reaches its maximum) when $P_{\nu_\mu\leftrightarrow\nu_\mu}(t) = P_{\nu_\mu\leftrightarrow\nu_e}(t) = \frac{1}{2}$

The inequality (4.71) describes the loss of purity of the neutrino state due to weak-interaction scattering processes.

We conclude this subsection with an important remark. It could be argued that the charged lepton, being part of the thermal bath, was not in a pure state, to begin with. While this is true in general, the reasoning that leads to the inequality (4.71) is unaffected, because it specifically pertains to the quantum correlations between the neutrino and the charged lepton. It is the latter that gets destroyed by the interactions with the medium, leading to a loss of purity in the neutrino state, regardless of the initial charged lepton state.

### Numerical Results

Before illustrating some numerical results let us discuss a crucial point. The criterion for the breakdown of the matter potential approximation is represented by the high density/high energy condition $G_F N_e \gg \omega_0$).

In main sequence stars, with electron densities comparable to that of the Sun $N_\odot$, the matter potential approximation breaks down only at extremely high energies ($E > 100 GeV$). On the other hand, when much denser objects are considered, such as white dwarfs with $N_{WD} \simeq 10^6 N_\odot$, the deviation from the matter potential approximation can be already evident at energies as low as a few $GeV$. However, the neutrino spectrum for these objects extends from 100 keV to 10 MeV [239], and so it is highly improbable that neutrinos produced within these stars reach the required energy to see appreciable modifications with respect to the MSW.

Moreover, within the core of a supernova, due to the high electron densities, a discrepancy with respect to the bare MSW prediction is to be expected for high energy neutrinos $E > 200 MeV$. The implications of this effect on the mechanism of supernova explosions require a detailed and careful analysis, which is beyond the scope of this paper.

On the other hand, the high density/high energy condition is well verified for ultra high energy neutrinos (see for instance Ref. [240]) propagating through the Earth that have been recently detected in the IceCube experiment[241]. For this reason in our numerical analysis we will focus on them.

In Fig.(4.9) we plot $P_{\nu_\mu\to\nu_e}$ and $P_{\bar{\nu}_e\to\bar{\nu}_e}$ for ultra high energy neutrinos propagating through the Earth as a function of the neutrino energy $E$. For sake of simplicity we consider neutrinos traveling on a diametral trajectory through the Earth and a constant electron density $N_e = 4.069 N_A cm^{-3}$ obtained as a weighted mean from the earth density profile of the preliminary reference earth model [238]. In the plots, the bare matter potential prediction (MSW effect and oscillations inhibited) (red dashed line) and the result obtained from Eq. (4.67) and Eq. (4.68) are compared. We can see that while the MSW formula does not predict any relevant oscillation probability, our formulae provide a transition probability that is remarkably different from zero in the energy range $1 - 10^4$ TeV. These predicted oscillations could be detected in future experiments. We recognize that in the energy range considered the transmission probability might be substantially lowered depending on the angle. Although this does not entirely rule out a possible observation of the phenomenon described, especially below 100 $TeV$ where the transmission probability is fairly high, it constitutes an important limitation to the possible experimental test of our results [242]. Other limitations may be represented by backgrounds, detector systematic and the atmospheric flux that are not negligible in this energy range.

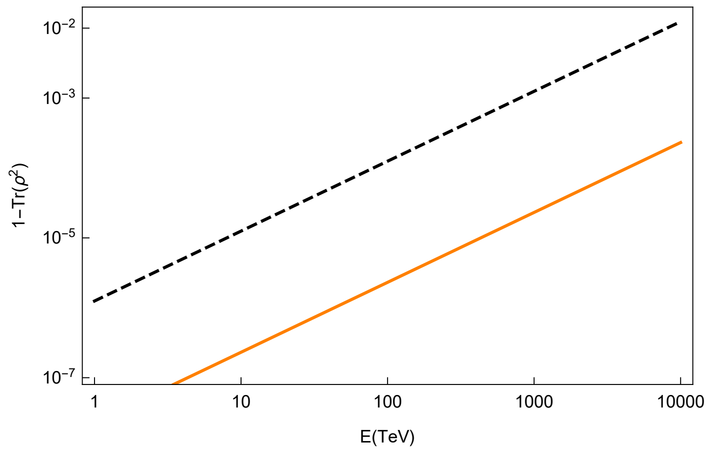


FIGURE 4.10: (color online)Plot of the impurity $1 - Tr(\rho^2)$ as a function of the neutrino energy $E$, for a neutrino travelling on a diametral trajectory through the Earth. The black dashed line refers to the muon neutrino state, whereas the orange solid line refers to the electron antineutrino state. We have assumed the same parameters as in fig. (4.9).

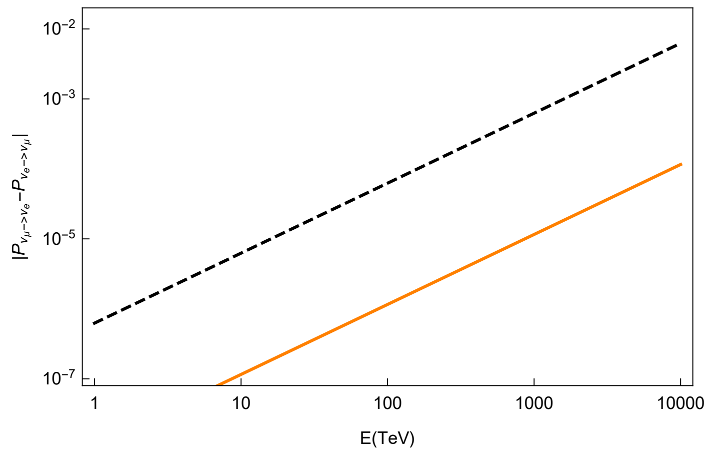


FIGURE 4.11: (color online) Plot of the $T$ asymmetries $\Delta_T^{\mu\to e} = P_{\nu_\mu\to\nu_e} - P_{\nu_e\to\nu_\mu}$ (black dashed line) and $\bar{\Delta}_T^{\mu\to e} = P_{\bar{\nu}_\mu\to\bar{\nu}_e} - P_{\bar{\nu}_e\to\bar{\nu}_\mu}$ (orange solid line) as a function of the neutrino energy $E$, for a neutrino travelling on a diametral trajectory through the Earth. The same parameters as in fig. (4.9) are assumed.

Also the impurity $1 - Tr(\rho^2)$ of the neutrino state $\rho$, which, as anticipated, is always zero in the matter potential approximation gain a non-trivial behavior due to the presence of the scattering processes. In fig. (4.10) we plot the impurity for an initial electron antineutrino and an initial muon neutrino propagating through the Earth, as a function of energy. As can be seen from fig. (4.10), the impurity of the neutrino state initially grows with the energy. At a specific value of the energy $E^*$, depending on the electron density and on the distance $R$ travelled in the medium, the neutrino state reaches the maximum impurity $1 - Tr(\rho_\nu^2(R)) = \frac{1}{2}$ when $P_{\nu_\mu\leftrightarrow\nu_\mu}(t) = P_{\nu_\mu\leftrightarrow\nu_e}(t)$. Beyond $E^*$ the collisions become so frequent that the initial neutrino is almost certainly converted into a neutrino with opposite flavor, approaching the related pure state as the energy grows.

Furthermore, also the asymmetries $\Delta_T^{\alpha\to\beta} = P_{\nu_\alpha\to\nu_\beta}(t) - P_{\nu_\beta\to\nu_\alpha}(t)$ and $\Delta_{CP}^{\alpha\to\beta} = P_{\nu_\alpha\to\nu_\beta}(t) - P_{\bar{\nu}_\alpha\to\bar{\nu}_\beta}(t)$ are also considerably affected by the evolution in a dense environment(see Fig.4.11) Indeed, in view of the possible reactions and due to the absence of muons in the medium, the $\nu_\mu \to \nu_e$ transition probability acquires a non–zero value, while the probability for the opposite transition $\nu_e \to \nu_\mu$ vanishes. Similarly, the antineutrino transition $\bar{\nu}_e \to \bar{\nu}_\mu$ is allowed, while the opposite transition $\bar{\nu}_\mu \to \bar{\nu}_e$ is suppressed. Overall, since $\Delta_T^{\alpha\to\beta} \neq \Delta_{CP}^{\alpha\to\beta}$, the $CPT$ symmetry is violated. The $CPT$ asymmetry is due to the additional scattering term and the related decoherence effect. This is in contrast with the matter potential approximation, for which, in the analyzed energy regime, $CP$, $T$ and $CPT$ violations would all vanish identically, since the oscillations are inhibited for the MSW effect. The $CPT$ violation due to the matter effect discussed here may have played an important role during the first phases of the universe, where high densities and high neutrino energies are to be expected. It is worth mentioning that all the effects discussed in this section are in principle significantly enhanced when the medium electron density $N_e$ is larger, as compared to the relatively small deviations that one has for the Earth electron density. An indication of the larger deviation is shown in the insets of Figure (1), where the transitions for a high energy (anti-)neutrino travelling in the Sun's core are shown. We stress that such high energy neutrinos are not produced within the Sun, and the plot serves merely as an indication of what one expects for high energy neutrinos in denser environments.

### 4.3.5 Discussion

In the MSW theory, the presence of the medium is described by an effective potential that modifies the Pontecorvo Hamiltonian and the oscillation frequencies (see chapter 1). The term introduced in the MSW theory acts as an effective field and does not affect the property of unitarity of the evolution. Thus, the MSW potential alone cannot provide phenomena as decoherence.

In this section we take into account the effects of the scattering processes of the neutrinos with the charged leptons in the medium. To describe this interaction we have introduced a Hamiltonian and a unitary operator that can model the different scattering processes. Then we have connected their elements with the scattering amplitudes derived in the context of quantum field theory.

Our approach is rather general and can provide predictions for a very wide class of physical situations. Possible limitations of the present approach are due to the complexity of the mathematical equations. This implies that a detailed analysis is possible only in some particular cases. Among them, two different situations have attracted our interest: 1) the case in which the probability for a single neutrino to have two or more scattering processes can be neglected, and 2) the high-energy neutrino/high-density medium case in which $G_F N_e \gg \omega_0$. We have shown that, in the first case the predicted results are very close to those of the MSW effect, while in the second appears a clear discrepancy between our results and the MSW ones. Indeed, in this second regime, the new oscillation formulae that we have developed for the muon neutrino and for the electronic antineutrino show an oscillation strongly dependent on the energy, in a region in which, for the MSW theory, no oscillation is allowed. Associated with this new oscillation formulae, we have predicted an effective violation of the $T$, $CP$, and $CPT$ symmetries as well as a loss of purity in the neutrino state.

A possible experimental test of our results could be made in future experiments probing neutrinos travelling through Earth at energies of the order of the TeV, where there is a difference between our prediction and those of the MSW theory.

We remark that, having neglected all the processes involving the emission or absorption of neutrinos, the dissipative evolution we obtain for neutrinos in a medium cannot be precisely compared with the gain-term and the loss-term structure obtained in various papers, as for instance in [243] in a different context. A further analysis of the neutrino propagation in a dense medium, including creation and destruction processes, shall be treated in a forthcoming paper.

For the sake of simplicity, we have developed our results in the framework of quantum mechanics. Obviously, the inclusion of field–theoretical effects can be of interest, with regards to the QFT effects on particle mixing and oscillations [35–38, 77–87, 183, 244] and and the curvature effects on neutrino oscillations ([197] and chapter 2).

# Conclusions

Dark matter is one of the most prominent puzzles in modern cosmology and the quest for its solution has driven an extensive research effort during the last decades, both theoretical and experimental. The issue is tied to and calls for particle physics beyond the standard model. In this thesis we have presented our contribution to the topic, touching on diverse contexts and phenomena, but all relating to the common thread of dark matter.

We have explored a pure field–theoretical explanation, according to which the flavor vacuum of fermion mixing may constitute a dark matter component. To provide solid theoretical grounds on which to study the hypothesis we have generalized the quantum field theory of fermion mixing. We have developed the formalism necessary to describe neutrino oscillations in curved space, deriving new oscillation formulae. In the same framework we have analyzed the energy–momentum tensor associated to the flavor vacuum. We have shown that in the FLRW metric, for an exponential expansion of the scale factor, the vacuum behaves as a pressure–less perfect fluid, analogous to dark matter. This gives a strong indication about the role that flavor mixing plays at a cosmological level. The research in this respect is still at the beginning. Future works will have to expand the results presented here in several directions. Firstly by enlarging the scope of the theory to include other metrics of interest, such as those required to describe the large scale structures in the universe. Secondly by developing, along the same lines, the quantum field theory of boson mixing in curved space.

We have also studied the most promising particle explanation for dark matter, namely axions and axionlike particles. We have introduced two new detection methods to reveal such elusive particles. We have shown that for fermions interacting through axion exchange, entanglement measures bear an observabe signature of the interaction. Consequently entanglement measurements may highlight the existence of axions and axionlike particles. We have also shown that the axion–mediated interaction induces a phase shift in the neutron wavefunction. We have then designed an interferometric setup to reveal the axion–induced phase shift. Both detection mechanisms work in presence of a generic pseudoscalar spin–spin interaction, and are thus sensitive to an eventual "fifth force". There is room for a consistent improvement of these proposals. Many of the simplyfing assumptions made in their conceptual description can be lifted, so to get a more realistic depiction and, eventually, a fully implementable experiment. Forthcoming works shall be aimed at such improvements.

Finally we have investigated the phenomenology of neutrino interactions and neutrino mixing. We have shown how the dark–matter–like behaviour of the mixing vacuum can be reproduced in laboratory, under adequate circumstances, by means of Rydberg atoms. Our results concerning the simulation must be completed by a consistent field theoretical treatment of neutrino mixing at finite temperature. In this direction is our study of neutrino propagation in a dense medium. Although the setting is that of ordinary quantum mechanics, our approach is already capable of catching the dissipative aspects of the neutrino propagation in a medium. Future studies will be concerned with a pure field theoretical description of neutrino mixing at finite temperature, for neutrinos interacting with a generic thermal bath. We have also demonstrated that trapped ions can simulate neutrino–neutrino gravitational interactions. This paves the way for a laboratory replication of the interactions that take place among neutrinos in astrophysical environments.

# Appendix A

# Special functions

In this appendix we provide some details about the special functions that appear in the thesis. The *Bessel functions* are ubiquitous in physics and arise in many contexts, from heat conduction to scattering problems. They solve the complex differential equation

$$z^2\frac{d^2 f}{dz^2}+z\frac{df}{dz}+\left(z^2-\nu^2\right)f=0\,, \tag{A.1}$$

where $\nu$ is an arbitrary complex number. The solutions are denoted $J_\nu(z)$ (Bessel functions of the first kind), $Y_\nu(z)$ (Bessel functions of the second kind) and $H_\nu^{(1)}(z), H_\nu^{(2)}(z)$ (Hankel functions). All these functions are holomorphic on the complex $z$ plane without the negative real axis. We remark that $\{J_\nu(z), Y_\nu(z)\}$ and $\{H_\nu^{(1)}(z), H_\nu^{(2)}(z)\}$ are linearly independent for all values of $\nu$. Unless $\nu$ is an integer $J_\nu(z)$ and $J_{-\nu}(z)$ are also linearly independent. The general solution of equation (A.1) can then be written in either of the forms

$$\begin{aligned} f(z) &= A_1 J_\nu(z)+B_1 Y_\nu(z) \qquad \forall\nu \\ &= A_2 H_\nu^{(1)}(z)+B_2 H_\nu^{(2)}(z) \qquad \forall\nu \\ &= A_3 J_\nu(z)+B_3 J_{-\nu}(z) \qquad \nu\notin\mathbb{Z} \end{aligned}$$

for some complex coefficients $A_j, B_j, j=1,2,3$. The Bessel functions satisfy some useful recurrence relations. If $f_\nu$ denotes any of the functions $J_\nu, Y_\nu, H_\nu^{(1)}, H_\nu^{(2)}$, the following relations hold:

$$\begin{aligned} f_{\nu-1}(z)+f_{\nu+1}(z) &= \frac{2\nu}{z}f_\nu(z) \\ f_{\nu-1}(z)-f_{\nu+1}(z) &= 2\frac{df_\nu}{dz} \\ f_{\nu-1}(z)-\frac{\nu}{z}f_\nu(z) &= \frac{df_\nu}{dz} \\ -f_{\nu+1}(z)+\frac{\nu}{z}f_\nu(z) &= \frac{df_\nu}{dz}\,. \end{aligned} \tag{A.2}$$

Other differential equations are closely related to eq. (A.1) and admit a solution in terms of Bessel functions. In particular, the equation

$$z^2\frac{d^2 f}{dz^2}+\left(\lambda^2 z^2-\nu^2+\frac{1}{4}\right)f=0 \tag{A.3}$$

for arbitrary complex $\lambda$ is solved by $f(z)=z^{\frac{1}{2}}f_\nu(\lambda z)$. We also make use of the asymptotic formulae for the Bessel functions of the first kind $J_\nu(z)$. For fixed $\nu$ not a negative integer and for $z\to 0$ one has

$$J_\nu(z)\sim\left(\frac{z}{2}\right)^\nu\frac{1}{\Gamma(\nu+1)}\,, \tag{A.4}$$

where $\Gamma(z)$ is the Euler Gamma function. For fixed $\nu$, $|\arg z| < \pi$ and $|z| \to \infty$ it holds that

$$J_\nu(z) \sim \sqrt{\frac{2}{\pi z}} \cos\left(z - \frac{\nu\pi}{2} - \frac{\pi}{4}\right) . \tag{A.5}$$

The *Euler Gamma function* $\Gamma(z)$ is a complex generalization of the factorial, holomorphic in the whole complex $z$ plane except for the negative integers and 0. The standard definition, limited to $\Re z > 0$, is

$$\Gamma(z) = \int_0^\infty dt\, t^{z-1} e^{-t} . \tag{A.6}$$

For positive integers $n$ the Gamma function directly yields the factorial $\Gamma(n+1) = n!$. In general, it holds the recurrence relation

$$\Gamma(z+1) = z\Gamma(z) , \tag{A.7}$$

as can be easily deduced from the definition (A.6) with integration by parts. Other useful properties are ($t \in \mathbb{R}$):

$$\begin{aligned} \Gamma(z^*) &= \Gamma^*(z) ; \\ \Gamma(z)\Gamma(1-z) &= \pi \csc \pi z ; \\ \Gamma\left(\frac{1}{2} + it\right)\Gamma\left(\frac{1}{2} - it\right) &= \left|\Gamma\left(\frac{1}{2} + it\right)\right|^2 = \frac{\pi}{\cosh \pi t} . \end{aligned} \tag{A.8}$$

*Whittaker's functions* belong to the class of confluent hypergeometric functions [90]. They solve the Whittaker's equation

$$\frac{d^2 f}{dz^2} + \left[-\frac{1}{4} + \frac{\kappa}{z} + \frac{(\frac{1}{4} - \mu^2)}{z^2}\right] f = 0 . \tag{A.9}$$

As a consequence Whittaker's functions are specified by two complex indices $\kappa, \mu$. In particular $W_{\kappa,\mu}$ is related to the Kummer's $U$ function as

$$W_{\kappa,\mu}(z) = e^{-\frac{z}{2}} z^{\frac{1}{2}+\mu} U(\frac{1}{2} + \mu - \kappa, 1 + 2\mu, z) \tag{A.10}$$

for $-\pi < \arg z <= \pi$.

The *Polylogarithm function* $\mathrm{Li}_s(z)$ is defined for real parameter $s$ and complex argument $z$ as

$$\mathrm{Li}_s(z) = \frac{z}{\Gamma(s)} \int_0^\infty dt\, \frac{t^{s-1}}{e^t - z} . \tag{A.11}$$

When $|z| < 1$ the Polylogarithm can also be written as a power series

$$\mathrm{Li}_s(z) = \sum_{k=1}^{\infty} \frac{z^k}{k^s} . \tag{A.12}$$

From the definition one can see that it holds the important recurrence relation

$$z \frac{d}{dz} \mathrm{Li}_s(z) = \mathrm{Li}_{s-1}(z) . \tag{A.13}$$

For some special values of $s$ the Polylogarithm reduces to other known functions. When $s = 1$ and $|z| < 1$ the power series (A.12) converges to the ordinary logarithm:

$$\mathrm{Li}_1(z) = \sum_{k=1}^{\infty} \frac{z^k}{k} = -\ln(1-z) \ . \tag{A.14}$$

For lower integer values of $s$, one can simply differentiate this expression and employ the recurrence relation to obtain the corresponding function, for instance

$$\mathrm{Li}_0 = z\frac{d}{dz}\mathrm{Li}_1(z) = \frac{z}{1-z} \ . \tag{A.15}$$

When $s = 2$ the Polylogarithm becomes the Spence's function (or dilogarithm). Finally, in the case of unit argument ($z = 1$) the Polylogarithm reduces to the *Riemann Zeta function* $\zeta(s)$:

$$\mathrm{Li}_s(1) = \sum_{k=1}^{\infty} \frac{1}{k^s} = \zeta(s) \ . \tag{A.16}$$

# Appendix B

# FLRW spacetimes

This appendix provides an elementary and self-contained introduction to FLRW spacetimes. To a very good extent the universe is homogeneous, meaning that it has the same physical properties at all points, and it is isotropic, having no preferred spatial direction. The class of metrics respecting these symmetries is that of the *FLRW metrics*, whose general form reads

$$ds^2 = dt^2 - C^2(t)d\Sigma^2 \; . \tag{B.1}$$

Here $C(t)$ is a smooth function of time known as the *scale factor*, having dimensions of length, and $d\Sigma^2$ is the line element of the spatial hypersurfaces with constant $t$. In comoving coordinates $(t, r, \theta, \phi)$ one writes explicitly

$$ds^2 = dt^2 - C^2(t)\left(\frac{dr^2}{1 - Kr^2} + r^2 d\theta^2 + r^2 \sin^2\theta d\phi^2\right), \tag{B.2}$$

where $r$ is dimensionless and is in the range $[0, 1]$ for $K = 1$. The parameter $K$ determines the $(3-)$space curvature and takes the values $K = \pm 1, 0$. For $K = 0$ (zero curvature) the spatial manifold is flat, for $K = 1$ (positive curvature) it is a 3-sphere and for $K = -1$ (negative curvature) it is a hyperboloid. In each case the spatial manifold has constant and homogeneous curvature. The non-zero components of the Ricci tensor for the metric of equation (B.2) are

$$R_{00} = -\frac{3\ddot{C}}{C} \quad ; \quad R_{ij} = -g_{ij}\left(\frac{\ddot{C}}{C} + 2\left(\frac{\dot{C}}{C}\right)^2 + \frac{K}{C^2}\right) . \tag{B.3}$$

Here the dots are used to denote time derivatives and $g$ is the metric tensor. The scalar curvature is evidently

$$R = g^{\mu\nu}R_{\mu\nu} = -6\left(\frac{\ddot{C}}{C} + \left(\frac{\dot{C}}{C}\right)^2 + \frac{K}{C^2}\right) . \tag{B.4}$$

From the equations (B.3) and (B.4) we can write down the left hand side of the Einstein field equations

$$R_{\mu\nu} - \frac{1}{2}g_{\mu\nu}R = 8\pi G T_{\mu\nu} \; . \tag{B.5}$$

The source term $T_{\mu\nu}$ is modelled, according with the requirement of isotropy and with the symmetries of the metric, as the energy-momentum tensor of a perfect fluid

$$T^{\mu}_{\nu} = \mathrm{diag}\,(\rho, -p, -p, -p) \; , \tag{B.6}$$

with (possibly time-dependent) energy density $\rho$ and pressure $p$. The information on the source of the Einstein equations is exhausted by specifying the fluid equation of state $p =$

$p(\rho)$. The typical contributions have the simple equation of state

$$p = w\rho \,, \tag{B.7}$$

with $w$ constant. Inserting the eqs. (B.3), (B.4) and (B.6) in (B.5), one arrives at the Friedmann equations

$$\begin{aligned} \left(\frac{\dot{C}}{C}\right)^2 + \frac{K}{C^2} &= \frac{8\pi G}{3}\rho \\ 2\frac{\ddot{C}}{C} + \left(\frac{\dot{C}}{C}\right)^2 + \frac{K}{C^2} &= -8\pi G p \end{aligned} \tag{B.8}$$

which combined yield

$$\frac{\ddot{C}}{C} = -\frac{4\pi G}{3}\left(\rho + 3p\right) \,. \tag{B.9}$$

In addition, from the covariant conservation of the energy-momentum tensor, $\nabla_\mu T^{\mu\nu} = 0$ one deduces

$$d\left[C^3\left(\rho + p\right)\right] = C^3 dp \,, \tag{B.10}$$

which is just the first law of thermodynamics. In particular, for a fluid satisfying the equation of state (B.7) one obtains

$$d\left[C^3\rho\left(1+w\right)\right] = wC^3 d\rho \implies \frac{d\rho}{\rho} = -3(1+w)\frac{dC}{C} \implies \rho \propto C^{-3(1+w)} \,. \tag{B.11}$$

Let us now consider the spatially flat ($K = 0$) metric and analyze some of the possible contributions to the energy-momentum tensor. The first Friedmann equation (B.8) becomes

$$\left(\frac{\dot{C}}{C}\right)^2 = \frac{8\pi G}{3}\rho \,, \tag{B.12}$$

which can be easily solved for the scale factor once the equation of state is specified. For non relativistic matter and cold dark matter, $w = 0$, so that $\rho_M \propto C^{-3}$. Writing $\rho_M = \rho_0\left(\frac{C}{C_0}\right)^{-3}$ and substituting in equation (B.12) we obtain

$$\dot{C} = \sqrt{\frac{8\pi G\rho_0 C_0^3}{3}}\, C^{-\frac{1}{2}} \tag{B.13}$$

whose solution gives $C \propto t^{\frac{2}{3}}$. For the cosmological constant contribution $T_{\mu\nu} = \Lambda g_{\mu\nu}$, $w = -1$ and so $\rho_\Lambda = constant$. Setting $H_0^2 = \frac{8\pi G}{3}\rho_\Lambda$, the Friedmann equation gives

$$C(t) \propto e^{H_0 t} \,. \tag{B.14}$$

We conclude by noting that, when $K = 0$, the coordinate transformation $dt \to d\tau = \frac{dt}{C(t)}$ shows explicitly that the FLRW line element (B.2) is confomally equivalent to the flat Minkowski space:

$$ds^2 = C^2(\tau)\left(d\tau^2 - dr^2 - r^2 d\theta^2 - r^2\sin^2\theta d\phi^2\right) \,. \tag{B.15}$$

The coordinate $\tau$ is known as *conformal time*, and often simplifies the calculations in FLRW metrics.

# Appendix C

# Conservation of the energy momentum tensor

In this appendix we prove explicitly the covariant conservation of the energy momentum tensor associated to the flavor vacuum. With reference to the notation of Chapter 2, we prove

$$\nabla_\mu \mathbb{T}^{\mu\nu} = 0 \tag{C.1}$$

with $\nabla_\mu$ denoting the covariant derivative. There is no need here to distinguish between $\mathbb{T}^{(MIX)}_{\mu\nu}$ and $\mathbb{T}^{(N)}_{\mu\nu}$, since both satisfy eq. (C.1), and so does the full energy-momentum tensor. Preliminarly we derive the connection coefficients for the metric of eq. (2.60). It is easy to see from the definition that the only non vanishing coefficients are

$$\Gamma^{\tau}_{\tau\tau} = \Gamma^{\tau}_{ii} = \Gamma^{i}_{\tau i} = \Gamma^{i}_{i\tau} = \frac{\dot{C}}{C} \, . \tag{C.2}$$

Here the dot denotes the derivative with respect to conformal time $\tau$ and no sum is intended over repeated indices. Notice that the coefficients depend only on $\tau$. In terms of the connection coefficients, the covariant divergence reads

$$\nabla_\mu \mathbb{T}^{\mu\nu} = \partial_\mu \mathbb{T}^{\mu\nu} + \Gamma^{\mu}_{\mu\sigma}\mathbb{T}^{\sigma\nu} + \Gamma^{\nu}_{\mu\sigma}\mathbb{T}^{\mu\sigma} \, . \tag{C.3}$$

- ($\nu = i$) For $\nu = i$, with $i = 1, 2, 3$ equation (C.3) becomes

  $$\nabla_\mu \mathbb{T}^{\mu i} = \partial_\mu \mathbb{T}^{\mu i} + \Gamma^{\mu}_{\mu\sigma}\mathbb{T}^{\sigma i} + \Gamma^{i}_{\mu\sigma}\mathbb{T}^{\mu\sigma} \, . \tag{C.4}$$

  From the diagonality of $\mathbb{T}^{\mu\nu}$ proved in Chapter 2, we can write

  $$\nabla_\mu \mathbb{T}^{\mu i} = \partial_i \mathbb{T}^{ii} + \sum_\mu \Gamma^{\mu}_{\mu i}\mathbb{T}^{ii} + \sum_\mu \Gamma^{i}_{\mu\mu}\mathbb{T}^{\mu\mu} \, , \tag{C.5}$$

  where no sum is intended over repeated indices and the summations are written out explicitly to avoid confusion. The first term on the right hand side of eq. (C.5) is zero, since $\mathbb{T}^{\mu\nu}$ depends only on $\tau$. Similarly, from eq. (C.2) we know that $\Gamma^{\mu}_{\mu i} = 0 = \Gamma^{i}_{\mu\mu}$ for each $\mu = 0, 1, 2, 3$ and each $i = 1, 2, 3$, so that also the second and the third term on the right hand side of eq. (C.5) vanish. Then

  $$\nabla_\mu \mathbb{T}^{\mu i} = 0 \quad \forall i \, . \tag{C.6}$$

- ($\nu = \tau$) Only a slightly longer calculation is needed to prove the statement for $\nu = \tau$. Starting from equation (C.3) we have

$$
\begin{aligned}
\nabla_\mu \mathbb{T}^{\mu\tau} &= \partial_\mu \mathbb{T}^{\mu\tau} + \Gamma^{\mu}_{\mu\sigma}\Gamma^{\sigma\tau} + \Gamma^{\tau}_{\mu\sigma}\mathbb{T}^{\mu\sigma} \\
&= \partial_\tau \mathbb{T}^{\tau\tau} + \left(\Gamma^{\tau}_{\tau\tau} + \sum_i \Gamma^{i}_{i\tau}\right)\mathbb{T}^{\tau\tau} + \Gamma^{\tau}_{\tau\tau}\mathbb{T}^{\tau\tau} + \sum_i \Gamma^{\tau}_{ii}\mathbb{T}^{ii} \\
&= \partial_\tau \mathbb{T}^{\tau\tau} + 5\Gamma^{\tau}_{\tau\tau}\mathbb{T}^{\tau\tau} + 3\Gamma^{\tau}_{\tau\tau}\mathbb{T}^{ii}\,, \qquad \text{(C.7)}
\end{aligned}
$$

where we have used the diagonality of $\mathbb{T}^{\mu\nu}$ and eqs. (C.2). For our purposes it is convenient to rewrite eq. (C.7) in terms of $\mathbb{T}_{\tau\tau}$ and the trace $\mathbb{T}^{\mu}_{\mu}$. To this end we employ eqs. (2.130), (C.2) and lower the indices through the metric of eq. (2.60), obtaining:

$$
\nabla_\mu \mathbb{T}^{\mu\tau} = \partial_\tau\left(C^{-4}\mathbb{T}_{\tau\tau}\right) + 6C^{-5}\dot{C}\mathbb{T}_{\tau\tau} - C^{-3}\dot{C}\mathbb{T}^{\mu}_{\mu}\,. \qquad \text{(C.8)}
$$

From equation (2.116), we know that each of the terms above is the integral of the auxiliary tensor components $L_{\tau\tau}, L^{\mu}_{\mu}$ weighted by $\tau$-independent coefficients (recall that the Bogoliubov coefficients are evaluated at a fixed time $\tau_0$). It is therefore sufficient to prove that

$$
\partial_\tau\left(C^{-4}L_{\tau\tau}(a,b)\right) + 6C^{-5}\dot{C}L_{\tau\tau}(a,b) - C^{-3}\dot{C}L^{\mu}_{\mu}(a,b) = 0 \qquad \text{(C.9)}
$$

for each $a, b = u_{\mathbf{p},\lambda;j}, v_{\mathbf{p},\lambda;j}$, to show that the divergence (C.8) vanishes. To this end we need the second order equations

$$
\begin{aligned}
\partial_\tau^2 \phi_{p;j} &= -\left(im_j\dot{C} + p^2 + m_j^2C^2\right)\phi_{p;j} \\
\partial_\tau^2 \gamma_{p;j} &= -\left(-im_j\dot{C} + p^2 + m_j^2C^2\right)\gamma_{p;j}\,. \qquad \text{(C.10)}
\end{aligned}
$$

The first of this equations is simply eq. (2.77), and the second can be likewise deduced from the system (2.76). For $L_{\mu\nu}(u_{\mathbf{p},\lambda;j}, u_{\mathbf{p},\lambda;j})$ we have, using the properties of the auxiliary tensor (cfr. Chapter 2)

$$
\begin{aligned}
&\partial_\tau\left(C^{-4}L_{\tau\tau}(u_{\mathbf{p},\lambda;j}, u_{\mathbf{p},\lambda;j})\right) + 6C^{-5}\dot{C}L_{\tau\tau}(u_{\mathbf{p},\lambda;j}, u_{\mathbf{p},\lambda;j}) - C^{-3}\dot{C}L^{\mu}_{\mu}(u_{\mathbf{p},\lambda;j}, u_{\mathbf{p},\lambda;j}) = \\
&2\partial_\tau\left[C^{-6}\left(\phi^*_{p;j}\overleftrightarrow{\partial_\tau}\phi_{p;j} + \gamma^*_{p;j}\overleftrightarrow{\partial_\tau}\gamma_{p;j}\right)\right] + 12C^{-7}\dot{C}\left(\phi^*_{p;j}\overleftrightarrow{\partial_\tau}\phi_{p;j} + \gamma^*_{p;j}\overleftrightarrow{\partial_\tau}\gamma_{p;j}\right) \\
&+4im_jC^{-6}\dot{C}\left(|\phi_{p;j}|^2 - |\gamma_{p;j}|^2\right) = \\
&2C^{-6}\partial_\tau\left(\phi^*_{p;j}\overleftrightarrow{\partial_\tau}\phi_{p;j} + \gamma^*_{p;j}\overleftrightarrow{\partial_\tau}\gamma_{p;j}\right) + 4im_jC^{-6}\dot{C}\left(|\phi_{p;j}|^2 - |\gamma_{p;j}|^2\right) = \\
&2C^{-6}\left(\phi^*_{p;j}\partial_\tau^2\phi_{p;j} - \phi_{p;j}\partial_\tau^2\phi^*_{p;j} + \gamma^*_{p;j}\partial_\tau^2\gamma_{p;j} - \gamma_{p;j}\partial_\tau^2\gamma^*_{p;j}\right) + 4im_jC^{-6}\dot{C}\left(|\phi_{p;j}|^2 - |\gamma_{p;j}|^2\right) = \\
&2C^{-6}\Big\{\phi^*_{p;j}\left[-\left(im_j\dot{C} + p^2 + m^2C^2\right)\right]\phi_{p;j} - \phi^*_{p;j}\left[-\left(-im_j\dot{C} + p^2 + m^2C^2\right)\right]\phi_{p;j} \\
&+\gamma^*_{p;j}\left[-\left(-im_j\dot{C} + p^2 + m^2C^2\right)\right]\gamma_{p;j} - \phi^*_{p;j}\left[-\left(im_j\dot{C} + p^2 + m^2C^2\right)\right]\gamma_{p;j}\Big\} \\
&+4im_jC^{-6}\dot{C}\left(|\phi_{p;j}|^2 - |\gamma_{p;j}|^2\right) = \\
&2C^{-6}\left\{|\phi_{p;j}|^2\left(-2im_j\dot{C}\right) + |\gamma_{p;j}|^2\left(2im_j\dot{C}\right)\right\}4im_jC^{-6}\dot{C}\left(|\phi_{p;j}|^2 - |\gamma_{p;j}|^2\right) = \\
&-4im_jC^{-6}\dot{C}\left(|\phi_{p;j}|^2 - |\gamma_{p;j}|^2\right) + 4im_jC^{-6}\dot{C}\left(|\phi_{p;j}|^2 - |\gamma_{p;j}|^2\right) = 0\,.
\end{aligned}
$$

In the fourth step we have used the equations (C.10) and their complex conjugates, and the $\tau$ argument of the functions has been suppressed for notational simplicity. Note that from the properties $L_{\tau\tau}(v_{\boldsymbol{p},\lambda;j}, v_{\boldsymbol{p},\lambda;j}) = -L_{\tau\tau}(u_{\boldsymbol{p},\lambda;j}, u_{\boldsymbol{p},\lambda;j})$ and $L^{\mu}_{\mu}(v_{\boldsymbol{p},\lambda;j}, v_{\boldsymbol{p},\lambda;j}) = -L^{\mu}_{\mu}(u_{\boldsymbol{p},\lambda;j}, u_{\boldsymbol{p},\lambda;j})$ (cfr. Chapter 2) the same relation is satisfied by the components of $L_{\mu\nu}(v_{\boldsymbol{p},\lambda;j}, v_{\boldsymbol{p},\lambda;j})$. Similarly one has

$$\begin{aligned}
&\partial_\tau \left(C^{-4}L_{\tau\tau}(u_{\boldsymbol{p},\lambda;j}, v_{\boldsymbol{p},\lambda;j})\right) + 6C^{-5}\dot{C}L_{\tau\tau}(u_{\boldsymbol{p},\lambda;j}, v_{\boldsymbol{p},\lambda;j}) - C^{-3}\dot{C}L^{\mu}_{\mu}(u_{\boldsymbol{p},\lambda;j}, v_{\boldsymbol{p},\lambda;j}) = \\
&\partial_\tau \left(4C^{-6}\phi^*_{p;j}\overleftrightarrow{\partial_\tau}\gamma^*_{p;j}\right) + 24C^{-7}\dot{C}\left(4C^{-6}\phi^*_{p;j}\overleftrightarrow{\partial_\tau}\gamma^*_{p;j}\right) + 8im_jC^{-6}\dot{C}\phi^*_{p;j}\gamma^*_{p;j} = \\
&4C^{-6}\partial_\tau\left(C^{-6}\phi^*_{p;j}\overleftrightarrow{\partial_\tau}\gamma^*_{p;j}\right) + 8im_jC^{-6}\dot{C}\phi^*_{p;j}\gamma^*_{p;j} = \\
&4\left[\phi^*_{p;j}\partial^2_\tau\gamma^*_{p;j} - \gamma^*_{p;j}\partial^2_\tau\phi^*_{p;j}\right] + 8im_jC^{-6}\dot{C}\phi^*_{p;j}\gamma^*_{p;j} = \\
&4C^{-6}\left\{\phi^*_{p;j}\left[-\left(im_j\dot{C} + p^2 + m^2C^2\right)\right]\gamma^*_{p;j} - \phi^*_{p;j}\left[-\left(-im_j\dot{C} + p^2 + m^2C^2\right)\right]\gamma^*_{p;j}\right\} \\
&+8im_jC^{-6}\dot{C}\phi^*_{p;j}\gamma^*_{p;j} = \\
&-8im_jC^{-6}\dot{C}\phi^*_{p;j}\gamma^*_{p;j} + +8im_jC^{-6}\dot{C}\phi^*_{p;j}\gamma^*_{p;j} = 0\,.
\end{aligned}$$

In the fourth step we have used the complex conjugates of eqs. (C.10). Finally, due to the properties $L_{\tau\tau}(v_{\boldsymbol{p},\lambda;j}, u_{\boldsymbol{p},\lambda;j}) = -L^*_{\tau\tau}(u_{\boldsymbol{p},\lambda;j}, v_{\boldsymbol{p},\lambda;j})$ and $L^{\mu}_{\mu}(v_{\boldsymbol{p},\lambda;j}, u_{\boldsymbol{p},\lambda;j}) = -L^{\mu *}_{\mu}(u_{\boldsymbol{p},\lambda;j}, v_{\boldsymbol{p},\lambda;j})$, the same relation is satisfied by the components of $L_{\mu\nu}(v_{\boldsymbol{p},\lambda;j}, u_{\boldsymbol{p},\lambda;j})$. This is sufficient to prove the statement for $\nu = \tau$.

# Appendix D

# Calculation of the 2-Renyi Entropy

In this appendix we compute explicitly the 2-Renyi entropy for the two fermion state of section 3.2. The total two–body Hamiltonian of eq. (3.17) can be rewritten as

$$H_T = \mathcal{L}_1(r)\sigma_1^z\sigma_2^z + \mathcal{L}_2(r)\left(\sigma_1^x\sigma_2^x + \sigma_1^y\sigma_2^y\right) , \tag{D.1}$$

with the functions

$$\begin{aligned}\mathcal{L}_1(r) &= -\frac{\mathcal{A}}{r^3}\left[2 + \mathcal{B}e^{-mr}\left(m^2r^2 + 2mr + 2\right)\right]\\ \mathcal{L}_2(r) &= \frac{\mathcal{A}}{r^3}\left[1 + \mathcal{B}e^{-mr}\left(mr + 1\right)\right] .\end{aligned}$$

Recalling that, by definition of the Pauli operators one has

$$\begin{aligned}\sigma_i^z\left|\uparrow\right\rangle_i &= \left|\uparrow\right\rangle_i ;\ \sigma_i^z\left|\downarrow\right\rangle_i = -\left|\downarrow\right\rangle_i\\ \sigma_i^x\left|\uparrow\right\rangle_i &= \left|\downarrow\right\rangle_i ;\ \sigma_i^x\left|\downarrow\right\rangle_i = \left|\uparrow\right\rangle_i\\ \sigma_i^y\left|\uparrow\right\rangle_i &= -i\left|\downarrow\right\rangle_i ;\ \sigma_i^y\left|\downarrow\right\rangle_i = i\left|\uparrow\right\rangle_i ,\end{aligned}$$

we note that the states

$$\begin{aligned}\left|\chi\right\rangle &= \cos^2\theta\left|\uparrow\uparrow\right\rangle + \sin^2\theta\left|\downarrow\downarrow\right\rangle\\ \left|\eta\right\rangle &= \cos\theta\sin\theta\left(\left|\uparrow\downarrow\right\rangle + \left|\downarrow\uparrow\right\rangle\right)\end{aligned} \tag{D.2}$$

are eigenstates of the Hamiltonian. In equation (D.2) we use the shorthand notation $\left|\uparrow\downarrow\right\rangle \equiv \left|\uparrow\right\rangle_1 \otimes \left|\downarrow\right\rangle_2$ and similar for the other states. Explicitly one has

$$H_T\left|\chi\right\rangle = \mathcal{L}_1(r)\left|\chi\right\rangle ;\quad H_T\left|\eta\right\rangle = \left(2\mathcal{L}_2(r) - \mathcal{L}_1(r)\right)\left|\eta\right\rangle . \tag{D.3}$$

The initial two–fermion state of equation (3.15) is simply written

$$\left|\psi(0)\right\rangle = \left|\chi\right\rangle + \left|\eta\right\rangle . \tag{D.4}$$

It follows immediately, from equation (D.3), that the state at later times $t$ is

$$\left|\psi(t)\right\rangle = e^{-iH_Tt}\left|\psi(0)\right\rangle = e^{-i\mathcal{L}_1(r)t}\left|\chi\right\rangle + e^{-i(2\mathcal{L}_2(r)-\mathcal{L}_1(r))t}\left|\eta\right\rangle . \tag{D.5}$$

Setting

$$\Gamma = 2\left(\mathcal{L}_2(r) - \mathcal{L}_1(r)\right) = \frac{6\mathcal{A}}{r^3} + \frac{2\mathcal{A}\mathcal{B}e^{-mr}}{r^3}\left(m^2r^2 + 3mr + 3\right) , \tag{D.6}$$

the density matrix of the two fermions at time $t$ can be written as

$$\rho(t) = \left|\psi(t)\right\rangle\left\langle\psi(t)\right| = \left|\chi\right\rangle\left\langle\chi\right| + \left|\eta\right\rangle\left\langle\eta\right| + e^{i\Gamma t}\left|\chi\right\rangle\left\langle\eta\right| + e^{-i\Gamma t}\left|\eta\right\rangle\left\langle\chi\right| . \tag{D.7}$$

The reduced density matrix is obtained by tracing with respect to one of the two fermions, say 2:

$$\rho_1(t) = \cos^2\theta \left|\uparrow\right\rangle_1 \left\langle\uparrow\right|_1 + \sin^2\theta \left|\downarrow\right\rangle_1 \left\langle\downarrow\right|_1 + \left(\cos^3\theta \sin\theta e^{i\Gamma t} + \cos\theta \sin^3\theta e^{-i\Gamma t}\right) \left|\uparrow\right\rangle_1 \left\langle\downarrow\right|_1$$
$$+ \left(\cos^3\theta \sin\theta e^{-i\Gamma t} + \cos\theta \sin^3\theta e^{i\Gamma t}\right) \left|\downarrow\right\rangle_1 \left\langle\uparrow\right|_1 \ . \tag{D.8}$$

Squaring the above equation and tracing one gets the purity

$$\mathcal{P}(\rho_1(t)) = \mathrm{Tr}\left(\rho_1^2(t)\right) = 1 - \frac{\sin^4 2\theta}{2} \sin^2 \Gamma t \tag{D.9}$$

and finally the result of eq. (3.18).

# Appendix E

# Scattering amplitudes for neutrino-lepton interactions

In this appendix we derive the scattering amplitudes for the various processes involved. We shall study the reactions in the rest frame of the initial charged lepton and assume that the 4-momentum exchange is small compared to the mass of the weak gauge bosons $m_W, m_Z$. The weak boson propagator in momentum space is given by

$$D^j_{\mu\nu}(q) = \frac{-i\left(g_{\mu\nu} - \frac{q_\mu q_\nu}{m_j^2}\right)}{q^2 - m_j^2 + i\epsilon} \tag{E.1}$$

with $j = W, Z$. When $q^2 \ll m_j^2$, we can neglect all the $q$ terms in Eq.(E.1). Correspondingly the weak propagator becomes a constant, and the weak interaction is replaced by the effective Fermi current-current interaction. There are three kinds of reactions to consider: neutral current interactions like $\nu_e + \mu \leftrightarrow \nu_e + \mu$, charged current interactions like $\nu_e + \mu \leftrightarrow \nu_\mu + e$ and reactions where both charged and neutral current contribute, like $\nu_e + e \leftrightarrow \nu_e + e$. We start by computing $\mathcal{M}(\nu_e + e \leftrightarrow \nu_e + e)$. We work in the rest frame of the initial electron, where $p_e \equiv (m_e, \mathbf{0})$ and $p_\nu \equiv (E_\nu, \boldsymbol{p_\nu})$. The hypothesis of vanishing 4-momentum exchange implies that $p'_\nu = p_\nu$ and $p'_e = p_e$. Without loss of generality, we align the $z$ axis with the neutrino 3-momentum $\boldsymbol{p_\nu} = \boldsymbol{p'_\nu}$. It is convenient to work in the helicity basis. Here the Dirac matrices are

$$\gamma^0 = \begin{pmatrix} 0 & -\mathbb{1} \\ -\mathbb{1} & 0 \end{pmatrix} \quad \boldsymbol{\gamma} = \begin{pmatrix} 0 & \boldsymbol{\sigma} \\ -\boldsymbol{\sigma} & 0 \end{pmatrix} \quad \gamma_5 = \begin{pmatrix} \mathbb{1} & 0 \\ 0 & -\mathbb{1} \end{pmatrix} \tag{E.2}$$

with $\mathbb{1}$ the $2 \times 2$ identity matrix and $\boldsymbol{\sigma}$ the vector of Pauli matrices. In this basis the spinors with helicity $h = \pm$ are

$$\begin{aligned} u^{(h)}(\boldsymbol{p}) &= \begin{pmatrix} -\sqrt{E_{\boldsymbol{p}} + h|\boldsymbol{p}|}\chi^{(h)}(\boldsymbol{p}) \\ \sqrt{E_{\boldsymbol{p}} - h|\boldsymbol{p}|}\chi^{(h)}(\boldsymbol{p}) \end{pmatrix} \\ v^{(h)}(\boldsymbol{p}) &= -h \begin{pmatrix} -\sqrt{E_{\boldsymbol{p}} - h|\boldsymbol{p}|}\chi^{(-h)}(\boldsymbol{p}) \\ \sqrt{E_{\boldsymbol{p}} + h|\boldsymbol{p}|}\chi^{(-h)}(\boldsymbol{p}) \end{pmatrix} \end{aligned}$$

respectively for the particle and the antiparticle. The two-spinors $\chi$ depend upon the orientation of $\boldsymbol{p}$. When $\boldsymbol{p}$ is along the $z$ axis or $\boldsymbol{p} = 0$ (this is the only case relevant to us), we have

$\chi^{(+)} = \begin{pmatrix} 1 \\ 0 \end{pmatrix}$ and $\chi^{(-)} = \begin{pmatrix} 0 \\ 1 \end{pmatrix}$. The charged current contribution is given by [54]

$$\begin{aligned} \mathcal{M}_{CC} &= -\frac{G_F}{\sqrt{2}} J^{\mu\dagger}_{\nu_e e} J_{\mu\nu_e e} \\ &= -\frac{G_F}{\sqrt{2}} \left(\bar{e}\gamma^\mu(1-\gamma_5)\nu_e\right) \left(\bar{\nu}_e\gamma_\mu(1-\gamma_5)e\right) \ . \end{aligned} \tag{E.3}$$

Only left-handed neutrinos participate in the weak interaction, whereas both the spin orientations must be considered for the electron. We then have

$$\begin{aligned} J^{\mu\dagger}_{\nu_e e(h)} &= 2\overline{u^{(h)}}(p'_e)\gamma^\mu P_L u^{(-)}(p_\nu) \\ J^{\mu}_{\nu_e e(h)} &= 2\overline{u^{(-)}}(p'_\nu)\gamma^\mu P_L u^{(h)}(p_e) \end{aligned} \tag{E.4}$$

where we have introduced the left-handed projector $P_L = (1-\gamma_5)/2$ for convenience. The currents can be easily computed, giving

$$\begin{aligned} J^{\mu\dagger}_{\nu_e e(+)} &= 2\sqrt{(E'_e - |\boldsymbol{p'_e}|)(E_\nu + |\boldsymbol{p_\nu}|)}\chi^{(+)\dagger}(\boldsymbol{p'_e})\bar{\sigma}^\mu\chi^{(-)}(\boldsymbol{p_\nu}) \\ J^{\mu\dagger}_{\nu_e e(-)} &= 2\sqrt{(E'_e + |\boldsymbol{p'_e}|)(E_\nu + |\boldsymbol{p_\nu}|)}\chi^{(-)\dagger}(\boldsymbol{p'_e})\bar{\sigma}^\mu\chi^{(-)}(\boldsymbol{p_\nu}) \\ J^{\mu}_{\nu_e e(+)} &= 2\sqrt{(E_e - |\boldsymbol{p_e}|)(E'_\nu + |\boldsymbol{p'_\nu}|)}\chi^{(-)\dagger}(\boldsymbol{p'_\nu})\bar{\sigma}^\mu\chi^{(+)}(\boldsymbol{p_e}) \\ J^{\mu}_{\nu_e e(-)} &= 2\sqrt{(E_e + |\boldsymbol{p_e}|)(E'_\nu + |\boldsymbol{p'_\nu}|)}\chi^{(-)\dagger}(\boldsymbol{p'_\nu})\bar{\sigma}^\mu\chi^{(-)}(\boldsymbol{p_e}) \end{aligned}$$

where $\bar{\sigma}^\mu \equiv (\mathbb{1}, -\boldsymbol{\sigma})$. Considered that $\boldsymbol{p_\nu} = \boldsymbol{p'_\nu} \,||\, z$, $|\boldsymbol{p}_\nu| \simeq E_\nu$ and that $\boldsymbol{p_e} = \boldsymbol{p'_e} = \boldsymbol{0}$, we have

$$\begin{aligned} J^{\mu\dagger}_{\nu_e e(+)} &\equiv -2\sqrt{2E_\nu m_e}(0,1,-i,0) \\ J^{\mu\dagger}_{\nu_e e(-)} &\equiv 2\sqrt{2E_\nu m_e}(1,0,0,1) \\ J^{\mu}_{\nu_e e(+)} &\equiv -2\sqrt{2E_\nu m_e}(0,1,i,0) \\ J^{\mu}_{\nu_e e(-)} &\equiv 2\sqrt{2E_\nu m_e}(1,0,0,1) \ . \end{aligned}$$

It follows immediately that the charged current contribution is zero for opposite initial and final electron spin projections. On the other hand we find

$$\mathcal{M}^{++}_{CC} = 8\sqrt{2}G_F E_\nu m_e \quad \mathcal{M}^{--}_{CC} = 0 \, , \tag{E.5}$$

Where $\mathcal{M}^{hh'}$ denotes the amplitude associated to the charged lepton with initial helicity $h$ and final helicity $h'$. The neutral current contribution for the same process is [54]

$$\mathcal{M}_{NC} = -\frac{G_F}{\sqrt{2}} \left(\overline{\nu_e}\gamma^\mu(1-\gamma_5)\nu_e\right) \left(\bar{e}\gamma_\mu(g^e_V - g^e_A\gamma_5)\right) \tag{E.6}$$

with $g^e_V = -\frac{1}{2} + \sin^2\theta_W$ and $g^e_A = -\frac{1}{2}$. The calculation follows the same steps as before, yielding $\mathcal{M}^{+-}_{NC} = 0 = \mathcal{M}^{-+}_{NC}$ and

$$\begin{aligned} \mathcal{M}^{++}_{NC} &= -8\sqrt{2}G_F E_\nu m_e \left(\sin^2\theta_W - \frac{1}{2}\right) \\ \mathcal{M}^{--}_{NC} &= -8\sqrt{2}G_F E_\nu m_e \sin^2\theta_W \ . \end{aligned} \tag{E.7}$$

The total amplitude for the process is therefore

$$\begin{aligned}\mathcal{M}^{++}(\nu_e + e^- \leftrightarrow \nu_e + e^-) &= -8\sqrt{2}G_F E_\nu m_e \left(\sin^2\theta_W + \frac{1}{2}\right) \\ \mathcal{M}^{--}(\nu_e + e^- \leftrightarrow \nu_e + e^-) &= -8\sqrt{2}G_F E_\nu m_e \sin^2\theta_W \,. \end{aligned} \tag{E.8}$$

The situation is similar for the other process in which both neutral and charged current contribute, i.e. $\nu_\mu + \mu \leftrightarrow \nu_\mu + \mu$:

$$\begin{aligned}\mathcal{M}^{++}(\nu_\mu + \mu^- \leftrightarrow \nu_\mu + \mu^-) &= -8\sqrt{2}G_F E_\nu m_\mu \left(\sin^2\theta_W + \frac{1}{2}\right) \\ \mathcal{M}^{--}(\nu_\mu + \mu^- \leftrightarrow \nu_\mu + \mu^-) &= -8\sqrt{2}G_F E_\nu m_\mu \sin^2\theta_W \,. \end{aligned} \tag{E.9}$$

For the elastic scatterings $\nu_e + \mu \leftrightarrow \nu_e + \mu$ and $\nu_\mu + e \leftrightarrow \nu_\mu + e$ only the neutral current contributes. We have

$$\begin{aligned}\mathcal{M}^{++}(\nu_e + \mu^- \leftrightarrow \nu_e + \mu^-) &= -8\sqrt{2}G_F E_\nu m_\mu \left(\sin^2\theta_W - \frac{1}{2}\right) \\ \mathcal{M}^{--}(\nu_e + \mu^- \leftrightarrow \nu_e + \mu^-) &= -8\sqrt{2}G_F E_\nu m_\mu \sin^2\theta_W \end{aligned} \tag{E.10}$$

and

$$\begin{aligned}\mathcal{M}^{++}(\nu_\mu + e^- \leftrightarrow \nu_\mu + e^-) &= -8\sqrt{2}G_F E_\nu m_e \left(\sin^2\theta_W - \frac{1}{2}\right) \\ \mathcal{M}^{--}(\nu_\mu + e^- \leftrightarrow \nu_\mu + e^-) &= -8\sqrt{2}G_F E_\nu m_e \sin^2\theta_W \end{aligned} \tag{E.11}$$

respectively. The quasi-elastic scattering $\nu_\mu + e \leftrightarrow \nu_e + \mu$ is the only process considered that has an energy threshold and cannot take place with vanishing 4-momentum exchange. Calling $p_\nu, p_e$ the initial 4-momenta and $p'_\nu, p_\mu$ the final 4-momenta, momentum conservation implies

$$\begin{aligned} m_e + E_\nu &= E'_\nu + E_\mu \\ \boldsymbol{p_\nu} &= \boldsymbol{p'_\nu} + \boldsymbol{p_\mu} \end{aligned}$$

as expressed in the rest frame of the initial electron. In order that the neutrino is forward scattered $\boldsymbol{p_\nu} \,||\, \boldsymbol{p'_\nu} \,||\, z$, all the three-momenta must lie on the $z$ axis. Projecting the second equation on this axis and recalling that $E_\nu \simeq p_\nu$, $E'_\nu \simeq p'_\nu$, we obtain by subtraction

$$E_\mu = p_\mu + m_e \,. \tag{E.12}$$

Squaring equation (E.12) we find the muon 4-momentum

$$p_\mu = \frac{m_\mu^2 - m_e^2}{2m_e} \Longrightarrow E_\mu = \frac{m_e^2 + m_\mu^2}{2m_e} \tag{E.13}$$

and the energy of the outcoming neutrino $E'_\nu = E_\nu - \frac{m_\mu^2 - m_e^2}{2m_e}$. Evidently the energy threshold is set by $\frac{m_\mu^2 - m_e^2}{2m_e} \simeq 10$ GeV and the (lightlike) 4-momentum exchange $q = p_\nu - p'_\nu$ has components of the same order $q^0 = q^z \simeq 10$ GeV. Since $q$ is lightlike, the denominator in the propagator expression (E.1) is again a constant, but we make an error of order $\left(\frac{q^0}{m_W}\right)^2 \simeq \frac{1}{64}$ in neglecting the $q$-term in the numerator. Nonetheless we stick to the current-current interaction, and find the amplitudes as

$$\mathcal{M}^{++}(\nu_\mu + e^- \to \nu_e + \mu^-) = 8\sqrt{2}G_F m_e \sqrt{E_\nu E'_\nu} \qquad \mathcal{M}^{--}(\nu_\mu + e^- \to \nu_e + \mu^-) = 0\,. \tag{E.14}$$

The calculation of the amplitudes for the antineutrinos follows the same steps, except that now only the right-handed antineutrino participates in the interaction and the quasi-elastic reactions are $\bar{\nu}_e + e \leftrightarrow \nu_\mu + \mu$. We have

$$\begin{aligned} \mathcal{M}^{++}(\bar{\nu}_e + e^- \leftrightarrow \bar{\nu}_e + e^-) &= 8\sqrt{2}G_F E_\nu m_e \left(\frac{3}{2} - \sin^2\theta_W\right) \\ \mathcal{M}^{--}(\bar{\nu}_e + e^- \leftrightarrow \bar{\nu}_e + e^-) &= -8\sqrt{2}G_F E_\nu m_e \sin^2\theta_W\,. \end{aligned} \tag{E.15}$$

for the $\bar{\nu}_e + e \leftrightarrow \bar{\nu}_e + e$ scattering and

$$\begin{aligned} \mathcal{M}^{++}(\bar{\nu}_\mu + \mu^- \leftrightarrow \bar{\nu}_\mu + \mu^-) &= 8\sqrt{2}G_F E_\nu m_\mu \left(\frac{3}{2} - \sin^2\theta_W\right) \\ \mathcal{M}^{--}(\bar{\nu}_\mu + \mu^- \leftrightarrow \bar{\nu}_\mu + \mu^-) &= -8\sqrt{2}G_F E_\nu m_\mu \sin^2\theta_W\,. \end{aligned} \tag{E.16}$$

for the $\bar{\nu}_\mu + \mu \leftrightarrow \bar{\nu}_\mu + \mu$ scattering. For the neutral current reactions one finds

$$\mathcal{M}^{++}(\bar{\nu}_\mu + e^- \leftrightarrow \bar{\nu}_\mu + e^-) = 8\sqrt{2}G_F E_\nu m_e \qquad \mathcal{M}^{--}(\bar{\nu}_\mu + e^- \leftrightarrow \bar{\nu}_\mu + e^-) = 0 \tag{E.17}$$

for $\bar{\nu}_\mu + e \leftrightarrow \bar{\nu}_\mu + e$ and

$$\mathcal{M}^{++}(\bar{\nu}_e + \mu^- \leftrightarrow \bar{\nu}_e + \mu^-) = 8\sqrt{2}G_F E_\nu m_\mu \qquad \mathcal{M}^{--}(\bar{\nu}_e + \mu^- \leftrightarrow \bar{\nu}_e + \mu^-) = 0 \tag{E.18}$$

for $\bar{\nu}_e + \mu \leftrightarrow \bar{\nu}_e + \mu$. Finally, the quasi-elastic scattering is described by the same kinematics of equation (E.13) and its amplitude is

$$\mathcal{M}^{++}(\bar{\nu}_e + e^- \to \bar{\nu}_\mu + \mu^-) = 8\sqrt{2}G_F m_e \sqrt{E_\nu E'_\nu} \qquad \mathcal{M}^{--}(\bar{\nu}_e + e^- \to \bar{\nu}_\mu + \mu^-) = 0\,. \tag{E.19}$$

# Bibliography


[1] G. Aad et al. (ATLAS Collaboration). In: *Physics Letters B* 716.1 (2012), pp. 1–29. URL: https://doi.org/10.1016/j.physletb.2012.08.020.

[2] B. P. Abbott et al. "Observation of Gravitational Waves from a Binary Black Hole Merger". In: *Phys. Rev. Lett.* 116 (6 Feb. 2016), p. 061102. DOI: 10.1103/PhysRevLett.116.061102. URL: https://link.aps.org/doi/10.1103/PhysRevLett.116.061102.

[3] Y. Fukuda et al. "Evidence for Oscillation of Atmospheric Neutrinos". In: *Phys. Rev. Lett.* 81 (8 Aug. 1998), pp. 1562–1567. DOI: 10.1103/PhysRevLett.81.1562. URL: https://link.aps.org/doi/10.1103/PhysRevLett.81.1562.

[4] Q. R. Ahmad et al. "Measurement of the Rate of $\nu_e + d \to p + p + e^-$ Interactions Produced by $^8B$ Solar Neutrinos at the Sudbury Neutrino Observatory". In: *Phys. Rev. Lett.* 87 (7 July 2001), p. 071301. DOI: 10.1103/PhysRevLett.87.071301. URL: https://link.aps.org/doi/10.1103/PhysRevLett.87.071301.

[5] Q. R. Ahmad et al. "Direct Evidence for Neutrino Flavor Transformation from Neutral-Current Interactions in the Sudbury Neutrino Observatory". In: *Phys. Rev. Lett.* 89 (1 June 2002), p. 011301. DOI: 10.1103/PhysRevLett.89.011301. URL: https://link.aps.org/doi/10.1103/PhysRevLett.89.011301.

[6] Howard Georgi and S. L. Glashow. "Unity of All Elementary-Particle Forces". In: *Phys. Rev. Lett.* 32 (8 Feb. 1974), pp. 438–441. DOI: 10.1103/PhysRevLett.32.438. URL: https://link.aps.org/doi/10.1103/PhysRevLett.32.438.

[7] Jogesh C. Pati and Abdus Salam. "Lepton number as the fourth "color"". In: *Phys. Rev. D* 10 (1 July 1974), pp. 275–289. DOI: 10.1103/PhysRevD.10.275. URL: https://link.aps.org/doi/10.1103/PhysRevD.10.275.

[8] Harald Fritzsch and Peter Minkowski. "Unified interactions of leptons and hadrons". In: *Annals of Physics* 93.1 (1975), pp. 193–266. ISSN: 0003-4916. DOI: https://doi.org/10.1016/0003-4916(75)90211-0. URL: https://www.sciencedirect.com/science/article/pii/0003491675902110.

[9] M. Fukugita and T. Yanagida. "Resurrection of Grand Unified Theory Baryogenesis". In: *Phys. Rev. Lett.* 89 (13 Sept. 2002), p. 131602. DOI: 10.1103/PhysRevLett.89.131602. URL: https://link.aps.org/doi/10.1103/PhysRevLett.89.131602.

[10] M. Blau and S. Theisen. "String theory as a theory of quantum gravity: a status report". In: *Gen. Relativ. Gravit.* 41 (2009), pp. 743–755. URL: https://doi.org/10.1007/s10714-008-0752-z.

[11] R Loll. "Quantum gravity from causal dynamical triangulations: a review". In: 37.1 (Dec. 2019), p. 013002. DOI: 10.1088/1361-6382/ab57c7. URL: https://doi.org/10.1088/1361-6382/ab57c7.

[12] Leonardo Modesto and Lesław Rachwał. “Nonlocal quantum gravity: A review”. In: *International Journal of Modern Physics D* 26.11 (2017), p. 1730020. DOI: 10.1142/S0218271817300208. eprint: https://doi.org/10.1142/S0218271817300208. URL: https://doi.org/10.1142/S0218271817300208.

[13] Alejandro Perez. “Spin foam models for quantum gravity”. In: 20.6 (Feb. 2003), R43–R104. DOI: 10.1088/0264-9381/20/6/202. URL: https://doi.org/10.1088/0264-9381/20/6/202.

[14] Glennys R. Farrar and M. E. Shaposhnikov. “Baryon asymmetry of the Universe in the minimal standard model”. In: *Phys. Rev. Lett.* 70 (19 May 1993), pp. 2833–2836. DOI: 10.1103/PhysRevLett.70.2833. URL: https://link.aps.org/doi/10.1103/PhysRevLett.70.2833.

[15] Andrei D Sakharov. “Violation ofCPin variance,Casymmetry, and baryon asymmetry of the universe”. In: 34.5 (May 1991), pp. 392–393. DOI: 10.1070/pu1991v034n05abeh002497. URL: https://doi.org/10.1070/pu1991v034n05abeh002497.

[16] Laurent Canetti, Marco Drewes, and Mikhail Shaposhnikov. “Matter and antimatter in the universe”. In: 14.9 (Sept. 2012), p. 095012. DOI: 10.1088/1367-2630/14/9/095012. URL: https://doi.org/10.1088/1367-2630/14/9/095012.

[17] Planck Collaboration et al. “Planck 2018 results - VI. Cosmological parameters”. In: *A&A* 641 (2020), A6. DOI: 10.1051/0004-6361/201833910. URL: https://doi.org/10.1051/0004-6361/201833910.

[18] P. J. E. Peebles and Bharat Ratra. “The cosmological constant and dark energy”. In: *Rev. Mod. Phys.* 75 (2 Apr. 2003), pp. 559–606. DOI: 10.1103/RevModPhys.75.559. URL: https://link.aps.org/doi/10.1103/RevModPhys.75.559.

[19] Joshua A. Frieman, Michael S. Turner, and Dragan Huterer. “Dark Energy and the Accelerating Universe”. In: *Annual Review of Astronomy and Astrophysics* 46.1 (2008), pp. 385–432. DOI: 10.1146/annurev.astro.46.060407.145243. eprint: https://doi.org/10.1146/annurev.astro.46.060407.145243. URL: https://doi.org/10.1146/annurev.astro.46.060407.145243.

[20] T. M. C. Abbott et al. “Dark Energy Survey year 1 results: Cosmological constraints from galaxy clustering and weak lensing”. In: *Phys. Rev. D* 98 (4 Aug. 2018), p. 043526. DOI: 10.1103/PhysRevD.98.043526. URL: https://link.aps.org/doi/10.1103/PhysRevD.98.043526.

[21] Justin Khoury and Amanda Weltman. “Chameleon cosmology”. In: *Phys. Rev. D* 69 (4 Feb. 2004), p. 044026. DOI: 10.1103/PhysRevD.69.044026. URL: https://link.aps.org/doi/10.1103/PhysRevD.69.044026.

[22] Thomas P. Sotiriou and Valerio Faraoni. “$f(R)$ theories of gravity”. In: *Rev. Mod. Phys.* 82 (1 Mar. 2010), pp. 451–497. DOI: 10.1103/RevModPhys.82.451. URL: https://link.aps.org/doi/10.1103/RevModPhys.82.451.

[23] Salvatore Capozziello and Mariafelicia De Laurentis. “Extended Theories of Gravity”. In: *Physics Reports* 509.4 (2011), pp. 167–321. ISSN: 0370-1573. DOI: https://doi.org/10.1016/j.physrep.2011.09.003. URL: https://www.sciencedirect.com/science/article/pii/S0370157311002432.

[24] Virginia Trimble. “Existence and Nature of Dark Matter in the Universe”. In: *Annual Review of Astronomy and Astrophysics* 25.1 (1987), pp. 425–472. DOI: 10.1146/annurev.aa.25.090187.002233. eprint: https://doi.org/10.1146/annurev.aa.25.090187.002233. URL: https://doi.org/10.1146/annurev.aa.25.090187.002233.

[25] Edvige Corbelli and Paolo Salucci. “The extended rotation curve and the dark matter halo of M33”. In: *Monthly Notices of the Royal Astronomical Society* 311.2 (Jan. 2000), pp. 441–447. ISSN: 0035-8711. DOI: 10.1046/j.1365-8711.2000.03075.x. eprint: https://academic.oup.com/mnras/article-pdf/311/2/441/2881340/311-2-441.pdf. URL: https://doi.org/10.1046/j.1365-8711.2000.03075.x.

[26] Vera C. Rubin and Jr. Ford W. Kent. “Rotation of the Andromeda Nebula from a Spectroscopic Survey of Emission Regions”. In: *Astrophysical Journal* 159 (Feb. 1970), p. 379. DOI: 10.1086/150317.

[27] V. C. Rubin, Jr. Ford W. K., and N. Thonnard. “Rotational properties of 21 SC galaxies with a large range of luminosities and radii, from NGC 4605 (R=4kpc) to UGC 2885 (R=122kpc).” In: *Astrophysical Journal* 238 (June 1980), pp. 471–487. DOI: 10.1086/158003.

[28] Douglas Clowe et al. “A Direct Empirical Proof of the Existence of Dark Matter”. In: 648.2 (Aug. 2006), pp. L109–L113. DOI: 10.1086/508162. URL: https://doi.org/10.1086/508162.

[29] Volker Springel et al. “Simulations of the formation, evolution and clustering of galaxies and quasars”. In: *Nature* 435.7042 (June 2005), pp. 629–636. DOI: 10.1038/nature03597. arXiv: astro-ph/0504097 [astro-ph].

[30] Leandros Perivolaropoulos and Foteini Skara. *Challenges for ΛCDM: An update*. 2021. arXiv: 2105.05208 [astro-ph.CO].

[31] Sébastien Clesse and Juan García-Bellido. “Seven hints for primordial black hole dark matter”. In: *Physics of the Dark Universe* 22 (2018), pp. 137–146. ISSN: 2212-6864. DOI: https://doi.org/10.1016/j.dark.2018.08.004. URL: https://www.sciencedirect.com/science/article/pii/S2212686418301250.

[32] Paul H Frampton et al. “Primordial black holes as all dark matter”. In: 2010.04 (Apr. 2010), pp. 023–023. DOI: 10.1088/1475-7516/2010/04/023. URL: https://doi.org/10.1088/1475-7516/2010/04/023.

[33] Gerard Jungman, Marc Kamionkowski, and Kim Griest. “Supersymmetric dark matter”. In: *Physics Reports* 267.5 (1996), pp. 195–373. ISSN: 0370-1573. DOI: https://doi.org/10.1016/0370-1573(95)00058-5. URL: https://www.sciencedirect.com/science/article/pii/0370157395000585.

[34] A. Capolupo. “"Dark Matter and Dark Energy Induced by Condensates"”. In: *Advances in High Energy Physics* 2016.8089142 (2016). URL: https://doi.org/10.1155/2016/8089142.

[35] Antonio) Capolupo. “"Quantum Vacuum, Dark Matter, Dark Energy, and Spontaneous Supersymmetry Breaking"”. In: *Advances in High Energy Physics* 2018.9840351 (2018). URL: https://doi.org/10.1155/2018/9840351.

[36] A. Capolupo, S. Capozziello, and G. Vitiello. “Dark energy and particle mixing”. In: *Physics Letters A* 373.6 (2009), pp. 601–610. ISSN: 0375-9601. DOI: https://doi.org/10.1016/j.physleta.2008.12.018. URL: https://www.sciencedirect.com/science/article/pii/S0375960108017593.

[37] A. Capolupo, S. Capozziello, and G. Vitiello. “Neutrino mixing as a source of dark energy”. In: *Physics Letters A* 363.1 (2007), pp. 53–56. ISSN: 0375-9601. DOI: https://doi.org/10.1016/j.physleta.2006.10.084. URL: https://www.sciencedirect.com/science/article/pii/S0375960106016860.

[38] A. CAPOLUPO, S. CAPOZZIELLO, and G. VITIELLO. “DARK ENERGY, COSMOLOGICAL CONSTANT AND NEUTRINO MIXING”. In: *International Journal of Modern Physics A* 23.31 (2008), pp. 4979–4990. DOI: 10.1142/S0217751X08042857. eprint: https://doi.org/10.1142/S0217751X08042857. URL: https://doi.org/10.1142/S0217751X08042857.

[39] Joan Solà. “Cosmological constant and vacuum energy: old and new ideas”. In: 453 (Aug. 2013), p. 012015. DOI: 10.1088/1742-6596/453/1/012015. URL: https://doi.org/10.1088/1742-6596/453/1/012015.

[40] Adrià Gómez-Valent, Joan Solà, and Spyros Basilakos. “Dynamical vacuum energy in the expanding Universe confronted with observations: a dedicated study”. In: 2015.01 (Jan. 2015), pp. 004–004. DOI: 10.1088/1475-7516/2015/01/004. URL: https://doi.org/10.1088/1475-7516/2015/01/004.

[41] Ronald J. Adler, Brendan Casey, and Ovid C. Jacob. “Vacuum catastrophe: An elementary exposition of the cosmological constant problem”. In: *American Journal of Physics* 63.7 (1995), pp. 620–626. DOI: 10.1119/1.17850. eprint: https://doi.org/10.1119/1.17850. URL: https://doi.org/10.1119/1.17850.

[42] Steven Weinberg. “The cosmological constant problem”. In: *Rev. Mod. Phys.* 61 (1 Jan. 1989), pp. 1–23. DOI: 10.1103/RevModPhys.61.1. URL: https://link.aps.org/doi/10.1103/RevModPhys.61.1.

[43] Alessandra Filippi and M. De Napoli. “Searching in the dark: the hunt for the dark photon”. In: *Reviews in Physics* 5 (2020), p. 100042. ISSN: 2405-4283. DOI: https://doi.org/10.1016/j.revip.2020.100042. URL: https://www.sciencedirect.com/science/article/pii/S2405428320300058.

[44] R. D. Peccei and Helen R. Quinn. “Constraints imposed by CP conservation in the presence of pseudoparticles”. In: *Phys. Rev. D* 16 (6 Sept. 1977), pp. 1791–1797. DOI: 10.1103/PhysRevD.16.1791. URL: https://link.aps.org/doi/10.1103/PhysRevD.16.1791.

[45] Peter Svrcek and Edward Witten. “Axions in string theory”. In: 2006.06 (June 2006), pp. 051–051. DOI: 10.1088/1126-6708/2006/06/051. URL: https://doi.org/10.1088/1126-6708/2006/06/051.

[46] Asimina Arvanitaki et al. “String axiverse”. In: *Phys. Rev. D* 81 (12 June 2010), p. 123530. DOI: 10.1103/PhysRevD.81.123530. URL: https://link.aps.org/doi/10.1103/PhysRevD.81.123530.

[47] Bobby Samir Acharya, Konstantin Bobkov, and Piyush Kumar. “An M theory solution to the strong CP-problem, and constraints on the axiverse”. In: *Journal of High Energy Physics* 2010, 105 (Nov. 2010), p. 105. DOI: 10.1007/JHEP11(2010)105. arXiv: 1004.5138 [hep-th].

[48] S.M. Bilenky and B. Pontecorvo. “Lepton mixing and neutrino oscillations”. In: *Physics Reports* 41.4 (1978), pp. 225–261. ISSN: 0370-1573. DOI: https://doi.org/10.1016/0370-1573(78)90095-9. URL: https://www.sciencedirect.com/science/article/pii/0370157378900959.

[49] S. M. Bilenky and S. T. Petcov. "Massive neutrinos and neutrino oscillations". In: *Rev. Mod. Phys.* 59 (3 July 1987), pp. 671–754. DOI: 10.1103/RevModPhys.59.671. URL: https://link.aps.org/doi/10.1103/RevModPhys.59.671.

[50] Massimo Blasone, Antonio Capolupo, and Giuseppe Vitiello. "Quantum field theory of three flavor neutrino mixing and oscillations with CP violation". In: *Phys. Rev. D* 66 (2 July 2002), p. 025033. DOI: 10.1103/PhysRevD.66.025033. URL: https://link.aps.org/doi/10.1103/PhysRevD.66.025033.

[51] Kanji Fujii, Chikage Habe, and Tetsuo Yabuki. "Note on the field theory of neutrino mixing". In: *Phys. Rev. D* 59 (11 Apr. 1999), p. 113003. DOI: 10.1103/PhysRevD.59.113003. URL: https://link.aps.org/doi/10.1103/PhysRevD.59.113003.

[52] Chueng-Ryong Ji and Yuriy Mishchenko. "General theory of quantum field mixing". In: *Phys. Rev. D* 65 (9 May 2002), p. 096015. DOI: 10.1103/PhysRevD.65.096015. URL: https://link.aps.org/doi/10.1103/PhysRevD.65.096015.

[53] Antonio Capolupo et al. "Phenomenology of flavor oscillations with non-perturbative effects from quantum field theory". In: *Physics Letters B* 594.1 (2004), pp. 135–140. ISSN: 0370-2693. DOI: https://doi.org/10.1016/j.physletb.2004.05.016. URL: https://www.sciencedirect.com/science/article/pii/S0370269304007506.

[54] Carlo Giunti and Chung W. Kim. *"Fundamentals of Neutrino Physics and Astrophysics"*. "Oxford University Press", 2007.

[55] L. Wolfenstein. "Neutrino oscillations in matter". In: *Phys. Rev. D* 17 (9 May 1978), pp. 2369–2374. DOI: 10.1103/PhysRevD.17.2369. URL: https://link.aps.org/doi/10.1103/PhysRevD.17.2369.

[56] L. Wolfenstein. "Neutrino oscillations and stellar collapse". In: *Phys. Rev. D* 20 (10 Nov. 1979), pp. 2634–2635. DOI: 10.1103/PhysRevD.20.2634. URL: https://link.aps.org/doi/10.1103/PhysRevD.20.2634.

[57] S. P. Mikheyev and A. Y. Smirnov. "Resonant amplification of $\nu$ oscillations in matter and solar-neutrino spectroscopy". In: *Il Nuovo Cimento C* 9 (1986), pp. 17–26. URL: https://doi.org/10.1007/BF02508049.

[58] P A (Particle Data Group) Zyla et al. "Review of Particle Physics". In: *Progress of Theoretical and Experimental Physics* 2020.8 (Aug. 2020). 083C01. ISSN: 2050-3911. DOI: 10.1093/ptep/ptaa104. eprint: https://academic.oup.com/ptep/article-pdf/2020/8/083C01/34673722/ptaa104.pdf. URL: https://doi.org/10.1093/ptep/ptaa104.

[59] Antonio Capolupo. "Aspects of particle mixing in Quantum Field Theory". In: *arXiv e-prints*, hep-th/0408228 (Aug. 2004), hep–th/0408228. arXiv: hep-th/0408228 [hep-th].

[60] Massimo Blasone and Jonathan S. Palmer. "Mixing and oscillations of neutral particles in quantum field theory". In: *Phys. Rev. D* 69 (5 Mar. 2004), p. 057301. DOI: 10.1103/PhysRevD.69.057301. URL: https://link.aps.org/doi/10.1103/PhysRevD.69.057301.

[61] Massimo Blasone and Giuseppe Vitiello. "Remarks on the neutrino oscillation formula". In: *Phys. Rev. D* 60 (11 Nov. 1999), p. 111302. DOI: 10.1103/PhysRevD.60.111302. URL: https://link.aps.org/doi/10.1103/PhysRevD.60.111302.

[62] R. Achilles and A Bonfiglioli. “The early proofs of the theorem of Campbell, Baker, Hausdorff and Dynkin”. In: *Archive for History of Exact Sciences* 66 (3 2012), pp. 295–358. URL: http://www.jstor.org/stable/41472234.

[63] S. W. Hawking. “Particle creation by black holes”. In: *Communications in Mathematical Physics* 43 (1975), pp. 199–220. URL: https://rdcu.be/czMxb.

[64] Leonard Parker. “Quantized Fields and Particle Creation in Expanding Universes. I”. In: *Phys. Rev.* 183 (5 July 1969), pp. 1057–1068. DOI: 10.1103/PhysRev.183.1057. URL: https://link.aps.org/doi/10.1103/PhysRev.183.1057.

[65] Julian Schwinger. “On Gauge Invariance and Vacuum Polarization”. In: *Phys. Rev.* 82 (5 June 1951), pp. 664–679. DOI: 10.1103/PhysRev.82.664. URL: https://link.aps.org/doi/10.1103/PhysRev.82.664.

[66] H. B. G. Casimir and D. Polder. “The Influence of Retardation on the London-van der Waals Forces”. In: *Phys. Rev.* 73 (4 Feb. 1948), pp. 360–372. DOI: 10.1103/PhysRev.73.360. URL: https://link.aps.org/doi/10.1103/PhysRev.73.360.

[67] J. Bardeen, L. N. Cooper, and J. R. Schrieffer. “Microscopic Theory of Superconductivity”. In: *Phys. Rev.* 106 (1 Apr. 1957), pp. 162–164. DOI: 10.1103/PhysRev.106.162. URL: https://link.aps.org/doi/10.1103/PhysRev.106.162.

[68] Anna Franckowiak. “Multimessenger Astronomy with Neutrinos”. In: 888 (Sept. 2017), p. 012009. DOI: 10.1088/1742-6596/888/1/012009. URL: https://doi.org/10.1088/1742-6596/888/1/012009.

[69] Kate Scholberg. “Supernova Neutrino Detection”. In: *Annual Review of Nuclear and Particle Science* 62.1 (2012), pp. 81–103. DOI: 10.1146/annurev-nucl-102711-095006. eprint: https://doi.org/10.1146/annurev-nucl-102711-095006. URL: https://doi.org/10.1146/annurev-nucl-102711-095006.

[70] Wilfried Buchmuller. “Neutrinos, Grand Unification and Leptogenesis”. In: (2002). URL: arXiv:hep-ph/0204288v2.

[71] M. Tanabashi et al. “Review of Particle Physics”. In: *Phys. Rev. D* 98 (3 Aug. 2018), p. 030001. DOI: 10.1103/PhysRevD.98.030001. URL: https://link.aps.org/doi/10.1103/PhysRevD.98.030001.

[72] Yuval Grossman and Harry J. Lipkin. “Flavor oscillations from a spatially localized source: A simple general treatment”. In: *Phys. Rev. D* 55 (5 Mar. 1997), pp. 2760–2767. DOI: 10.1103/PhysRevD.55.2760. URL: https://link.aps.org/doi/10.1103/PhysRevD.55.2760.

[73] Dardo Pıriz, Mou Roy, and José Wudka. “Neutrino oscillations in strong gravitational fields”. In: *Phys. Rev. D* 54 (2 July 1996), pp. 1587–1599. DOI: 10.1103/PhysRevD.54.1587. URL: https://link.aps.org/doi/10.1103/PhysRevD.54.1587.

[74] Christian Y. Cardall and George M. Fuller. “Neutrino oscillations in curved spacetime: A heuristic treatment”. In: *Phys. Rev. D* 55 (12 June 1997), pp. 7960–7966. DOI: 10.1103/PhysRevD.55.7960. URL: https://link.aps.org/doi/10.1103/PhysRevD.55.7960.

[75] N. Birrell and P. Davies. *"Quantum Fields in Curved Space (Cambridge Monographs on Mathematical Physics)"*. Cambridge: "Cambridge University Press", 1982.

[76] R. Wald. *"Quantum Field Theory in Curved Spacetime and Black Hole Thermodynamics (Chicago Lectures in Physics)"*. "The University of Chicago Press", 1994.

[77] A. Capolupo et al. “Axion–photon mixing in quantum field theory and vacuum energy”. In: *Physics Letters B* 790 (2019), pp. 427–435. ISSN: 0370-2693. DOI: https://doi.org/10.1016/j.physletb.2019.01.056. URL: https://www.sciencedirect.com/science/article/pii/S0370269319300814.

[78] Kanji Fujii, Chikage Habe, and Tetsuo Yabuki. “Remarks on flavor-neutrino propagators and oscillation formulas”. In: *Phys. Rev. D* 64 (1 June 2001), p. 013011. DOI: 10.1103/PhysRevD.64.013011. URL: https://link.aps.org/doi/10.1103/PhysRevD.64.013011.

[79] K C Hannabuss and D C Latimer. “The quantum field theory of fermion mixing”. In: 33.7 (Feb. 2000), pp. 1369–1373. DOI: 10.1088/0305-4470/33/7/307. URL: https://doi.org/10.1088/0305-4470/33/7/307.

[80] Chueng-Ryong Ji and Yuriy Mishchenko. “Time-to-space conversion in quantum field theory of flavor mixing”. In: *Annals of Physics* 315.2 (2005), pp. 488–504. ISSN: 0003-4916. DOI: https://doi.org/10.1016/j.aop.2004.09.004. URL: https://www.sciencedirect.com/science/article/pii/S0003491604001708.

[81] Massimo Blasone et al. “Quantum field theory of boson mixing”. In: *Phys. Rev. D* 63 (12 May 2001), p. 125015. DOI: 10.1103/PhysRevD.63.125015. URL: https://link.aps.org/doi/10.1103/PhysRevD.63.125015.

[82] Massimo Blasone et al. “Lepton charge and neutrino mixing in pion decay processes”. In: *Phys. Rev. D* 72 (1 July 2005), p. 013003. DOI: 10.1103/PhysRevD.72.013003. URL: https://link.aps.org/doi/10.1103/PhysRevD.72.013003.

[83] M. Blasone et al. “Neutrino mixing, flavor states and dark energy”. In: *Nuclear Instruments and Methods in Physics Research Section A: Accelerators, Spectrometers, Detectors and Associated Equipment* 588.1 (2008). Proceedings of the First International Conference on Astroparticle Physics, pp. 272–275. ISSN: 0168-9002. DOI: https://doi.org/10.1016/j.nima.2008.01.050. URL: https://www.sciencedirect.com/science/article/pii/S0168900208000855.

[84] Massimo Blasone, Antonio Capolupo, and Giuseppe Vitiello. “Particle mixing, flavor condensate and dark energy”. In: *Progress in Particle and Nuclear Physics* 64.2 (2010). Neutrinos in Cosmology, in Astro, Particle and Nuclear Physics, pp. 451–453. ISSN: 0146-6410. DOI: https://doi.org/10.1016/j.ppnp.2009.12.073. URL: https://www.sciencedirect.com/science/article/pii/S0146641009001513.

[85] M. Blasone et al. “Neutrino mixing contribution to the cosmological constant”. In: *Physics Letters A* 323.3 (2004), pp. 182–189. ISSN: 0375-9601. DOI: https://doi.org/10.1016/j.physleta.2004.02.004. URL: https://www.sciencedirect.com/science/article/pii/S0375960104001720.

[86] Antonio Capolupo, Marco Di Mauro, and Alfredo Iorio. “Mixing-induced spontaneous supersymmetry breaking”. In: *Physics Letters A* 375.39 (2011), pp. 3415–3418. ISSN: 0375-9601. DOI: https://doi.org/10.1016/j.physleta.2011.07.046. URL: https://www.sciencedirect.com/science/article/pii/S0375960111009182.

[87] A. Capolupo et al. “Probing quantum field theory particle mixing and dark–matter–like effects with Rydberg atoms”. In: *The European Physical Journal C* 80.423 (2020). DOI: https://doi.org/10.1140/epjc/s10052-020-7959-x.

[88] L. Biedenharn, J. Louck, and P. Carruthers. *"Angular Momentum in Quantum Physics: Theory and Application (Encyclopedia of Mathematics and its Applications"*. Cambridge: "Cambridge University Press", 1984. DOI: doi:10.1017/CBO9780511759888.

[89] B. Thaller. *"Advanced Visual Quantum Mechanics"*. New York: "Springer-Verlag", 2005. DOI: doi:10.1007/b138654.

[90] M. Abramowitz and I. A. Stegun. *"Handbook of Mathematical Functions"*. New York: "Dover Publications Inc.", 1965. ISBN: 9780486612720.

[91] A. O. Barut and I. H. Duru. “Exact solutions of the Dirac equation in spatially flat Robertson-Walker space-times”. In: *Phys. Rev. D* 36 (12 Dec. 1987), pp. 3705–3711. DOI: 10.1103/PhysRevD.36.3705. URL: https://link.aps.org/doi/10.1103/PhysRevD.36.3705.

[92] Ryan Kerner and R B Mann. “Fermions tunnelling from black holes”. In: 25.9 (Apr. 2008), p. 095014. DOI: 10.1088/0264-9381/25/9/095014. URL: https://doi.org/10.1088/0264-9381/25/9/095014.

[93] G. Lambiase et al. “Neutrino optics and oscillations in gravitational fields”. In: *Phys. Rev. D* 71 (7 Apr. 2005), p. 073011. DOI: 10.1103/PhysRevD.71.073011. URL: https://link.aps.org/doi/10.1103/PhysRevD.71.073011.

[94] G. Lambiase. “Pulsar kicks induced by spin flavour oscillations of neutrinos in gravitational fields”. In: *Monthly Notices of the Royal Astronomical Society* 362.3 (Sept. 2005), pp. 867–871. ISSN: 0035-8711. DOI: 10.1111/j.1365-2966.2005.09317.x. eprint: https://academic.oup.com/mnras/article-pdf/362/3/867/2991360/362-3-867.pdf. URL: https://doi.org/10.1111/j.1365-2966.2005.09317.x.

[95] Luca Visinelli. “Neutrino flavor oscillations in a curved space-time”. In: *General Relativity and Gravitation* 47, 62 (May 2015), p. 62. DOI: 10.1007/s10714-015-1899-z. arXiv: 1410.1523 [gr-qc].

[96] Robert M. Wald. “The back reaction effect in particle creation in curved spacetime”. In: *Communications in Mathematical Physics* 54.1 (Feb. 1977), pp. 1–19. DOI: 10.1007/BF01609833.

[97] P. K. Kabir. *"The CP puzzle"*. London: Academic Press, 1968.

[98] O. Nachtmann. *"Elementary Particle Physics: Concepts and Phenomena"*. Berlin: Springer, 1990.

[99] R. D. Peccei and Helen R. Quinn. “CP Conservation in the Presence of Pseudoparticles”. In: *Phys. Rev. Lett.* 38 (25 June 1977), pp. 1440–1443. DOI: 10.1103/PhysRevLett.38.1440. URL: https://link.aps.org/doi/10.1103/PhysRevLett.38.1440.

[100] John Ellis. “Physics Beyond the Standard Model”. In: *Nuclear Physics A* 827.1 (2009). PANIC08, pp. 187c–198c. ISSN: 0375-9474. DOI: https://doi.org/10.1016/j.nuclphysa.2009.05.034. URL: https://www.sciencedirect.com/science/article/pii/S0375947409002966.

[101] Roberto D. Peccei. “The Strong CP Problem and Axions”. In: *Axions: Theory, Cosmology, and Experimental Searches*. Ed. by Markus Kuster, Georg Raffelt, and Berta Beltrán. Berlin, Heidelberg: Springer Berlin Heidelberg, 2008, pp. 3–17. ISBN: 978-3-540-73518-2. DOI: 10.1007/978-3-540-73518-2_1. URL: https://doi.org/10.1007/978-3-540-73518-2_1.

[102] F. Wilczek. “Problem of Strong $P$ and $T$ Invariance in the Presence of Instantons”. In: *Phys. Rev. Lett.* 40 (5 Jan. 1978), pp. 279–282. DOI: 10.1103/PhysRevLett.40.279. URL: https://link.aps.org/doi/10.1103/PhysRevLett.40.279.

[103] Steven Weinberg. “A New Light Boson?” In: *Phys. Rev. Lett.* 40 (4 Jan. 1978), pp. 223–226. DOI: 10.1103/PhysRevLett.40.223. URL: https://link.aps.org/doi/10.1103/PhysRevLett.40.223.

[104] J. M. Pendlebury et al. “Revised experimental upper limit on the electric dipole moment of the neutron”. In: *Phys. Rev. D* 92 (9 Nov. 2015), p. 092003. DOI: 10.1103/PhysRevD.92.092003. URL: https://link.aps.org/doi/10.1103/PhysRevD.92.092003.

[105] C. Abel et al. “Measurement of the Permanent Electric Dipole Moment of the Neutron”. In: *Phys. Rev. Lett.* 124 (8 Feb. 2020), p. 081803. DOI: 10.1103/PhysRevLett.124.081803. URL: https://link.aps.org/doi/10.1103/PhysRevLett.124.081803.

[106] B. Graner et al. “Reduced Limit on the Permanent Electric Dipole Moment of $^{199}$Hg”. In: *Phys. Rev. Lett.* 116 (16 Apr. 2016), p. 161601. DOI: 10.1103/PhysRevLett.116.161601. URL: https://link.aps.org/doi/10.1103/PhysRevLett.116.161601.

[107] V. V. Flambaum et al. “Sensitivity of EDM experiments in paramagnetic atoms and molecules to hadronic $CP$ violation”. In: *Phys. Rev. D* 102 (3 Aug. 2020), p. 035001. DOI: 10.1103/PhysRevD.102.035001. URL: https://link.aps.org/doi/10.1103/PhysRevD.102.035001.

[108] G G Raffelt. “Axions—motivation, limits and searches”. In: 40.25 (June 2007), pp. 6607–6620. DOI: 10.1088/1751-8113/40/25/s05. URL: https://doi.org/10.1088/1751-8113/40/25/s05.

[109] Jihn E. Kim. “Weak-Interaction Singlet and Strong CP Invariance”. In: *Phys. Rev. Lett.* 43 (2 July 1979), pp. 103–107. DOI: 10.1103/PhysRevLett.43.103. URL: https://link.aps.org/doi/10.1103/PhysRevLett.43.103.

[110] M.A. Shifman, A.I. Vainshtein, and V.I. Zakharov. “Can confinement ensure natural CP invariance of strong interactions?” In: *Nuclear Physics B* 166.3 (1980), pp. 493–506. ISSN: 0550-3213. DOI: https://doi.org/10.1016/0550-3213(80)90209-6. URL: https://www.sciencedirect.com/science/article/pii/0550321380902096.

[111] A. R. Zhitnitsky. “"On Possible Suppression of the Axion Hadron Interactions". (In Russian)”. In: *Sov. J. Nucl. Phys.* 31 (980), p. 260.

[112] Michael Dine, Willy Fischler, and Mark Srednicki. “A simple solution to the strong CP problem with a harmless axion”. In: *Physics Letters B* 104.3 (1981), pp. 199–202. ISSN: 0370-2693. DOI: https://doi.org/10.1016/0370-2693(81)90590-6. URL: https://www.sciencedirect.com/science/article/pii/0370269381905906.

[113] Jihn E. Kim and David J. E. Marsh. "An ultralight pseudoscalar boson". In: *Phys. Rev. D* 93 (2 Jan. 2016), p. 025027. DOI: 10.1103/PhysRevD.93.025027. URL: https://link.aps.org/doi/10.1103/PhysRevD.93.025027.

[114] Ivan De Martino et al. "Recognizing Axionic Dark Matter by Compton and de Broglie Scale Modulation of Pulsar Timing". In: *Phys. Rev. Lett.* 119 (22 Nov. 2017), p. 221103. DOI: 10.1103/PhysRevLett.119.221103. URL: https://link.aps.org/doi/10.1103/PhysRevLett.119.221103.

[115] V. A. Rubakov. "Grand unification and heavy axion". In: *JETP Lett.* 65 (Apr. 1997), pp. 621–624. DOI: https://doi.org/10.1134/1.567390. URL: https://rdcu.be/czQSk.

[116] David J. E. Marsh. "Axion cosmology". In: *Physics Reports* 643 (July 2016), pp. 1–79. DOI: 10.1016/j.physrep.2016.06.005. arXiv: 1510.07633 [astro-ph.CO].

[117] G. Lambiase and S. Mohanty. *Hydrogen spin oscillations in a background of axions and the 21-cm brightness temperature*. 2020. arXiv: 1804.05318 [hep-ph].

[118] Adrien Auriol, Sacha Davidson, and Georg Raffelt. "Axion absorption and the spin temperature of primordial hydrogen". In: *Phys. Rev. D* 99 (2 Jan. 2019), p. 023013. DOI: 10.1103/PhysRevD.99.023013. URL: https://link.aps.org/doi/10.1103/PhysRevD.99.023013.

[119] Nick Houston et al. "Natural Explanation for 21 cm Absorption Signals via Axion-Induced Cooling". In: *Phys. Rev. Lett.* 121 (11 Sept. 2018), p. 111301. DOI: 10.1103/PhysRevLett.121.111301. URL: https://link.aps.org/doi/10.1103/PhysRevLett.121.111301.

[120] E. Zavattini et al. "New PVLAS results and limits on magnetically induced optical rotation and ellipticity in vacuum". In: *Phys. Rev. D* 77 (3 Feb. 2008), p. 032006. DOI: 10.1103/PhysRevD.77.032006. URL: https://link.aps.org/doi/10.1103/PhysRevD.77.032006.

[121] Pierre Pugnat et al. "Results from the OSQAR photon-regeneration experiment: No light shining through a wall". In: *Phys. Rev. D* 78 (9 Nov. 2008), p. 092003. DOI: 10.1103/PhysRevD.78.092003. URL: https://link.aps.org/doi/10.1103/PhysRevD.78.092003.

[122] R. Ballou et al. "New exclusion limits on scalar and pseudoscalar axionlike particles from light shining through a wall". In: *Phys. Rev. D* 92 (9 Nov. 2015), p. 092002. DOI: 10.1103/PhysRevD.92.092002. URL: https://link.aps.org/doi/10.1103/PhysRevD.92.092002.

[123] Klaus Ehret et al. "New ALPS results on hidden-sector lightweights". In: *Physics Letters B* 689.4 (2010), pp. 149–155. ISSN: 0370-2693. DOI: https://doi.org/10.1016/j.physletb.2010.04.066. URL: https://www.sciencedirect.com/science/article/pii/S0370269310005526.

[124] M. Arik et al. "Search for Sub-eV Mass Solar Axions by the CERN Axion Solar Telescope with $^3$He Buffer Gas". In: *Phys. Rev. Lett.* 107 (26 Dec. 2011), p. 261302. DOI: 10.1103/PhysRevLett.107.261302. URL: https://link.aps.org/doi/10.1103/PhysRevLett.107.261302.

[125] N. Du et al. "Search for Invisible Axion Dark Matter with the Axion Dark Matter Experiment". In: *Phys. Rev. Lett.* 120 (15 Apr. 2018), p. 151301. DOI: 10.1103/PhysRevLett.120.151301. URL: https://link.aps.org/doi/10.1103/PhysRevLett.120.151301.

[126] A. Capolupo, G. Lambiase, and G. Vitiello. “"Probing Mixing of Photons and Axion-Like Particles by Geometric Phase"”. In: *Advances in High Energy Physics* 2015.826051 (2015). URL: https://doi.org/10.1155/2015/826051.

[127] V. B. Bezerra et al. “Constraining axion coupling constants from measuring the Casimir interaction between polarized test bodies”. In: *Phys. Rev. D* 94 (3 Aug. 2016), p. 035011. DOI: 10.1103/PhysRevD.94.035011. URL: https://link.aps.org/doi/10.1103/PhysRevD.94.035011.

[128] R. Barbieri et al. “Searching for galactic axions through magnetized media: The QUAX proposal”. In: *Physics of the Dark Universe* 15 (2017), pp. 135–141. ISSN: 2212-6864. DOI: https://doi.org/10.1016/j.dark.2017.01.003. URL: https://www.sciencedirect.com/science/article/pii/S2212686417300031.

[129] Georg Raffelt and Leo Stodolsky. “Mixing of the photon with low-mass particles”. In: *Phys. Rev. D* 37 (5 Mar. 1988), pp. 1237–1249. DOI: 10.1103/PhysRevD.37.1237. URL: https://link.aps.org/doi/10.1103/PhysRevD.37.1237.

[130] Ryuji Daido and Fuminobu Takahashi. “The sign of the dipole–dipole potential by axion exchange”. In: *Physics Letters B* 772 (2017), pp. 127–129. ISSN: 0370-2693. DOI: https://doi.org/10.1016/j.physletb.2017.06.027. URL: https://www.sciencedirect.com/science/article/pii/S0370269317304951.

[131] J. E. Moody and Frank Wilczek. “New macroscopic forces?” In: *Phys. Rev. D* 30 (1 July 1984), pp. 130–138. DOI: 10.1103/PhysRevD.30.130. URL: https://link.aps.org/doi/10.1103/PhysRevD.30.130.

[132] K. Simonov, A. Capolupo, and S. M. Giampaolo. “Gravity, entanglement and CPT-symmetry violation in particle mixing”. In: *European Physical Journal C* 79.11, 902 (Nov. 2019), p. 902. DOI: 10.1140/epjc/s10052-019-7407-y. arXiv: 1903.10266 [hep-th].

[133] Salvatore Marco Giampaolo and Tommaso Macrı. “Entanglement, holonomic constraints, and the quantization of fundamental interactions”. In: *Scientific Reports* 9, 11362 (Aug. 2019), p. 11362. DOI: 10.1038/s41598-019-47844-8. arXiv: 1806.08383 [quant-ph].

[134] Charles H. Bennett et al. “Entanglement-Assisted Classical Capacity of Noisy Quantum Channels”. In: *Phys. Rev. Lett.* 83 (15 Oct. 1999), pp. 3081–3084. DOI: 10.1103/PhysRevLett.83.3081. URL: https://link.aps.org/doi/10.1103/PhysRevLett.83.3081.

[135] Paweł Horodecki and Artur Ekert. “Method for Direct Detection of Quantum Entanglement”. In: *Phys. Rev. Lett.* 89 (12 Aug. 2002), p. 127902. DOI: 10.1103/PhysRevLett.89.127902. URL: https://link.aps.org/doi/10.1103/PhysRevLett.89.127902.

[136] Martin B. Plenio and Shashank Virmani. “An Introduction to Entanglement Measures”. In: *Quantum Info. Comput.* 7.1 (Jan. 2007), pp. 1–51. ISSN: 1533-7146.

[137] M. A. Nielsen and I. L. Chuang. *"Quantum Computation and Quantum Information"*. Cambridge University Press, 2010.

[138] S. M. Giampaolo et al. "Universal aspects in the behavior of the entanglement spectrum in one dimension: Scaling transition at the factorization point and ordered entangled structures". In: *Phys. Rev. B* 88 (12 Sept. 2013), p. 125142. DOI: 10.1103/PhysRevB.88.125142. URL: https://link.aps.org/doi/10.1103/PhysRevB.88.125142.

[139] Fabio Antonio Bovino et al. "Direct Measurement of Nonlinear Properties of Bipartite Quantum States". In: *Phys. Rev. Lett.* 95 (24 Dec. 2005), p. 240407. DOI: 10.1103/PhysRevLett.95.240407. URL: https://link.aps.org/doi/10.1103/PhysRevLett.95.240407.

[140] Tiff Brydges et al. "Probing Rényi entanglement entropy via randomized measurements". In: *Science* 364.6437 (2019), pp. 260–263. DOI: 10.1126/science.aau4963. eprint: https://www.science.org/doi/pdf/10.1126/science.aau4963. URL: https://www.science.org/doi/abs/10.1126/science.aau4963.

[141] Bernhard Lesche. "Rényi entropies and observables". In: *Phys. Rev. E* 70 (1 July 2004), p. 017102. DOI: 10.1103/PhysRevE.70.017102. URL: https://link.aps.org/doi/10.1103/PhysRevE.70.017102.

[142] Rajibul Islam et al. "Measuring entanglement entropy in a quantum many-body system". In: *Nature* 528.7580 (Dec. 2015), pp. 77–83. DOI: 10.1038/nature15750.

[143] Dmitry A. Abanin and Eugene Demler. "Measuring Entanglement Entropy of a Generic Many-Body System with a Quantum Switch". In: *Phys. Rev. Lett.* 109 (2 July 2012), p. 020504. DOI: 10.1103/PhysRevLett.109.020504. URL: https://link.aps.org/doi/10.1103/PhysRevLett.109.020504.

[144] V. B. Bezerra et al. "Constraining axion-nucleon coupling constants from measurements of effective Casimir pressure by means of micromachined oscillator". In: *European Physical Journal C* 74, 2859 (May 2014), p. 2859. DOI: 10.1140/epjc/s10052-014-2859-6. arXiv: 1402.3228 [hep-ph].

[145] G. Bimonte, D. López, and R. S. Decca. "Isoelectronic determination of the thermal Casimir force". In: *Phys. Rev. B* 93 (18 May 2016), p. 184434. DOI: 10.1103/PhysRevB.93.184434. URL: https://link.aps.org/doi/10.1103/PhysRevB.93.184434.

[146] G. L. Klimchitskaya and V. M. Mostepanenko. "Improved constraints on the coupling constants of axion-like particles to nucleons from recent Casimir-less experiment". In: *European Physical Journal C* 75, 164 (Apr. 2015), p. 164. DOI: 10.1140/epjc/s10052-015-3401-1. arXiv: 1503.04982 [hep-ph].

[147] Y.-J. Chen et al. "Stronger Limits on Hypothetical Yukawa Interactions in the 30–8000 nm Range". In: *Phys. Rev. Lett.* 116 (22 June 2016), p. 221102. DOI: 10.1103/PhysRevLett.116.221102. URL: https://link.aps.org/doi/10.1103/PhysRevLett.116.221102.

[148] G. L. Klimchitskaya and V. M. Mostepanenko. "Constraints on axionlike particles and non-Newtonian gravity from measuring the difference of Casimir forces". In: *Phys. Rev. D* 95 (12 June 2017), p. 123013. DOI: 10.1103/PhysRevD.95.123013. URL: https://link.aps.org/doi/10.1103/PhysRevD.95.123013.

[149] Jae Hyeok Chang, Rouven Essig, and Samuel D. McDermott. "Supernova 1987A constraints on sub-GeV dark sectors, millicharged particles, the QCD axion, and an axion-like particle". In: *Journal of High Energy Physics* 2018.9, 51 (Sept. 2018), p. 51. DOI: 10.1007/JHEP09(2018)051. arXiv: 1803.00993 [hep-ph].

[150] Koichi Hamaguchi et al. "Limit on the axion decay constant from the cooling neutron star in Cassiopeia A". In: *Phys. Rev. D* 98 (10 Nov. 2018), p. 103015. DOI: 10.1103/PhysRevD.98.103015. URL: https://link.aps.org/doi/10.1103/PhysRevD.98.103015.

[151] Asimina Arvanitaki, Masha Baryakhtar, and Xinlu Huang. "Discovering the QCD axion with black holes and gravitational waves". In: *Phys. Rev. D* 91 (8 Apr. 2015), p. 084011. DOI: 10.1103/PhysRevD.91.084011. URL: https://link.aps.org/doi/10.1103/PhysRevD.91.084011.

[152] C. Marletto and V. Vedral. "Gravitationally Induced Entanglement between Two Massive Particles is Sufficient Evidence of Quantum Effects in Gravity". In: *Phys. Rev. Lett.* 119 (24 Dec. 2017), p. 240402. DOI: 10.1103/PhysRevLett.119.240402. URL: https://link.aps.org/doi/10.1103/PhysRevLett.119.240402.

[153] Sougato Bose et al. "Spin Entanglement Witness for Quantum Gravity". In: *Phys. Rev. Lett.* 119 (24 Dec. 2017), p. 240401. DOI: 10.1103/PhysRevLett.119.240401. URL: https://link.aps.org/doi/10.1103/PhysRevLett.119.240401.

[154] Jen-Feng Hsu et al. "Cooling the Motion of Diamond Nanocrystals in a Magneto-Gravitational Trap in High Vacuum". In: *Scientific Reports* 6, 30125 (July 2016), p. 30125. DOI: 10.1038/srep30125. arXiv: 1603.09243 [quant-ph].

[155] H. Rauch and S. A. Werner. *"Neutron Interferometry–Lessons in Experimental Quantum Mechanics, Wave–Particle Duality, and Entanglement" (2nd Edition)*. Oxford: Oxford University Press, 2015.

[156] S. A. Werner, J. -L. Staudenmann, and R. Colella. "Effect of Earth's Rotation on the Quantum Mechanical Phase of the Neutron". In: *Phys. Rev. Lett.* 42 (17 Apr. 1979), pp. 1103–1106. DOI: 10.1103/PhysRevLett.42.1103. URL: https://link.aps.org/doi/10.1103/PhysRevLett.42.1103.

[157] B. E. Allman et al. "Observation of geometric and dynamical phases by neutron interferometry". In: *Phys. Rev. A* 56 (6 Dec. 1997), pp. 4420–4439. DOI: 10.1103/PhysRevA.56.4420. URL: https://link.aps.org/doi/10.1103/PhysRevA.56.4420.

[158] Apoorva G. Wagh and Veer Chand Rakhecha. "Geometric phase in neutron interferometry". In: *Physics Letters A* 148.1 (1990), pp. 17–19. ISSN: 0375-9601. DOI: https://doi.org/10.1016/0375-9601(90)90566-7. URL: https://www.sciencedirect.com/science/article/pii/0375960190905667.

[159] Apoorva G. Wagh et al. "Neutron Interferometric Observation of Noncyclic Phase". In: *Phys. Rev. Lett.* 81 (10 Sept. 1998), pp. 1992–1995. DOI: 10.1103/PhysRevLett.81.1992. URL: https://link.aps.org/doi/10.1103/PhysRevLett.81.1992.

[160] Frédéric Ott et al. "Shaping micron-sized cold neutron beams". In: *Nuclear Instruments and Methods in Physics Research Section A: Accelerators, Spectrometers, Detectors and Associated Equipment* 788 (2015), pp. 29–34. ISSN: 0168-9002. DOI: https://doi.org/10.1016/j.nima.2015.03.057. URL: https://www.sciencedirect.com/science/article/pii/S0168900215003824.

[161] I. S. Gradshteyn and I. M. Ryzhik. "Table of Integrals, Series and Products". In: 7th ed. Academic Press, 2007, pp. 110–111.

[162] A. Steyerl. “Measurements of total cross sections for very slow neutrons with velocities from 100 m/sec to 5 m/sec”. In: *Physics Letters B* 29.1 (1969), pp. 33–35. ISSN: 0370-2693. DOI: https://doi.org/10.1016/0370-2693(69)90127-0. URL: https://www.sciencedirect.com/science/article/pii/0370269369901270.

[163] *Compendium of Neutron Beam Facilities for High Precision Nuclear Data Measurements*. TECDOC Series 1743. Vienna: INTERNATIONAL ATOMIC ENERGY AGENCY, 2014. ISBN: 978-92-0-106614-5. URL: https://www.iaea.org/publications/10738/compendium-of-neutron-beam-facilities-for-high-precision-nuclear-data-measurements.

[164] G. L. Klimchitskaya, P. Kuusk, and V. M. Mostepanenko. “Constraints on non-Newtonian gravity and axionlike particles from measuring the Casimir force in nanometer separation range”. In: *Phys. Rev. D* 101 (5 Mar. 2020), p. 056013. DOI: 10.1103/PhysRevD.101.056013. URL: https://link.aps.org/doi/10.1103/PhysRevD.101.056013.

[165] Joerg Jaeckel and Michael Spannowsky. “Probing MeV to 90 GeV axion-like particles with LEP and LHC”. In: *Physics Letters B* 753 (2016), pp. 482–487. ISSN: 0370-2693. DOI: https://doi.org/10.1016/j.physletb.2015.12.037. URL: https://www.sciencedirect.com/science/article/pii/S0370269315009855.

[166] Martin Bauer, Matthias Neubert, and Andrea Thamm. “Collider probes of axion-like particles”. In: *Journal of High Energy Physics* 2017.12, 44 (Dec. 2017), p. 44. DOI: 10.1007/JHEP12(2017)044. arXiv: 1708.00443 [hep-ph].

[167] Wolfgang Altmannshofer, Stefania Gori, and Dean J. Robinson. “Constraining axion-like particles from rare pion decays”. In: *Phys. Rev. D* 101 (7 Apr. 2020), p. 075002. DOI: 10.1103/PhysRevD.101.075002. URL: https://link.aps.org/doi/10.1103/PhysRevD.101.075002.

[168] Peter W. Graham et al. “Experimental Searches for the Axion and Axion-Like Particles”. In: *Annual Review of Nuclear and Particle Science* 65.1 (2015), pp. 485–514. DOI: 10.1146/annurev-nucl-102014-022120. eprint: https://doi.org/10.1146/annurev-nucl-102014-022120. URL: https://doi.org/10.1146/annurev-nucl-102014-022120.

[169] Paul Frederik Depta, Marco Hufnagel, and Kai Schmidt-Hoberg. “Robust cosmological constraints on axion-like particles”. In: 2020.05 (May 2020), pp. 009–009. DOI: 10.1088/1475-7516/2020/05/009. URL: https://doi.org/10.1088/1475-7516/2020/05/009.

[170] OPAL Collaboration, G. Abbiendi, and et al. “Multi-photon production in ee collisions at $\sqrt{}\{s\}$ = 181-209 GeV”. In: *European Physical Journal C* 26.3 (Jan. 2003), pp. 331–344. DOI: 10.1140/epjc/s2002-01074-5. arXiv: hep-ex/0210016 [hep-ex].

[171] Simon Knapen et al. “Searching for Axionlike Particles with Ultraperipheral Heavy-Ion Collisions”. In: *Phys. Rev. Lett.* 118 (17 Apr. 2017), p. 171801. DOI: 10.1103/PhysRevLett.118.171801. URL: https://link.aps.org/doi/10.1103/PhysRevLett.118.171801.

[172] Martin Bauer et al. “Axion-like particles at future colliders”. In: *European Physical Journal C* 79.1, 74 (Jan. 2019), p. 74. DOI: 10.1140/epjc/s10052-019-6587-9. arXiv: 1808.10323 [hep-ph].

[173] T F Gallagher. “Rydberg atoms”. In: 51.2 (Feb. 1988), pp. 143–188. DOI: 10.1088/0034-4885/51/2/001. URL: https://doi.org/10.1088/0034-4885/51/2/001.

[174] Jianing Han et al. “Rb $nf$ quantum defects from millimeter-wave spectroscopy of cold $^{85}$Rb Rydberg atoms”. In: *Phys. Rev. A* 74 (5 Nov. 2006), p. 054502. DOI: 10.1103/PhysRevA.74.054502. URL: https://link.aps.org/doi/10.1103/PhysRevA.74.054502.

[175] Wenhui Li et al. “Millimeter-wave spectroscopy of cold Rb Rydberg atoms in a magneto-optical trap: Quantum defects of the ns, np, and nd series”. In: *Phys. Rev. A* 67 (5 May 2003), p. 052502. DOI: 10.1103/PhysRevA.67.052502. URL: https://link.aps.org/doi/10.1103/PhysRevA.67.052502.

[176] K.-H. Weber and Craig J. Sansonetti. “Accurate energies of nS, nP, nD, nF, and nG levels of neutral cesium”. In: *Phys. Rev. A* 35 (11 June 1987), pp. 4650–4660. DOI: 10.1103/PhysRevA.35.4650. URL: https://link.aps.org/doi/10.1103/PhysRevA.35.4650.

[177] P. Schauß et al. “Crystallization in Ising quantum magnets”. In: *Science* 347.6229 (2015), pp. 1455–1458. DOI: 10.1126/science.1258351. eprint: https://www.science.org/doi/pdf/10.1126/science.1258351. URL: https://www.science.org/doi/abs/10.1126/science.1258351.

[178] Jian Cui et al. “Optimal control of Rydberg lattice gases”. In: 2.3 (Aug. 2017), p. 035006. DOI: 10.1088/2058-9565/aa7daf. URL: https://doi.org/10.1088/2058-9565/aa7daf.

[179] D. J. Griffiths. “Elementary Particles”. In: 2nd ed. Wiley-VCH, 2008, p. 149.

[180] B. Aubert et al. “Measurement of *CP*-Violating Asymmetries in $B^0$ Decays to *CP* Eigenstates”. In: *Phys. Rev. Lett.* 86 (12 Mar. 2001), pp. 2515–2522. DOI: 10.1103/PhysRevLett.86.2515. URL: https://link.aps.org/doi/10.1103/PhysRevLett.86.2515.

[181] R N Mohapatra. “Neutron–anti-neutron oscillation: theory and phenomenology”. In: 36.10 (Sept. 2009), p. 104006. DOI: 10.1088/0954-3899/36/10/104006. URL: https://doi.org/10.1088/0954-3899/36/10/104006.

[182] K. van Bibber et al. “Design for a practical laboratory detector for solar axions”. In: *Phys. Rev. D* 39 (8 Apr. 1989), pp. 2089–2099. DOI: 10.1103/PhysRevD.39.2089. URL: https://link.aps.org/doi/10.1103/PhysRevD.39.2089.

[183] D V Naumov and V A Naumov. “A diagrammatic treatment of neutrino oscillations”. In: 37.10 (Aug. 2010), p. 105014. DOI: 10.1088/0954-3899/37/10/105014. URL: https://doi.org/10.1088/0954-3899/37/10/105014.

[184] H. Umezawa, H. Matsumoto, and M. Tachiki. *Thermo Field Dynamics and Condensed States*. Amsterdam, New York: North-Holland, 1982.

[185] C Marletto, V Vedral, and D Deutsch. “Quantum-gravity effects could in principle be witnessed in neutrino-like oscillations”. In: 20.8 (Aug. 2018), p. 083011. DOI: 10.1088/1367-2630/aad5d8. URL: https://doi.org/10.1088/1367-2630/aad5d8.

[186] John Ellis et al. “Search for violations of quantum mechanics”. In: *Nuclear Physics B* 241.2 (1984), pp. 381–405. ISSN: 0550-3213. DOI: https://doi.org/10.1016/0550-3213(84)90053-1. URL: https://www.sciencedirect.com/science/article/pii/0550321384900531.

[187] G. Amelino-Camelia. "Towards Quantum Gravity". In: Springer, 2000, pp. 1–49.

[188] C. Rovelli. *Quantum Gravity*. Cambridge University Press, 2004.

[189] A. M. Gago et al. "Quantum dissipative effects and neutrinos: Current constraints and future perspectives". In: *Phys. Rev. D* 63 (7 Feb. 2001), p. 073001. DOI: 10.1103/PhysRevD.63.073001. URL: https://link.aps.org/doi/10.1103/PhysRevD.63.073001.

[190] Marcelo M. Guzzo, Pedro C. de Holanda, and Roberto L.N. Oliveira. "Quantum dissipation in a neutrino system propagating in vacuum and in matter". In: *Nuclear Physics B* 908 (2016). Neutrino Oscillations: Celebrating the Nobel Prize in Physics 2015, pp. 408–422. ISSN: 0550-3213. DOI: https://doi.org/10.1016/j.nuclphysb.2016.04.030. URL: https://www.sciencedirect.com/science/article/pii/S0550321316300682.

[191] E. Lisi, A. Marrone, and D. Montanino. "Probing Possible Decoherence Effects in Atmospheric Neutrino Oscillations". In: *Phys. Rev. Lett.* 85 (6 Aug. 2000), pp. 1166–1169. DOI: 10.1103/PhysRevLett.85.1166. URL: https://link.aps.org/doi/10.1103/PhysRevLett.85.1166.

[192] Fabio Benatti and Roberto Floreanini. "Open system approach to neutrino oscillations". In: 2000.02 (Feb. 2000), pp. 032–032. DOI: 10.1088/1126-6708/2000/02/032. URL: https://doi.org/10.1088/1126-6708/2000/02/032.

[193] F. Benatti and R. Floreanini. "Massless neutrino oscillations". In: *Phys. Rev. D* 64 (8 Sept. 2001), p. 085015. DOI: 10.1103/PhysRevD.64.085015. URL: https://link.aps.org/doi/10.1103/PhysRevD.64.085015.

[194] A. Capolupo et al. "Geometric phase of neutrinos: Differences between Dirac and Majorana neutrinos". In: *Physics Letters B* 780 (2018), pp. 216–220. ISSN: 0370-2693. DOI: https://doi.org/10.1016/j.physletb.2018.03.016. URL: https://www.sciencedirect.com/science/article/pii/S0370269318302053.

[195] A. Capolupo, S.M. Giampaolo, and G. Lambiase. "Decoherence in neutrino oscillations, neutrino nature and CPT violation". In: *Physics Letters B* 792 (2019), pp. 298–303. ISSN: 0370-2693. DOI: https://doi.org/10.1016/j.physletb.2019.03.062. URL: https://www.sciencedirect.com/science/article/pii/S037026931930231X.

[196] Luca Buoninfante et al. "Revealing neutrino nature and CPT violation with decoherence effects". In: *European Physical Journal C* 80.11, 1009 (Nov. 2020), p. 1009. DOI: 10.1140/epjc/s10052-020-08549-9. arXiv: 2001.07580 [hep-ph].

[197] A. Capolupo, G. Lambiase, and A. Quaranta. "Neutrinos in curved spacetime: Particle mixing and flavor oscillations". In: *Phys. Rev. D* 101 (9 May 2020), p. 095022. DOI: 10.1103/PhysRevD.101.095022. URL: https://link.aps.org/doi/10.1103/PhysRevD.101.095022.

[198] M. H. Abobeih et al. "One-second coherence for a single electron spin coupled to a multi-qubit nuclear-spin environment". In: *Nature Communications* 9, 2552 (June 2018), p. 2552. DOI: 10.1038/s41467-018-04916-z. arXiv: 1801.01196 [quant-ph].

[199] Nicolai Friis et al. "Observation of Entangled States of a Fully Controlled 20-Qubit System". In: *Phys. Rev. X* 8 (2 Apr. 2018), p. 021012. DOI: 10.1103/PhysRevX.8.021012. URL: https://link.aps.org/doi/10.1103/PhysRevX.8.021012.

[200] Stephan A Schulz et al. “Sideband cooling and coherent dynamics in a microchip multi-segmented ion trap”. In: 10.4 (Apr. 2008), p. 045007. DOI: 10.1088/1367-2630/10/4/045007. URL: https://doi.org/10.1088/1367-2630/10/4/045007.

[201] D. Kielpinski, C. Monroe, and D. J. Wineland. “Architecture for a large-scale ion-trap quantum computer”. In: *Nature* 417.6890 (June 2002), pp. 709–711. DOI: 10.1038/nature00784.

[202] S. Zippilli et al. “Adiabatic quantum simulation with a segmented ion trap: Application to long-distance entanglement in quantum spin systems”. In: *Phys. Rev. A* 89 (4 Apr. 2014), p. 042308. DOI: 10.1103/PhysRevA.89.042308. URL: https://link.aps.org/doi/10.1103/PhysRevA.89.042308.

[203] C. Kokail et al. “Self-verifying variational quantum simulation of lattice models”. In: *Nature* 569.7756 (May 2019), pp. 355–360. DOI: 10.1038/s41586-019-1177-4. arXiv: 1810.03421 [quant-ph].

[204] Erez Zohar, J Ignacio Cirac, and Benni Reznik. “Quantum simulations of lattice gauge theories using ultracold atoms in optical lattices”. In: 79.1 (Dec. 2015), p. 014401. DOI: 10.1088/0034-4885/79/1/014401. URL: https://doi.org/10.1088/0034-4885/79/1/014401.

[205] D. Kaufmann et al. “Thick-film technology for ultra high vacuum interfaces of micro-structured traps”. In: *Applied Physics B: Lasers and Optics* 107.4 (June 2012), pp. 935–943. DOI: 10.1007/s00340-012-4951-7. arXiv: 1107.4082 [quant-ph].

[206] Florian Mintert and Christof Wunderlich. “Ion-Trap Quantum Logic Using Long-Wavelength Radiation”. In: *Phys. Rev. Lett.* 87 (25 Nov. 2001), p. 257904. DOI: 10.1103/PhysRevLett.87.257904. URL: https://link.aps.org/doi/10.1103/PhysRevLett.87.257904.

[207] J. Chiaverini and W. E. Lybarger. “Laserless trapped-ion quantum simulations without spontaneous scattering using microtrap arrays”. In: *Phys. Rev. A* 77 (2 Feb. 2008), p. 022324. DOI: 10.1103/PhysRevA.77.022324. URL: https://link.aps.org/doi/10.1103/PhysRevA.77.022324.

[208] A. Khromova et al. “Designer Spin Pseudomolecule Implemented with Trapped Ions in a Magnetic Gradient”. In: *Phys. Rev. Lett.* 108 (22 June 2012), p. 220502. DOI: 10.1103/PhysRevLett.108.220502. URL: https://link.aps.org/doi/10.1103/PhysRevLett.108.220502.

[209] Michael Johanning, Andrés F Varón, and Christof Wunderlich. “Quantum simulations with cold trapped ions”. In: 42.15 (July 2009), p. 154009. DOI: 10.1088/0953-4075/42/15/154009. URL: https://doi.org/10.1088/0953-4075/42/15/154009.

[210] Harald Wunderlich et al. “Two-dimensional cluster-state preparation with linear ion traps”. In: *Phys. Rev. A* 79 (5 May 2009), p. 052324. DOI: 10.1103/PhysRevA.79.052324. URL: https://link.aps.org/doi/10.1103/PhysRevA.79.052324.

[211] Donald J. Douglas, Aaron J. Frank, and Dunmin Mao. “Linear ion traps in mass spectrometry”. In: *Mass Spectrometry Reviews* 24.1 (2005), pp. 1–29. DOI: https://doi.org/10.1002/mas.20004. eprint: https://analyticalsciencejournals.onlinelibrary.wiley.com/doi/pdf/10.1002/mas.20004. URL: https://analyticalsciencejournals.onlinelibrary.wiley.com/doi/abs/10.1002/mas.20004.

[212] F. Vannucci. "Interactions of neutrinos with matter". In: *Progress in Particle and Nuclear Physics* 95 (2017), pp. 1–47. ISSN: 0146-6410. DOI: https://doi.org/10.1016/j.ppnp.2017.03.003. URL: https://www.sciencedirect.com/science/article/pii/S0146641017300340.

[213] F. P. An et al. "Observation of Electron-Antineutrino Disappearance at Daya Bay". In: *Phys. Rev. Lett.* 108 (17 Apr. 2012), p. 171803. DOI: 10.1103/PhysRevLett.108.171803. URL: https://link.aps.org/doi/10.1103/PhysRevLett.108.171803.

[214] J. K. Ahn et al. "Observation of Reactor Electron Antineutrinos Disappearance in the RENO Experiment". In: *Phys. Rev. Lett.* 108 (19 May 2012), p. 191802. DOI: 10.1103/PhysRevLett.108.191802. URL: https://link.aps.org/doi/10.1103/PhysRevLett.108.191802.

[215] Y. Abe et al. "Indication of Reactor $\overline{\nu}_e$ Disappearance in the Double Chooz Experiment". In: *Phys. Rev. Lett.* 108 (13 Mar. 2012), p. 131801. DOI: 10.1103/PhysRevLett.108.131801. URL: https://link.aps.org/doi/10.1103/PhysRevLett.108.131801.

[216] K. Abe et al. "Indication of Electron Neutrino Appearance from an Accelerator-Produced Off-Axis Muon Neutrino Beam". In: *Phys. Rev. Lett.* 107 (4 July 2011), p. 041801. DOI: 10.1103/PhysRevLett.107.041801. URL: https://link.aps.org/doi/10.1103/PhysRevLett.107.041801.

[217] P. Adamson et al. "Improved Search for Muon-Neutrino to Electron-Neutrino Oscillations in MINOS". In: *Phys. Rev. Lett.* 107 (18 Oct. 2011), p. 181802. DOI: 10.1103/PhysRevLett.107.181802. URL: https://link.aps.org/doi/10.1103/PhysRevLett.107.181802.

[218] J. Beringer et al. "Review of Particle Physics". In: *Phys. Rev. D* 86 (1 July 2012), p. 010001. DOI: 10.1103/PhysRevD.86.010001. URL: https://link.aps.org/doi/10.1103/PhysRevD.86.010001.

[219] G. Lindblad. "On the generators of quantum dynamical semigroups". In: *Communications in Mathematical Physics* 48.2 (June 1976), pp. 119–130. DOI: 10.1007/BF01608499.

[220] Vittorio Gorini, Andrzej Kossakowski, and E. C. G. Sudarshan. "Completely positive dynamical semigroups of N-level systems". In: *Journal of Mathematical Physics* 17.5 (1976), pp. 821–825. DOI: 10.1063/1.522979. eprint: https://aip.scitation.org/doi/pdf/10.1063/1.522979. URL: https://aip.scitation.org/doi/abs/10.1063/1.522979.

[221] Dean Morgan et al. "Probing quantum decoherence in atmospheric neutrino oscillations with a neutrino telescope". In: *Astroparticle Physics* 25.5 (2006), pp. 311–327. ISSN: 0927-6505. DOI: https://doi.org/10.1016/j.astropartphys.2006.03.001. URL: https://www.sciencedirect.com/science/article/pii/S0927650506000338.

[222] G. L. Fogli et al. "Probing nonstandard decoherence effects with solar and KamLAND neutrinos". In: *Phys. Rev. D* 76 (3 Aug. 2007), p. 033006. DOI: 10.1103/PhysRevD.76.033006. URL: https://link.aps.org/doi/10.1103/PhysRevD.76.033006.

[223] Yasaman Farzan, Thomas Schwetz, and Alexei Yu Smirnov. "Reconciling results of LSND, MiniBooNE and other experiments with soft decoherence". In: 2008.07 (July 2008), pp. 067–067. DOI: 10.1088/1126-6708/2008/07/067. URL: https://doi.org/10.1088/1126-6708/2008/07/067.

[224] R. L. N. Oliveira and M. M. Guzzo. “Quantum dissipation in vacuum neutrino oscillation”. In: *European Physical Journal C* 69.3-4 (Oct. 2010), pp. 493–502. DOI: 10.1140/epjc/s10052-010-1388-1.

[225] R. L. N. Oliveira and M. M. Guzzo. “Dissipation and $\theta_{13}$ in neutrino oscillations”. In: *European Physical Journal C* 73, 2434 (May 2013), p. 2434. DOI: 10.1140/epjc/s10052-013-2434-6.

[226] Roberto L. N. Oliveira. “Dissipative effect in long baseline neutrino experiments”. In: *European Physical Journal C* 76.7, 417 (July 2016), p. 417. DOI: 10.1140/epjc/s10052-016-4253-z. arXiv: 1603.08065 [hep-ph].

[227] Pouya Bakhti, Yasaman Farzan, and Thomas Schwetz. “Revisiting the quantum decoherence scenario as an explanation for the LSND anomaly”. In: *Journal of High Energy Physics* 2015, 7 (May 2015), p. 7. DOI: 10.1007/JHEP05(2015)007. arXiv: 1503.05374 [hep-ph].

[228] G. Balieiro Gomes et al. “Parameter limits for neutrino oscillation with decoherence in KamLAND”. In: *Phys. Rev. D* 95 (11 June 2017), p. 113005. DOI: 10.1103/PhysRevD.95.113005. URL: https://link.aps.org/doi/10.1103/PhysRevD.95.113005.

[229] Marcelo M. Guzzo, Pedro C. de Holanda, and Roberto L.N. Oliveira. “Quantum dissipation in a neutrino system propagating in vacuum and in matter”. In: *Nuclear Physics B* 908 (2016). Neutrino Oscillations: Celebrating the Nobel Prize in Physics 2015, pp. 408–422. ISSN: 0550-3213. DOI: https://doi.org/10.1016/j.nuclphysb.2016.04.030. URL: https://www.sciencedirect.com/science/article/pii/S0550321316300682.

[230] L. Stodolsky. “Treatment of neutrino oscillations in a thermal environment”. In: *Phys. Rev. D* 36 (8 Oct. 1987), pp. 2273–2277. DOI: 10.1103/PhysRevD.36.2273. URL: https://link.aps.org/doi/10.1103/PhysRevD.36.2273.

[231] G. Sigl and G. Raffelt. “General kinetic description of relativistic mixed neutrinos”. In: *Nuclear Physics B* 406.1 (1993), pp. 423–451. ISSN: 0550-3213. DOI: https://doi.org/10.1016/0550-3213(93)90175-O. URL: https://www.sciencedirect.com/science/article/pii/055032139390175O.

[232] Tobias Stirner, Günter Sigl, and Georg Raffelt. “Liouville term for neutrinos: flavor structure and wave interpretation”. In: 2018.05 (May 2018), pp. 016–016. DOI: 10.1088/1475-7516/2018/05/016. URL: https://doi.org/10.1088/1475-7516/2018/05/016.

[233] Alexey Vlasenko, George M. Fuller, and Vincenzo Cirigliano. “Neutrino quantum kinetics”. In: *Phys. Rev. D* 89 (10 May 2014), p. 105004. DOI: 10.1103/PhysRevD.89.105004. URL: https://link.aps.org/doi/10.1103/PhysRevD.89.105004.

[234] Daniel N. Blaschke and Vincenzo Cirigliano. “Neutrino quantum kinetic equations: The collision term”. In: *Phys. Rev. D* 94 (3 Aug. 2016), p. 033009. DOI: 10.1103/PhysRevD.94.033009. URL: https://link.aps.org/doi/10.1103/PhysRevD.94.033009.

[235] R. R. Lewis. “Coherent detector for low-energy neutrinos”. In: *Phys. Rev. D* 21 (3 Feb. 1980), pp. 663–668. DOI: 10.1103/PhysRevD.21.663. URL: https://link.aps.org/doi/10.1103/PhysRevD.21.663.

[236] Jose A Helayël-Neto, Andre B Penna-Firme, and Ilya L Shapiro. “Scalar QED hbar-corrections to the Coulomb potential”. In: 2000.01 (Jan. 2000), pp. 009–009. DOI: 10.1088/1126-6708/2000/01/009. URL: https://doi.org/10.1088/1126-6708/2000/01/009.

[237] S. Weinberg. *The Quantum Theory of Fields vol. 1: Foundations*. 1st ed. Cambridge University Press, 1995.

[238] A. et al. Ereditato. *The State of the Art of Neutrino Physics*. Vol. 28. Advanced Series on Directions in High Energy Physics. World Scientific, 2018.

[239] D´Angelo, D. et al. “Recent Borexino results and prospects for the near future”. In: *EPJ Web Conf.* 126 (2016), p. 02008. DOI: 10.1051/epjconf/201612602008. URL: https://doi.org/10.1051/epjconf/201612602008.

[240] James Madsen. *Ultra-High Energy Neutrinos*. 2019. arXiv: 1901.02528 [astro-ph.HE].

[241] Aya Ishihara and. “Extremely high energy neutrinos in six years of IceCube data”. In: 718 (May 2016), p. 062027. DOI: 10.1088/1742-6596/718/6/062027. URL: https://doi.org/10.1088/1742-6596/718/6/062027.

[242] M. G. Aartsen et al. “Measurement of the multi-TeV neutrino interaction cross-section with IceCube using Earth absorption”. In: *Nature* 551.7682 (Nov. 2017), pp. 596–600. DOI: 10.1038/nature24459. arXiv: 1711.08119 [hep-ex].

[243] Jean-Sébastien Gagnon and Mikhail Shaposhnikov. “Baryon asymmetry of the Universe without Boltzmann or Kadanoff-Baym equations”. In: *Phys. Rev. D* 83 (6 Mar. 2011), p. 065021. DOI: 10.1103/PhysRevD.83.065021. URL: https://link.aps.org/doi/10.1103/PhysRevD.83.065021.

[244] E. Alfinito et al. “Squeezed neutrino oscillations in quantum field theory”. In: *Physics Letters B* 362.1 (1995), pp. 91–96. ISSN: 0370-2693. DOI: https://doi.org/10.1016/0370-2693(95)01171-L. URL: https://www.sciencedirect.com/science/article/pii/037026939501171L.